

The biochemical basis of plant ATG8 substrate specificity

Erin Zess

Thesis submitted to the University of East Anglia for the
Degree of Doctor of Philosophy

September 2019

© This copy of the thesis has been supplied on condition that anyone who consults it is understood to recognize that its copyright rests with the author and that use of any information derived there from must be in accordance with current UK Copyright Law. In addition, any quotation or extract must include full attribution.

Abstract

Autophagy is an essential eukaryotic cellular quality control pathway that involves the degradation of self- and non-self macromolecules, with multiple layers of specificity defining the dynamics of substrate uptake, sub-cellular trafficking, and turnover. ATG8 is a highly-conserved ubiquitin-like protein that is central to the selectivity of the autophagy pathway, directly or indirectly binding desired autophagic cargo. Throughout plant evolution, ATG8 has expanded from a single protein in algae to multiple isoforms in higher plants. However, the degree to which ATG8 isoforms have functionally specialized to bind distinct proteins is unclear. In this thesis, I described the potato ATG8 interactome using *in planta* immunoprecipitation followed by mass spectrometry, discovering that potato ATG8 isoforms bind distinct sets of plant proteins with varying degrees of overlap. In addition, I defined the biochemical basis of potato ATG8 specialization. I revealed that the ATG8 N-terminal β -strand underpins binding specificity to substrates that contain ATG8-interacting motifs (AIMs), including the ATG8-targetting effector from the potato late blight pathogen *Phytophthora infestans*, PexRD54. To approach the question of ATG8 substrate specificity from the opposing direction, I also explored the evolutionary dynamics of PexRD54 in different host-specific lineages of *Phytophthora*. I found that the PexRD54 ortholog from *P. mirabilis*, a closely related species to *P. infestans*, has a polymorphism in its AIM which nearly abolishes binding to the ATG8s of its host, *Mirabilis jalapa*. These results provide insights into the requirements of a functional ATG8-interacting motif, as well as raise questions as to whether specific selective pressures of the *M. jalapa* host environment have shaped the evolution the *P. mirabilis* PexRD54.

Table of Contents

<i>Abstract</i>	2
<i>Table of Contents</i>	3
<i>Abbreviations</i>	10
<i>Acknowledgements</i>	12
Chapter 1: General Introduction	13
1.1 Plant autophagy—overview	13
1.2 Molecular mechanisms of plant autophagy	14
1.2.1 Autophagy-related (ATG) proteins	14
1.2.2 Phagophore initiation.....	14
1.2.3 Phagophore expansion	15
1.2.4 Autophagosome maturation	18
1.2.5 Autophagosome trafficking and vacuolar fusion.....	18
1.2.6 Regulation of the plant autophagy pathway	20
1.3 Roles of autophagy in plants	20
1.3.1 Development.....	21
1.3.2 Metabolism	21
1.3.3 Abiotic stress	22
1.3.4 Biotic stress.....	23
1.4 Plant selective autophagy—layers of specificity	24
1.4.1 Autophagy cargo receptors	25
1.4.2 ATG8-interacting motif.....	29
1.4.3 ATG8 diversification	30
1.4.4 Regulation of plant selective autophagy components.....	31
1.5 Tools to study plant selective autophagy	32
1.6 Plant pathogen effectors	33
1.6.1 Classes of effectors.....	33
1.6.2 Effector functions	34
1.6.3 Detection of effectors by intracellular immune receptors	35
1.6.4 Effectors as molecular probes	36
1.7 Evolution of plant pathogen effectors	36
1.7.1 Genomic localization	37
1.7.2 Extreme patterns of mutations.....	38
1.7.3 Presence/ absence polymorphisms	39

1.7.4	Structurally-defined classes of effectors.....	40
1.8	Aims of the thesis	41
Chapter 2: Materials and Methods		43
2.1	Molecular biology methods	43
2.1.1	Gateway cloning	43
2.1.2	Golden Gate cloning.....	43
2.1.3	In-Fusion cloning	43
2.1.4	Bacterial transformation	44
2.1.5	PCR product purification, colony PCR, and plasmid preparation.....	44
2.2	Biochemistry methods	44
2.2.1	<i>In planta</i> protein expression.....	44
2.2.2	Plant total protein extraction	45
2.2.3	Co-immunoprecipitation	45
2.2.4	SDS-PAGE electrophoresis.....	46
2.2.5	Immunoblot analysis	46
2.2.6	Heterologous protein production and purification.....	46
2.2.7	Isothermal titration calorimetry	47
2.3	Plant material	47
2.3.1	<i>Nicotiana benthamiana</i>	47
2.3.2	<i>Mirabilis jalapa</i>	48
2.4	Plant genotyping	48
2.4.1	<i>Mirabilis jalapa</i> DNA extraction	48
2.4.2	<i>Mirabilis jalapa</i> genotyping by PCR.....	48
2.5	Cloning	49
2.5.1	ATG8s.....	49
2.5.2	ATG8-interacting proteins and ATG8-interacting motif (AIM) mutants.....	51
2.5.3	PexRD54 variants and mutants.....	52
2.5.4	PexRD54-interacting proteins	53
2.6	Phylogenetic analyses	53
2.6.1	Phylogenetic analysis of Solanaceous ATG8s.....	53
2.6.2	Phylogenetic analysis of <i>Mirabilis jalapa</i> ATG8s.....	54
2.7	Immunoprecipitation-mass spectrometry (IP-MS).....	54
2.7.1	Sample preparation.....	54
2.7.2	Nano liquid chromatography mass spectrometry (LC-MS) analysis, data processing, and peptide identification.....	55
2.7.3	Data filtering.....	56

2.7.4 Network analysis.....	57
2.7.5 ATG8-interacting motif prediction and conservation.....	57
Chapter 3: Solanaceous ATG8 isoforms associate with distinct sets of plant proteins.....	58
3.1 Introduction	58
3.2 Results and Discussion.....	61
3.2.1 <i>Solanum tuberosum</i> ATG8s have distinct interactor profiles.....	61
3.2.2 Validation of the potato ATG8 interactome.....	66
3.2.3 The <i>S. tuberosum</i> ATG8 interactome contains known ATG8-interacting proteins, novel autophagy-associated proteins, and organellar proteins	68
3.2.4 ATG8 functional diversification—a broader view.....	74
3.3 Conclusions.....	75
Chapter 4: N-terminal β-strand underpins biochemical specialization of a plant ATG8 isoform.....	76
4.1 Introduction	76
4.2 Results and Discussion.....	78
4.2.1 ATG8 isoforms show differential binding to PexRD54.....	78
4.2.2 The first β -strand of ATG8 underpins discriminatory binding to PexRD54 ...	80
4.2.3 A single residue in the first β -strand underpins discriminatory binding to the substrate PexRD54.....	82
4.2.4 The N-terminal β -strand defines the protein interactor profiles of ATG8-2.2 and ATG8-4.....	85
4.2.5 Low expression of ATG8-4-V32I construct precluded IP-MS analysis.....	88
4.3 Conclusions.....	89
Chapter 5: Evolutionary dynamics of the <i>Phytophthora</i> effector PexRD54 following a host jump	90
5.1 Introduction	90
5.2 Results and Discussion.....	93
5.2.1 The <i>P. mirabilis</i> PexRD54 has a fixed amino acid polymorphism in its ATG8-interacting motif	93
5.2.2 <i>P. mirabilis</i> PexRD54 AIM polymorphism reduces binding to <i>M. jalapa</i> ATG8s ..	95
5.2.3 What is the role of <i>Pm</i> PexRD54 during <i>P. mirabilis</i> infection of <i>M. jalapa</i> ?.....	101
5.3 Conclusions.....	104
Chapter 6: Discussion.....	106
6.1 ATG8 functional specialization: a layer of specificity defining the plant selective autophagy pathway	106
6.2 What drove the diversification of plant ATG8s?	107

6.3	Multiple structural features shape ATG8 substrate specificity	109
6.4	Potato ATG8-4: an ATG8 apart?	110
6.5	Aiming higher: improving the accuracy of AIM predictions	112
6.6	<i>Phytophthora mirabilis</i> PexRD54 has evolved away from direct ATG8 targeting	113
6.7	What we talk about when we talk about evolutionary plant-microbe interactions	114
6.8	Concluding remarks and future challenges	115
	<i>Appendix I</i>	116
	<i>Appendix II</i>	121
	<i>Appendix III</i>	147
	<i>Appendix IV</i>	155
	<i>Appendix V</i>	169
	<i>References</i>	180

List of Tables

Table 2.1 List of primers used for genotyping of <i>M. jalapa</i> transgenics	48
Table 2.2 List of <i>S. tuberosum</i> ATG8 accessions	49
Table 2.3 List of primers used for ATG8 cloning.....	50
Table 2.4 List of ATG8-interacting proteins and accessions.....	52
Table 2.5 List of primers used for PexRD54 cloning.....	53
Table A.2.1 ATG8 interactome	122
Table A.2.2 Overlap between the potato ATG8 interactome and the human ATG8 interactome from Behrends et al (2010)	139
Table A.4.1 Comparative ATG8-4-S3 mutant analysis dataset	156
Table A.5.1 Summary of the thermodynamic and kinetic data for the isothermal titration calorimetry experiments.....	179

List of Figures

Figure 1.1 Schematic representation of known or proposed steps within the autophagy (ATG)-mediated autophagic system in yeasts, animals, and plants.....	16
Figure 3.1 Schematic representation of the selective autophagy pathway	61
Figure 3.2 Potato ATG8s are sequence diverse	62
Figure 3.3 Potato ATG8 isoforms have distinct protein interaction profiles	63
Figure 3.4 Potato ATG8s differentially interact with proteins from different cellular compartments, including the core autophagy machinery.....	65
Figure 3.5 Non-specific interaction of two ATG8 interactome proteins	68
Figure 3.6 Network representation of interaction between potato ATG8s and endogenous <i>N. benthamiana</i> ATG8s.....	69
Figure 3.7 Potato ATG8-4 shows selectivity towards a subset of substrates.....	71
Figure 4.1 ATG8 isoforms show differential binding to PexRD54.....	79
Figure 4.2 The ATG8 region surrounding the first β -strand is responsible for discriminatory binding to PexRD54.....	81
Figure 4.3 A Comparison of ATG8-2.2 structure and ATG8-4 model identifies polymorphic residues within the AIM binding site.....	83
Figure 4.4 A single amino acid residue, Val-32 in the first β -strand, determines differential binding affinity of ATG8-4 towards PexRD54.....	84
Figure 4.5 The first β -strand defines the AIM-dependent interaction profiles of ATG8 isoforms	87
Figure 5.1 Host specialization of related <i>Phytophthora</i> species	93
Figure 5.2 The <i>P. mirabilis</i> PexRD54 has an AIM polymorphism and is expressed during infection	94
Figure 5.3 <i>Mirabilis jalapa</i> ATG8s are not orthologous to ATG8s from other plant taxa	96
Figure 5.4 The <i>P. mirabilis</i> PexRD54 AIM polymorphism reduces binding to <i>M. jalapa</i> ATG8s.....	97
Figure 5.5 <i>PmPexRD54</i> peptide binds weakly to ATG8s in isothermal titration calorimetry experiments	99
Figure 5.6 <i>PmPexRD54</i> does not associate with <i>M. jalapa</i> Rab8a	103
Figure 5.7 Evolutionary dynamics of PexRD54 following a host jump	103
Figure A.1.1 Orthologous relationships between Solanaceous ATG8 isoforms	117
Figure A.1.2 Network representation of the interactions between ATG8s and protein groups defined by biological process gene ontology (GO) annotations ...	118
Figure A.1.3 ATG8 interactome data is reproducible across replicates	119
Figure A.1.4 Significant level of overlap between the <i>N. benthamiana</i> ATG8 interactome and the human ATG8 interactome from Behrends et al (2010).....	120
Figure A.3.1 Normal distribution of comparative ATG8-4-S3 mutant IP-MS data	148
Figure A.3.2 The first β -strand of ATG8 underpins interaction with plant proteins ...	149
Figure A.3.3 The ATG8 region surrounding the first β -strand is responsible for discriminatory binding to potato Vps4.....	150
Figure A.3.4 Candidate ATG8-interacting proteins do not express <i>in planta</i>	152
Figure A.3.5 The ATG8-4-V32I bait construct is weakly expressed.....	153
Figure A.3.6 Network representation of the interaction between ATG8-2.2, ATG8-4, and ATG8-4-S3 and endogenous <i>N. benthamiana</i> ATG8s	154
Figure A.5.1 Diversity of <i>Phytophthora</i> clade 1c PexRD54 sequences	170

Figure A.5.2 Sequence diversity of <i>M. jalapa</i> ATG8s	171
Figure A.5.3 <i>Mirabilis jalapa</i> ATG8s are not orthologous to ATG8s from other plant taxa.....	173
Figure A.5.4 Mutation of the <i>P. mirabilis</i> PexRD54 AIM to match the <i>P. infestans</i> sequence is sufficient to reconstitute ATG8 binding	174
Figure A.5.5 <i>Pi</i> PexRD54 AIM peptide interaction with <i>St</i> ATG8-2.2, <i>Mj</i> ATG8-I and <i>Mj</i> ATG8-III in isothermal titration calorimetry.....	175
Figure A.5.6 <i>Pm</i> PexRD54 AIM peptide interaction with <i>St</i> ATG8-2.2, <i>Mj</i> ATG8-I and <i>Mj</i> ATG8-III in isothermal titration calorimetry.....	177

Abbreviations

AIM	ATG8-interacting motif
AMPK	AMP-activated protein kinase
At	<i>Arabidopsis thaliana</i>
ATG	autophagy-related
ATG8	autophagy-related protein 8
ATI1	ATG8-interacting protein 1
ATI2	ATG8-interacting protein 2
ATI3	ATG8-interacting protein 3
AVR	avirulence protein
BAR-SH3	bin amphiphysin rvs src homology 3
BES1	BRI1-EMS suppressor 1
CaMV	cauliflower mosaic virus
CDC	conditionally dispensable chromosomes
CHMP1	charged multivesicular body protein 1
co-IP	co-immunoprecipitation
COPII	coat protein complex II
dN	nonsynonymous nucleotide substitutions
dpi	days post infiltration/infection
dS	synonymous substitutions
DYRK	dual-specificity tyrosine regulated protein kinase
EF1a	elongation factor 1-alpha
ER	endoplasmic reticulum
ERES	ER exit sites
ESCRT	endosomal sorting complex required for transport
FREE1	FYVE domain protein required for endosomal sorting 1
GABARAP	gamma-aminobutyric receptor-associated protein
GAPDH	glyceraldehyde-3-phosphate dehydrogenase
GFP	green fluorescent protein
GIM	GABARAP interaction motif
HMA	heavy metal-associated domain
HOPS	homotypic fusion and protein sorting
HR	hypersensitive response
HsfA1a	heat-shock transcription factor A1a
IP	immunoprecipitate
IP-MS	immunoprecipitation with tandem mass spectrometry
ITC	isothermal titration calorimetry
K_D	equilibrium dissociation constant
LCAT	lecithin-cholesterol acyltransferase
LIR	LC3-interacting region
MAP1LC3	microtubule-associated protein 1 light chain 3
MAX	<i>Magnaporthe</i> AVR and ToxB-like
<i>Mj</i>	<i>Mirabilis jalapa</i>
NBR1	neighbour of BRCA1
NLR	nucleotide-binding domain leucine-rich repeat-containing protein
PAMP	pathogen associated molecular pattern
PE	phosphatidylethanolamine

<i>Pi</i>	<i>Phytophthora infestans</i>
PI3K	phosphatidylinositol-3-kinase
PI3P	phosphatidylinositol-3-phosphate
<i>Pm</i>	<i>Phytophthora mirabilis</i>
PRR	pattern recognition receptor
PSM	peptide spectrum match
Pst	<i>Pseudomonas syringae</i> pv. tomato DC3000
RPN10	regulatory particle non-ATPase subunit
RCLR	Arg-X-Leu-Arg
S6PDH	NADP-dependent d-sorbitol-6-phosphate dehydrogenase
SH3P2	SH3 domain-containing protein 2
SKD1	suppressor of K ⁺ transport growth defect 1
SNARE	soluble N-ethylmaleimide-sensitive factor attachment receptors
<i>St</i>	<i>Solanum tuberosum</i>
SUMO	small ubiquitin-like modifier
TALE	transcription activator-like effectors
TE	transposable elements
TMT	tandem mass tag
TOR	target of rapamycin
TPM	transcripts per million
TPSO	tryptophan-rich sensory protein/ translocator
UBL	ubiquitin-like modifier
UIM	ubiquitin interacting motif
VPS34	vacuolar protein sorting 34

Acknowledgements

Firstly, I would like to thank the John Innes Centre/ The Sainsbury Laboratory Rotation PhD program for giving me the opportunity to pursue a PhD in such a vibrant, stimulating, and rigorous environment. I am grateful to Sophien Kamoun for his guidance over the course of my PhD, and for fundamentally reshaping my view of what makes a great scientist. I will strive to emulate your scientific vision, as well as your clarity of thought and expression. I would also like to thank my secondary supervisor, Mark Banfield, for being a consistently engaged, insightful, and encouraging presence on my committee.

I want to extend my sincere appreciation to everyone who worked on the project that forms the bulk of this thesis—it was a pleasure to participate in such an expansive, productive collaboration. Thank you especially to Yasin Dagdas, for contributing a boundless enthusiasm that buoyed this project through the challenging times.

I feel incredibly privileged to have been able to work with each of the past and present members of the Kamoun Lab. Thank you all for helping me grow as a scientist, for providing a consistent source of inspiration, and for being such great colleagues. I would like to extend a special thank you to my constant companion in the Kamoun Lab, Ola Bialas—I like to think that sum of all of our office chats add up to something productive. I am eternally indebted to my mentor, Lida Derivnina, for providing a model for the kind of scientist I want to be. ~~Moreover,~~ thank you to Lida, Ola, Abbas Maqbool, Adeline Harant, and Mauricio Contreras for providing helpful feedback on my thesis, the final product has benefited immensely from your input.

To my TSLytherins, I am proud of the community that we built together—it stands as a testament to the fact that possessing ‘great ambition’ does not preclude the desire to invest in the success and wellbeing of those around you. Thank you for making my time at TSL more personally enriching, and fun, than I ever could have imagined it would be.

I am grateful for my years spent in Norwich, a city I love. Thank you to the Book Hive for nourishing my soul, and to Take Thai for nourishing my body. To the Boots Rewards Program, thank you for the points; those that I cannot spend before I leave, I will carry in my heart.

For my London Thesis Writing Retreat, I am thankful to Ann Wright and Andy Whittaker, whose generosity made this final month a significantly less stressful endeavour.

Words cannot contain my appreciation for all of the friends that I have made during my PhD. I cherish you all, so deeply.

And, to the friendships that I brought with me, thank you for being the continuous lights of my life. Thank you to Kelly, for showing me what strength looks like.

Lastly, to my family. A big slobbery thanks to Badger, for surviving. Thank you to my extended family, especially my beloved aunts, for showering me with love from afar. To my brothers, well, pray my head never gets too big in your presence. Most importantly, thank you to my parents—all that I can do is because of you.

It’s a good start.

Chapter 1: General Introduction

1.1 Plant autophagy—overview

Autophagy—“self-eating”—is an essential eukaryotic cellular process that involves the degradation of cellular components, either as a housekeeping function or as a stress response (Dikic and Elazar, 2018; Lamb et al., 2013). Three distinct autophagy routes have been identified in eukaryotes: chaperone-mediated autophagy, microautophagy, and macroautophagy (Rabinowitz and White, 2010; Klionsky, 2007; Nakatogawa et al., 2009). The chaperone-mediated pathway, which has not yet been reported in plants, uses specific receptors to target individual proteins for import into the vacuole for degradation (Li and Vierstra, 2012). By contrast, microautophagy involves the direct sequestration of cytoplasmic material by invagination of the tonoplast, which then undergoes scission to release autophagic bodies into the vacuole that are subsequently degraded (Li and Vierstra, 2012). In macroautophagy (hereafter ‘autophagy’), targeted cytoplasmic contents are engulfed in *de novo* formed vesicles, termed ‘autophagosomes’, which are trafficked to the vacuole for degradation, or elsewhere in the cell as part of a more general trafficking pathway (Marshall and Vierstra, 2018; Dagdas et al., 2018; Dupont et al., 2011).

Autophagy was first described as a non-selective bulk degradation pathway that provides essential components for survival during starvation stress. However, it is now well-established that autophagy is a highly selective and tightly regulated pathway (Johansen and Lamark, 2011; Svenning and Johansen, 2013; Kraft et al., 2010; Kadandale and Kiger, 2010). A number of studies in *Saccharomyces cerevisiae* (yeast), metazoans, and plants have shown that autophagy selectively degrades cargo material such as aggregated proteins, damaged mitochondria, excess peroxisomes, and invading pathogens (Zaffagnini and Martens, 2016). Although the characterization of selective autophagy mechanisms in plants has lagged behind studies in these other systems, it is widely recognized that this pathway is crucial for plants to rapidly modulate their organelle and proteome content to maintain homeostasis, contributing to their robust phenotypic plasticity (Stephani and Dagdas, 2019).

1.2 Molecular mechanisms of plant autophagy

1.2.1 Autophagy-related (ATG) proteins

Autophagosome formation proceeds in three major steps: initiation, expansion, and maturation. Genes required for the full function of autophagy were initially identified via screens in yeast—foundational work pioneered by Yoshinori Ohsumi, who won the 2016 Nobel Prize in Physiology or Medicine for his discoveries (Tooze and Dikic, 2016). In all, the autophagy pathway requires the concerted action of around 40 conserved proteins that have been grouped into the autophagy-related (ATG) protein family, with 15 proteins constituting the core machinery (Wen and Klionsky, 2016; Kraft and Martens, 2012). The autophagy machinery is highly conserved in eukaryotes, with most ATG proteins discovered in yeast also present in both metazoans and plants (Wen and Klionsky, 2016; Kraft and Martens, 2012). Interestingly, many ATG components in plants are synthesized from small gene families, representing a marked mechanistic divergence (Doelling et al., 2002; Chung et al., 2009; Suttangkakul et al., 2011; Hanaoka et al., 2002; Avin-Wittenberg et al., 2012). Although our understanding of the molecular mechanisms that underpin autophagy in plants is incomplete, we have a burgeoning understanding of the genetic requirements for autophagosome formation, expansion, trafficking, and vacuolar fusion (**Fig 1.1**) (Wang et al., 2018).

1.2.2 Phagophore initiation

The early steps of autophagosome formation have not been well-defined in plants (Michaeli et al., 2016), but much can be concluded from analogy to yeast and metazoan systems. First, inducing signals, such as starvation or infection, converge on ATG1, a serine/threonine kinase. ATG1, together in complex with ATG13, ATG17, ATG29, and ATG31, initiates the formation of a membranous structure named the ‘phagophore’ (**Fig 1.1**) (Yamamoto et al., 2016; Suzuki et al., 2015; Popelka and Klionsky, 2015). Interestingly, additional evidence in metazoans has indicated that autophagic cargo can also directly induce phagophore formation, serving as a template to recruit the ATG machinery, although this has not been observed in plants (Lazarou et al., 2015; Shibutani and Yoshimori, 2014; Youle and Narendra, 2011; Fujita et al., 2013). In either case, upon induction of autophagy, ATG proteins involved in phagophore initiation and expansion rapidly re-localize from the cytoplasm to punctate structures termed ‘phagophore

assembly sites' (Reggiori and Klionsky, 2013). These initial phagophore nucleation events remain poorly characterized, especially in plants, with both the nature and architecture of phagophore assembly sites still under debate (Gomez et al., 2018).

1.2.3 Phagophore expansion

1.2.3.1 *Phosphatidylinositol-3-kinase (PI3K) complex*

Following the convergence of signals on ATG1, the ATG1 complex activates the phosphatidylinositol-3-kinase (PI3K) complex at the phagophore assembly site (**Fig 1.1**) (Vicinanza et al., 2015; Ge et al., 2014; Xu et al., 2017). The PI3K complex is formed of VACUOLAR PROTEIN SORTING 34 (VPS34), which provides the kinase activity, together with three accessory subunits, ATG6, ATG14, and VPS15 (Lee et al., 2018). This complex is required for the expansion of the phagophore and decorates the growing phagophore with its product, phosphatidylinositol-3-phosphate (PI3P), serving as a signal to recruit further downstream ATG proteins (Liu et al., 2005). The four PI3K components—VPS34, ATG6, ATG14, and VPS15—have been studied in the model flowering plant *Arabidopsis thaliana*, and been found to carry out similar functions (Welters et al., 1994; Wang et al., 2012; Lee et al., 2018; Patel and Dinesh-Kumar, 2008; Gao et al., 2015; Li et al., 2016; Xu et al., 2017).

1.2.3.2 *ATG8-phosphatidylethanolamine conjugation*

Two linked catalytic conjugation cascades are essential for autophagosome formation, both of which are analogous to the ubiquitination conjugation system (**Fig 1.1**) (Mizushima et al., 1998; Ichimura et al., 2000). In this context, both ATG12 and ATG8 function as ubiquitin-like modifiers (Tooze and Dikic, 2016). Before activation, ATG8 is first processed by the cysteine protease ATG4, revealing a C-terminal glycine residue (Tooze and Dikic, 2016). Then, both ATG12 and ATG8 are activated by the common E1-like protein ATG7 and transferred to the E2-like enzymes ATG10 and ATG3, respectively (Tooze and Dikic, 2016). The ATG5-ATG10 conjugate forms a complex with ATG16, which then function as an E3-like enzyme, conjugating ATG8 to phosphatidylethanolamine (PE) for insertion into the growing phagophore (Kaufmann et al., 2014).

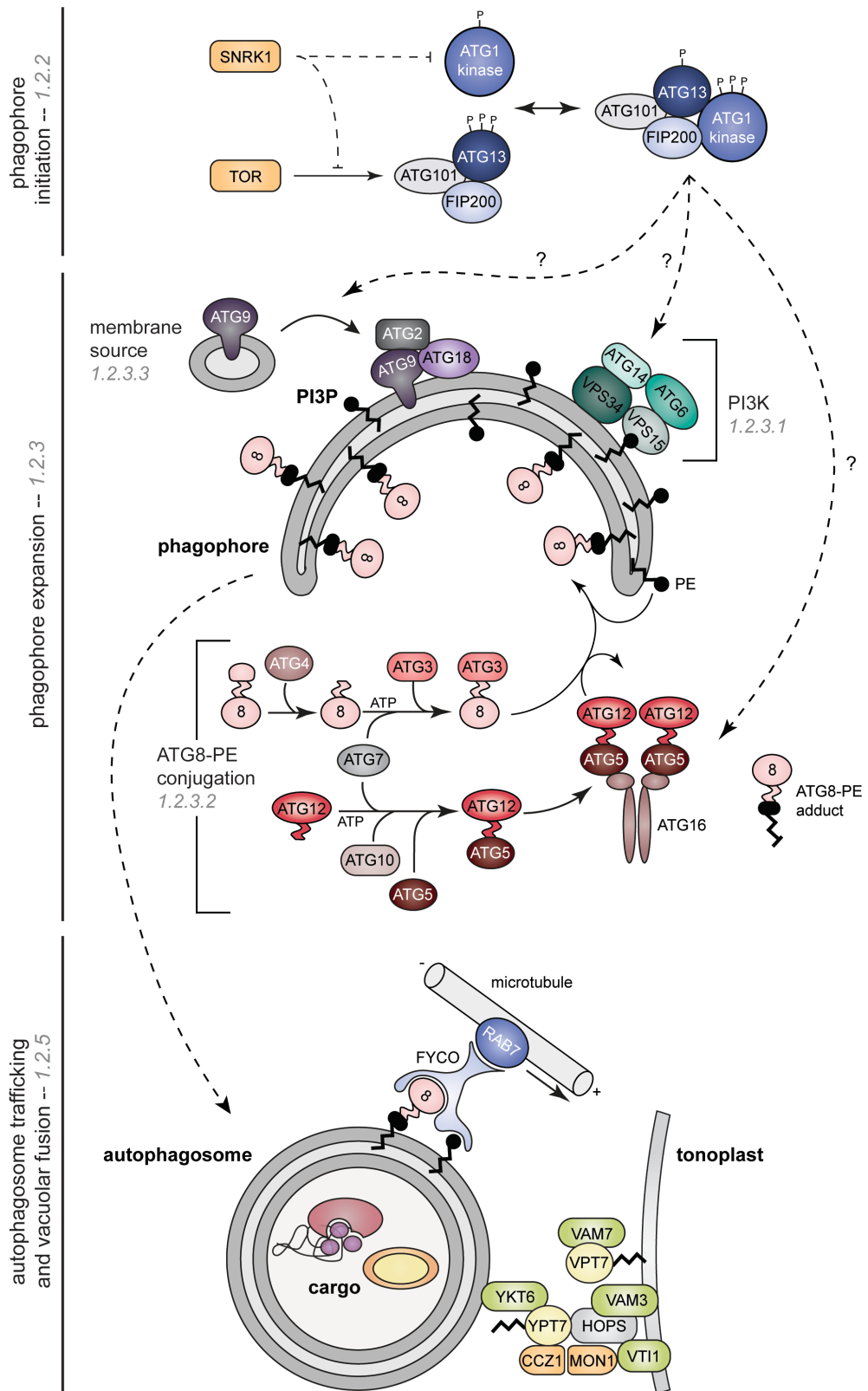


Figure 1.1 Schematic representation of known or proposed steps within the autophagy (ATG)-mediated autophagic system in yeasts, animals, and plants.

Figure 1.1 Schematic representation of known or proposed steps within the autophagy (ATG)-mediated autophagic system in yeasts, animals, and plants.

Phagophore initiation (**section 1.2.2**) is controlled by the ATG1/ATG13 kinase complex, the activation of which is regulated via phosphorylation by the upstream kinases SnRK1 and TOR (**section 1.2.6**). Phagophore expansion (**section 1.2.3**) proceeds by ATG1-mediated activation of the PI3K complex (**section 1.2.3.1**); ATG8-phosphatidylethanolamine (PE) conjugation and membrane insertion (**section 1.2.3.2**); and lipid delivery to the developing phagophore (**section 1.2.3.3**). Following autophagosome maturation (**section 1.2.4**, not depicted), the fully formed autophagosome is transported to the vacuole where hemifusion with the tonoplast is mediated by SNARE proteins (green), Rab-like GTPases (yellow), HOPS complex members, and guanine nucleotide exchange factors (orange) (**section 1.2.5**). Figure inspired by Li and Vierstra, 2012.

The ATG8-PE adduct coats the expanding phagophore membrane, providing a docking platform for a suite of ATG8-interacting proteins that are essential for autophagosome maturation, closure, and vacuolar fusion, as well as cargo recruitment (**Section 1.4.1**) (Johansen and Lamark, 2011; Noda et al., 2010). Moreover, ATG8 serves as a major structural component of autophagosome membrane (Klionsky and Schulman, 2014). ATG8 also interacts with several ATG proteins that are essential for autophagy signaling—such as ATG1 (Nakatogawa et al., 2012; Noda et al., 2010), ATG6, and ATG7 (Stanley et al., 2014; Kaufmann et al., 2014; Kaufmann and Wollert, 2014)—which could be essential for regulating the localization and concentration of autophagy components, ensuring optimal autophagic flux (Khaminets et al., 2016).

1.2.3.3 Membrane source

The origin of the phagophore membrane in plants remains elusive—essentially every organelle of the endomembrane system has been implicated (Reggiori and Klionsky, 2013). Recent evidence suggests that the endoplasmic reticulum (ER) might serve as a membrane source and signaling platform for autophagosome biogenesis (Zhuang et al., 2013; Le Bars et al., 2014; Zhuang et al., 2017; Liu et al., 2012). Microscopy studies have revealed that phagophore assembly sites localize in close proximity to ER exit sites (ERES), as well as ATG9 vesicles (Graef et al., 2013). ATG9 is a multispinning membrane protein that localizes to cytoplasmic mobile vesicles—which, in yeast, are derived from the Golgi apparatus—that provide an important membrane source during the early steps of autophagosome formation (**Fig 1.1**) (Yamamoto et al., 2012). Further studies have shown that ERES-derived coat protein complex II (COPII) vesicles are

recruited to the phagophore assembly site, tethering with ATG9 vesicles to deliver a membrane source to the growing phagophore (Tan et al., 2013). Moreover, some ERES-defective mutants show deficiencies in autophagy, providing an additional indication that ERES contribute to phagophore formation (Graef et al., 2013).

1.2.4 Autophagosome maturation

Membrane-bound ATG8-PE interacts with a number of proteins involved in autophagosome maturation and closure, including members of the lipid-binding BIN/AMPHIPHYSIN RVS (BAR)/SRC HOMOMOLOGY 3 (SH3) family (Zhuang et al., 2013). These BAR-SH3 family proteins likely work cooperatively with ATG8 to stimulate curvature of the developing phagophore, ensuring proper autophagosome architecture (Zhuang et al., 2013). This leads to the formation of a mature autophagosome, a double-membrane vesicle decorated with ATG8 on both surfaces (Zaffagnini and Martens, 2016; Wurzer et al., 2015). Majority of the ATG8-PE adducts lining the outer membrane are eventually delipidated by ATG4 and released, whereas ATG8-PE lining the inner membrane is consumed in the vacuole (Kirisako et al., 2000).

1.2.5 Autophagosome trafficking and vacuolar fusion

Mature autophagosomes are carried on cytoskeletal tracks to the vacuole for recycling, or delivered elsewhere in the cell (Rubinsztein et al., 2012; Moreau et al., 2011; Jahreiss et al., 2008; Nakatogawa et al., 2007). A number of plant endosomal trafficking proteins have been found to be involved in these processes, suggesting crosstalk between autophagy and other intracellular trafficking pathways (Kalinowska and Isono, 2018). These proteins include: the endosomal sorting complex required for transport (ESCRT); subunits of the homotypic fusion and protein sorting (HOPS)-tethering complex; subunits of the exocyst complex; soluble N-ethylmaleimide-sensitive factor attachment protein receptors (SNAREs); and RAB GTPases (Kalinowska and Isono, 2018) (**Fig 1.1**). Although the phenotypes of trafficking mutants in plants are highly pleiotropic, defects in many of these proteins have been shown to cause impairment of autophagosome formation, transport, fusion, and degradation (Kalinowska and Isono, 2018).

Accumulating evidence has implicated the endosomal complex required for transport (ESCRT) in the regulation of autophagy both in metazoans (Filimonenko et al., 2007; Lee

et al., 2007; Rusten et al., 2007) and plants (Katsiarimpa et al., 2013; Gao et al., 2015; Kolb et al., 2015; Spitzer et al., 2015). The plant-specific ESCRT component FYVE DOMAIN PROTEIN REQUIRED FOR ENDOSOMAL SORTING 1 (FREE1) has recently been shown to be required for vacuolar protein transport and control of autophagic degradation by facilitating fusion of autophagosomes with the vacuole (Gao et al., 2015; Kolb et al., 2015). FREE1 has also been shown to directly interact with SH3 DOMAIN-CONTAINING PROTEIN 2 (SH3P2), a BAR-SH3 family protein which functions in autophagosome maturation (Gao et al., 2015; Zhuang et al., 2013). FREE1 depletion leads to a defect in autophagosome–vacuole fusion, thus leading to the accumulation of autophagosomes (Gao et al., 2015). In addition, *free1* mutants displayed defects in central vacuole formation, instead exhibiting many small vacuoles (Gao et al., 2015; Kolb et al., 2015).

In yeast and metazoans, the Ras-related GTPase RAB7 localizes to autophagosomal membranes, and has been shown to be involved in the regulation of autophagosome–lysosome fusion (**Fig 1.1**) (Gutierrez et al., 2004; Balderhaar et al., 2010; Hegedus et al., 2016). Moreover, in human cells it was shown that an autophagy adaptor, a FYVE and coiled-coil (CC) domain-containing protein FYCO1, binds ATG8, Rab7, and phosphatidylinositol-3-phosphate, to promote microtubule plus end-directed transport of autophagic vesicles (**Fig 1.1**) (Pankiv et al., 2010). In *A. thaliana*, one of the RAB7 GTPase homologs, RABG3B, was shown to localize to autophagosomes, as well as control xylem formation through positive regulation of autophagy (Kalinowska and Isono, 2018). RABG3B also positively regulates immunity-associated hypersensitive cell death, although the dependency of this function on autophagy is unclear (Kwon et al., 2013). Whether plant RAB7 homologs, or indeed other plant RAB GTPases, can regulate autophagosome–vacuole fusion remains to be determined.

Another ATG8-interacting protein, EXO70B1, an exocyst component, is essential for autophagosome formation and transport to the vacuole in Arabidopsis (Kulich et al., 2013). EXO70B1—one of 23 paralogs of *A. thaliana* EXO70 exocyst subunits—interacts with SEC5 and EXO84 and forms an exocyst subcomplex involved in autophagy-related, Golgi-independent membrane traffic to the vacuole (Kulich et al., 2013). A follow-up study bioinformatically predicted that EXO70B1, and 20 additional *A. thaliana* EXO70 paralogs, have putative ATG8-interacting motifs, suggesting that these components may

directly interact with ATG8 (Tzfadia and Galili, 2013). Interestingly, EXO70B1 is also involved in plant defense against pathogens, as the *A. thaliana* *exo70B1* mutant was reported to be less resistant to *Pseudomonas syringae* pv. tomato DC3000 than the wild type plants (Stegmann et al., 2013).

1.2.6 Regulation of the plant autophagy pathway

Autophagy signaling is intricately linked with many processes, such as cellular energy metabolism, vesicle trafficking, secretion, organelle dynamics, protein synthesis, and the cell cycle (Zaffagnini and Martens, 2016; Kraft et al., 2010; Liu and Debnath, 2016; Martens and Bachmair, 2015). The best-studied regulators of plant autophagy are the upstream nutrient and energy sensors TARGET OF RAPAMYCIN (TOR), a kinase, and the AMP-ACTIVATED PROTEIN KINASE (AMPK, known as SnRK1 in plants) (Pu et al., 2017; Soto-Burgos and Bassham, 2017). Transcriptional, cell biological, and proteomic data show that TOR and SnRK1 upregulate autophagy upon nutrient deprivation (**Fig 1.1**) (Contento et al., 2004; Yimo Liu and Bassham, 2010; Pu et al., 2017; Soto-Burgos and Bassham, 2017; Suttangkakul et al., 2011). TOR seems to be a particularly important regulator, as its overexpression is enough to block autophagy induced by a number of stress conditions, including starvation, salt, and drought (Pu et al., 2017). TOR activity can be inhibited by SnRK1, and a catalytic subunit of SnRK1, KIN10, was shown to act upstream of TOR (Inoue et al., 2006). SnRK1 activity has been shown to be modulated by cellular sugar phosphates, providing a multilayered mechanism to sense and respond to different abiotic stress conditions (Nukarinen et al., 2016; Lastdrager et al., 2014). The mechanistic details of these regulatory mechanisms remain to be described, as do the mechanisms underpinning the links between autophagy and other plant processes.

1.3 Roles of autophagy in plants

In plants, autophagy plays a central role in development, metabolism, and responses to abiotic and biotic stresses (Yang and Bassham, 2015; Michaeli et al., 2016). Whether through remobilizing nutrients, breaking down energy storage molecules, turning over target proteins, or regulating cell death, autophagy plays a critical role in many aspects of

plant life. Considering the centrality of this pathway, it is surprising that autophagy is not essential in certain plant species—for example, *A. thaliana* and maize mutants in core autophagy components complete their life cycle and produce viable seeds (Marshall and Vierstra, 2018). However, even in these cases, autophagy-defective plants exhibit striking phenotypes when they are grown under nutrient-deficient conditions—including slow growth, enhanced senescence, lower fecundity, and reduced survival—pointing to the context-dependent roles of autophagy (Doelling et al., 2002; Hanaoka et al., 2002; Li et al., 2015; Thompson et al., 2005; Xiong et al., 2005).

1.3.1 Development

Autophagy is important for both plant senescence and seed germination, two processes that require the large-scale remobilization of nutrients (Liu and Bassham, 2012). During leaf senescence, autophagy has dual functions—one is to maintain tissue longevity through nutrient recycling, while the other is to participate in the systematic breakdown of tissue components to remobilize nutrients to areas of growth and storage (Masclaux-Daubresse et al., 2017). In particular, autophagy has been implicated in chloroplast degradation during senescence (**section 1.4.1.3**), providing a rich source of remobilized nitrogen to developing vegetative tissues and seeds (Have et al., 2017). Moreover, evidence in maize supports a role for autophagy in mobilizing nutrients from the endosperm during seed germination, with increased levels of lipidated ATG8 observed during this developmental transition, indicating increased autophagic activity (Chung et al., 2009). Interestingly, there is other evidence that increasing nutrient mobilization via autophagy could increase fecundity, as overexpression of *ATG5* or *ATG7* in *A. thaliana*, or of different *ATG8* genes in both *A. thaliana* and rice, increased seed yields (Chung et al., 2009; Avin-Wittenberg et al., 2015).

1.3.2 Metabolism

Although the phenotypic effects of autophagy mutants appear limited under nutrient-rich growth conditions, several metabolomics studies have revealed that autophagy defects have a pervasive effect on plant metabolism. Metabolomic analyses of wild-type and autophagy-defective *A. thaliana* rosettes revealed that autophagy plays a role in amino acid catabolism, as these molecules hyperaccumulate in the absence of autophagy

(Masclaux-Daubresse et al., 2014). Moreover, it was shown that autophagy is involved in sugar redox management, with mutants accumulating fewer hexoses, but more of their corresponding sugar alcohols (Guiboileau et al., 2013; Masclaux-Daubresse et al., 2014). Autophagy is also required for normal lipid metabolism in maize, potentially implying that it has a role in membrane turnover (Marshall and Vierstra, 2018). Additionally, there is emerging evidence to show that autophagy is involved in modulating starch levels to maintain the pools of organic substrates needed for mitochondrial respiration (Wang et al., 2013). Furthermore, a direct connection between metabolism and autophagy was discovered in tobacco, involving the glyceraldehyde-3-phosphate dehydrogenase (GAPDH) enzyme (Wang et al., 2013). GAPDH catalyzes the conversion of glyceraldehyde-3-phosphate to 1,3-bisphosphoglycerate, linking the energy-consuming steps of glycolysis with its energy-producing steps; in tobacco, the cytosolic GAPDHs have been demonstrated to interact with ATG3 to regulate autophagy (Wang et al., 2013).

1.3.3 Abiotic stress

Autophagy can be induced by various abiotic stresses—including starvation, heat, oxidative, salt, and drought—and autophagy-defective mutants are hypersensitive to these stress conditions (Xiong et al., 2005; 2007; Liu et al., 2009; Zhou et al., 2013; Zhou, Zhang, et al., 2014; Shin et al., 2009). Autophagy also plays a crucial role in response to nutrient starvation; ATG genes are upregulated upon carbon or nitrogen starvation, and autophagy-deficient mutants show reduced fitness under these conditions (Thompson and Vierstra, 2005; Doelling et al., 2002; Hanaoka et al., 2002; Yoshimoto et al., 2004; Phillips et al., 2008; Xiong et al., 2005; Rose et al., 2006; Breeze et al., 2011; Xia et al., 2011). Additionally, autophagy is important for heat stress, targeting misfolded or denatured proteins for degradation through the activity of specific autophagy cargo receptors (**section 1.4.1.2**) (Zhou et al., 2013). Heat stress can also trigger ER degradation to balance cellular homeostasis (Deng et al., 2011), and autophagy is reported to play a role in ER turnover (Liu et al., 2012; Yang et al., 2016) (**section 1.4.1.6**). In tomato, a heat-shock transcription factor A1a (HsfA1a) was shown to upregulate ATG10 and ATG18 under drought stress to stimulate autophagic flux, indicating the involvement of this pathway in maintaining homeostasis (Wang et al., 2015).

Additional examples of the role of autophagy in abiotic stress involve the targeted degradation of specific proteins via the activity of autophagy receptors—proteins that bridge ATG8 and targeted cellular components (**section 1.4.1**). A recent study characterized the role of an autophagy receptor in balancing plant growth and survival under multiple stress conditions (Nolan et al., 2017). This study showed that the brassinosteroid-regulated and growth-promoting transcription factor BRI1-EMS SUPPRESSOR 1 (BES1) is degraded by autophagy during drought and starvation stress via DSK2, a phosphorylation-regulated selective autophagy receptor (Nolan et al., 2017). There is also evidence that autophagy is involved in turnover of aquaporins via the ATG8-interacting autophagy receptor TRYPTOPHAN-RICH SENSORY PROTEIN/TRANSLOCATOR (TPSO). This receptor is upregulated upon heat and drought stress perception, and can target free heme groups (Vanhee et al., 2011), cytosolic porphyrins, and plasma membrane localized aquaporin PIP2;7 for degradation, to decrease water losses within the cell (Hachez et al., 2014; Jurkiewicz et al., 2018).

1.3.4 Biotic stress

Autophagy is engaged in various aspects of plant immunity—it has been shown to regulate basal resistance, as well as cell death responses related to both immunity and disease (Zhou, Yu, et al., 2014). One of the most well-studied plant defence mechanisms is the hypersensitive response (HR), a form of programmed cell death that has a role in restricting pathogen invasion (Coll et al., 2011). Depending on the pathosystem and pathogenic lifestyle, autophagy appears to be necessary for extending HR cell death or restricting the HR to cells in the immediate area surrounding an infection (Seay et al., 2006). This implies that autophagy can play opposing, complementary roles in plant innate immunity (Hayward and Dinesh-Kumar, 2011; Teh and Hofius, 2014; Zhou et al., 2014).

Autophagy has been shown to be upregulated in response to pathogen challenge. For example, the majority of plant ATG genes are expressed preferentially upon challenge with the aphid *Myzus persicae* or the bacterium *Pseudomonas syringae* (Zimmermann et al., 2004). Moreover, autophagy has a positive function in preventing infection and restricting the spread of cell death from necrotrophic pathogen infection (Kabbage et al., 2013; Lai et al., 2011). Autophagy also regulates programmed cell death during plant-virus interactions, restricting the HR to the viral infection site, a function linked to ATG6

(Kwon et al., 2013). In addition, autophagy mediates the degradation of viral components or particles, acting as an antiviral mechanism (Ismayil et al., 2019). Similarly, autophagy is involved in the plant response to bacterial and oomycete infection, likely participating in a focal immune response in the latter case (**section 1.4.1.5**). However, due to the involvement of plant autophagy in homeostatic, metabolic, and developmental processes, the dissection of autophagic mechanisms underlying host immunity and microbial pathogenesis is still in its infancy (Hofius et al., 2017).

Consistent with an evolving ‘arms race’ between pathogens and their hosts, some pathogens modulate the autophagic machinery of their host to their advantage (Popa et al., 2016; Dagdas et al., 2016; Ustun et al., 2018). Plant viruses have evolved multiple mechanisms to counteract or hijack autophagic processes to promote viral infection (Ismayil et al., 2019). Moreover, the potato late blight pathogen *Phytophthora infestans* secretes a virulence protein, PexRD54, which translocates inside the plant host cell and perturbs autophagy by binding ATG8 (Dagdas et al., 2016) (**section 1.4.1.5**). As secreted plant pathogen virulence proteins, termed ‘effectors’, often converge on proteins or pathways important for successful infection (**section 1.6.2**), the evolution of these pathogen strategies provides additional evidence that the autophagy pathway is an important aspect of the plant immune response.

1.4 Plant selective autophagy—layers of specificity

Autophagy has multiple layers of specificity defining the dynamics of uptake, sub-cellular trafficking, and turnover of substrates (Stolz et al., 2014; Zaffagnini and Martens, 2016). However, the molecular details of how various autophagy cargoes and components are recognized, recruited, and recycled remain to be fully elucidated, especially in plants (Bento et al., 2016; Mizushima, 2018). ATG8 is known to serve as the lynch-pin in selectivity of the autophagy pathway, directly binding autophagy receptors that provide a mechanism to selectively eliminate desired cargo (Stolz et al., 2014; Marshall and Vierstra, 2018). An emerging view is that, in species with multiple ATG8 isoforms, the specialization of ATG8s could form a layer of specificity in the selective autophagy pathway.

1.4.1 Autophagy cargo receptors

1.4.1.1 Introduction to autophagy receptors

The selectivity in the autophagy pathway is primarily conferred by autophagy receptors, which tether cargo to nascent autophagosome via ATG8 binding, such as in the aforementioned examples DSK2 and TPO (section 1.3.3) (Zaffagnini and Martens, 2016). Autophagy receptors often recognize autophagic labels, such as polyubiquitin chains or cytosolic lectins, and subsequently recruit tagged components into autophagosomes (Randow and Youle, 2014; Boyle and Randow, 2013). The interaction of autophagy receptors with ATG8 leads to the formation of supramolecular structures, facilitating the engulfment of high molecular weight cargo into autophagosomes (Wurzer et al., 2015; Bertipaglia et al., 2016). The activity of autophagy receptors is tightly regulated by inducible expression, spatial organization and cellular localization, and multiple post-translational modifications (Stolz et al., 2014).

In mammalian cells, more than two dozen autophagy receptors have been identified by yeast two-hybrid and proteomic screens (Rogov et al., 2014; Behrends et al., 2010; Stolz et al., 2014). The human autophagy cargo receptor p62/SQSTM1 mediates the degradation of ubiquitinated cargo material, such as aggregated proteins or cytosolic bacteria, homopolymerizing to bind clustered ubiquitin at a high affinity (Wurzer et al., 2015; Zheng et al., 2009; Pankiv et al., 2007). Another human autophagic receptor NEIGHBOR OF BRCA1 (NBR1) interacts with p62 and plays an essential role in p62-dependent sequestration and degradation of aggregated proteins (Kirkin et al., 2009), peroxisomes (Deosaran et al., 2013), and mid body rings (Isakson et al., 2013). In contrast, the autophagy receptor NDP52 acts during the selective autophagy of intracellular bacteria and damaged mitochondria; but, similar to p62, self-association confers binding specificity towards specific ubiquitin tags marking the components for degradation (Heo et al., 2015; Mostowy et al., 2011; Thurston et al., 2009; von Muhlinen et al., 2012; Lazarou et al., 2015).

In plants, increasing evidence has suggested that selective autophagic routes play critical roles in clearance of ubiquitylated protein aggregates (aggrephagy), damaged or excess chloroplasts (chlorophagy), proteasomes (proteaphagy), and invading pathogens (xenophagy). Additional findings support a role for autophagy in turnover of mitochondria (mitophagy), ribosomes (ribophagy), endoplasmic reticulum components

(ER-phagy), and peroxisomes (pexophagy) (Marshall and Vierstra, 2018). Although autophagy has been implicated in the clearance or trafficking of these many cellular components, only in a few cases have the selective autophagy receptors been identified.

1.4.1.2 Aggrephagy

An *A. thaliana* homolog of the human autophagy receptor NBR1 was the first non-metazoan aggrephagy cargo receptor to be described in detail. *A. thaliana* NBR1 (AtNBR1) mutants are highly sensitive to various stress conditions and accumulate polyubiquitinated protein aggregates (Zhou, Zhang, et al., 2014). AtNBR1 was shown to be able to homopolymerize, suggesting that it is a functional hybrid of the human NBR1 and p62 (Svenning et al., 2011). Indeed, AtNBR1 and its tobacco homolog (JOKA2) bind to both ATG8 and ubiquitin, and are delivered to the vacuole (Svenning et al., 2011; Zientara-Rytter et al., 2011). Evidently, there is also a tight relationship between AtNBR1 and catalase proteins, as several catalase isoforms accumulate in an *nbr1* mutant following heat stress (Zhou, Zhang, et al., 2014). This suggests that AtNBR1 may act in the selective clearance of catalases, either directly or as part of pexophagy (**section 1.4.1.6**), a function that was already demonstrated for this protein in animals (Deosaran et al., 2013).

1.4.1.3 Chlorophagy

Autophagy has been shown to play an active role in regulating the degradation of chloroplast proteins, as well as whole photodamaged chloroplasts (Ishida et al., 2008; Michaeli et al., 2014; Izumi et al., 2017). During senescence and starvation, piecemeal chlorophagy mediates nutrient remobilization by recycling starch- and Rubisco-containing protein-rich vesicles that bud off from chloroplasts (Izumi et al., 2010). The *A. thaliana* ATG8-interacting protein 1 (ATI1) has been suggested to play a role in the piecemeal pathway, targeting plastid bodies to the vacuole (Michaeli et al., 2014). In contrast, the accumulation of reactive oxygen species triggered by high light stress seems to induce degradation of entire chloroplasts (Izumi et al., 2017). Chlorophagy is more common in senescing leaves, and is also stimulated by prolonged darkness (Li and Vierstra, 2012).

Interestingly, a recent study suggests that the ESCRT machinery is also involved in chlorophagy. The *A. thaliana* ESCRT-III accessory protein CHARGED MULTIVESICULAR BODY PROTEIN 1 (CHMP1), which plays crucial roles in the

biogenesis of multivesicular bodies and vacuolar sorting of membrane proteins, has been implicated in the autophagic clearance of chloroplast proteins (Spitzer et al., 2009; Spitzer et al., 2015). Depletion of CHMP1 specifically affects phagophore closure and loading of chloroplast proteins, causing the accumulation of plastid proteins in cytoplasmic bodies that resemble Rubisco-containing bodies (Spitzer et al., 2015).

1.4.1.4 Proteaphagy

A novel type of selective autophagy, proteaphagy, was discovered in *A. thaliana*, in which inactive 26S proteasome complexes are degraded via the direct interaction between the 26S proteasome regulatory subunit RPN10 and ATG8 (Marshall et al., 2015). This degradation is induced separately by nutrient starvation and proteasome inhibition, implying that both bulk and selective routes exist (Marshall et al., 2015). Inhibited proteasomes become extensively ubiquitylated, and subsequent proteaphagy is mediated by RPN10, which contains three ubiquitin-interacting motifs (UIMs), with UIM1 necessary for binding ubiquitylated proteasome subunits and UIM2 for binding lipidated ATG8 (Marshall et al., 2019; 2015). Proteaphagy likely plays a key role in modulating proteasome abundance by removing inactive or excess particles (Marshall et al., 2015). Although the RPN10 UIM2 motif essential ATG8 binding is conserved in plants, this motif is missing from the yeast RPN10 homolog, suggesting that—if proteaphagy is a conserved selective autophagy pathway—a different receptor is likely involved (Marshall et al., 2015).

1.4.1.5 Xenophagy

As described previously (**section 1.3.4**), autophagy plays multiple roles in plant defence against pathogens. NBR1/JOKA2—the aforementioned aggrephagy receptor—has also been characterized as a xenophagy receptor. NBR1/JOKA2 is involved in the plant response to bacterial, oomycete, and viral infection, with characterized functions in focal immunity and selective removal of pathogen components. NBR1/JOKA2-mediated autophagy counteracts *Pseudomonas syringae* pv. tomato DC3000 (Pst) infection, as well as limits formation of disease-associated water-soaked lesions (Ustun et al., 2018). In addition, NBR1/JOKA2 is reported to function in mediating immunity against the potato late blight pathogen *Phytophthora infestans* (Dagdas et al., 2018). In this case, NBR1/JOKA2-ATG8 labelled autophagosomes are diverted to the haustorium interface

to restrict *P. infestans* growth, implicating NBR1/JOKA2 in focal immunity (Dagdás et al., 2018). Consistent with the diversion of autophagosomes to the haustorium, degradation of NBR1/JOKA2 is reduced during *P. infestans* infection, much like during Pst infection (Dagdás et al., 2018; Ustun et al., 2018), suggesting a potential non-degradative function of autophagy. Moreover, this receptor mediates the degradation of non-assembled and virus particle-forming capsid proteins, restricting the establishment of cauliflower mosaic virus (CaMV) infection (Hafren et al., 2017).

Interestingly, in multiple cases, the role of NBR1/JOKA2 in plant immunity is subverted by the pathogen. As previously mentioned (**section 1.3.4**), during *P. infestans* infection, the effector PexRD54 perturbs the potato host selective autophagy pathway via ATG8 binding, an interaction that occludes NBR1/JOKA2 binding (Dagdás et al., 2016). Here, PexRD54 dampens the NBR1/JOKA2-mediated focal immune response, as well as re-routes autophagosome trafficking to the host-pathogen interface, presumably carrying cargo that benefit pathogen infection (Dagdás et al., 2016; Dagdás et al., 2018). During CaMV infection, NBR1/JOKA2-mediated antiviral xenophagy is also counteracted by the protective functions of autophagy-resistant CaMV inclusion bodies (Hafren et al., 2017). This survival function extends the timespan of virus production, increasing the chances for virus particle acquisition by aphid vectors and thus CaMV transmission (Hafren et al., 2017).

1.4.1.6 Other selective autophagy pathways

In addition to the aforementioned examples of cargo receptor-mediated degradation of specific cellular components or invading pathogens, there are also a number of less well-characterized examples of the involvement of autophagy in the turnover of mitochondria (mitophagy), endoplasmic reticulum components (ER-phagy), ribosomes (ribophagy), and peroxisomes (pexophagy) (Marshall and Vierstra, 2018).

Although plants lack many of the known mitophagy receptors and regulators, it was recently reported that, during senescence, mitochondrial proteins and mitochondrial vesicles were degraded by autophagy in *A. thaliana* (Broda et al., 2018). For ER-phagy, the dicot-specific ATG8-interacting protein ATI3 has been implicated in ER turnover, but no potential autophagy receptors have been identified outside of this group of flowering plants (Zhou et al., 2018). Moreover, so far, none of the plant homologs of metazoan ER-phagy receptors have been found to share the same function. Ribophagy *per se* has yet to

be demonstrated in plants, but there is evidence for autophagy-dependent pathways of rRNA turnover in *A. thaliana* (Wang et al., 2018). Similarly, there is clear genetic evidence for the involvement of autophagy in peroxisome recycling, but there are no characterized receptors (Young et al., 2019). NBR1/JOKA2 is the only characterized pexophagy receptor with a plant homolog, but there is no direct evidence connecting NBR1/JOKA2 to pexophagy in plants (Svenning et al., 2011).

1.4.2 ATG8-interacting motif

The interaction of ATG8 with the core autophagy machinery, autophagy adaptors, and autophagy receptors is mediated by a conserved motif called the ATG8-interacting motif (AIM) (or, in mammals, LC3-interacting region (LIR)) (Birgisdottir et al., 2013). The core AIM sequence is composed of an aromatic amino acid followed by two amino acids and then a branched-chain amino acid, W/F/Y-XX-L/I/V, that is generally surrounded by negatively charged residues (Birgisdottir et al., 2013). The first and last hydrophobic residues of AIM bind to the W-site and L-site on the ATG8 surface, respectively, and the nearby acidic residues strengthen the interaction by forming non-covalent bonds with the residues surrounding the conserved hydrophobic pockets (Klionsky and Schulman, 2014). Moreover, negatively charged residues in proximity to the core AIM were shown to contribute to ATG8 binding (Rogov et al., 2014; Pankiv et al., 2007; Wild et al., 2011), and the AIM sequence or the neighboring residues can be phosphorylated to enhance the interaction with ATG8 (Farré and Subramani, 2016; Matsumoto et al., 2011).

Two online tools are available to computationally predict AIMs in various organisms, including *A. thaliana* (Kalvari et al., 2014; Jacomin et al., 2016; Xie et al., 2016). However, these tools can both miss true AIMs, as well as falsely predict AIMs. A number of characterized AIMs are noncanonical, and thus would not be predicted using the available tools. For example, the AIM in the human autophagy receptor NDP52 lacks an aromatic residue, a deficiency which is balanced by several surrounding residues that form additional electrostatic interactions with the cognate ATG8, LC3C (von Muhlinen et al., 2012). Moreover, considering the short length of the AIM, computational predictions will invariably result in a number of false positives. Structural information can be useful to distinguish functional AIMs from non-functional AIM-like sequences, as an AIM has to

have a flexible conformation to be able to interact with ATG8 (Noda et al., 2010). If structural information is not available, predicting the structurally disordered region from the primary sequence may also be effective in some cases (Noda et al., 2010).

1.4.3 ATG8 diversification

1.4.3.1 *Functional diversification of human ATG8 isoforms*

Unlike yeast, where there is only one copy of ATG8, many eukaryotes have multiple ATG8 isoforms. For example, there are six ATG8s in mammalian cells: three microtubule-associated protein 1 light chain 3 (MAP1LC3) subfamily members (LC3A, B, C), and three gamma-aminobutyric receptor-associated protein (GABARAP) subfamily members (GABARAP, GABARAP-L1, GABARAP-L2/GATE-16) (Zaffagnini and Martens, 2016). Multiple studies have shown that these isoforms exhibit a degree of functional diversity. For example, LC3A, B, and C have been shown to mostly be involved in autophagosome formation, while GABARAP, GABARAL1, and GATE-16 are involved downstream in the maturation step (Weidberg et al., 2010). Moreover, studies performing large-scale screens of the ATG8 interactors, using either immunoprecipitation with tandem mass spectrometry (IP-MS) (Behrends et al., 2010; Wild et al., 2014) or proximity labelling proteomics (Le Guerroue et al., 2017), showed that the isoforms have limited overlap in their interacting protein complements. Human ATG8s have also been shown to undergo different post-translational modifications (Joachim et al., 2017; Huang et al., 2015) and exhibit unique sub-cellular localizations (Winer et al., 2018; Joachim et al., 2015).

There is also specificity in how human ATG8s interact with known cargo receptors. The cytosolic bacteria receptor NDP52 preferentially interacts with LC3C, an interaction underpinned by four amino acids unique to LC3C (von Muhlinen et al., 2012). Similarly, the autophagy-linked FYVE protein, ALFY, binds preferentially to the GABARAPs (Lystad et al., 2014). Three conserved residues in the GABARAPs are responsible for binding to ALFY, and introduction of these residues in LC3B is sufficient to enable its interaction with ALFY (Lystad et al., 2014). In addition, both the autophagy adaptor PLEKHM1 and the tumor necrosis factor FN14 preferentially bind to the GABARAPs (McEwan et al., 2015; Winer et al., 2018); recently, a GABARAP interaction motif (GIM)

was identified that mediates the high affinity binding of GABARAP-interacting proteins (Rogov et al., 2017).

1.4.3.2 Plant ATG8 expansion—a driver of functional diversification?

ATG8 has dramatically expanded and diversified in plants, from a single protein in algae to multiple isoforms in flowering plants (Kellner et al., 2017). Extensive phylogenetic analyses revealed that each plant family has its own set of ATG8 isoforms that have been maintained over millions of years of evolution (Kellner et al., 2017). It is hypothesized that the ATG8 expansion was driven by functional diversification, which may have been shaped by coevolution with pathogen effectors (Kellner et al., 2017). It is thought that the plant family-specific expansion and diversification of ATG8s may have facilitated in the subcellular compartmentalization of different selective autophagy pathways, as well as increased the robustness of the plant autophagy network (Kellner et al., 2017; Stephani and Dagdas, 2019).

1.4.4 Regulation of plant selective autophagy components

As in metazoans, plant selective autophagy is tightly regulated at the transcriptional, post-transcriptional, and post-translational levels (Stephani and Dagdas, 2019). Some plant ATG family members have subfunctionalized with respect to expression patterns, including the *A. thaliana* ATG8s (ATG8a-i) (Thompson et al., 2005; Contento et al., 2004; Slavikova et al., 2005) and ATG12s (ATG12a and ATG12b) (Chung et al., 2010). Because *A. thaliana* ATG8 family members are differentially expressed in different organs, tissues, and cell types under different stress conditions (Hayward et al., 2009; Slavikova et al., 2005), it has been hypothesized that individual ATG8 members may function in specific developmental or stress responses (Woo et al., 2014).

Moreover, post-translational regulation of autophagy is indispensable for plants to adapt to various environmental stresses. There is evidence that regulation of autophagy by TOR is dependent on its ability to phosphorylate ATG13, thereby repressing autophagy under nutrient-rich conditions (Van Leene et al., 2019). In addition, the stability and function of several core ATG components is highly influenced by ubiquitination (Xie et al., 2015). In particular, ubiquitination of ATG6 serves to regulate the autophagy pathway, under nutrient-rich conditions, two RING finger E3 ligases are

recruited to ATG6 to ubiquitylate and degrade this protein; upon starvation, this recruitment is disrupted, and the subsequent stabilization of ATG6 leads to autophagy activation (Qi et al., 2017).

1.5 Tools to study plant selective autophagy

Our understanding of plant selective autophagy has developed significantly through the use of traditional genetic, biochemical, and cellular approaches. To continue to dissect the complex mechanisms that underpin plant autophagy function and regulation, we will need to also employ additional creative tools. Recently, researchers established a robust pipeline for the identification of chemical compounds that specifically modulate plant autophagy, which will hopefully lead to the development of chemical tools to study plant autophagy from many vantages (Dauphinee et al., 2019). In addition, the early diverging land plant *Marchantia polymorpha* has emerged as a powerful model organism to carry out further genetic analysis of plant autophagy, due to its reduced genetic redundancy (Norizuki et al., 2019). For example, this species has only two copies of ATG8, and one copy of most other core ATG genes, providing a simpler genetic system to identify the plant-specific requirements for the autophagy pathway (Norizuki et al., 2019).

As the study of plant selective autophagy advances, it will also be necessary to study selective autophagy in specific stimulus conditions, cell types, and in different subcellular locations. Studying selective autophagy at these finer resolutions will help us understand the multiple layers of specificity that define the plasticity and selectivity of the pathway. At present, however, we are limited in these studies due to a lack of available tools (Stephani and Dagdas, 2019). So far, a number of promoter systems have been developed to perform tissue specific genetic analysis, which could be applied to study cell type-specific selective autophagy pathways (Schurholz et al., 2018; Shulse et al., 2019; Ryu et al., 2019).

To gain a more integrated understanding of the autophagy, it will also be important to examine this pathway using global techniques. ‘Omics’ approaches—including transcriptomics, metabolomics, and proteomics—have begun to be successfully employed to dissect the molecular mechanisms of plant autophagy (Liu, Marshall, & Li, 2018). Transcriptomic studies have elucidated the expression profiles of ATG genes, and

uncovered novel transcriptional regulatory mechanisms of autophagy (Liu, Marshall, & Li, 2018). In addition, proteomic and metabolomic profiling have been used to assess how autophagy affects plant growth and development via modulating the relative abundance of specific proteins and metabolites (Liu et al., 2018). For human ATG8s, proteomics approaches have been used to show that isoforms exhibit unique complements of interacting proteins (**section 1.4.3.1**). One of the aims of this work was to use a proteomics approach to define the ATG8-interacting proteins for potato ATG8 isoforms, both to provide a global understanding of plant autophagy-associated proteins and determine the degree to which plant ATG8 isoforms are functionally specialized (**Chapter 3**). An additional aim was to use the ATG8-targeting *P. infestans* effector PexRD54 as a molecular probe to understand the structural determinants of ATG8 substrate specificity (**Chapter 4**).

1.6 Plant pathogen effectors

Plant pathogen effectors are any secreted proteins or small molecules that alter host-cell structure and function (Hogenhout et al., 2009). In this, effectors are a salient examples of Richard Dawkin’s concept of the ‘extended phenotype,’ which postulates that there are certain classes of genes whose effects reach beyond the cells in which they reside (Hughes and Libersat, 2019). Indeed, effectors are fine-tuned to function in the context of the plant, exhibiting an astonishing array of activities in modulating plant physiology, often to the direct benefit of pathogen infection.

1.6.1 Classes of effectors

There are two broad classes of effectors, apoplastic and cytoplasmic effectors, distinguished by the host cellular space in which they function. Members of the former class of effectors accumulate in the plant intercellular space, the apoplast (Haas et al., 2009; van den Burg et al., 2006; Bolton et al., 2008). In contrast, cytoplasmic effectors are translocated inside the host cell, often trafficking to different subcellular compartments to carry out their functions (Win et al., 2012). Bacterial plant pathogens use a variety of secretion systems to deliver effectors, including the well-characterized type II secretion system, which delivers effectors to the apoplast (Cianciotto, 2005), and the type III

secretion system, which delivers effectors into the cytoplasm of plant cells (Alfano and Collmer, 2004; Pfeilmeier et al., 2016). In contrast, the mechanisms that underpin the delivery of effectors from filamentous plant pathogens—fungi and oomycetes—remain poorly understood.

1.6.2 Effector functions

Within the past decade, a number of studies have characterized the functions of plant pathogen effectors and, collectively, this body of research has pointed to the incredible diversity in effector activities. A number of effectors exhibit enzymatic activity, with examples of secreted proteases, hydrolases, phosphatases, kinases, transferases, and ubiquitin ligases in the literature (Janjusevic et al., 2006; Shao et al., 2003; Fu et al., 2007; Lee et al., 2012; Rodriguez-Herva et al., 2012; van Damme et al., 2012). Other effectors act by binding host proteins and modulating their activity, either through inhibition, aberrant stabilization, or dysregulation. Many such effectors inhibit plant enzymes such as kinases, proteases, glucanases, and peroxidases (Tian et al., 2004; 2007; Rooney et al., 2005; Damasceno et al., 2008; Xiang et al., 2008; Song et al., 2009; Hemetsberger et al., 2012). Some effectors can disrupt entire host pathways, such as vesicle trafficking, autophagy or hormone synthesis (Bozkurt et al., 2011; Sugio et al., 2011; Tanaka et al., 2009). Additional effectors bind nucleic acids, modulating host gene expression or sequestering target transcripts (Lakatos et al., 2004; Domingues et al., 2010; de Souza et al., 2012). Further studies have characterized effectors that are nucleic acids, involved in regulating the abundance of target transcripts (Weiberg et al., 2013; Wang et al., 2017).

Although effector functions are incredibly diverse, the effector complement of any given pathogen often exhibits some level of redundancy, particularly in targeting plant processes essential for infection success. An example of this evolutionary “bet-hedging” strategy comes from *Pseudomonas syringae* infection of *A. thaliana*, where three different *P. syringae* effectors target the negative regulator of defence RIN4 (Grant et al., 2006). Examples of effectors that converge on related host proteins also include the rice blast pathogen *Magnaporthe oryzae* effectors AVR-Pik, AVR-Pia, and AVR1-CO39. Each of these effectors bind rice proteins with heavy metal-associated (HMA) domains (Ortiz et al., 2017; Kanzaki et al., 2012; Maqbool et al., 2015). Although the precise identity of the

host targets of these effectors is not yet clear, AVR-Pik, AVR-Pia and AVR1-CO39 are thought to bind HMA-containing proteins to promote infection.

Effectors from different pathogens also converge on the same host proteins and pathways, which are sometimes termed ‘hubs.’ These hubs are often essential targets for successful pathogen infection, and many are involved in the first layer of plant immunity (Macho and Zipfel, 2014; Chisholm et al., 2006; Jones and Dangl, 2006; Dodds and Rathjen, 2010). The first layer of defence is triggered by pathogen-associated molecular patterns, or PAMPs, and leads to the activation of cell surface receptors and downstream signaling to ward off infection (Couto and Zipfel, 2016). Many pathogens deploy effectors to both dampen PAMP-triggered immunity and to disrupt downstream signaling. For example, bacterial plant pathogen effectors target a number of components of the immune pathway triggered by the bacteria-associated molecular patterns flagellin and EF-Tu (Block and Alfano, 2011), and fungal pathogens deploy a suite of effectors to suppress immune responses elicited by the fungal cell wall component chitin (de Jonge et al., 2011). Similarly, many plant viruses have multiple effectors that target different aspects of the RNA silencing pathway, thereby dampening the systemic response to viral infection (Burgyan and Havelda, 2011).

Regardless of precise function, all effectors can be considered ‘operational’ plant proteins—meaning that, although they are encoded by pathogen genes, effectors are fine-tuned to function in the context of the plant. As such, the evolution of effectors is profoundly shaped by the host environment.

1.6.3 Detection of effectors by intracellular immune receptors

Some pathogen effectors ‘trip the wire’ of the second layer of the plant immune system. These effectors—sometimes termed ‘avirulence effectors’ to denote the phenotype that they cause in certain host environments—are recognized by intracellular host receptors, leading to a robust immune response that effectively halts pathogen ingress. Most of these host receptors belong to a superfamily of intracellular nucleotide-binding leucine-rich repeat (NLR) receptors, with specific NLRs able to recognize specific pathogen effectors (Dodds and Rathjen, 2010). NLRs recognize effectors either via direct interaction, as receptor and ligand, or indirectly, with the NLR detecting the modifications of an effector host target (or, even a decoy of the effector target) (Dodds and Rathjen,

2010). In activating an immune response after recognition, some NLRs function as singletons, some function in pairs, and some even function in complex networks (Wu et al., 2017; Dodds and Rathjen, 2010). Regardless of the precise mechanism, effector detection is a liability for the pathogen, driving the covert mutation or loss of effector genes to enable the pathogen to evade host immunity.

1.6.4 Effectors as molecular probes

Studying effectors has helped uncover novel components of cellular processes—such as plant immune signaling, intracellular trafficking, and transcription—as well as characterize the molecular functions of these components (Lee et al., 2013; Bozkurt et al., 2011; Feng and Zhou, 2012; Mitchum et al., 2013). Additional studies have used effectors as synthetic biology tools to rewire host immune signaling pathways (Wei et al., 2012) and study aspects of primary metabolism (Biemelt and Sonnewald, 2006).

Perhaps the most striking example of using effectors as molecular probes comes from the transcription activator-like effectors (TALEs) of the β - and γ -Proteobacteria, with the majority occurring in plant-pathogenic *Xanthomonas* species (Schornack et al., 2013). TALEs have modular DNA-binding domains that, in the context of *Xanthomonas* infection, bind specific host promoters to regulate target gene expression (Schornack et al., 2013). The unique utility of TALEs stems from this binding specificity being encoded within repetitive 33-35-aa elements in the DNA-binding domain, and thus subsequent studies have leveraged this modularity to engineer TALEs to manipulate plant genomes and control transcription (Schornack et al., 2013; Sanjana et al., 2012). Further studies capitalizing on the utility of effectors as molecular probes stand to unveil additional aspects of plant physiology, as well as positively impact efforts to engineer plants for agriculture.

1.7 Evolution of plant pathogen effectors

Evolutionary biologist J. B. S. Haldane wrote that, “that the struggle against disease, and particularly infectious disease, has been a very important evolutionary agent” (Lederberg, 1999). However, the same can be said from the opposing perspective: the struggle to *maintain* disease has been, and continues to be, a very powerful evolutionary

agent. Evidence of this struggle can be seen in effector genes, which are under pressure to both retain their function in aiding infection and to skirt detection by the plant. These dual selection pressures on effectors manifest in a number of ways, including the localization of effector genes in repeat-rich genomic regions, the lineage-specific loss of effector genes, the extreme pattern of mutations in effector genes, and the structurally defined classes of effectors.

1.7.1 Genomic localization

Effectors are often located in unstable genomic regions to facilitate rapid evolution. In many filamentous plant pathogens—including the oomycete *Phytophthora* spp., *Leptosphaeria maculans*, and *Verticillium dahliae*—effectors tend to be associated with gene-sparse compartments enriched in repetitive sequences and transposable elements (TEs) (Dong et al., 2015; Faino et al., 2016). Sequence repeats and TEs create hot-spots for duplication, deletion, and recombination, leading to increased structural variation in these genome positions (Dong et al., 2015; Kaessmann, 2010; Feschotte, 2008; Hua-Van et al., 2011). In a model termed the ‘two-speed genome,’ Dong et al. hypothesized that these unstable repeat-rich regions serve as cradles for adaptive evolution, particularly for effector genes, which exhibit higher levels of both presence/ absence polymorphisms and positive selection when located in these compartments (Dong et al., 2015).

Although other filamentous plant pathogens—such as *Magnaporthe oryzae* and *Blumeria graminis*—don’t have the typical signatures of a two-speed genome, their effector genes are commonly linked to TEs or flanked by repetitive sequences (Yoshida et al., 2016; de Jonge et al., 2013; Wicker et al., 2013; Thon et al., 2006; Robberecht et al., 2013). Effectors in these unstable locations show increased incidences of presence/ absence polymorphisms and nucleotide polymorphisms, leading some to hypothesize that the plasticity conferred by repetitive elements is adaptive (Yoshida et al., 2016; Baer et al., 2007; Xue et al., 2012) . Similarly, in some fungal plant pathogens, effectors are often located near telomeres, which are known to serve as recombination hot spots during sexual reproduction and tend to evolve at higher rates than the rest of the genome (Cuomo et al., 2007; Orbach et al., 2000; Chuma et al., 2011; Croll and McDonald, 2012).

In other pathogenic fungi, effectors are overrepresented on conditionally dispensable chromosomes (CDCs), which differ structurally from the rest of the genome and persist

in a pathogen population only if they confer an adaptive advantage (Ma et al., 2010; Akagi et al., 2009; Wittenberg et al., 2009; Han et al., 2001). CDCs are also thought to be hotspots for accelerated evolution; for example, CDCs from the fungal pathogen *Mycosphaerella graminicola* exhibit increased non-synonymous substitution rates compared to the rest of the genome (Stukenbrock et al., 2010). This is strikingly similar to some bacterial pathogens which carry many of their effector genes on plasmids that exhibit high frequencies of gain and loss in pathogen populations (Hacker and Kaper, 2000). Across phytopathogenic microorganisms, the localization of effector genes to unstable genomic regions often impacts both nucleotide substitution rates and the frequency of presence/absence polymorphisms, enhancing their evolutionary potential.

1.7.2 Extreme patterns of mutations

Many effectors show signatures of positive selection, with nonsynonymous nucleotide substitutions exceeding synonymous substitutions ($dN/dS > 1$) (Allen et al., 2004; Dodds et al., 2006; Huang et al., 2014; Raffaele et al., 2010; Yoshida et al., 2009; Liu et al., 2005). Such patterns of sequence polymorphisms are a hallmark of positive selection, and are thought to reflect the coevolutionary arms race of these effectors with host components. In effector genes, positively selected sites are frequently concentrated in the C-termini of effectors that encode the biochemical activity, or surface exposed residues involved in protein-protein interactions (Boutemy et al., 2011; Win et al., 2007; Yaeno et al., 2011; Chou et al., 2011).

The coevolution of hosts and pathogens is driven by antagonistic molecular interactions in which both pathogen and plant components are under selection to adapt. Some of the most extreme examples of positive selection in effector genes can be traced to the pressure to evade host detection. One of the best-characterized examples can be seen between the rice blast fungus *Magnaporthe oryzae* and its host, *Oryza sativa*. Allelic variants of the *M. oryzae* effector AVR-Pik exhibit four amino acid replacements, but no synonymous changes (Huang et al., 2014; Yoshida et al., 2009; Kanzaki et al., 2012). These polymorphisms are located in regions involved in recognition by the cognate NLR, Pik-1, which also occurs in an allelic series (Kanzaki et al., 2012). Reconstructing the evolutionary history of AVR-Pik and Pik-1 indicates that the positive selection observed in the effector gene is imposed by the NLR (Kanzaki et al., 2012).

Another remarkable case of positive selection in an effector gene comes from the *Phytophthora* clade 1c species (Dong et al., 2014). This clade arose through a series of host jumps to botanically distant plant species, followed by adaptation and specialization on these disparate hosts (Raffaele et al., 2010). The *Phytophthora* clade 1c includes the ‘sister’ species *Phytophthora infestans* and *Phytophthora mirabilis*—which infect *Solanum* species and the ornamental plant *Mirabilis jalapa* (colloquially known as four o’clock flower), respectively—which are estimated to have split about 1,300 years ago (Raffaele et al., 2010). Comparative genomic analyses between *P. infestans* and *P. mirabilis* revealed signatures of positive selection in a large number of effector genes (Raffaele et al., 2010). For one of these effectors, the protease inhibitor EPIC1, the changes involved in the process of host adaptation were mapped to the level of single amino acid residues (Dong et al., 2014). A single polymorphism between the *P. infestans* and *P. mirabilis* EPIC1 orthologs was shown to greatly determine the activity of these effectors towards their respective potato and *M. jalapa* host proteases (Dong et al., 2014).

1.7.3 Presence/ absence polymorphisms

The dynamic gain and loss of effector genes is a common response to host genotype, and is important for the process of host adaptation (Yoshida et al., 2016). As previously mentioned, presence/ absence polymorphisms in effector genes is commonly due to chromosomal rearrangements associated with unstable genomic locations (Yoshida et al., 2016). There are countless examples of effector gene gain and loss that can be tied to the host environment, but some of the best characterized come from *M. oryzae*. For *M. oryzae* isolates from rice, loss of effector genes with avirulence activity is one of the predominant mechanisms to avoid effector-triggered immunity in host cultivars (Huang et al., 2014; Yoshida et al., 2009). Among *M. oryzae* field isolates, the effectors AVR-Pita, AVR-Pia, and AVR-Pii all exhibit exceptionally high frequencies of presence/ absence polymorphisms (Huang et al., 2014). In each case, there is a direct link to genomic features: AVR-Pita is flanked by repetitive sequences, AVR-Pia is linked to a transposable element, and AVR-Pii is located in a telomeric region (Yoshida et al., 2009; Huang et al., 2014). Notably, both AVR-Pita and AVR-Pia are found to be variably located between different *M. oryzae* chromosomes, suggesting that they are in regions particularly prone to chromosome rearrangement (Sone et al., 2013).

Similar trends have also been observed in other filamentous plant pathogens, including the oomycetes *Phytophthora infestans* and *Phytophthora sojae*, and the smut fungus *Melanopsichium pennsylvanicum* (Raffaele et al., 2010; Sharma et al., 2014). In *P. infestans*, genes located in repeat-rich regions have significantly higher frequencies of presence/ absence polymorphisms, overall affecting the distribution of effector genes with avirulence activity (Raffaele and Kamoun, 2012; Raffaele et al., 2010).

1.7.4 Structurally-defined classes of effectors

Filamentous plant pathogen effectors are typically small secreted proteins that exhibit rapid levels of sequence diversification. One of the signatures of effector proteins is that they tend to have little sequence similarity to each other, or to other known proteins. The three-dimensional structures of effector proteins have, however, revealed unexpected similarities between unrelated proteins. In a recent paper by de Guillen et al. 2015, the authors hypothesized that most plant pathogen effectors belong to structurally defined families whose members are phylogenetically related (de Guillen et al., 2015). They further hypothesized that evolution of individual effectors is so rapid that obvious phylogenetic signals are subsequently lost, but the basic protein architecture remains intact due to constraints posed by stability and translocation (de Guillen et al., 2015). These hypotheses are in part borne out by computational and structural studies of the pathogens *Magnaporthe oryzae* and *Phytophthora* spp., which both have families of structurally-related proteins (de Guillen et al., 2015; Boutemy et al., 2011; Win et al., 2012).

The aforementioned paper by de Guillen et al. 2015 solved the crystal structures of two *M. oryzae* effectors, which bear striking structural similarity to other sequence-unrelated *M. oryzae* effectors and to the *Pyrenophora tritici-repentis* host-specific toxin ToxB (de Guillen et al., 2015). The authors termed this group of structurally related proteins *Magnaporthe* Avr_s and ToxB-like (MAX) effectors, and further structure-informed pattern searches found additional MAX-effector candidates in a wide range of ascomycete phytopathogens (de Guillen et al., 2015). MAX effectors form six-stranded β -sandwich structures, with the extended and exposed hydrophobic surface in multiple MAX effectors implicated in protein-protein interactions (de Guillen et al., 2015). Further, a study of the variation in the *M. oryzae* MAX effector Avr-Pik posited that the structure of

MAX-effectors may enable accumulation of adaptive mutations, especially at the hydrophobic interface (Yoshida et al., 2016).

The RXLR family of effectors in the Peronosporales clade, which includes the plant pathogens *Hyaloperonospora arabidopsidis*, *Phytophthora infestans*, and *Phytophthora sojae*, are modular secreted proteins containing an amino-terminal motif Arg-X-Leu-Arg (RXLR) that defines the domain required for delivery inside plant cells (Haas et al., 2009; J Win et al., 2012). In this class of effectors, the RXLR motif is followed by diverse, rapidly evolving carboxy-terminal effector domains which encode the biochemical activities of the effectors (Haas et al., 2009; Win et al., 2012). Bioinformatic and structural studies have revealed that the positively selected sites are not random in these effectors, but rather that polymorphic residues tend to be on the surface of the proteins, similar to MAX-effectors (Raffaele and Kamoun, 2012).

Many RXLRs have conserved sequence motifs (W, Y, and L) in their C-terminal domains, and structural studies revealed that this motif is defined by an α -helical bundle with buried hydrophobic residues, since termed the WY-domain or LWY-domains (Boutemy et al., 2011; Win et al., 2012; He et al., 2019). The WY-domain can occur as a single unit, duplicated, or in tandem repeats (Raffaele and Kamoun, 2012). Bioinformatic analyses show that the WY-domain-containing proteins are limited to a single clade within the oomycetes, and are exclusively associated with plant pathogens (Win et al., 2012). Computational analyses suggest that at least 44% of annotated *Phytophthora* RXLR effectors and 26% of *H. arabidopsidis* RXLR effectors contain the WY-domain (Boutemy et al., 2011). Similar to the MAX-effectors, WY-domain-containing proteins are sequence divergent; for example, the *Phytophthora capsici* effector AVR3a11 and *Phytophthora infestans* effector PexRD2 share less than 20% sequence identity, but exhibit striking structural similarity (Boutemy et al., 2011). It is hypothesized that the α -helical fold of the WY-domain enables functional adaptation of effectors, similar to what has been hypothesized for MAX-effectors (Boutemy et al., 2011; de Guillen et al., 2015).

1.8 Aims of the thesis

The primary aim of this thesis was to understand the biochemical basis of ATG8 substrate specificity. To determine the degree to which plant family-specific ATG8

isoforms have functionally specialized, together with my collaborator (Dr. Yasin Dagdas, Gregor Mendel Institute) I used *in planta* immunoprecipitation followed by mass spectrometry (IP-MS) to characterize the plant interactor profiles of the six potato ATG8 isoforms. The results revealed that these isoforms interact with that ATG8 isoforms bind distinct sets of plant proteins with varying degrees of overlap (**Chapter 3**). Additionally, I used the ATG8-interacting *Phytophthora infestans* effector PexRD54 as a molecular probe to define the structural determinants of ATG8 specialization, using both *in vivo* protein interaction assays and additional IP-MS experiments. These experiments revealed that the N-terminal β -strand underpins binding specificity to the substrate PexRD54, as well as shapes the broader ATG8 interactor profiles, presumably by shaping the hydrophobic pocket that accommodates this protein's ATG8-interacting motif (**Chapter 4**). To approach the question of substrate specificity from the opposing direction, I aimed to understand how the host environment has shaped the evolution of PexRD54. The results revealed that the PexRD54 ortholog in a closely related *Phytophthora* species to *P. infestans*, *P. mirabilis*, has a polymorphism in its ATG8-interacting motif, which prevents strong binding to the *Mirabilis jalapa* host ATG8s (**Chapter 5**). Altogether, these results provide new insights into the molecular mechanisms of the selective autophagy pathway and shed light on the evolutionary dynamics of an ATG8-targeting effector.

Chapter 2: Materials and Methods

2.1 Molecular biology methods

2.1.1 Gateway cloning

Gateway cloning (Invitrogen) was performed following the manufacturer's instructions. PCR-amplified sequences were cloned into the entry vector pENTR/D-TOPO and transformed into the *Escherichia coli* chemically competent cells One Shot TOP10 (Invitrogen). LR reactions were performed by mixing 0.5 μ L LR Clonase II (Invitrogen), 100 ng entry clone, and 250 ng destination vector in TE buffer (pH 8.0) to a final volume of 5 μ L. Reactions were incubated at room temperature for a minimum of two hours before transformation into subcloning efficiency *E. coli* DH5 α chemically competent cells (Invitrogen).

2.1.2 Golden Gate cloning

Golden gate assembly was performed using a protocol modified from the literature (Weber et al., 2011). The restriction-ligation reactions consisted of a mix of: 100 ng of each level 0 module and the binary vector; 2 U (units) of *Bsa*I (NEB); 4 U T4 DNA ligase (Invitrogen); 1x BSA (NEB) in T4 DNA ligase buffer (Invitrogen), to a final volume of 20 μ L. Using a thermocycler, the reaction was incubated at 37°C, followed by 50 cycles of 5 minutes (min) at 37°C, 5 min at 20°C, and 10 min at 50°C, and finally 10 min at 80°C. The reaction was then transformed into subcloning efficiency DH5 α chemically competent cells (Invitrogen).

2.1.3 In-Fusion cloning

In-Fusion cloning (Clontech) was performed following the manufacturer's instructions. Reactions were performed by mixing 2 μ L 5x In-Fusion HD enzyme mix (Clontech), 100 ng of linearized vector, 10 ng of insert, and dH₂O to a total volume of 10 μ L, followed by incubation for 15 minutes at 50°C. These reactions were transformed into subcloning efficiency DH5 α chemically competent cells (Invitrogen).

2.1.4 Bacterial transformation

Transformations of *E. coli* One Shot Top10 and subcloning efficiency DH5 α chemically competent cells were performed according to the manufacturer's instructions (Invitrogen). Reaction products were mixed with competent cells and incubated on ice for up to 30 minutes. Cells were then heat shocked by incubation at 42°C for 45 seconds. Immediately following, 200 μ L of lysogeny broth (LB) medium was added to the cells, which were incubated at 37°C for 45 minutes, with constant agitation. The cells were plated on LB agar plates with the appropriate antibiotics (kanamycin or spectinomycin, 50 μ g/mL) and incubated at 37°C overnight. Transformations of *E. coli* BL21 (DE3) chemically competent cells were performed following the same protocol.

Agrobacterium tumefaciens strain GV3101 was used for all leaf infiltration experiments, whereas *A. tumefaciens* AGL1 was used for plant transformation. For both, electroporation was performed using an electroporation cuvette with a width of 1 mm and an electroporator (Biorad) with the settings: voltage = 1.8 kV, capacitance = 25 μ F, resistance = 200 Ω . Immediately following electroporation, 500 μ L of LB medium was added to the cells, which were then incubated at 28°C for an hour, with constant agitation. The cells were plated on LB agar plates with the appropriate antibiotics (kanamycin 50 μ g/mL and rifampicin 100 μ g/mL; or spectinomycin 50 μ g/mL and rifampicin 100 μ g/mL) and incubated at 28°C for approximately 48 hours.

2.1.5 PCR product purification, colony PCR, and plasmid preparation

PCR products were purified using a QIAquick PCR purification kit (Qiagen). Colony PCR was performed using DreamTaq DNA polymerase according to the manufacturer's instructions (ThermoFisher Scientific). Plasmid extraction was performed using QIAprep Spin Miniprep Kit according to the manufacturer's instructions (Qiagen).

2.2 Biochemistry methods

2.2.1 *In planta* protein expression

Transient gene expression *in planta* was performed by delivering T-DNA constructs with *A. tumefaciens* strain GV3101 into 3– 4-week old *N. benthamiana* plants as described previously (Win et al., 2011). *A. tumefaciens* strains carrying the plant expression constructs

were diluted in agroinfiltration medium (10 mM MgCl₂, 5 mM 2-[N-morpholine]-ethanesulfonic acid [MES], pH 5.6) to a final OD₆₀₀ of 0.2, unless stated otherwise. For transient co-expression assays, *A. tumefaciens* strains were mixed in a 1:1 ratio. *N. benthamiana* leaves were harvested 2–3 days after infiltration.

2.2.2 Plant total protein extraction

Protein extraction was performed as described previously (Win et al., 2011). *N. benthamiana* leaves were ground into a fine powder in liquid nitrogen with a mortar and pestle. Ground tissue was mixed with GTEN buffer (150 mM Tris-HCl, pH 7.5; 150 mM NaCl; 10% (w/v) glycerol; 10 mM EDTA) augmented with 10mM dithiothreitol, 2% (w/v) PVPP, 1% (v/v) protease inhibitor cocktail (Sigma), and 0.2% (v/v) iGepal, at a ratio of 2x buffer volume to tissue weight. After full mixture, the samples were centrifuged at 45000 rpm at 4°C for 30 min and the supernatants were filtered through 0.45 µm filters, resulting in the total protein extracts. For SDS-PAGE electrophoresis, total protein extracts were mixed with protein loading dye (5x final concentration: 0.2% (w/v) bromophenol blue, 200 mM Tris-HCl (pH 6.8), 2.5% (v/v) glycerol, and 4% (w/v) SDS) and incubated at 70°C for 10 minutes before electrophoresis.

2.2.3 Co-immunoprecipitation

Co-immunoprecipitation (co-IP) was carried out following the protocol described previously (Win et al., 2011). Immunoprecipitation was performed using affinity chromatography with GFP_Trap_A beads (Chromotek) by adding 40 µL of beads resuspended 1:1 in IP buffer (GTEN with 0.1% iGepal) to 1 mL of total protein extract, and mixing the beads and extract well by turning end-over-end for two hours at 4°C. Samples were then centrifuged at 1000 rcf at 4°C for 1 min; the supernatant was discarded using a needle attached to a syringe, before the beads were resuspended in 1 mL of fresh IP buffer. Samples were washed as such a total of five times before being resuspended in an equal volume of loading dye with 10 mM DTT. Elution of the proteins from the beads was performed by heating 10 minutes at 70°C.

2.2.4 SDS-PAGE electrophoresis

For western blot analysis, commercial 4- 20% SDS-PAGE gels (Bio-Rad) were used for protein electrophoresis in Tris-glycine buffer (25 mM Tris, 250 mM glycine (pH 8.3), 0.1% (w/v) SDS) for approximately two hours at 120 V. For analysing *in vitro* produced proteins, commercial 16% RunBlue™ TEO-Tricin SDS gels (Expedeon) were used for electrophoresis in RunBlue™ SDS Running Buffer (Expedeon) for approximately two hours at 120 V; gels were stained with InstantBlue™ Protein Stain (Expedeon). For both, PageRuler Plus (Fermentas) was used as a protein size marker.

2.2.5 Immunoblot analysis

Following SDS-PAGE electrophoresis, proteins were transferred onto a polyvinylidene difluoride membrane using a Trans-Blot Turbo transfer system (Bio-Rad) according to the manufacturer's instructions. The membrane was blocked with 5% milk in Tris-buffered saline and Tween 20. GFP detection was performed in a single step by a GFP (B2):sc-9996 horseradish peroxidase (HRP)-conjugated antibody (Santa Cruz Biotechnology); RFP detection was performed with a rat anti-RFP 5F8 antibody (Chromotek) and an HRP-conjugated anti-rat antibody. Pierce ECL Western Blotting Substrate (ThermoFisher Scientific) or SuperSignal West Femto Maximum Sensitivity Substrate (ThermoFisher Scientific) were used for detection. Membrane imaging was carried out with an ImageQuant LAS 4000 luminescent imager (GE Healthcare Life Sciences). SimplyBlue™ SafeStain (Invitrogen) staining of rubisco was used as a loading control.

2.2.6 Heterologous protein production and purification

Bacteria expressing heterologous proteins were pre-cultured in 100 mL volumes of LB overnight at 37°C with constant agitation at 180 rpm, then used to inoculate 1L volumes of auto-induction media, which were grown at 37°C with constant agitation before being transferred to 18°C overnight upon induction at OD₆₀₀ 0.4- 0.6. Cell pellets were collected by centrifugation at 5,000 rpm for 10 minutes, before being resuspended in buffer A1 (50 mM Tris-HCl pH 8.0, 500 mM NaCl, 50 mM glycine, 5% (v/v) glycerol, 20 mM imidazole, and EDTA-free protease inhibitor). The cells were lysed by sonication and subsequently centrifuged at 18,000 rpm for 30 minutes at 4°C to produce the clear

lysate. A Ni²⁺-NTA capture step produced fractions containing His-tagged protein of interest, which were concentrated as appropriate. The concentration was judged by absorbance at 280 nm, using a calculated molar extinction coefficient of each protein. For proteins with cleavable His tags (pOPINF constructs), 3c-protease was added at 10 µg/mg protein and incubated overnight at 4°C. A final Ni²⁺-NTA capture step, to isolate the cleaved His tag, was followed by a final gel filtration onto a Superdex 75 26/600 gel filtration column pre-equilibrated in buffer A4 (20 mM HEPES pH 7.5, 500 mM NaCl). The fractions containing the protein of interest were pooled and concentrated as appropriate, as above. The purity of proteins was judged by running 16% SDS-PAGE gels and staining with InstantBlue™ (Expedeon). PexRD54 was purified as described previously (Dagdas et al., 2016).

2.2.7 Isothermal titration calorimetry

All calorimetry experiments were recorded using a MicroCal PEAQ-ITC (Malvern, UK). To test the interaction of ATG8 proteins with PexRD54 peptides, experiments were carried out at room temperature (20°C) in A4 buffer (20 mM HEPES pH 7.5, 500 mM NaCl). The calorimetric cell was filled with 90 µM ATG8 protein and titrated with 1 mM PexRD54 peptide. For each ITC run, a single injection of 0.5 µL of ligand was followed by 19 injections of 2 µL each. Injections were made at 120s intervals with a stirring speed of 750 rpm. The raw titration data for the replicates of each experiment were integrated and fit to a single-site binding model using AFFINImeter software. A global analysis of the interactions were performed using AFFINImeter software, where the isotherms for the experimental replicates were simultaneously fit to the same single-site binding model.

2.3 Plant material

2.3.1 *Nicotiana benthamiana*

Wild-type *N. benthamiana* plants were primarily grown under glasshouse conditions, supplemented with light for a 16/8-hour light/dark cycle. For experiments testing the expression of putative ATG8-interacting proteins, *N. benthamiana* lines were grown in a controlled growth chamber with temperature 22- 25°C, humidity 45- 65% and 16/8-hour light/dark cycle, due to a change a space availability.

2.3.2 *Mirabilis jalapa*

M. jalapa plants were grown in glasshouse conditions, supplemented with light for a 16/8-hour light/dark cycle.

2.4 Plant genotyping

2.4.1 *Mirabilis jalapa* DNA extraction

M. jalapa seedling leaf tissue (<50 mg) was collected and disrupted in lysis buffer (Qiagen) using manual agitation. Following disruption, lysis filtration was performed using the QIAshredder spin column as part in the DNeasy Plant Mini Kit (Qiagen), per the manufacturer's instructions. DNA extraction and elution were performed using the same kit, per the manufacturer's instructions. DNA concentration was determined by nanodrop and quality was verified by running diluted samples on a 1.5 % agarose gels.

2.4.2 *Mirabilis jalapa* genotyping by PCR

PCR reactions screening for three genes were performed on each extracted *M. jalapa* DNA sample using primers listed in **Table 2.1**: an endogenous *M. jalapa* ATG8, *Mj*ATG8-I, was screened to validate DNA quality; the PexRD54 effector (*Pm*PexRD54, *Pj*PexRD54^{PmAIM}) was screened to detect transgene insertion; and the kanamycin resistance gene was also screened to detect transgene insertion. PCRs were run on 1.5% agarose gels to check amplification and product size against positive controls.

Table 2.1 List of primers used for genotyping of *M. jalapa* transgenics

Primer name	Sequence (5'-3')	Size (bp)	Usage in this study	Reference
g-MjATG8-I_F	ATGGCTAAGAGTTACTTCAAG		Genotyping <i>M. jalapa</i>	This study
g-MjATG8-I_R	GGAGATCGCAACAGTGTAG	366	Genotyping <i>M. jalapa</i>	This study
g-PmRD54_F	GTTGGTCCCTCTTGGCTATC		Genotyping <i>M. jalapa</i>	This study
g-PiRD54_F	GTTGGTCCCTCTTGGCTAGC		Genotyping <i>M. jalapa</i>	This study
g-PmRD54_R	CACAATTTTCCAGTCGAACTC	1146	Genotyping <i>M. jalapa</i>	This study
g-Kan_F	CGATACCGTAAAGCACGAGG		Genotyping <i>M. jalapa</i>	This study
g-Kan_R	ATCTGGACGAAGAGCATCAG	768	Genotyping <i>M. jalapa</i>	This study

2.5 Cloning

2.5.1 ATG8s

The *Solanum tuberosum* ATG8 (*St*ATG8) isoforms (**Table 2.2**) were amplified from cDNA using primers listed in **Table 2.3** and cloned into the Gateway destination pK7WGF2 vector; ATG8-2.2 and ATG8-4 were also cloned as level 0 modules for Golden Gate cloning. The *St*ATG8 swap and point mutants were synthesized as level 0 modules for Golden Gate cloning (Weber et al., 2011). Using these modules, GFP:ATG8-2.2, GFP:ATG8-4, GFP:ATG8-4 swap and GFP:ATG8-4 point mutant constructs were generated by Golden Gate assembly with pICSL13001 (long 35s promoter, The Sainsbury Laboratory (TSL) SynBio), pICSL30006 (N-terminal GFP, TSL SynBio), pICH41414 (35s terminator, TSL SynBio), into the binary vector pICH47732 (Karimi et al., 2002). All constructs were verified by DNA sequencing.

The *Mirabilis jalapa* ATG8 (*Mj*ATG8) isoforms were identified using RNA sequencing datasets, amplified from cDNA using primers listed in **Table 2.3**, and cloned into the Gateway destination vector pK7WGF2. *Mj*ATG8-I and *Mj*ATG8-III were also amplified using primers listed in **Table 2.3** and cloned into the pOPINF vector using In-Fusion cloning (Berrow et al., 2007), generating cleavable N-terminal 6xHis-tagged proteins for purification. then transformed into the *E. coli* strain BL21 (DE3) for recombinant protein production. All constructs were verified by DNA sequencing.

Table 2.2 List of *S. tuberosum* ATG8 accessions

Gene	Protein accession (Sol Genomics)	Transcript accession (Sol Genomics)
StATG8-1.1	PGSC0003DMP400008510	PGSC0003DMT400012239
StATG8-1.2	PGSC0003DMP400022074	PGSC0003DMT400032486
StATG8-2.2	PGSC0003DMP400038670	PGSC0003DMT400057469
StATG8-3.1	PGSC0003DMP400028821	PGSC0003DMT400042494
StATG8-3.2	PGSC0003DMP400009038	PGSC0003DMT400013024
StATG8-4	PGSC0003DMP400009229	PGSC0003DMT400013320

Table 2.3 List of primers used for ATG8 cloning

Primer name	Sequence (5'-3')	Size (bp)	Usage in this study	Reference
StATG8-1.1_F	<i>CACCATGGCTAAGAGCTCAT TCAAG</i>		Gateway cloning of StATG8-1.1	Zess et al 2019
StATG8-1.1_R	<i>CTACAGTTCGCTCAGACCC</i>	366	Gateway cloning of StATG8-1.1	Zess et al 2019
StATG8-1.2_F	<i>CACCATGGCAAAGAGTTCGT TCAAG</i>		Gateway cloning of StATG8-1.2	Zess et al 2019
StATG8-1.2_R	<i>CTACACTAAGTTAAGGTCCC</i>	366	Gateway cloning of StATG8-1.2	Zess et al 2019
StATG8-2.2_F	<i>CACCATGGCCAAAAGCTCCT TCAAAT</i>		Gateway cloning of StATG8-2.2	Zess et al 2019
StATG8-2.2_R	<i>TCAAAAGGATCCGAAGGTAT TC</i>	357	Gateway cloning of StATG8-2.2	Zess et al 2019
StATG8-3.1_F	<i>CACCATGGCCAAAAGTTCTT TCAAG</i>		Gateway cloning of StATG8-3.1	Zess et al 2019
StATG8-3.1_R	<i>TTAATTTCCAAGCTCAACAAA C</i>	369	Gateway cloning of StATG8-3.1	Zess et al 2019
StATG8-3.2_F	<i>CACCATGGCTAAGAGTTCTT TCAAG</i>		Gateway cloning of StATG8-3.2	Zess et al 2019
StATG8-3.2_R	<i>TTAATTCCTCAAGCTCGAGG</i>	369	Gateway cloning of StATG8-3.2	Zess et al 2019
StATG8-4_F	<i>CACCATGGGGAAGACCTTCA AAGATG</i>		Gateway cloning of StATG8-4	Zess et al 2019
StATG8-4_R	<i>CTAAGAGTGACCACCAAAGG</i>	357	Gateway cloning of StATG8-4	Zess et al 2019
MjATG8-I_F	<i>CACCATGGCTAAGAGTTACT TCAAG</i>		Gateway cloning of MjATG8-I	This study
MjATG8-I_R	<i>CTACACTGTTGCGATCTCCC</i>	366	Gateway cloning of MjATG8-I	This study
MjATG8-II_F	<i>CACCATGGCCAATAATTCGT TCC</i>		Gateway cloning of MjATG8-II	This study
MjATG8-II_R	<i>TCAGAAGCCATCGCATTTTG ATC</i>	369	Gateway cloning of MjATG8-II	This study
MjATG8-III_F	<i>CACCATGGTTAAGCCTCAAG TTTTC</i>		Gateway cloning of MjATG8-III	This study
MjATG8-III_R	<i>TCACCCGCCACCAAAGGTC</i>	360	Gateway cloning of MjATG8-III	This study
MjATG8-IV_F	<i>CACCATGGCTAAAAGCTCCT TCAAAT</i>		Gateway cloning of MjATG8-IV	This study
MjATG8-IV_R	<i>TCAGTTAATTCCAAATGCCG</i>	369	Gateway cloning of MjATG8-IV	This study
MjATG8-V_F	<i>CACCATGGCTAAAAGCTCCT TCAAAT</i>		Gateway cloning of MjATG8-V	This study
MjATG8-V_R	<i>TCATCCAAACACATTCTCCC C</i>	351	Gateway cloning of MjATG8-V	This study
MjATG8-VI_F	<i>CACCATGGCTAAAAGCTCTT TCAAGC</i>		Gateway cloning of MjATG8-VI	This study
MjATG8-VI_R	<i>CTACATGTCTGCACTGCATG</i>	372	Gateway cloning of MjATG8-VI	This study

Table 2.3 List of primers used for ATG8 cloning (continued)

Primer name	Sequence (5'-3')	Size (bp)	Usage in this study	Reference
MjATG8-I_pOPINF_F	AAGTTCTGTTTCAGGGCCCCG GCTAAGAGTTACTTCAAGCA		In-Fusion cloning of MjATG8-I	This study
MjATG8-I_pOPINF_R	ATGGTCTAGAAAGCTTTACA CTGTTGCGATCTCCCCAA	363	In-Fusion cloning of MjATG8-I	This study
MjATG8-III_pOPINF_F	AAGTTCTGTTTCAGGGCCCCG GTTAAGCCTCAAGTTTTCAA		In-Fusion cloning of MjATG8-III	This study
MjATG8-III_pOPINF_R	TGGTCTAGAAAGCTTTACCC GCCACCAAAGGTCTTTT	357	In-Fusion cloning of MjATG8-III	This study

2.5.2 ATG8-interacting proteins and ATG8-interacting motif (AIM) mutants

The *N. benthamiana* protein sequences of the putative ATG8-interacting proteins identified using immunoprecipitation followed by mass spectrometry (IP-MS) were used to identify homologs in the *S. tuberosum* protein database (potato ITAG release 1 predicted proteins) on the Sol Genomics Network (SGN) (**Table 2.4**). For each candidate, ATG8-interacting motif (AIM) sequences were determined using the iLIR online tool (Kalvari et al., 2014), which defines an AIM as a sequence of [ADEFGLPRSK] [DEGMSTV] [WFY] [DEILQTV] [ADEFHIKLMPSV] [ILV] based on experimentally verified AIMs. For each candidate ATG8-interacting protein, an AIM mutant construct was designed substituting each of the two key hydrophobic residues (underlined) for an alanine (eg. DGYEDV to DGAAEDA). *S. tuberosum* candidates and candidate AIM mutants were synthesized as level 0 modules for Golden Gate cloning (Weber et al., 2011). Using these modules, expression constructs featuring N-terminal tags were generated by Golden Gate assembly with pICSL13001 (long 35s promoter, The Sainsbury Laboratory (TSL) SynBio), pICSL30003 (N-terminal RFP, TSL SynBio), pICH41414 (35s terminator, TSL SynBio), into the binary vector pICH47732 (Weber et al., 2011). Using the same level 0 modules, expression constructs featuring C-terminal tags were generated by Golden Gate assembly with pICSL1266 (long 35s promoter, The Sainsbury Laboratory (TSL) SynBio), pICSL50004 (C-terminal RFP, TSL SynBio), pICH41414 (35s terminator, TSL SynBio), into the binary vector pICH47732 (Weber et al., 2011). All constructs were verified by DNA sequencing.

Table 2.4 List of ATG8-interacting proteins and accessions

Description	Nb Accession	St Accession	Abbrev.	Reference
40S ribosomal protein S15a-1	NbS00013115g0003.1	PGSC0003DMC400043932 (SGN)	r_40s_S15	This study
60s ribosomal protein l21-1-like	Nbv6.1trP56805	PGSC0003DMC400020280 (SGN)	r_60s_l21	This study
26s proteasome regulatory subunit 6a	Nbv6.1trP48334	PGSC0003DMC400042798 (SGN)	p_26s_6a	This study
Low-temp-induced cysteine protease-like	Nbv6.1trA201272	XM_015312063.1 (NCBI)	cys_prot	This study
Cathepsin B cysteine protease	NbC26208175g0003.1	XM_006342582.2 (NCBI)	RD21	This study
Protein transport protein sec61 subunit α -like	Nbv6.1trP32384	PGSC0003DMC400049442 (SGN)	Sec61a	This study

2.5.3 PexRD54 variants and mutants

*Pi*PexRD54 (PITG_09316) and the *Pi*PexRD54 AIM mutant (*Pi*PexRD54^{AIM}) were cloned previously using Gateway cloning into the destination vectors pH7WGR2 (N-terminal RFP fusion) and PK7WGF2 (N-terminal GFP) (Karimi et al., 2002), generating the constructs RFP:*Pi*PexRD54, RFP:*Pi*PexRD54^{AIM}, GFP:*Pi*PexRD54, and GFP:*Pi*PexRD54^{AIM} (Dagdas et al., 2016). *Pm*PexRD54 was amplified from genomic DNA of *Phytophthora mirabilis* isolate 3008 (*Pm*3008), and cloned into the same set of Gateway destination vectors, generating RFP:*Pm*PexRD54 and GFP:*Pm*PexRD54. Constructs swapping the AIM sequences between *Pi*PexRD54 and *Pm*PexRD54—*Pi*PexRD54^{*Pm*AIM} and *Pm*PexRD54^{*Pi*AIM}—were cloned into the same Gateway destination vectors following site-directed mutagenesis, generating the constructs: RFP:*Pi*PexRD54^{*Pm*AIM}, RFP:*Pm*PexRD54^{*Pi*AIM}, GFP:*Pi*PexRD54^{*Pm*AIM}, and RFP:*Pi*PexRD54^{*Pi*AIM}. Primers used in **Table 2.5** were used to introduce the mutations by inverse PCR with Phusion High-Fidelity DNA Polymerase (Thermo); constructs were verified by DNA sequencing.

Table 2.5 List of primers used for PexRD54 cloning

Primer name	Sequence (5'-3')	Size (bp)	Usage in this study	Reference
PmPexRD54_F	ATGCGTTTCCAGAGCATT ATG		Gateway cloning <i>PmPexRD54</i>	This study
PmPexRD54_R	TTACACAATTTTCCAGTCG	1146	Gateway cloning <i>PmPexRD54</i>	This study
sdm- PmPexRD54_PiAIM_F	CAAACCGCTGGAGTTCGA CTGAAAAATTGTGT		Site-directed mutagenesis <i>PmPexRD54</i>	This study
sdm- PmPexRD54_PiAIM_R	ACACAATTTTTCAGTCGA ACTCCAGCGGTTTG	*	Site-directed mutagenesis <i>PmPexRD54</i>	This study
sdm- PiPexRD54_PmAIM_F	CCGCTGGATTTTCGACTGG GGAATTGTGTAA		Site-directed mutagenesis <i>PIPexRD54</i>	This study
sdm- PiPexRD54_PmAIM_R	TTACACAATTTCCCAGTC GAAATCCAGCGG	*	Site-directed mutagenesis <i>PIPexRD54</i>	This study

*size dependent on vector context

2.5.4 PexRD54-interacting proteins

The *S. tuberosum* protein Rab8a (StRab8a) (accession PGSC0003DMP400048235, Sol Genomics Network) was cloned previously using Gateway cloning into the destination vector pH7WGR2 (N-terminal RFP fusion). The *M. jalapa* homolog of Rab8a (*MjRab8a*) was synthesized as a synthetic fragment, and an expression construct featuring an N-terminal RFP tag was generated by Golden Gate assembly with pICSL13001 (long 35s promoter, The Sainsbury Laboratory (TSL) SynBio), pICSL30003 (N-terminal RFP, TSL SynBio), pICH41414 (35s terminator, TSL SynBio), into the binary vector pICH47732 (Weber et al., 2011).

2.6 Phylogenetic analyses

2.6.1 Phylogenetic analysis of Solanaceous ATG8s

Nucleotide sequences of Solanaceous ATG8s from select species (*Solanum tuberosum*, *Nicotiana benthamiana*, *Capsicum annuum*, *Solanum lycopersicum*) were collected from Kellner et al., 2017. The phylogenetic tree was calculated in MEGA7 (Kumar et al., 2016) from a 369-nucleotide alignment (MUSCLE (Edgar, 2004), codon-based) with bootstrap values

based on 1000 iterations, and visualized using FigTree v1.4.3 (<http://tree.bio.ed.ac.uk/software/figtree/>).

2.6.2 Phylogenetic analysis of *Mirabilis jalapa* ATG8s

Nucleotide sequences of ATG8s from Solanales and Brassicales were collected from Kellner et al., 2017. The potato ATG8-2.2 sequence was used to identify the homologs from the Chenopodiaceae and Nyctaginaceae families (Order: Caryophyllales) using BLAST (NCBI). The phylogenetic tree showing all ATG8s was calculated in MEGA7 (Kumar et al., 2016) from a 444-nucleotide alignment (MUSCLE (Edgar, 2004), codon-based) with bootstrap values based on 1000 iterations and visualized using FigTree v1.4.3 (<http://tree.bio.ed.ac.uk/software/figtree/>). To simplify the phylogenetic tree, some branches were collapsed into clades according to the bootstrap values of the nodes; Solanales and Brassicales clades were labelled using the conventions in Kellner et al., 2017. The phylogenetic tree showing the ATG8s from Caryophyllales was calculated in MEGA7 (Kumar et al., 2016) from a 372-nucleotide alignment (MUSCLE (Edgar, 2004), codon-based) with bootstrap values based on 1000 iterations and visualized using FigTree v1.4.3 (<http://tree.bio.ed.ac.uk/software/figtree/>).

2.7 Immunoprecipitation-mass spectrometry (IP-MS)

2.7.1 Sample preparation

For the ATG8 interactome and ATG8-4-32I mutant experiment, these methods were performed by the the Vienna Biocenter Protein Chemistry core facilities (Vienna, Austria). Following co-immunoprecipitation, the beads were resuspended in 100 mM ammonium bicarbonate (Fluka 09830-500G). Proteins were digested from the beads by addition of 400 ng Lys-C (Wako PEF 7041) and incubation on a Thermoshaker at 1,300 rpm for 4 hours at 37°C. Subsequently, the supernatant was transferred to a fresh tube and reduced in 0.6 mM TCEP-HCl (Tris 2-carboxyethyl phosphine hydrochloride, Sigma 646547-10 x 1ml) for 30 min at 60°C followed by an alkylation reaction in 4 mM MMTS (methyl methanethiosulfonate, Fluka 64306) for 30 min at room temperature in the dark. Peptides were further digested by addition of 400 ng Trypsin (Trypsin Gold Promega V5280) and

overnight incubation at 37°C. The digestion was stopped by addition of TFA (trifluoroacetic acid, Aldrich T63002) to a final concentration of 1%.

For the ATG8-4-S3 mutant experiment, these methods were performed by The Sainsbury Laboratory core Proteomics facilities (Norwich, UK). Immunoprecipitated protein samples were separated by SDS-PAGE (4-20% gradient gel, Biorad), and after staining with Coomassie brilliant blue G-250 (SimplyBlue Safe stain, Invitrogen) the proteins were cut out and gel slices were destained in 50% acetonitrile. Reduction and alkylation were done by incubation for 45 min in 10 mM DTT, followed for 30 min in the dark in 55 mM chloroacetamide. After several washes with 25 mM ammonium bicarbonate, 50% acetonitrile gel slices were dehydrated in 100% acetonitrile. Gel pieces were rehydrated with 50 mM ammonium bicarbonate and 5% acetonitrile containing 20 ng/μL trypsin (Pierce), and digested overnight at 37°C. Tryptic peptides were sonicated from the gel in 5% formic acid, 50% acetonitrile, and the total extracts were evaporated until dry.

2.7.2 Nano liquid chromatography mass spectrometry (LC-MS) analysis, data processing, and peptide identification

For the ATG8 interactome and ATG8-4-32I mutant experiment, LC-MS analysis was done as described previously by the Vienna Biocenter Protein Chemistry core facilities (Zess et al., 2019). In short, LC-MS/MS analysis was performed with an UltiMate 3000 RSLC nano system (Thermo Fisher Scientific), equipped with a Proxeon nanospray source (Thermo Fisher Scientific). The raw files were loaded into Proteome Discoverer (version 2.1.0.81, Thermo Fisher Scientific), and peptide identification was performed by searching the in-house *N. benthamiana* database Nicotiana_Benthamiana_Nbv6trPAplusSGNUniq_20170808 (398,682 sequences; 137,880,484 residues), supplemented with common contaminants, using MS Amanda v2.1.5.9849, Engine version v2.0.0.9849 (Dorfer et al., 2014). The localization of the post-translational modification sites within the peptides was performed with the tool ptmRS, based on the tool phosphoRS (Taus et al., 2011). Peptide areas have been quantified using in-house-developed tool APQuant. The mass spectrometry proteomics data have been deposited to the ProteomeXchange Consortium via the PRIDE (Vizcaino et al., 2016) partner repository with the dataset identifier PXD011226.

For the ATG8-4-S3 mutant experiment, IP-MS analysis was done as previously described by The Sainsbury Laboratory Proteomics core facilities (Zess et al., 2019). In brief, LC-MS/MS analysis was performed with an Orbitrap Fusion Trihybrid mass spectrometer (Thermo Scientific) and a nanoflow-HPLC system (Dionex Ultimate3000, Thermo Scientific). The peptide identification was performed by searching the aforementioned *N. benthamiana* database using Mascot (v 2.4.1 Matrix Science) with the modification of allowing Trypsin peptide termini. Scaffold (v4; Proteome Software) was used to validate MS/MS-based peptide and protein identifications and annotate spectra using a search criterium of a minimum of two peptides with MASCOT ion scores above 20 and 95% peptide identity. Selected spectra were manually inspected before acceptance. The mass spectrometry proteomics data have been deposited to the ProteomeXchange Consortium via the PRIDE (Vizcaino et al., 2016) partner repository with the dataset identifier PXD011484.

2.7.3 Data filtering

For both the ATG8 interactome and the ATG8-4-32I mutant IP-MS data analysis, the peptide spectrum match (PSM) values were averaged between the replicates of each assayed construct. The unfiltered datasets contained 2,349 and 2,550 proteins, respectively. The dataset was then filtered to remove any proteins that showed a PSM value >10 with the GFP empty vector control (GFP-EV), as well as any proteins where none of the ATG8-GFP fusions exhibited an average PSM value >10. After this basic filtering, the dataset was further filtered such that for all interactors with a GFP-EV average PSM value >4, at least one of the ATG8-GFP fusions had to exhibit >3x the EV PSM value (e.g. for GFP-EV average PSM = 9.5, one GFP-ATG8 > 28.5). This resulted in a final list of 621 proteins.

For ATG8-4-S3 mutant IP-MS data analysis, the peptide count values were first normalized to the peptide counts for GFP in each sample to adjust for varying expression levels. The unfiltered dataset contained 1,994 proteins. Then, after averaging the replicate values for each assayed construct, the dataset was filtered to remove any proteins that showed a peptide count of >6 with the GFP empty vector control, as well as any proteins where none of the GFP-ATG8 fusions exhibited a peptide count >10. This resulted in a list of 496 proteins. This dataset was further filtered by removing proteins that showed

extreme unevenness among replicates, resulting in a final ATG8-4-S3 dataset of 291 proteins amenable to statistical analysis.

2.7.4 Network analysis

For each interactor in the ATG8 interactome dataset, the closest *Arabidopsis thaliana* homolog was predicted using BLAST, and the gene ontology (GO) annotations were obtained using Blast2GO (Gotz et al., 2008). The interactors were sorted by cellular compartment or biological process, respectively, and then collapsed based on shared annotations. The number of interactors in each shared annotation group was recorded, and the average PSM values were calculated for each group for every ATG8; the resulting tables were imported into Cytoscape (Shannon et al., 2003) to make network representations. The former values were used to scale the node sizes across all network representations, and the latter values were used to weight the edges for each individual ATG8-group connection.

2.7.5 ATG8-interacting motif prediction and conservation

For all of the proteins in each of the interactomes, ATG8-interacting motif (AIM) sequences were predicted using iLIR (Kalvari et al., 2014). This prediction tool defines the sequence feature of functional AIM as [ADEFGLPRSK] [DEGMSTV] [WFY] [DEILQTV] [ADEFHIKLMPTV] [ILV] based on experimentally verified AIMs, scoring sequences against a position-specific scoring matrix (PSSM). For each *N. benthamiana* protein, the position, sequence, and PSSM score of the predicted AIM was recorded. To look at conservation, the *A. thaliana* and *Marchantia polymorpha* homologs of the interactome proteins with predicted AIMs were also analysed using iLIR. An AIM was considered evolutionarily conserved if four out of six amino acid residues were conserved and the AIM position in the protein was within 50 residues of the *N. benthamiana* position, in at least one of the homologs. An alignment was consulted in the case of unclear positional conservation, such as with large insertions or deletions in one of the proteins.

Chapter 3: Solanaceous ATG8 isoforms associate with distinct sets of plant proteins¹

3.1 Introduction

Autophagy is an essential eukaryotic cellular process that involves the degradation or trafficking of cellular components, either as a housekeeping function or as a stress response (Dikic and Elazar, 2018; Lamb et al., 2013). Autophagy employs specialized double membrane-bound vesicles, termed autophagosomes, which are formed by the expansion of a cup-shaped phagophore that encapsulates the targeted cytoplasmic material (**Fig 3.1**) (Marshall and Vierstra, 2018). The autophagosomes are either trafficked to the vacuole, where the contents are degraded and the components returned to the cytoplasm, via vacuolar membrane fusion, lysis, and export, or elsewhere in the cell as part of a more general trafficking pathway (**Fig 3.1**) (Marshall and Vierstra, 2018; Dagdas et al., 2018; Dupont et al., 2011). Autophagy was initially described as a non-selective bulk process, but it is now clear that the pathway is highly selective and tightly regulated, requiring cargo recognition by the autophagy machinery, resulting in the more accurate moniker, “selective autophagy” (Yang and Klionsky, 2010).

A number of studies, based on a variety of experimental systems, have together identified the key genes that comprise the autophagy machinery, termed autophagy-related (ATG) proteins. More than 30 ATG proteins have been identified in yeast (Tsukada and Ohsumi, 1993; Thumm et al., 1994). Autophagy-related protein 8 (ATG8), in particular, is a key player in the selective autophagy pathway. Through the activities of other ATG proteins, ATG8 is conjugated to the lipid phosphatidylethanolamine (PE), and the resulting ATG8-PE adduct is inserted into the growing phagophore membrane (**Fig 3.1**) (Phillips et al., 2008; Thompson et al., 2005; Fujioka et al., 2010). ATG8 interacts with proteins required for autophagosome closure and autophagosome-vacuolar fusion,

¹ Most parts of this chapter have been published in the following literature: Zess, E. K., Jensen, C., Cruz-Mireles, N., De la Concepcion, J. C., Sklenar, J., Stephani, M., ... Dagdas, Y. F. (2019). N-terminal β -strand underpins biochemical specialization of an ATG8 isoform. *PLOS Biology*, 17(7), e3000373.

The permission to reuse the contents is under the Creative Commons Attribution License.

and functions as a major structural component of autophagosome membrane (Reggiori and Ungermann, 2017; Kumar et al., 2018; McEwan et al., 2015; Alemu et al., 2012; Zhuang et al., 2013).

Selective autophagy has multiple layers of specificity defining the dynamics of uptake, sub-cellular trafficking, and turnover of autophagic substrates (Stolz et al., 2014; Zaffagnini and Martens, 2016). However, the molecular details of how various autophagy cargoes and components are recognized, recruited, and recycled remain to be fully elucidated (Bento et al., 2016; Noboru Mizushima, 2018). An emerging view is that ATG8 specialization could form a layer of specificity in selective autophagy pathways. This could occur through ATG8 interaction with different sets of proteins (Behrends et al., 2010; Wild et al., 2014; Cheng et al., 2016), post-translational modifications—such as ubiquitination (Joachim et al., 2017) and acetylation (Huang et al., 2015)—and sub-cellular localization (Winer et al., 2018; Joachim et al., 2015). ATG8 is known to serve as the lynch-pin in selectivity of the autophagy pathway, directly binding receptors and adaptors that have affinity for specific cargo and machinery, respectively (Dikic, 2017; Farré and Subramani, 2016; Li and Vierstra, 2012). Autophagy receptors bridge ATG8 and autophagic cargo, providing a mechanism to selectively eliminate specific proteins, protein aggregates, organelles, and even invading pathogens (**Fig 3.1**) (Stolz et al., 2014; Marshall and Vierstra, 2018). Many ATG8-interacting proteins, including cargo receptors, carry a conserved motif named the ATG8-interacting motif (AIM)—also known as the LC3-interacting motif (LIR) in animal systems—which follows a W/Y/F-X-X-L/I/V consensus sequence, surrounded by negatively charged residues (**Fig 3.1**) (Birgisdottir et al., 2013).

Unlike in yeast and metazoan systems, determining the importance of ATG8 specialization and cargo receptor specificity in defining the selectivity of the autophagy pathway has lagged behind in plants. Plant ATG proteins can generally be annotated based on similarity to yeast ATG proteins, which has enabled our understanding of the basic mechanics of plant autophagy through analogy to the yeast system (Thompson and Vierstra, 2005; Kellner et al., 2017; Chung et al., 2009; Xia et al., 2011; Zhou et al., 2015). Notably, a number of the plant autophagy proteins are expanded, implying mechanistic diversification of the plant system or sub-functionalization of individual components (Kellner et al., 2017; Xiong et al., 2005). In particular, previous phylogenetic analyses

revealed that the ATG8 gene family is expanded in plants and that plant ATG8s form well-supported family-specific clades, suggesting maintenance of distinct sets of ATG8 isoforms for over millions of years of evolution (Kellner et al., 2017). Plant ATG8 isoforms fall into two major clades, I and II, which share more sequence similarity with ATG8s from fungi and oomycetes, and animals, respectively (Kellner et al., 2017). Although the multiple expansions of the ATG8 protein family across plant lineages suggests the possibility of functional diversification, this hypothesis has not been experimentally challenged. To date no large-scale characterization of plant ATG8 interacting proteins has been undertaken.

In addition to our limited understanding of ATG8 functional diversification, only a handful of autophagy cargo receptors have been characterized in plants. These are limited to: homologs of the human receptor NEIGHBOR OF BRCA1 GENE 1 (NBR1), named AtNBR1 in *A. thaliana* (Svenning et al., 2011) and JOKA2 in tobacco (Zientara-Rytter et al., 2011); ATG8 INTERACTING 1 AND 2 (ATI1 and ATI2) (Honig et al., 2012); TRYPTOPHAN-RICH SENSORY PROTEIN (TPSO) (Vanhee et al., 2011); and REGULATORY PARTICLE NON-ATPASE SUBUNIT (RPN10) (Marshall et al., 2015). This short list pales in comparison to the number of autophagy cargo receptors characterized in metazoans, and further identification of plant cargo receptors is essential to understand the molecular mechanisms that underpin the specificity of parallel plant selective autophagy pathways.

In this chapter I aimed to define the interacting proteins for a complement of ATG8 isoforms, towards addressing a fundamental gap in knowledge regarding plant selective autophagy—the extent to which plant ATG8 isoforms are functionally specialized. I focused on the Solanaceae, a plant family that has experienced a sizeable expansion of ATG8 proteins (Kellner et al., 2017). I determined that the Solanaceae provide an excellent experimental system to study ATG8-interacting proteins, because this plant family includes economically important species, such as *Solanum lycopersicum* (tomato) and *Solanum tuberosum* (potato), as well as the model species *Nicotiana benthamiana*, a relative of tobacco (Derevnina et al., 2019). Of the solanaceous species, I was interested in studying the specialization of the potato ATG8s, in particular, due to the well-characterized intersection of the potato selective autophagy pathway and plant immunity (Dagdas et al., 2016).

In this work, I used immunoprecipitation coupled with mass spectrometry to investigate the extent to which the potato ATG8 isoforms are functionally specialized, and determine novel ATG8-associated proteins. Here, I present original insights into the plant selective autophagy pathway, and provide an invaluable resource for the autophagy research community.

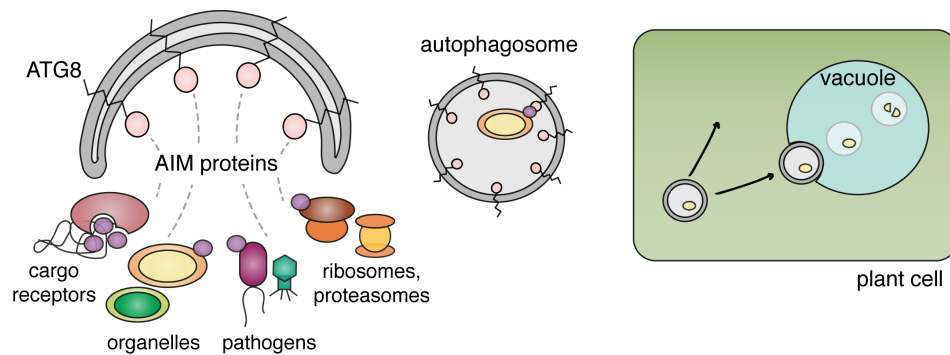


Figure 3.1 Schematic representation of the selective autophagy pathway

(Left) Cellular components—including cargo receptors, organelles, and invading pathogens—are taken up by the selective autophagy pathway. Some of these components interact directly with autophagy-related protein 8 (ATG8), which is embedded in the phagophore membrane, via ATG8-interacting motifs (AIMs); others interact in-directly, dependent on secondary modification. (Center, Right) Mature autophagosomes carrying cargo are trafficked to the vacuole for degradation, or elsewhere in the plant cell as part of a more general trafficking pathway.

3.2 Results and Discussion

3.2.1 *Solanum tuberosum* ATG8s have distinct interactor profiles

In the Solanaceae, ATG8s cluster into four clades (I–IV), one which belongs to the major clade II, one which belongs to the land plant-specific clade I subclade 1, and two of which belong to the flowering plant-specific clade I subclade 2 (Kellner et al., 2017). Potato encodes seven ATG8 isoforms that cluster in the Solanaceae ATG8 clades among close homologs from other species, two of which (ATG8-2.1 and ATG8-2.2) have the same amino acid sequence (**Fig 3.2**). Based on protein sequence divergence (**Fig 3.2C**), we hypothesized that these clade-specific ATG8s would interact with specific plant proteins and thus exhibit a degree of functional specialization.

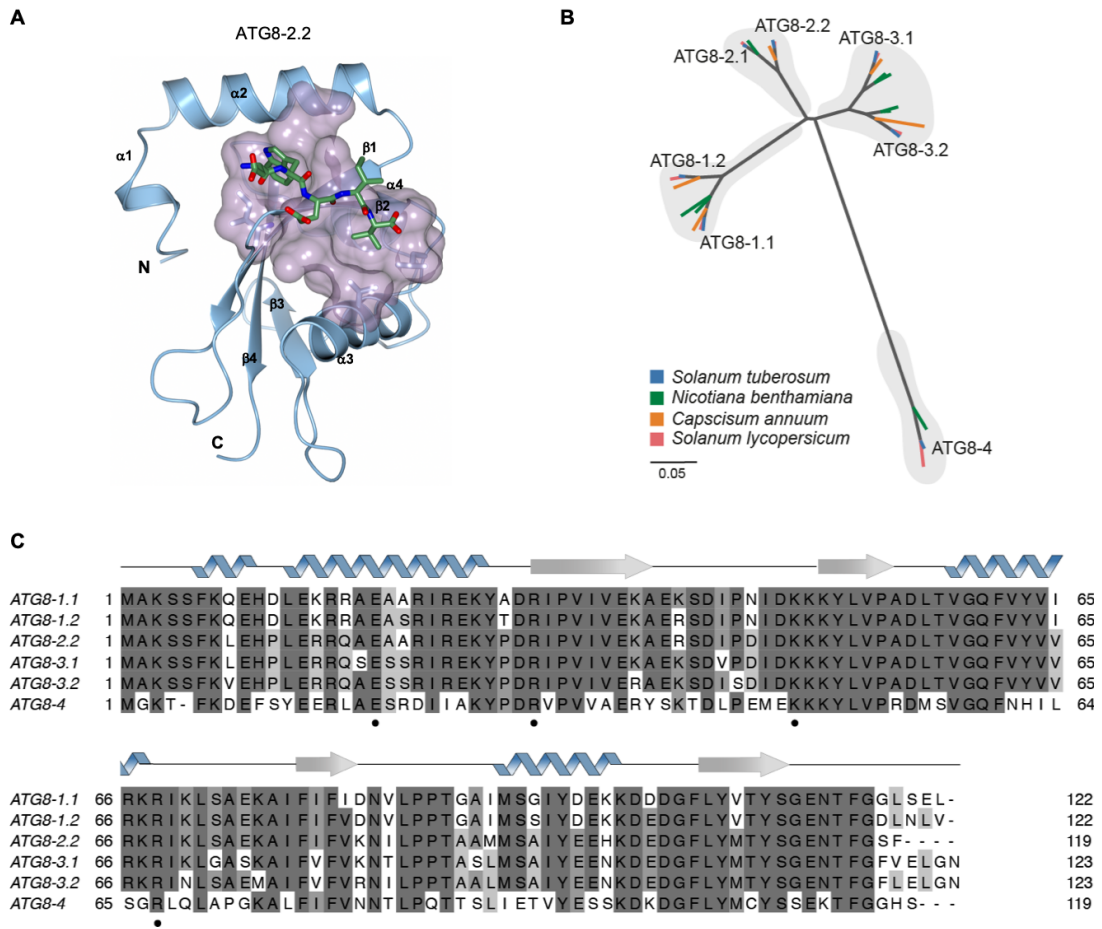


Figure 3.2 Potato ATG8s are sequence diverse

(a) Schematic representation of ATG8-2.2 with an ATG8-interacting motif peptide in the binding cavity, from Maqbool et al. 2015. The ATG8 molecular surface that contacts the AIM peptide is shown in purple. The α -helices, β -strands, N and C termini of ATG8-2.2 are labelled. (b) Orthologous relationships between solanaceous ATG8 isoforms. Unrooted maximum-likelihood phylogenetic tree of 29 ATG8 isoforms with gray shading highlighting clades, and colors indicating plant species. The tree was calculated in MEGA7 (Kumar et al., 2016) from a 369 nucleotide alignment (MUSCLE (Edgar, 2004) codon-based). The bootstrap supports of the major nodes are indicated. The scale bar indicates the evolutionary distance based on nucleotide substitution rate. (c) Alignment of all *S. tuberosum* ATG8s (MUSCLE (Edgar, 2004), visualized with Jalview). The protein model above corresponds to the ATG8-2.2 structure, and the residues that form electrostatic contacts with AIMs are marked below (•). ATG8s are named as in (a); only ATG8-2.2 is included in the alignment, as both ATG8-2.1 and ATG8-2.2 have the same amino acid sequence.

To investigate this hypothesis, we determined the interactor profiles of the six potato ATG8 proteins using immunoprecipitation (IP) coupled with mass spectrometry (MS) following transient expression in *N. benthamiana*. Our interactome analyses included two replicates and revealed 621 proteins, as defined by a unique *N. benthamiana* accession, that associated with at least one ATG8 isoform, but not with the control, green fluorescent protein (GFP) (**Fig 3.3; Table A.2.1**). Consistent with the hypothesis, the potato ATG8s associated with unique complements of proteins with varying degrees of similarity, with ATG8-4 exhibiting the most selectivity (**Fig 3.3**). By heatmap (**Fig 3.3A**) the finer differences in interactor profiles are more difficult to appreciate, but the patterns are striking when viewed by correlation matrix (**Fig 3.3B**). It should be noted that IP-MS data is only semi-quantitative, so peptide count values cannot necessarily be taken as a proxy for association strength; however, peptide count values can be compared between bait proteins for any given interactor.

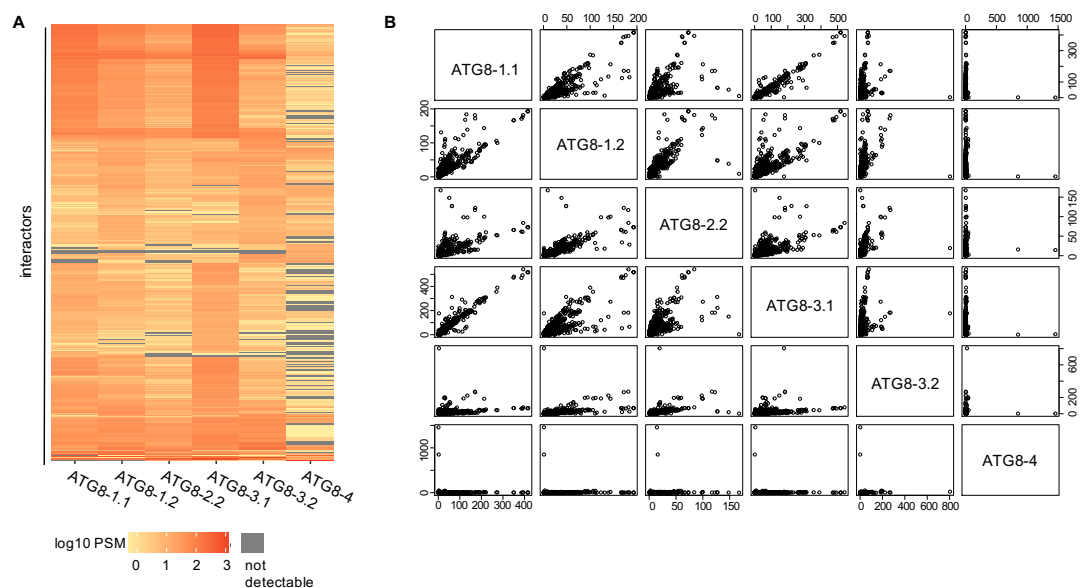


Figure 3.3 Potato ATG8 isoforms have distinct protein interaction profiles

(a) Heatmap showing the interaction profiles of all ATG8 isoforms. The average PSM data from two replicates was log₁₀ normalized, and then used to construct a hierarchically clustered heatmap with the scale as shown. (b) The average PSM values for each ATG8 isoform in the interactome dataset (621 interactors) were used to generate a correlation matrix, showing distinct interaction profiles for each ATG8, with varying degrees of overlap. Experiment performed by a collaborator.

The ATG8s showed differential interactions with a number of protein sets grouped by predicted cellular compartments (**Fig 3.4.A**) and biological processes (**Fig A.1.2**). Although ATG8-4 has a reduced number of interactors in the global analysis (**Fig 3.3**), grouping the proteins shows that ATG8-4 still interacts with predicted autophagosome membrane and microtubule proteins to a similar level as other ATG8s (**Fig 3.4.A**), suggesting that the selectivity may be more towards predicted cargo. Relatedly, examining interactors grouped based on predicted biological processes, it's clear that proteins involved in autophagy are, on average, similarly common to all ATG8s (**Fig A.1.2**). Another trend that emerges from looking at the network representation of the data is that ATG8-1.1 and ATG8-3.1 associate with proteins predicted to be involved in translation stronger than all other ATG8s (**Fig A.1.2**). The translation machinery could represent background contamination, as these proteins are highly abundant in the cell (Carroll, 2013), but the near-absence of these proteins in the pull-downs of the other ATG8s would suggest that the observation may be biologically relevant. Overall, although parsing the data in this way reveals interesting trends, intrinsic limitations with this analysis preclude more definitive conclusions. These limitations include that the protein groups represent averages of semi-quantitative data, and that gene ontology terms were predicted based on homology to *A. thaliana* proteins.

However, in looking at the interaction between the ATG8 isoforms and the autophagy machinery in more detail, more striking patterns emerge, particularly for ATG8-4 (**Fig 3.4.B**). Compared to the other ATG8s, ATG8-4 interacts very weakly with proteins involved in phagophore initiation (ATG1) and ATG8 processing for phosphatidylethanolamine (PE) conjugation (ATG4) (**Fig 3.4.B**). Interestingly, both ATG8-3.2 and ATG8-4 interact stronger with autophagy proteins that are involved in the final transfer of ATG8 to PE (ATG16 and ATG5). It is tempting to speculate that the differential interactions between the ATG8 isoforms and these core autophagy machinery proteins reflect varying mechanisms for ATG8 membrane insertion.

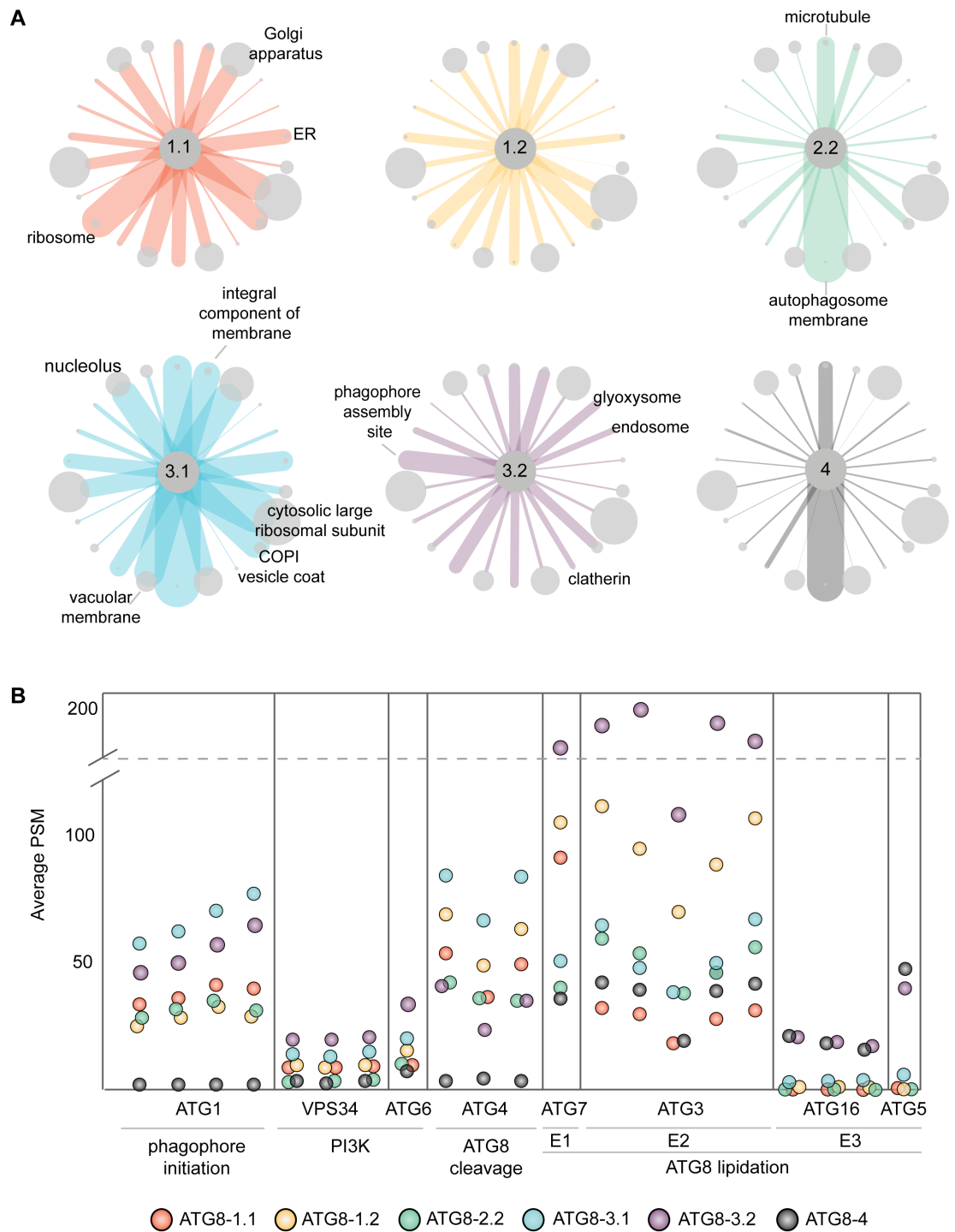


Figure 3.4 Potato ATG8s differentially interact with proteins from different cellular compartments, including the core autophagy machinery

(A) Network representation of the interactions between ATG8s and protein groups defined by gene ontology (GO) cellular compartment annotations. Proteins were grouped based on the cellular compartment annotations, and a subset of groups were chosen for representation. The sizes of the nodes are scaled to the number of interactors in each respective group, and the edges

are weighted to the average PSM values for all the interactors in each respective group for each ATG8. Nodes are labelled where the average PSM value is most differential compared to the other ATG8s. (B) Interaction between ATG8 isoforms and core autophagy (ATG) machinery. Representation of the average PSM values mapping to the ATG proteins found in the interactome for each ATG8 isoform. Each of the ATG protein homologs are shown separately; ATG proteins are grouped based on the process they are involved in, including: phagophore initiation, phosphatidylinositol-3-kinase (PI3K) complex, ATG8 cleavage, as well as the various steps of the ATG8 conjugation to phosphatidylethanolamine (PE), analogous to ubiquitin conjugation (E1, E2, E3).

3.2.2 Validation of the potato ATG8 interactome

3.2.2.1 *The underlying IP-MS data is of high quality*

As a first check to assess the quality of the underlying data, I determined that the levels of bait protein were relatively equal across all samples by looking at the peptide values corresponding to green fluorescent protein, the tag common to all of the expressed constructs. Then, as previously mentioned, the raw IP-MS data was filtered—removing all proteins that interacted with green fluorescent protein above a strict threshold—to exclude nonspecific interactors, resulting in the final list of 621 proteins used for further analysis. With this interactor list, I observed that the PSM values for the two biological replicates were positively correlated for each construct (R^2 range 0.622–0.9845), with ATG8-1.2 and ATG8-2.2 showing the most variability between replicates (**Fig A.1.3**). The correlation between the replicates confirms the reproducibility of the results and indicates that the data is of high quality.

3.2.2.2 *High degree of shared interactors with the human ATG8 interactome*

Although this is the first large-scale investigation of plant ATG8 interactors, previous analyses have been performed in metazoans (Behrends et al., 2010; Le Guerroue et al., 2017; Wild et al., 2014). About half (297/621 proteins, 48%) of the proteins in our ATG8 interactome had closely related proteins within the human ATG8 interactome defined by Behrends et al. (2010) using IP-MS, the most methodologically comparative study (**Fig A.1.4**). This degree of overlap is markedly higher compared to random sets of proteins of the same size (66/621 proteins, 10%) (**Fig A.1.4**). The overlapping proteins included other autophagy related (ATG) proteins, such as ATG4 and ATG7; homologs of the cargo receptor NBR1; cytoskeleton proteins, including actin and tubulin; and a large

number of housekeeping proteins, including ribosomal and proteasomal machinery (**Table A.2.2**). In addition to confirming the reliability of the interactors captured in this experiment, as well as the potential evolutionary relationship between ATG8 cargoes, this high degree of overlap may also reflect the consistency in the types of proteins detected by IP-MS (**Table A.2.2**).

3.2.2.3 Some proteins in the ATG8 interactome associate non-specifically

Previous studies have characterized the common false positive proteins observed in immunoprecipitation experiments (Trinkle-Mulcahy et al., 2008; Mellacheruvu et al., 2013). Contaminants often include highly abundant proteins, such as translation elongation factors and histones, as well as proteins associated with RNA functions (Mellacheruvu et al., 2013). Although we used green fluorescent protein (GFP) as a negative control to identify nonspecific interactions in our experiment, this approach may not capture all contaminants, especially since our bait proteins are membrane-associated. The ATG8 interactome features a number of highly abundant proteins in plant leaf tissue, including ribosome and proteasome subunits. However, these components are also known to undergo autophagic degradation (Marshall et al., 2015; An and Harper, 2018), making the distinction between possible contaminants and cargo more challenging.

As a check, I tested the interaction specificity of two abundant proteins present in the interactome—60s ribosomal protein I21-1-like (r_60s_I21) and 26s proteasome regulatory subunit 6a (p_26a)—via co-immunoprecipitation. Both proteins were found to associate with free GFP, in addition to ATG8-2.2 and ATG8-4, indicating that these interactors may be non-specific (**Fig 3.5**). However, this does not preclude the possibility that other ribosomal and proteasomal proteins may form specific interactions with ATG8, in a condition-dependent manner. This highlights the need to validate interactions observed in IP-MS, and suggests that a plant-specific repository for common background contaminants would improve to the interpretation of large-scale IP-MS results.

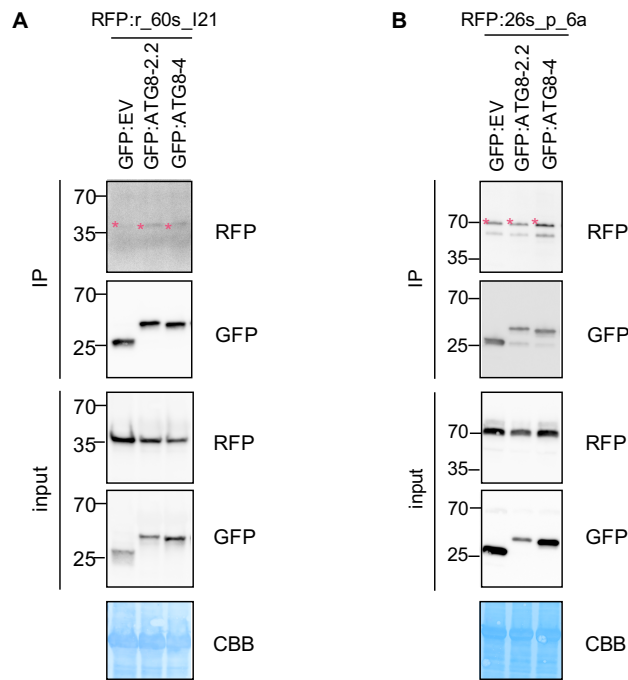


Figure 3.5 Non-specific interaction of two ATG8 interactome proteins

Co-immunoprecipitation experiment between candidate ATG8-interacting proteins 60s ribosomal protein I21-1 (r_60s_I21) and 26s proteasome regulatory subunit 6a (26a_p_6a) and GFP:EV and ATG8s. (a) RFP: r_60s_I21 was transiently co-expressed with GFP:EV, GFP:ATG8-2.2, and GFP:ATG8-4. (b) RFP:26a_p_6a was transiently co-expressed with GFP:EV, GFP:ATG8-2.2, and GFP:ATG8-4. For (a-b), immunoprecipitates (IPs) were obtained with anti-GFP antiserum and total protein extracts were immunoblotted with appropriate antisera (listed on the right). Stars indicate expected band sizes.

3.2.3 The *S. tuberosum* ATG8 interactome contains known ATG8-interacting proteins, novel autophagy-associated proteins, and organellar proteins

3.2.3.1 Known ATG8-associated proteins

Four of the endogenous *N. benthamiana* ATG8s were present in the interactome (**Table A.2.1**). One of the ATG8s, NbATG8-4, exhibited a selective interaction pattern, interacting almost exclusively with ATG8-4, its closest homolog (**Fig 3.6**), supporting a model that autophagosomes may carry different populations of ATG8s. Although this is not the case for potato and *N. benthamiana* ATG8-4 isoforms, some clade II ATG8s lack amino acid residues after the terminal glycine, rendering them ‘pre-activated’ for membrane insertion without processing (Kellner et al., 2017). This could provide a mechanistic understanding for how the autophagy machinery discriminates between

ATG8 isoforms at the stage of membrane insertion, but additional discriminatory mechanisms must exist for other ATG8s, such as the Solanaceae ATG8-4 isoforms, that do not differ in their processing requirements but appear to self-segregate.

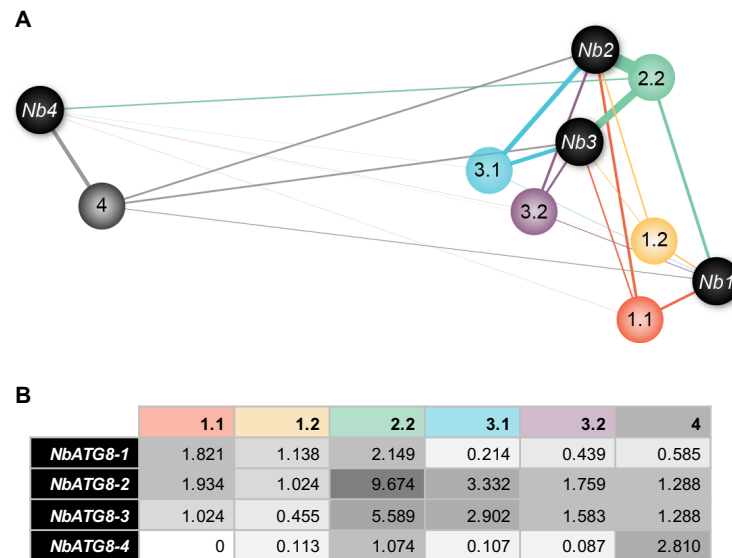


Figure 3.6 Network representation of interaction between potato ATG8s and endogenous *N. benthamiana* ATG8s

(a) Network representation of the interactions between potato ATG8s and endogenous *N. benthamiana* ATG8s. The edge widths are weighted to the GFP normalized peptide counts shown in (b). The spatial relationships between the ATG8s are scaled to amino acid sequence identity, with more sequence related ATG8s clustering together, using Cytoscape (Shannon et al., 2003). The four *N. benthamiana* ATG8s present in the ATG8 interactome dataset—labelled here NbATG8-1- NbATG8-4—are correspondingly labelled in Fig A.1.1 for reference.

In addition, the ATG8 interactome contains homologs of many of the known ATG8-associated proteins, such as members of the core autophagy machinery (ATG1, VPS34, ATG6, ATG4, ATG7, ATG3, ATG16, ATG5) (**Fig 3.4.B**) and the autophagy receptor NBR1/JOKA2 (**Table A.2.1**). The dataset also captured a number of vesicle trafficking-related proteins, including Rab GTPases, Rab GTPase activating proteins, ESCRT complex subunits, myosins, clathrin and coatamer subunits (**Table A.2.1**), which is consistent with the proteins identified in interactome studies using human ATG8 isoforms (Behrends et al., 2010; Wild et al., 2014). Interestingly, multiple homologs of

three of these proteins—myosin XII (six proteins), myosin-binding protein (six proteins), and Rab11 family-interacting protein (four proteins)—were identified in the interactome and shown to selectively associate with the ATG8 isoforms (**Fig 3.7**). All of these proteins consistently showed no interaction with ATG8-4, but interacted quite strongly with the other ATG8s, with the Rab11 family-interacting proteins showing the most striking differential (**Fig 3.7**).

3.2.3.2 Novel ATG8-associated proteins

I found several hitherto unknown ATG8-associated proteins in the interactome, a number of which have known roles in autophagy. One of these proteins, early endosome antigen homolog, is a tethering factor that provides specificity and promotes membrane fusion in intracellular membrane trafficking, including autophagy (Tooze et al., 2014)(**Table A.2.1**). Altogether, there were nine different early endosome antigen homologs identified in the interactome, and all of these proteins showed a selective interaction pattern, with no detectable interaction with ATG8-4 (**Fig 3.7**). In addition, I identified multiple phosphatidic acid phosphatases, a homolog of which has been identified to be involved in regulating autophagic flux in mice (Zhang, Verity, and Reue 2014)(**Table A.2.1**). I also identified multiple cytosolic glyceraldehyde-3-phosphate dehydrogenase (GAPDH) enzyme homologs, which are known to interact with ATG3 to regulate autophagy (Han et al., 2015), although no direct interaction with ATG8 has previously been described (**Table A.2.1**). Lastly, the interactome featured a number of catalase enzymes, which genetic evidence suggests are selectively degraded by the cargo receptor NBR1/JOKA2 (Zhou et al. 2014) (**Table A.2.1**).

These novel ATG8-associated proteins all have a known connection to autophagy in metazoan systems. However, there are a large number of proteins in this list that do not have a known connection to autophagy—perhaps hundreds of proteins—and a subset of these may represent plant-specific autophagy components. I noted the presence of a dual-specificity tyrosine regulated protein kinase (also known as DYRKs), which have not previously been implicated in autophagy, but are involved in cell cycle control and various stress responses in mammalian systems (Yoshida, 2008; Becker, 2012)(**Table A.2.1**). The interactome also contained multiple 14-3-3 homologs (9 proteins), which are important proteins in signal transduction pathways regulated by phosphorylation (DeLille et al.,

2001). Interestingly, these proteins were among some of the few proteins to preferentially interact with ATG8-4 (**Fig 3.7**). Although human 14-3-3 proteins are known to bind TOR and VPS34, and thus are connected to the autophagy pathway (Pozuelo-Rubio, 2012), this has not been shown for plant 14-3-3 family proteins.

The other novel ATG8-associated proteins identified in the interactome shown to selectively interact with ATG8-4 were NADP-dependent d-sorbitol-6-phosphate dehydrogenase (S6PDH) and lecithin-cholesterol acyltransferase (LCAT) (**Fig 3.7**). S6PDH is involved in the synthesis of sorbitol-6-phosphate, a key intermediate in the synthesis of sorbitol, a sugar associated with osmotic stress (Wang, 1999). The potential turnover of S6PDH via ATG8-4-mediated selective autophagy could be a potential mechanism by which the pathway senses and responds to cellular stress. Moreover, the *Arabidopsis* homolog of the LCAT protein in the IP-MS dataset was found to act as a cytosolic phospholipase A (Chen, 2012). In plants, phospholipase A proteins participate in plant signal transduction for growth, as well as defense (Chandra, 1996); as such, an interaction between ATG8-4 and LCAT could be involved in regulating or carrying out these process via selective autophagy trafficking or turnover.

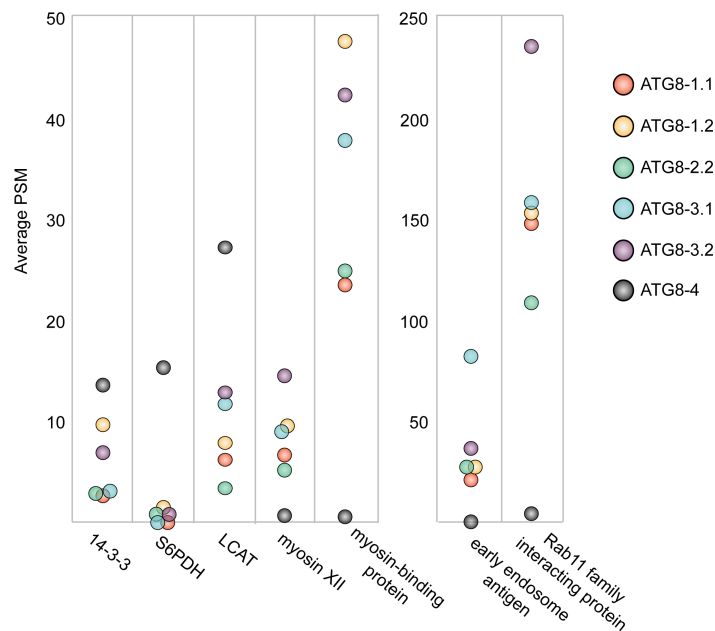


Figure 3.7 Potato ATG8-4 shows selectivity towards a subset of substrates

Potato ATG8 substrate specificity. For each group of related proteins (14-3-3, (eight proteins)); NADP-dependent d-sorbitol-6-phosphate dehydrogenase (S6PDH, (four proteins)); lecithin-

cholesterol acyltransferase (LCAT, (one protein)); myosin XII (six proteins); myosin-binding protein (six proteins); early endosome antigen (nine proteins); and Rab11 family-interacting protein (four proteins) found to show a differential interaction with ATG8-4, the average PSM value was calculated across the group for each ATG8 isoform. These values were then plotted, with two separate graphs to optimize the scale.

Using the potato ATG8 interactome to identify additional plant selective autophagy receptors would further increase the robustness of this dataset, and additional studies will have to determine whether any of these proteins are involved in selective cargo recruitment. Much of what we know about plant autophagy derives from analogy to other systems, so investigating plant-specific autophagy components will provide an opportunity to discover how this pathway differs in plants. Overall, for researchers trying to identify novel autophagy-related proteins, this dataset provides a valuable discovery resource, and will hopefully serve as the foundation for more in-depth studies.

3.2.3.3 Organellar proteins

I identified a number of proteins in the interactome that are predicted to localize to various organelles, making this dataset a useful resource for future functional studies interrogating organelle recycling (**Fig 3.4**). Autophagic turnover of organelles is critical for the maintenance of cellular homeostasis by preserving organelle integrity and number despite varying conditions (Anding and Baehrecke, 2017). In plants, organelle-specific autophagy has been found to clear chloroplasts, proteasomes, mitochondria, ribosomes, the endoplasmic reticulum, and peroxisomes (Anding and Baehrecke, 2017; Marshall and Vierstra, 2018), although molecular details remain largely obscure.

For example, the selective removal of damaged chloroplasts by autophagy, termed ‘chlorophagy’, happens both during leaf senescence and after photoinhibition, which is when light levels exceed the capacity of the photosynthetic apparatus (Nakamura and Izumi, 2018). However, how damaged chloroplasts are recruited to the core autophagy machinery, and whether chlorophagy involves cargo receptor proteins, remain open questions (Anding and Baehrecke, 2017). This dataset includes a number of predicted chloroplast-localized proteins, such as thioredoxins, chlorophyll biosynthesis enzymes, and proteins involved in weak chloroplast movement under blue light, which may provide

clues about the mechanisms underlying chlorophagy. Future studies could take a comparative proteomics approach under the relevant stress conditions to further narrow down candidate proteins involved in chloroplast recruitment and recycling by selective autophagy.

3.2.3.4 ATG8-interacting motif (AIM) containing proteins

Many proteins that directly interact with ATG8s do so via an ATG8-interacting motif (AIM), which dock into the hydrophobic surface of ATG8. Around 40% of all the interactors in the interactome are predicted to contain AIMs. A majority (73%) are conserved in either *Arabidopsis thaliana* or *Marchantia polymorpha*, an early diverging land plant that occupies an ideal phylogenetic position for reconstructing ancient evolutionary changes (Rich and Delaux, 2018). The high proportion of evolutionarily conserved AIMs suggests the utility of this dataset in furthering selective autophagy studies in plants, insofar as it underscores that many of the captured proteins may be direct ATG8 interactors.

Considering the short length of the AIM, at just five core amino acid residues, bioinformatic prediction of the motif within a large protein dataset will invariably result in a number of false positives. However, assuming that ATG8 interaction is a conserved protein property, we posit that integrating the parameter of AIM conservation, both by position and sequence, helps to delimit true AIM sequences. A more advanced approach than the one taken herein would also consider the overall amino acid conservation of a given protein when assessing AIM conservation, such as to further differentiate potentially functional AIMs. Additionally, predicting structurally disordered regions would improve the ability to infer true AIMs, as ATG8 binding requires a flexible AIM conformation (Noda et al., 2010). Although the prediction and evaluation of AIMs is important to determine direct ATG8-interacting proteins, interactors without AIMs may still directly interact with ATG8s, via non-canonical AIMs (von Muhlinen et al., 2012) or other ATG8-binding motifs, such as the ubiquitin-interacting motif (UIM) (Marshall et al., 2019).

3.2.3.5 Limitations of the results

It is important to note that the ATG8 interactome described herein reflects plant autophagic cargo under specific conditions, *Agrobacterium* infiltration and ATG8 overexpression, which likely have an effect on the observed ATG8 proteomic profiles. Future work describing plant ATG8 interactomes under alternate conditions—such as basal cell maintenance, using transgenic epitope-tagged ATG8-expressing lines, as well as a range of biotic and abiotic stress responses—would add to our understanding of how different ATG8 isoforms contribute to the dynamics of the selective autophagy pathway. Using quantitative proteomics in these studies, such as tandem mass tag (TMT) labelling, would also expand the breadth of the conclusions that are able to be drawn, providing information on the relative abundance of different interactors with accuracy (Zhang and Elias 2017). With this in mind, I designed an additional experiment to use TMT labelling proteomics to describe the potato ATG8 interactome and prepared a considerable number of experimental replicates, but technical challenges with execution of the method prevented meaningful interpretation.

3.2.4 ATG8 functional diversification—a broader view

A number of studies—both large-scale, and at the level of individual proteins—have shown that human ATG8s are functionally specialized. The interactor profiles of human ATG8 isoforms has been explored using IP-MS (Behrends et al., 2010; Wild et al., 2014) and proximity labeling proteomics (Le Guerroue et al., 2017). These studies revealed limited overlap between different ATG8 isoforms, particularly with proximity labeling proteomics, which primarily identifies cargoes within various ATG8 autophagosomes (Le Guerroue et al., 2017). In addition, mechanistic studies of ATG8-interacting proteins support specialization of human ATG8 isoforms. For example, the cytoplasmic bacteria receptor NDP52 specifically binds the ATG8 protein LC3C (von Muhlinen et al., 2012), whereas the autophagy adaptor PLEKHM1, the autophagy receptor ALFY, and the tumor necrosis factor Fn14 prefer to bind a different ATG8, GABARAP (McEwan et al., 2015; Winer et al., 2018; Lystad et al., 2014). A recent study even revealed the GABARAP interaction motif (GIM) that mediates the high affinity binding of GABARAP-interacting proteins (Rogov et al., 2017). Moreover, a recent study has approached specificity from the side of interacting proteins, showing that residues within the core ATG8-interacting

motif (in mammals, LC3-interacting region or LIR) and adjacent C-terminal region are critical for binding to the GABARAPs (Wirth et al., 2019).

Our finding that ATG8s differentially interact with different types of cargo is consistent with the view that ATG8s directly contribute to functional diversification of selective autophagy pathways in plants, as in mammals. Considering that some plant species have over 20 ATG8 isoforms, compared to 6 in humans, it is interesting to speculate the extent to which ATG8s have functionally specialized in different plant lineages, and whether the expansion of ATG8s in certain lineages could be associated with specific life history strategies or environmental pressures. A large-scale phylogenomic analysis of ATG8 expansion could generate interesting hypotheses and ultimately broaden our understanding of the role of selective autophagy in plants.

3.3 Conclusions

Overall, the IP-MS screen indicated that solanaceous ATG8s have distinct interactor profiles. Although these results fit well within the context of studies carried out with human ATG8s, they go against the prevailing trend in plant autophagy studies to treat ATG8 isoforms as functionally redundant. Our results tell a different story—that each ATG8 isoform mutant will be deficient in its own way. In this, the results of this study complicate the current view of plant selective autophagy, and add a level of nuanced understanding that should recolor conclusions from previous studies and be considered in the design of future experiments. Our evidence that plant ATG8s are functionally specialized not only warrants more careful consideration of studies involving ATG8 isoform mutants, but the interactome provides a strong foundation for follow-up studies to characterize novel autophagy-associated proteins. Through these multiple outcomes, this ATG8 interactome dataset will hopefully expand our understanding of plant selective autophagy.

Chapter 4: N-terminal β -strand underpins biochemical specialization of a plant ATG8 isoform²

4.1 Introduction

One of the most compelling lines of biological research is that which aims to unravel the molecular mechanisms that underpin complex functions and, at the same time, discover how evolution has shaped what we seek to understand. Following the observation that plant ATG8 isoforms are functionally specialized, the next question felt obvious: How? Or, more specifically: What are the structural determinants of plant ATG8 substrate specificity, and how have these features evolved?

The core ATG8 structure is composed of four α -helices and four β -strands, forming a β -grasp fold which is shared with ubiquitin and other ubiquitin-like modifiers (UBLs) (Burroughs et al., 2012). Compared to other UBLs, ATG8s also have a variable N-terminal extension, which mediates the growth of the nascent autophagosome via fusion of ATG8-containing vesicles (Slobodkin and Elazar, 2013; Noda et al., 2010; Klionsky and Schulman, 2014). The ATG8 surface features two hydrophobic pockets termed the W-site and L-site, respectively—so-named for the ATG8-interacting motif (AIM) residues that they accommodate—that serve as the major docking site for ATG8-interacting proteins (Maqbool et al., 2016). This interface corresponds to what is referred to as the ' α/β groove' in other UBLs, and it is also a well-characterized interaction interface in small ubiquitin-like modifier (SUMO) isoforms (Hecker et al., 2006).

A previous study solved the crystal structure of a potato ATG8 isoform, ATG8-2.2, in complex with the AIM from PexRD54, a secreted virulence effector from the Irish potato famine pathogen *Phytophthora infestans* (Maqbool et al., 2016). Previous work had

² Most parts of this chapter have been published in the following literature: Zess, E. K., Jensen, C., Cruz-Mireles, N., De la Concepcion, J. C., Sklenar, J., Stephani, M., ... Dagdas, Y. F. (2019). N-terminal β -strand underpins biochemical specialization of an ATG8 isoform. *PLOS Biology*, 17(7), e3000373.

The permission to reuse the contents is under the Creative Commons Attribution License.

demonstrated that, during *P. infestans* infections of potato, PexRD54 binds ATG8-2.2 via a C-terminal AIM, subverting the function of selective autophagy in plant immunity and re-routing autophagosome trafficking towards the host-pathogen interface (Dagdaz et al., 2016; Dagdas et al., 2018). The structure of ATG8-2.2 in complex with the PexRD54 AIM showed that ATG8-2.2 adopts a very similar structure to that observed for ATG8s from other organisms, including the human ATG8s GATE-16 and GABARAP (Maqbool et al., 2016). Additionally, the PexRD54 AIM was shown to dock within the ATG8 hydrophobic pockets, similar to the yeast and metazoan ATG8-AIM complexes (Maqbool et al., 2016). In this interaction, the AIM adopts a β -strand structure that extends the ATG8 β -sheet (Ichimura et al., 2008; Noda et al., 2008; Klionsky and Schulman, 2014). It was also shown that PexRD54 has a ten-fold higher binding affinity towards ATG8-2.2 compared to the clade II ATG8-4 isoform, and it was hypothesized that subtle structural differences in the hydrophobic pockets may be responsible for this interaction differential (Dagdaz et al., 2016; Maqbool et al., 2016).

We leveraged our unique grounding in effector biology, and our detailed understanding of the PexRD54-ATG8 interaction, and used PexRD54 as a probe to dissect the structural elements within potato ATG8s that determine binding specificity to AIM-containing substrates (Dagdaz et al., 2016; Maqbool et al., 2016). In recent years, pathogen effectors have emerged as molecular probes for unravelling host processes (Win et al., 2012). Studying effectors has helped uncover novel components of other cellular processes—such as plant immune signaling, intracellular trafficking, and transcription—as well as characterize the molecular functions of these components (Lee et al., 2013; Bozkurt et al., 2011; Feng and Zhou, 2012; Mitchum et al., 2013). Additional studies have used effectors as tools to rewire host immune signaling pathways, as well as probes to study aspects of primary metabolism (Wei et al., 2012; Biemelt and Sonnewald, 2006). As such, this work provides a further example of the utility of using an effector-guided approach to answer fundamental questions about plant biology.

4.2 Results and Discussion

4.2.1 ATG8 isoforms show differential binding to PexRD54

To get a sense of the range of association strengths between potato ATG8 isoforms and PexRD54, I tested the six ATG8 isoforms for association with PexRD54 in *in planta* co-immunoprecipitation (co-IP) experiments. The ATG8 isoforms exhibited a range of binding strengths with PexRD54, showing that ATG8s selectively bind the same substrate (**Fig 4.1.A**). ATG8-2.2 exhibited the strongest interaction with PexRD54, followed by ATG8-3.1 and ATG8-3.2, then ATG8-1.1 and ATG8-1.2, and finally ATG8-4, which showed the weakest interaction. This trend in association strengths was highly reproducible across replicates—however, co-IP results are, at best, only semi-quantitative.

To quantify these affinity differences *in vitro*, a number of collaborators on the project, led by Abbas Maqbool, expressed and purified all potato ATG8 isoforms from *E. coli*, and then tested these ATG8s for binding with the PexRD54 AIM peptide using isothermal titration calorimetry (ITC) experiments (**Fig 4.1.B**). In their experiments, the ATG8 isoforms interacted with the AIM peptide with varying degrees of strength, ranging from 29 nM to 287 nM (**Fig 4.1.C**). Overall, the ITC affinity measurements correlated with the trends in binding strength that I observed in co-IP experiments. Considering that the co-IP experiments were carried out with the full length PexRD54 protein, and the ITC experiments with only the PexRD54 AIM peptide, this correlation suggests that the AIM peptide alone is sufficient to recapitulate ATG8 binding specificities. In both methods, ATG8-2.2 and ATG8-4 displayed the greatest difference in PexRD54 binding strength, in a range that is consistent with our previous findings (**Fig 4.1**).

Previous studies investigating ATG8-AIM peptide complexes have shown that both hydrophobic and electrostatic interactions underlie interaction specificity (Cheng et al., 2016; Noda et al., 2008; Wu et al., 2015; Lystad et al., 2014). However, all of the ATG8 residues involved in forming electrostatic interactions with AIM residues are conserved between the potato ATG8 isoforms (**Fig A.1.2**), suggesting that hydrophobic interactions drive their marked differences in association with PexRD54. Future studies should address the balance between these two interaction forces in contributing to the substrate specificity of other plant ATG8 isoforms which do exhibit variation at residues involved in electrostatic interactions with the AIM.

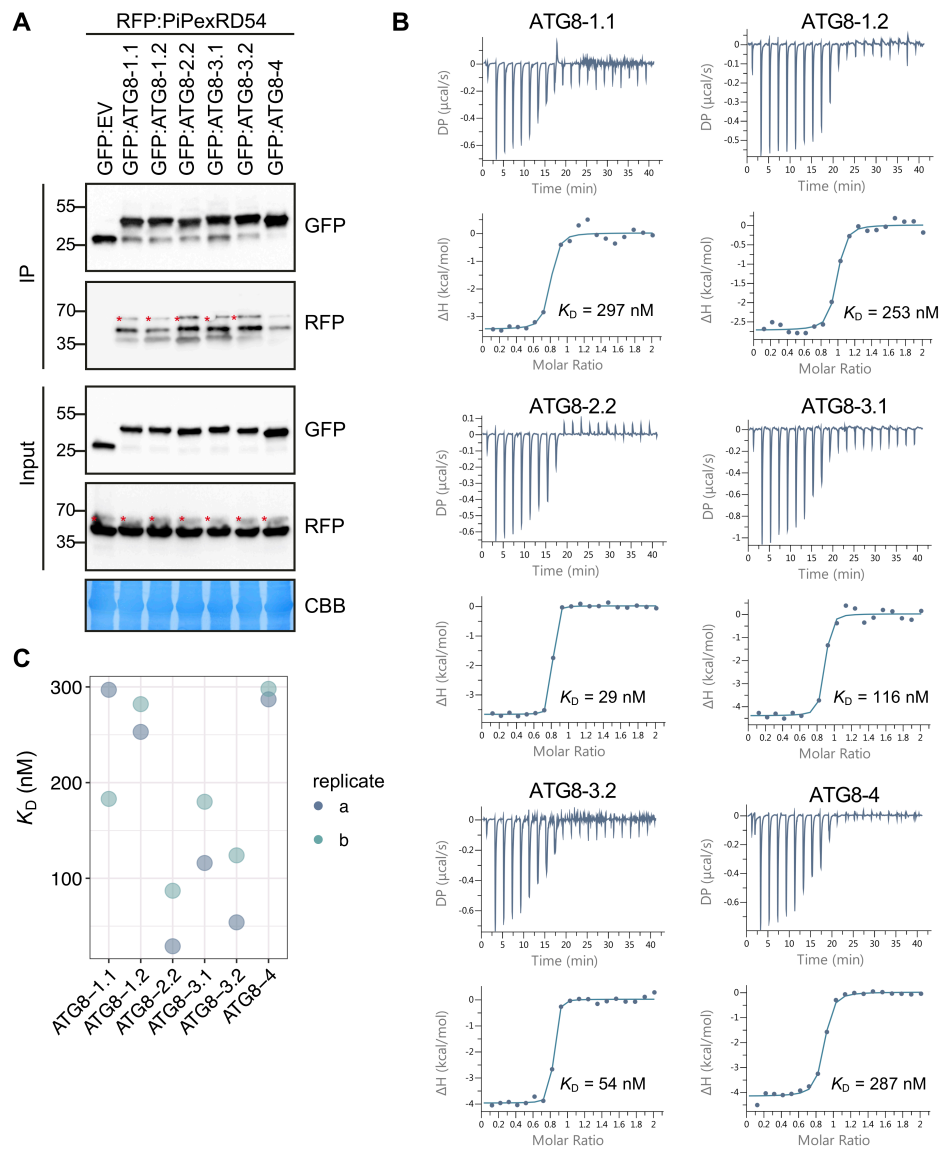


Figure 4.1 ATG8 isoforms show differential binding to PexRD54

(a) Co-Immunoprecipitation experiment between PexRD54 and all potato ATG8 isoforms. RFP:PiPexRD54 was transiently co-expressed with GFP:EV and all potato GFP:ATG8s. Immunoprecipitates (IPs) were obtained with anti-GFP antiserum and total protein extracts were immunoblotted with appropriate antisera (listed on the right). Stars indicate expected band sizes.

(b) The binding affinities between ATG8 isoforms and the PexRD54 AIM peptide were determined using isothermal titration calorimetry (ITC). The top panels show heat differences upon injection of peptide ligands and lower panels show integrated heats of injection (\bullet) and the best fit (solid line) to a single site binding model using MicroCal PEAQ-ITC analysis software

(c) Chart summarizing the K_D value for each interaction across two replicates and highlighting variation within the replicates. (b-c) Experiments performed by collaborators, led by Abbas Maqbool.

4.2.2 The first β -strand of ATG8 underpins discriminatory binding to PexRD54

To further investigate the ATG8 structural features that underpin discriminatory binding to PexRD54, and by proxy AIM-containing substrates, we generated chimeric proteins between ATG8-2.2 and ATG8-4 (**Fig 4.2.A**). We sequentially replaced ATG8-4 domains, the weakest PexRD54 interactor, with the corresponding domains from ATG8-2.2, the strongest interactor. Altogether we obtained a suite of eight ATG8 chimeras (Swaps 1- 8), and I assayed these for gain-of-binding to PexRD54 (**Fig 4.2.B**). In co-IP experiments, ATG8 chimera swap 3 (ATG8-4-S3), encompassing the first β -strand (β 1), consistently restored binding to PexRD54 (**Fig 4.2.B**). ATG8 chimera swap 1 (ATG8-4-S1) showed weak interaction with PexRD54, although this result was not consistent across replicates (**Fig 4.2.B**).

To validate these results using quantitative assays, a collaborator on the project, Abbas Maqbool, purified ATG8-4-S1 and ATG8-4-S3 from *E. coli* and tested for binding to both PexRD54 full length proteins and the PexRD54 AIM peptide (**Fig 4.2.C**). Consistent with the co-IP results, isothermal titration calorimetry measurements showed that the chimera ATG8-4-S3 bound to PexRD54 full length protein as well as the AIM peptide with a similar affinity as ATG8-2.2, whereas ATG8-4-S1 bound weakly (**Fig 4.2.C**). They also repeated these experiments and obtained similar results (**Fig 4.2.D**). Together, our results indicate that the ATG8 region encompassing the first β -strand (β 1) is crucial for binding to PexRD54, specifically via this substrate's AIM.

The first β -strand is central to the formation of the core β -grasp fold (**Fig 4.3**), and is positioned behind the W- and L-sites, shaping their precise contours. One of the residues in this region, arginine-29 (arginine-28 in ATG8-4), directly contacts the PexRD54 AIM, and diversity at the analogous residue in human ATG8s has been shown to be involved in preferential substrate binding (Rogov et al., 2017). However, besides this residue known to be important for AIM binding, this region has not been previously implicated in ATG8 binding specificity. This raises the possibility that the involvement of the first β -strand in discriminatory cargo binding is a plant-specific—or, even a Solanaceae-specific—innovation. It will be interesting to see if future studies in other systems, plant or otherwise, implicate this region in ATG8 binding specificity.

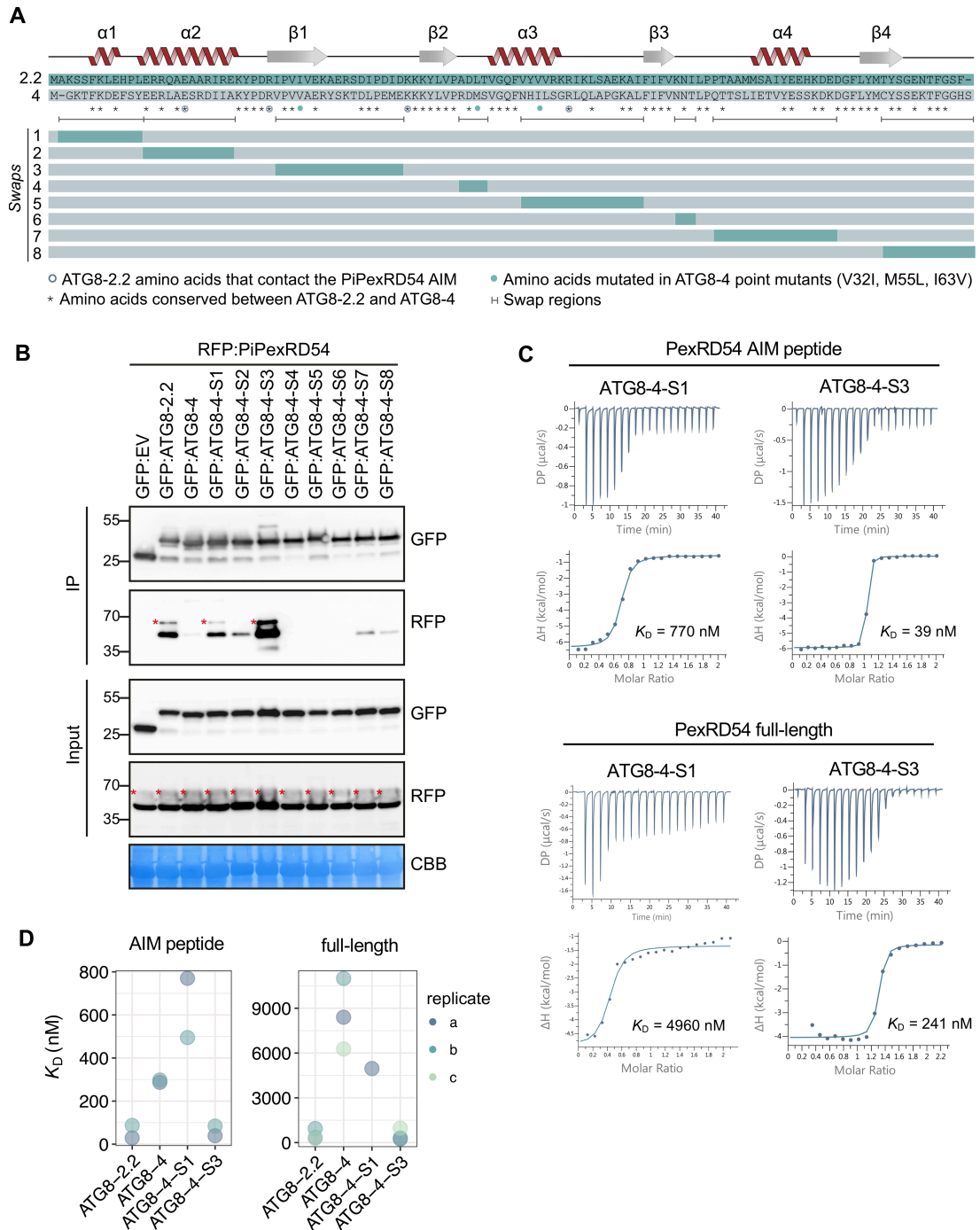


Figure 4.2 The ATG8 region surrounding the first β -strand is responsible for discriminatory binding to PexRD54

(a) Schematic showing the ATG8 swap chimeras and point mutants. The amino acid sequences of ATG8-2.2 and ATG8-4 are aligned, with the protein model above corresponding to the ATG8-2.2 structure. The brackets beneath the alignment indicate the boundaries of the swaps, with the color-coded rectangles below showing the chimeras made for each swap. The symbols beneath the alignment correspond to different features of the sequences: (i) the asterisks (*) mark conserved residues between ATG8-2.2 and ATG8-4, (ii) open circles mark residues that directly

contact the *Pi*PexRD54 AIM, and (iii) the filled circles mark the ATG8-4 residues used in structure guided mutagenesis experiments to match ATG8-2.2 (V32I, M55L, I63V). (b) Co-immunoprecipitation experiment between PexRD54 and all ATG8 swap chimeras. RFP:*Pi*PexRD54 was transiently co-expressed with the controls GFP:EV, GFP:ATG8-2.2, and GFP:ATG8-4, and all of the GFP:ATG8 swap chimeras (Swaps 1-8). Immunoprecipitates (IPs) were obtained with anti-GFP antibody and total protein extracts were immunoblotted with appropriate antibodies (listed on the right). Stars indicate expected band sizes. (c) The binding affinities of ATG8-4-S1 and ATG8-4-S3 towards PexRD54 AIM peptide and full-length PexRD54 were determined using isothermal titration calorimetry (ITC). The top panels show heat differences upon interaction and lower panels show integrated heats of injection (●) and the best fit (solid line) to a single site binding model using MicroCal PEAQ-ITC analysis software. (d) Chart summarizing the K_D values for all ATG8 swap chimera interactions tested, including two replicates with the PexRD54 AIM peptide and three replicates with full-length PexRD54. (c-d) Experiments performed by project collaborator Abbas Maqbool.

4.2.3 A single residue in the first β -strand underpins discriminatory binding to the substrate PexRD54

In parallel with the chimeric ATG8 approach, I took a structure-guided approach to identify single amino acids that could also be important for discriminatory AIM binding. Three residues that contribute to shaping the hydrophobic pockets that accommodate the AIM peptide are polymorphic between ATG8-2.2 and ATG8-4 (**Fig 4.3**). Isoleucine 33 (Ile-33), which is located in the W-site of ATG8-2.2, is changed to a valine (Val-32) in ATG8-4. Similarly, leucine 56 (Leu-56) and valine 64 (Val-64), located in L-site of ATG8-2.2, are replaced by a methionine (Met-55) and an isoleucine (Ile-63), respectively, in ATG8-4. This suggested that these three polymorphic residues between ATG8-4 and ATG8-2.2 could contribute to the differential interactions with the PexRD54 AIM.

To test if these residues underpin the binding specificity, I mutated each one in the ATG8-4 background to match ATG8-2.2 (**Fig 4.2.A**). I also generated a combined triple mutant (ATG8-4-3x) and assayed all of these variants for gain-of-binding to PexRD54 (**Fig 4.2.A**). The ATG8-4 point mutant Val-32 to Ile-32 (ATG8-4-V32I), within the first β -strand, partially restored binding to PexRD54 in co-IP experiments (**Fig 4.4.A**). A collaborator, Abbas Maqbool, then purified ATG8-4-V32I variant and quantified the gain-of-binding phenotype using ITC (**Fig 4.4.B**). Remarkably, with both PexRD54 AIM peptide and the full-length PexRD54, the ATG8-4-V32I mutant showed a strong gain-of-binding phenotype, restoring binding to levels that are similar to ATG8-2.2 (**Fig**

4.4.C). These results were consistent across multiple biological replicates (**Fig 4.4.C**). Altogether, these results suggest that a single amino acid residue, Val-32 in the first β -strand, largely determines the differential binding affinity of ATG8-4 towards PexRD54.

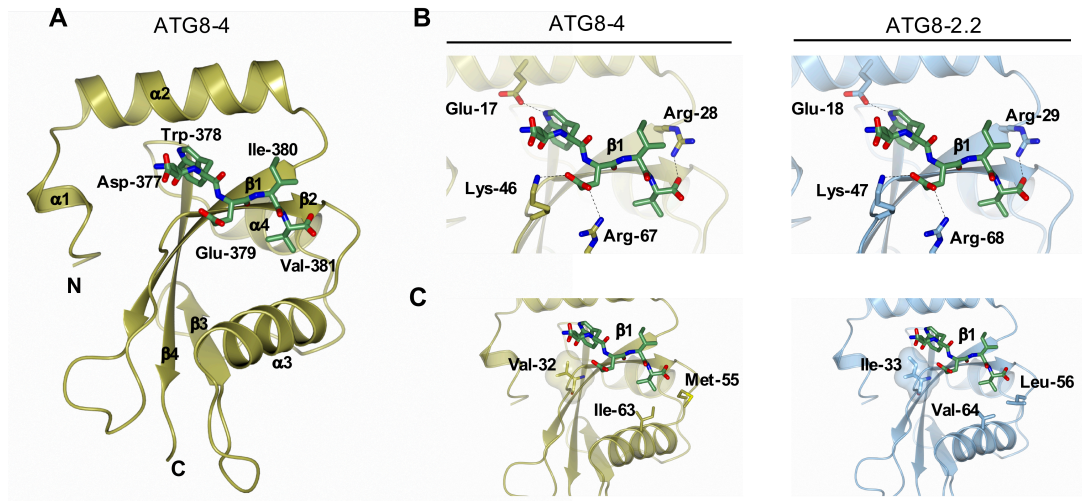


Figure 4.3 A Comparison of ATG8-2.2 structure and ATG8-4 model identifies polymorphic residues within the AIM binding site

(a) Homology model of ATG8-4 and PexRD54 AIM peptide complex. ATG8-4 and PexRD54 AIM are illustrated in cartoon and stick representation. β -helices, β -strands, N- and C-termini of ATG8-4 are labelled. (b) Zoomed in view of the AIM peptide binding pocket of ATG8-4 (left) and ATG8-2.2 (right), with amino acids making electrostatic interactions (dashed lines) labelled. (c) Zoomed in view of the AIM binding pocket of ATG8-4 (left) and ATG8-2.2 (right), highlighting differential residues contributing to hydrophobic interactions with the PexRD54 AIM peptide. Figure made in collaboration with Abbas Maqbool.

Isoleucine is only one methyl group larger than valine, making it perhaps surprising that the difference between these residues primarily underlies differential binding of ATG8-2.2 and ATG8-4 to PexRD54. We hypothesize that the isoleucine in ATG8-2.2 may better fill the hydrophobic cavity, and thus lead to stronger interactions with the PexRD54 AIM peptide. Ile-33 is highly conserved in various ATG8 isoforms (Kellner et al., 2017), suggesting that the valine polymorphism in ATG8-4 is recently derived in the solanaceae lineage. It is tempting to speculate that this polymorphism was selected to evade PexRD54 binding, and thus subversion of autophagy by the pathogen. Complementation of higher order ATG8 mutants with valine-substituted ATG8 isoforms

could challenge this hypothesis, and reveal whether valine substitution has an adverse effect on autophagy in general. It is also possible that some other selection force—or, indeed, neutral drift—led to the fixation of this polymorphism.

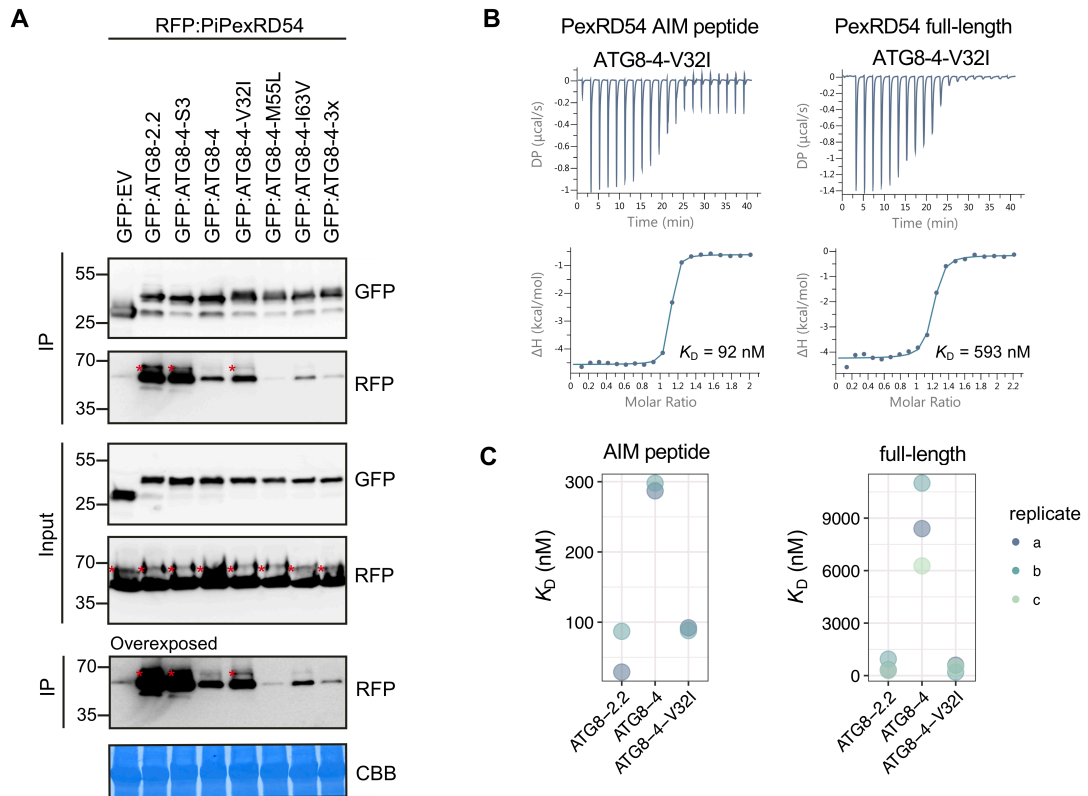


Figure 4.4 A single amino acid residue, Val-32 in the first β -strand, determines differential binding affinity of ATG8-4 towards PexRD54

(a) Co-immunoprecipitation experiment between PexRD54 and all ATG8-4 point mutants. RFP:PiPexRD54 was transiently co-expressed with the controls GFP:EV, GFP:ATG8-2.2, GFP:ATG8-4-S3, and GFP:ATG8-4, and all of the GFP:ATG8-4 point mutants. Immunoprecipitates (IPs) were obtained with anti-GFP antibody and total protein extracts were immunoblotted with appropriate antisera (listed on the right of each). Stars indicate expected band sizes. (b) The binding affinity of ATG8-4-V32I with PexRD54-AIM peptide and full-length PexRD54 was determined by ITC. The top panels show heat differences upon injection of ligands and lower panels show integrated heats of injection (•) and the best fit (solid line) to a single site binding model using MicroCal PEAQ-ITC analysis software. (c) Chart summarizing the KD values for each interaction, including two replicates with the PexRD54 AIM peptide and three replicates with full-length PexRD54. (b-c) Experiments performed by project collaborator Abbas Maqbool.

4.2.4 The N-terminal β -strand defines the protein interactor profiles of ATG8-2.2 and ATG8-4

Since we found that the first β -strand contributes to selective binding to the AIM-containing substrate PexRD54, we hypothesized that this region also underpins binding specificity to other ATG8 interacting proteins. To test this, I performed *in planta* immunoprecipitation with tandem mass spectrometry (IP-MS) experiments with ATG8-4-S3, ATG8-2.2 and ATG8-4, in three biological replicates, resulting in a final list of 291 proteins amenable to statistical analysis (**Fig 4.5.A; Fig A.3.1**). ATG8-4-V32I was also included in this experiment, but to repeated low expression of this construct, as determined by western blot analysis, it was not included in the final analysis.

Firstly, I detected significant overlap with our ATG8 interactome data (~40% of interactors), validating the IP-MS approach (**Table A.4.1**). This represents a considerable amount of overlap, as the sample preparation and mass spectrometry analyses were performed with different methods. Much like the ATG8 interactome dataset, this dataset also had an overrepresentation of predicted AIM-containing proteins (50%), with a majority of those AIMs evolutionarily conserved (70%), as compared to a random set of *N. benthamiana* proteins of the same size (35% and 27%, respectively) (**Fig 4.5.B**). This AIM ‘bootstrapping’ further validates the utility of using conservation as an additional parameter to delimit true AIM sequences, as discussed previously.

I then interrogated this dataset to see if we could identify proteins enriched for interaction with either of the ATG8 isoforms. Similar to our first ATG8 interactome screen, ATG8-2.2 and ATG8-4 associated with distinct sets of proteins (**Fig 4.5.A; Fig A.3.2**). Close to two-thirds of the proteins in the dataset were found to be significantly enriched in their interaction with either ATG8-2.2 (177 proteins) or ATG8-4 (6 proteins) using an ANOVA analysis with a post-hoc Tukey HSD test, while remaining proteins similarly interacted with both isoforms (105 proteins) (**Fig A.3.2**). We then compared the interaction profile of ATG8-4-S3 to those of ATG8-2.2 and ATG8-4. The ATG8-4-S3 interaction profile more closely resembled ATG8-2.2 than ATG8-4, indicating that inclusion of the first β -strand from ATG8-2.2 in the ATG8-4 background was sufficient to shift the specificity of the resulting chimera (**Fig 4.5.A**). ATG8-4-S3 associated with around 40% of the proteins that were significantly enriched in the ATG8-2.2 pull-down to a level statistically indistinguishable from ATG8-2.2 (**Fig A.3.2**). In addition, ATG8-

4-S3 does not interact with two of the six ATG8-4 enriched interactors, and maintains a similar level of interaction with all interactors common to both ATG8-2.2 and ATG8-4 (Fig A.3.2).

To see if the interactors significantly enriched in both the ATG8-2.2 and ATG8-4-S3 pull-downs had any specific properties, I performed AIM prediction, gene ontology analyses, and homology searches. These analyses revealed that the group of proteins that preferentially interact based on the ATG8-2.2 first β -strand have an overrepresentation of evolutionarily conserved AIMs (Fig 4.5.D). Within the set of ATG8-2.2 and ATG8-4-S3 enriched proteins, there was an overrepresentation of predicted AIM-containing proteins (53%), of which a majority of AIMs were conserved (83%), compared to the ATG8-2.2 enriched proteins that ATG8-4-S3 does not interact with (45% and 61%, respectively) (Fig 4.5.D). Based on these results, I hypothesize that the ATG8 N-terminal β -strand is crucial for shaping the hydrophobic pockets essential for AIM accommodation, and that the residues in this region in ATG8-4 reduce AIM binding.

In addition, the role of the ATG8-2.2 N-terminal β -strand region in conferring binding to AIM-containing proteins was confirmed by a collaborator on the project, Yasin Dagdas, for one of the interactors identified in the IP-MS screen, Vps4, providing further validation for the dataset (Fig A.3.3). Vps4—also known as Suppressor of K⁺ Transport Growth Defect 1 (SKD1) in *Arabidopsis thaliana*—is essential for the function of the Endosomal Sorting Complex Required for Transport (ESCRT) and is required for multivesicular body formation (Reyes et al., 2014). Although previous research has linked ESCRT components to autophagic degradation in plants (Katsiarimpa et al., 2013; Gao et al., 2015), the molecular basis of this connection was not clear. Our results reveal a direct interaction between Vps4 and ATG8. Considered together with the recent studies in metazoans revealing a role for ESCRT complex in phagophore closure (Zhou et al., 2019; Takahashi et al., 2018), our results provide a basis for future studies to further investigate the interplay between ESCRT complex and autophagy pathways.

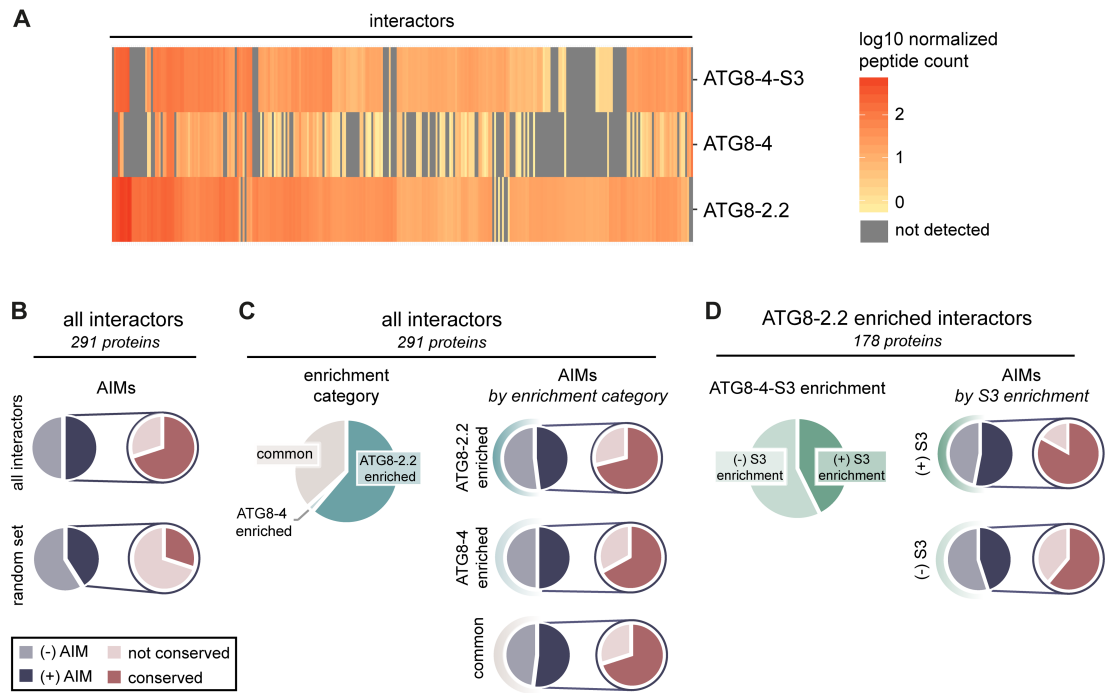


Figure 4.5 The first β -strand defines the AIM-dependent interaction profiles of ATG8 isoforms

(a) Heatmap showing the interaction profiles of ATG8-2.2, ATG8-4, and ATG8-4-S3. The average peptide count data from three replicates was \log_{10} normalized, and then used to construct a hierarchically clustered heatmap with the scale as shown. (b) All interactors in the dataset (291 proteins) and their closest *Arabidopsis thaliana* and *Marchantia polymorpha* homologs were analyzed for predicted AIMs using iLIR software (Kalvari et al., 2014). The proportion of interactors that contain a predicted AIM—as well as the proportion of those AIMs that are conserved—are summarized. These are compared to the analogous values calculated from the average of three sets of random proteins from the *Nicotiana benthamiana* proteome (291 proteins/ set). (c) All interactors were divided into enrichment categories based on whether they showed a significantly ($p < 0.05$) stronger interaction with ATG8-2.2 or ATG8-4 as determined by an ANOVA with a post-hoc Tukey's test; interactors that showed no significant difference in their interaction with either protein were categorized as 'common'. For each enrichment category, the proportion of interactors that contain a predicted AIM, and those AIMs that are conserved, are summarized. (d) For each interactor enriched in ATG8-2.2 pull-downs, we determined whether ATG8-4-S3 showed a significant ($p < 0.05$) difference in its interaction strength compared to ATG8-2.2 using an ANOVA with a post-hoc Tukey's test. Proteins that showed no statistical difference in their interaction with ATG8-4-S3 compared to ATG8-2.2 are categorized as '(+) S3 enrichment'; those that showed a statistical difference are categorized as '(-) S3 enrichment'. The proportion of interactors that contain a predicted AIM, and those AIMs that are conserved, are summarized for each ATG8-4-S3 enrichment category.

Our findings also demonstrate how to leverage the IP-MS data presented herein to identify novel autophagic cargoes or regulators. I also tried to pursue additional interactors to validate the role of the ATG8 N-terminal β -strand in AIM binding. I nominated candidates based on the criteria of having an evolutionary conserved AIM, being present in the all-ATG8 interactome, and being of a small size (<500 amino acids), to facilitate cloning. These criteria resulted in a list of four proteins: 40s ribosomal protein S15a-1 (r_40s_S15), a low-temperature induced cysteine protease (cys_prot), a cathepsin B cysteine protease (RD21), and sec61 subunit α -like (Sec61a). I attempted to clone each of these proteins, and each respective AIM mutant, but none of the resulting proteins were expressed under the tested conditions (**Fig A.3.4**).

4.2.5 Low expression of ATG8-4-V32I construct precluded IP-MS analysis

Having established the role of the first ATG8 β -strand in defining the interactor profiles for ATG8-2.2 and ATG8-4, I wanted to determine whether the ATG8-4 Val-32 residue is the main driver of the selectivity observed for this ATG8. Since the ATG8-4-V32I construct did not express well enough for inclusion in the previous IP-MS analysis, we repeated this experiment, performing IP-MS with ATG8-4-V32I, ATG8-4-S3, ATG8-2.2 and ATG8-4, in three biological replicates. In analyzing the resulting data, I found that, again, the ATG8-4-V32I construct expressed considerably weaker, thus giving the appearance of selective interaction (**Fig A.3.5**). ATG8-4-V32I had 5- to 20-fold lower peptide counts as compared to the ATG8-4 bait, as measured by peptides mapping to: the bait proteins themselves, ATG8-4 and ATG8-4-V32I; the common ATG8 interactor autophagy-related protein 3 (ATG3); and green fluorescent protein (GFP), the tag common to these bait proteins (**Fig A.3.5.B**).

I attempted to normalize the peptide data based on the values for the common interactor ATG3, but application of the large normalization factors across the ATG8-4-V32I peptide values for each replicate (factors of 5.1, 5.6, and 9.1, respectively) amplified variation between the replicates. This reduced the amount of significance in the dataset and undermined the ability to perform meaningful statistical analysis. In sum, no conclusions about the interactor profile of ATG8-4-V32I could be drawn from this data.

However, this dataset could be used to independently verify the results observed for ATG8-4-S3. Indeed, the interaction pattern observed for ATG8-4-S3 is the same as previously reported, with the ATG8-4-S3 interaction profile more closely resembling ATG8-2.2 than ATG8-4 (**Fig A.3.5.A**). Moreover—due to differences in how peptide searches were performed—four of the endogenous *N. benthamiana* ATG8s were present in this dataset, whereas these proteins were not present in the previous ATG8-4-S3 IP-MS dataset. The interaction pattern of NbATG8-4 was the most selective, interacting almost exclusively with ATG8-4 (**Fig A.3.6**), consistent with my previous findings (**Fig 3.3**). Although ATG8-4-S3 is more sequence-related to NbATG8-4, it exhibits a stronger interaction with NbATG8-2 (**Fig A.3.6**), suggesting that the N-terminal β -strand may be involved in the mechanism that sorts ATG8s into autophagosomes.

4.3 Conclusions

In this work, we used the *Phytophthora infestans* effector PexRD54 as a probe to show that the ATG8 N-terminal β -strand—and, in particular, a single residue within this region—determines binding specificity to AIM-containing substrates. These results demonstrate that ATG8 structure forms a layer of specificity in the plant selective autophagy pathway, contributing to the dynamics of cargo uptake, trafficking, and turnover. Follow-up studies should determine additional structural features involved in specifying these dynamics, towards a more complete understanding of how ATG8 specialization is biochemically coded. Future work should also investigate how this layer of ATG8 specialization intersects with other known contributing factors, such as interaction with different sets of proteins, post-translational modifications, and localization to different sub-cellular compartments.

Chapter 5: Evolutionary dynamics of the *Phytophthora* effector PexRD54 following a host jump

5.1 Introduction

Plant pathogen effectors are secreted proteins or small molecules that alter host-cell structure and function (Hogenhout et al., 2009). There are two broad classes of effectors, apoplastic and cytoplasmic effectors, distinguished by the host cellular space in which they function (Haas et al., 2009; Win et al., 2012). Within the past decade, a number of studies have characterized the functions of plant pathogen effectors and, collectively, this body of research has pointed to the incredible diversity in effector activities, which includes suppression of host immunity, re-routing of vesicle trafficking, disruption of hormone signalling, and modulating expression of target genes. (Win et al., 2012; Hogenhout et al., 2009).

Regardless of their precise function, all effectors can be considered ‘operational’ plant proteins—meaning that, although they are encoded by pathogen genes, effectors are fine-tuned to function in the context of the plant. As such, the evolution of effectors is shaped by changes in the host environment, including the evolution of effector targets or a shift in host species. In the latter case, a ‘host shift’ may progress to a ‘host jump’ following specialization on the alternate host species. Moreover, some effectors are recognized by intracellular host receptors, leading to a robust immune response that effectively halts pathogen ingress. Effector detection is a liability for the pathogen, driving the covert mutation or loss of effector genes to enable the pathogen to evade host immunity. These dual selection pressures on effectors—to retain their function in aiding infection, and to skirt detection by the plant—create an inherently unsettled biotic environment that generates an evolutionarily unstable framework (Upton et al., 2018). These selective pressures manifest in a number of ways, including extreme patterns of mutations in effector genes, genomic localization of effector genes in repeat-rich regions, lineage-specific loss of effector genes, and structurally-defined effector families. By studying these manifestations, we can shed light on many different aspects of effector evolution and

function, towards a better understanding of how pathogens successfully infect their plant hosts and how they coevolve with their hosts.

The work in this chapter is related to the remarkable pattern of mutations often observed in effector genes. Many effectors show high levels of nonsynonymous sequence substitutions relative to synonymous substitutions (Allen et al., 2004; Dodds et al., 2006; Huang et al., 2014; Raffaele et al., 2010; Yoshida et al., 2009; Liu et al., 2005). Such patterns of sequence polymorphisms are a hallmark of positive selection, and are thought to reflect the coevolutionary arms race of these effectors with host components. Positively selected sites in effector genes are frequently concentrated in the C-termini that encode the biochemical activity, or surface exposed residues involved in host protein interactions (Raffaele and Kamoun, 2012; Boutemy et al., 2011). In some cases, the signatures of positive selection observed in effector genes are extreme, with only a few synonymous or no synonymous polymorphisms. A striking example comes from the rice blast pathogen *Magnaporthe oryzae*, where allelic variants of the effector AVR-Pik exhibit four amino acid replacements, but no synonymous changes (Huang et al., 2014; Yoshida et al., 2009; Kanzaki et al., 2012). Remarkably, all non-synonymous AVR-Pik polymorphisms are presumably adaptive, since they map to regions in the protein structure that interface with the cognate immune receptor (Maqbool et al. 2015).

Another remarkable case of positive selection in an effector gene comes from the *Phytophthora* clade 1c species (Dong et al., 2014). This clade arose through a series of host jumps to botanically distant plant species, followed by adaptation and specialization on these disparate hosts (**Fig 5.1**) (Raffaele et al., 2010). The *Phytophthora* clade 1c includes the ‘sister’ species *Phytophthora infestans* and *Phytophthora mirabilis*—which infect *Solanum* species and the ornamental plant *Mirabilis jalapa* (colloquially known as four o’clock flower), respectively—and are estimated to have split about 1,300 years ago (**Fig 5.1**) (Raffaele et al., 2010). Comparative genomic analyses between *P. infestans* and *P. mirabilis* revealed signatures of positive selection in a high proportion of effector genes (300 out of 796 predicted genes) (Raffaele et al., 2010). For one of these effectors, the protease inhibitor EPIC1, the changes involved in the process of host adaptation were mapped to the level of single amino acid residues (Dong et al., 2014). A single polymorphism between the *P. infestans* and *P. mirabilis* EPIC1 orthologs was shown to greatly determine the activity of these effectors towards their respective potato and *M.*

jalapa host proteases (Dong et al., 2014). This provides a striking example of evolution driving the functional specialization of effectors during plant–pathogen coevolution.

Building on this work, the objective of the research summarized herein was to understand how changes in the host environment generated by a host jump shaped the evolution of the *Phytophthora* clade 1c RXLR effector PexRD54. PexRD54 is comprised of five tandem structural domains, termed WY-domains, that pack to form an elongated molecule (Maqbool et al., 2016). During *P. infestans* infection of potato, *P. infestans* PexRD54 (*Pi*PexRD54) is translocated inside the plant cell and binds the autophagy protein ATG8-2.2 via a C-terminal ATG8-interacting motif (AIM) that extends after the five WY domains (Dagdas et al., 2016). This interaction stimulates autophagosome formation, as well as interferes with the role of selective autophagy in plant immunity by depleting the immune-responsive autophagy cargo receptor JOKA2 out of ATG8-2.2 complexes (Dagdas et al., 2016). *Pi*PexRD54-labelled autophagosomes are then trafficked to the host-pathogen interface, supporting the view that *P. infestans* deploys PexRD54 to remodel the host-microbe interface by co-opting the host autophagy machinery (Dagdas et al., 2018). The *Pi*PexRD54 WY-domains also appear to contribute to the function of this protein by stimulating autophagosome formation or interacting with ‘cargo’ proteins that are brought into the re-directed autophagy pathway (Maqbool et al., 2016). This is evidenced by the retention of some *Pi*PexRD54 activities in a mutant with a non-functional AIM, including re-routing autophagosome trafficking to the host-pathogen interface, although at a reduced occurrence (Dagdas et al., 2018).

Leveraging this detailed mechanistic understanding of *Pi*PexRD54 function, and the established framework of studying effector evolution within the *Phytophthora* clade 1c, I aimed to explore how the ATG8-targeting effector, PexRD54, has evolved in the clade 1c lineages. My approach was to relate lineage-specific PexRD54 polymorphisms to the respective host environments and, in this, contribute to our understanding of evolutionary dynamics at the resolution of single amino acids.

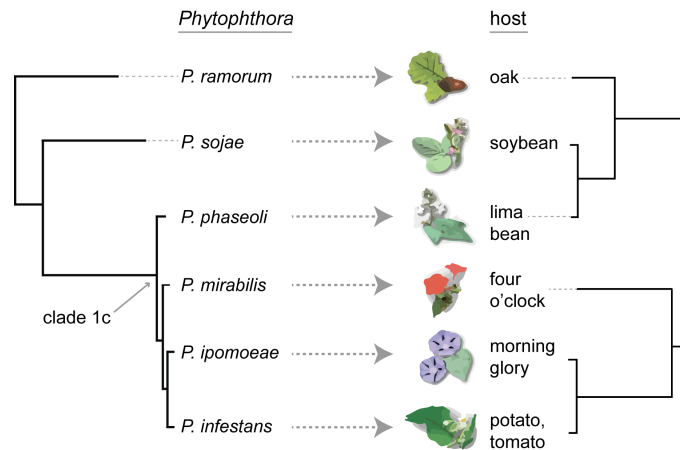


Figure 5.1 Host specialization of related *Phytophthora* species

Depiction of related *Phytophthora* species and their botanically distant hosts, with the respective simplified phylogenies.

5.2 Results and Discussion

5.2.1 The *P. mirabilis* PexRD54 has a fixed amino acid polymorphism in its ATG8-interacting motif

5.2.1.1 *P. mirabilis* PexRD54 is polymorphic

Species within the closely related *Phytophthora* clade 1c—*P. infestans*, *P. ipomoeae*, and *P. mirabilis*—were found to have PexRD54 orthologs, as determined by BLAST searches against available genome and transcriptome sequences (**Fig 5.2A**). Interestingly, the *P. mirabilis* PexRD54 ortholog (*PmPexRD54*) has a fixed amino acid polymorphism in its ATG8-interacting motif (AIM) region, with the central glutamate residue substituted for a lysine (DWEIV to DWKIV, E to K), whereas this AIM motif is invariant in all other PexRD54 orthologs in clade 1c (**Fig 5.2A; Fig A.5.1**). *PmPexRD54* has eleven additional unique amino acid polymorphisms relative to the other clade 1c PexRD54 orthologs, which are spread throughout the WY domains and linker regions (**Fig A.5.1**). In comparison, the *P. ipomoeae* PexRD54 has three unique polymorphisms relative to its orthologs, whereas *P. infestans* PexRD54 has two (**Fig A.5.1**). Due to the importance of the AIM in mediating PexRD54 activity, I chose to focus on investigating the evolutionary dynamics of *P. mirabilis* PexRD54 and I hypothesize that this polymorphism may reflect the specific selective pressures of functioning within the *M. jalapa* host environment.

Despite what seems like a comparatively high level of polymorphisms in the *P. mirabilis* PexRD54 ortholog, this gene was not deemed to be under positive selection based on the analyses of Raffaele et al., 2010. This study compared *Phytophthora* clade 1c species and found that a total of 2572 genes (14.2% of the whole genome) are under positive selection in the clade 1c strains, with the highest number in *P. mirabilis* (1004 genes) (Raffaele et al., 2010). The lack of evidence that positive selection is operating on the *PmPexRD54* gene does not preclude the possibility that the AIM polymorphism represents a positively selected site within the gene, as dN/dS ratios calculated over a large, multi-domain protein may dilute the signal from a specific site.

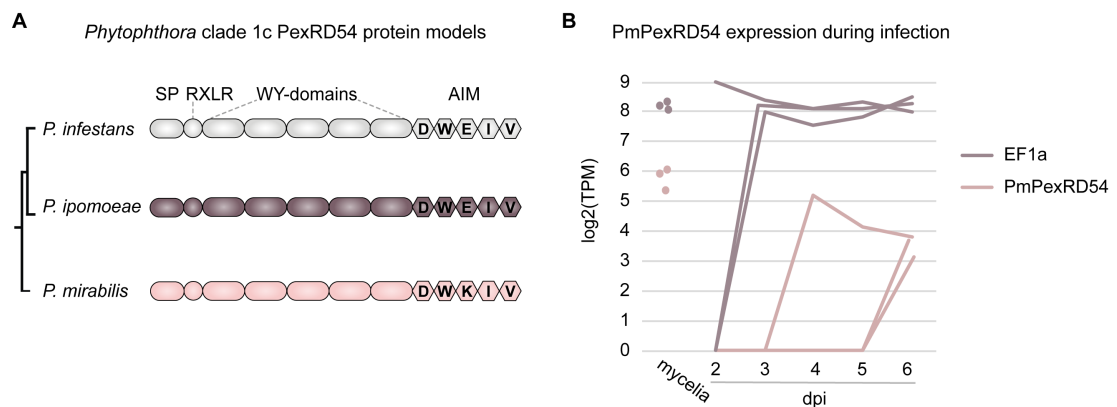


Figure 5.2 The *P. mirabilis* PexRD54 has an AIM polymorphism and is expressed during infection

(a) Protein models of the *Phytophthora* clade 1c PexRD54 homologs (381 aa), including the signal peptide (SP), RXLR motif, five tandem WY-domains and the C-terminal AIM motif. (b) *PmPexRD54* is expressed during *P. mirabilis* infection of *M. jalapa*. Graph representing the transcript abundance for *PmPexRD54* and the control elongation factor 1-alpha (EF1a) in *P. mirabilis* strain 09316 mycelia and 2–6 days post infection (dpi) of *M. jalapa*, across three technical replicates. Transcript abundance was measured by RNAseq and is reported in transcripts per million (TPM), a normalized value.

5.2.1.2 *P. mirabilis* PexRD54 is expressed during *M. jalapa* infection

I analyzed the expression pattern of *PmPexRD54* during *P. mirabilis* infection of *M. jalapa* using previously generated RNAseq dataset. This analysis showed that *PmPexRD54* is expressed during infection, with the highest average expression level at six days post infection (**Fig 5.2B**). Interestingly, *PmPexRD54* is expressed more highly in

mycelium, counter to the trend that *Phytophthora* effector genes, including *PiPexRD54*, are induced during infection (**Fig 5.2B**). This could indicate that this RNAseq experiment did not capture the timepoint at which *PmPexRD54* is most highly expressed, or that *PmPexRD54* has an alternate expression pattern during infection.

5.2.2 *P. mirabilis* PexRD54 AIM polymorphism reduces binding to *M. jalapa* ATG8s

5.2.2.1 *M. jalapa* ATG8s are not orthologous to ATG8s from other plant taxa

Following my hypothesis that the *PmPexRD54* AIM polymorphism may reflect the specific selective pressures of functioning within the *M. jalapa* host environment, I next explored how this residue impacts interaction with the *M. jalapa* host ATG8s (*MjATG8s*). First, I searched for *M. jalapa* ATG8 sequences using available genomic and transcriptomic sequence data, identifying six *MjATG8* isoforms (**Fig A.5.2; Fig 5.3**). These *MjATG8* isoforms cluster in four well-supported clades among other Caryophyllales ATG8s (**Fig A.5.2A**). The *MjATG8s* exhibit marked sequence diversity at their N-terminus, and also feature variation in regions known to mediate interaction with AIM-containing proteins, such as the second β -strand (**Fig A.5.2B**).

In line with previous findings that ATG8s from different plant lineages form monophyletic clades of higher taxonomic order (Kellner et al., 2017), phylogenetic evidence shows that the Caryophyllales ATG8s have undergone lineage specific expansions and are not orthologous to ATG8s from other plant taxa, such as the Solanales and the Brassicales (**Fig 5.3**). The Caryophyllales have both clade I and II ATG8s, with the *MjATG8*-III falling in the latter major clade (**Fig 5.3**). Due to the phylogenetic distance between the *M. jalapa* ATG8s and the potato ATG8s, I hypothesized that the *MjATG8s*, or a subset thereof, may exhibit subtle structural differences in their hydrophobic binding pockets that would result in preferential binding to the *PmPexRD54* AIM over the *PiPexRD54* AIM.

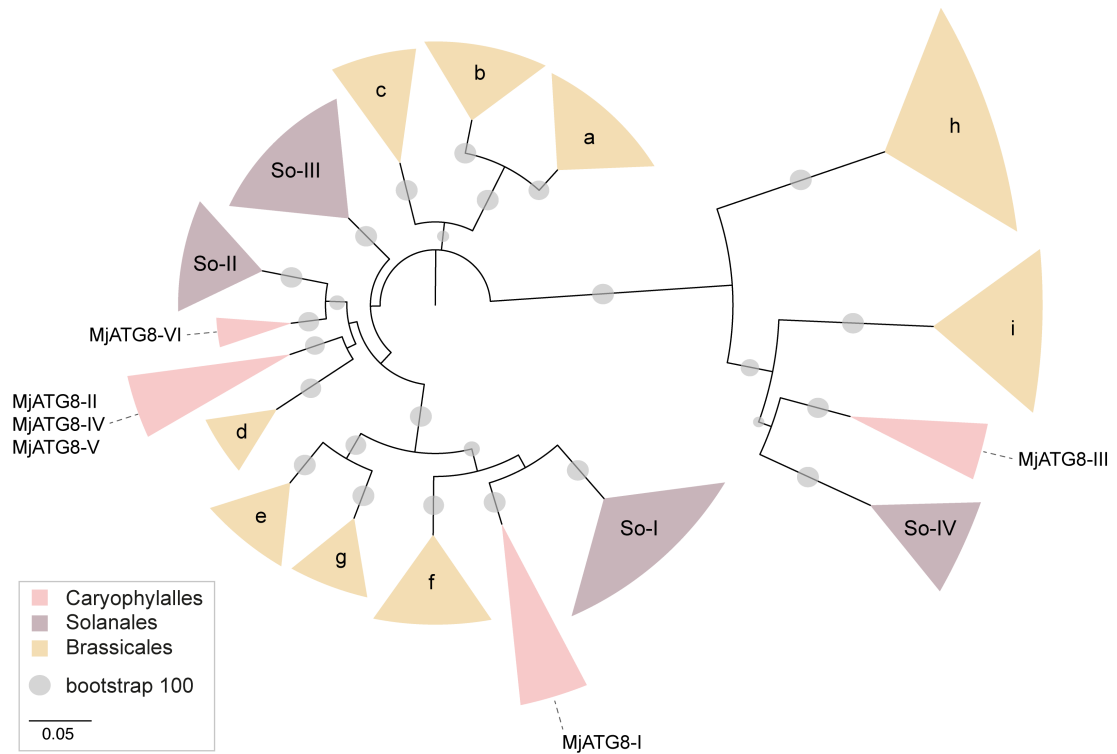


Figure 5.3 *Mirabilis jalapa* ATG8s are not orthologous to ATG8s from other plant taxa

Phylogenetic relationship between ATG8s from the Caryophyllales, Solanales, and Brassicales. Unrooted maximum-likelihood tree of 186 ATG8 isoforms, with clades collapsed based on bootstrap support and colors indicating plant order; the full tree is in the appendix, **Fig A.5.3**. The tree was calculated in MEGA7 (Sudhir Kumar et al., 2016) from a 445 nucleotide alignment (MUSCLE (Edgar, 2004), codon-based). The Solanales and Brassicales ATG8 clades are named following the conventions in Kellner et al. 2016, and the *Mirabilis jalapa* ATG8s are marked within their respective Caryophyllales clades. The bootstrap values of the major nodes are indicated by gray circles, with the scale as shown. The scale bar indicates the evolutionary distance based on nucleotide substitution rate.

5.2.2.2 The *P. mirabilis* PexRD54 AIM polymorphism precludes binding to *M. jalapa* ATG8s in co-immunoprecipitation experiments

I tested *Pm*PexRD54 for interaction with the six *M. jalapa* ATG8s using *in planta* co-immunoprecipitation (co-IP). I could not detect *Pm*PexRD54 association with the six *Mj*ATG8s or potato ATG8-2.2, although *Pi*PexRD54 associated with all of the tested ATG8s (**Fig 5.4**). Moreover, I could map this reduction in binding for *Pm*PexRD54 to the glutamate to lysine polymorphism in the AIM, as introducing a mutation in the

*Pi*PexRD54 AIM to alter the motif from ‘DWEIV’ to ‘DWKIV’ to match the *Pm*PexRD54 AIM (*Pi*PexRD54^{*Pm*AIM}) abolished binding to all of the tested ATG8s (Fig 5.4). Moreover, in a reciprocal experiment, introducing a mutation in the *Pm*PexRD54 AIM to alter the motif from ‘DWKIV’ to ‘DWEIV’ (*Pm*PexRD54^{*Pi*AIM}) was sufficient to recapitulate ATG8 binding to a similar level as *Pi*PexRD54 (Fig A.5.4). These experiments conclusively show that a single amino acid difference explains the differential binding observed between the two PexRD54 orthologs.

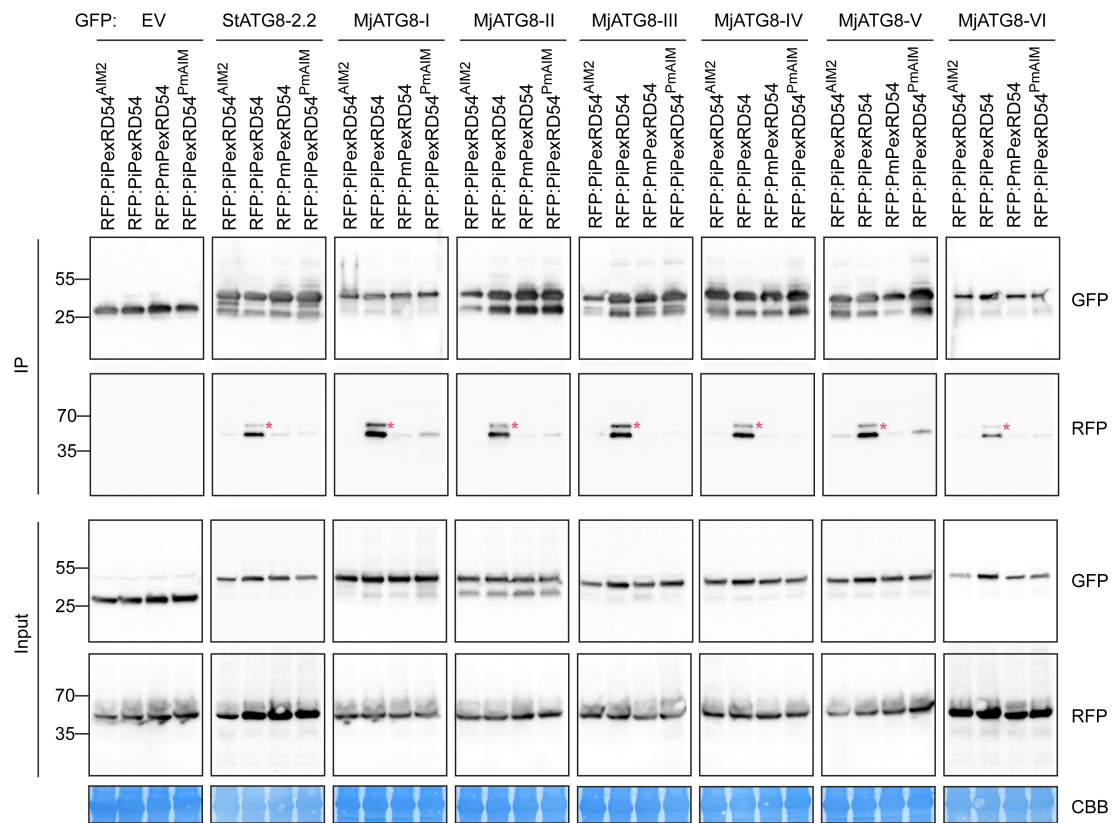


Figure 5.4 The *P. mirabilis* PexRD54 AIM polymorphism reduces binding to *M. jalapa* ATG8s

Co-immunoprecipitation experiment between PexRD54 variants (*Pi*PexRD54^{AIM}, *Pi*PexRD54, *Pm*PexRD54, *Pi*PexRD54^{*Pm*AIM}) and *M. jalapa* ATG8s (*Mj*ATG8s). RFP:PexRD54 variants were transiently co-expressed with GFP:EV, GFP:*St*ATG8-2.2, and all GFP:*Mj*ATG8s. Immunoprecipitates (IPs) were obtained with anti-GFP antiserum and total protein extracts were immunoblotted with appropriate antisera (listed on the right). Stars indicate expected band sizes.

5.2.2.3 The *P. mirabilis* PexRD54 AIM peptide binds weakly to ATG8s in isothermal titration calorimetry experiments

To quantify the reduction in binding caused by the *Pm*PexRD54 AIM polymorphism, I carried out isothermal titration calorimetry (ITC) experiments. I assayed the strength of interaction between 10 amino acid long peptides matching the *Pi*PexRD54 and *Pm*PexRD54 AIM regions, respectively, and a subset of the ATG8s tested in the co-IP experiment, potato ATG8-2.2, *Mj*ATG8-I, and *Mj*ATG8-III. The interaction between the *Pi*PexRD54 AIM peptide and potato ATG8-2.2 was included as a control, as this interaction has been studied extensively *in vitro* (Dagdas et al., 2016; Maqbool et al., 2016). *Mj*ATG8-I and *Mj*ATG8-III were selected to represent the *M. jalapa* ATG8s due to their phylogenetic distance, belonging to the major ATG8 clades, I and II, respectively (**Fig 5.3**). I found that the *Pm*PexRD54 AIM peptide bound weakly to all of the tested ATG8s, in each case exhibiting an affinity measurement an order of magnitude weaker than that observed for the *Pi*PexRD54 AIM peptide, using two different methods to derive the thermodynamic information (**Fig 5.5; Table A.5.1**).

First, I individually fit the isotherm data for each technical replicate for each interaction to a single-site binding model using AFFINImeter software (**Fig A.5.5; Fig A.5.6; Table A.5.1**). I checked the quality of these data, noting no irregularities in the heat differences upon injection or the integrated heats of injection (**Fig A.5.5; Fig A.5.6**). I observed close agreement between the integrated heats of injection and the best fit of the data (**Fig A.5.5; Fig A.5.6**). The experimental replicates for each interaction also had comparable equilibrium dissociation constant (K_D) values (**Table A.5.1**), and I noted that the values obtained for the control interaction, between the *Pi*PexRD54 peptide and potato ATG8-2.2, were in line with previous experiments. The K_D values ranged from 35–116 nM (**Table A.5.1**), which is comparable to the measurements reported in Chapter 4 (**Fig 4.1**).

In addition, for each interaction, I used the replicate data to perform a global analysis using the AFFINImeter software (**Fig 5.5**). In a global analysis, the isotherms for the experimental replicates are simultaneously fitted to the same binding model, producing a single, robust K_D estimate for each interaction. This method ultimately integrates more information into deriving the thermodynamic and kinetic information for a given interaction, and thus provide the most reliable results. In this analysis, I found that the

PmPexRD54 AIM peptide bound up to an order of magnitude weaker than the *PiPexRD54* AIM peptide for all of the tested ATG8s, with *PmPexRD54* binding in the low millimolar range (**Fig. 5.5**), similar to the analysis of the individual replicates (**Table A.5.1**). These differences in binding affinity can be visually appreciated by comparing the slopes of the best fit lines for the *PmPexRD54* interactions versus the *PiPexRD54* interactions, with a steeper slope indicating a stronger binding affinity (**Fig. 5.5**).

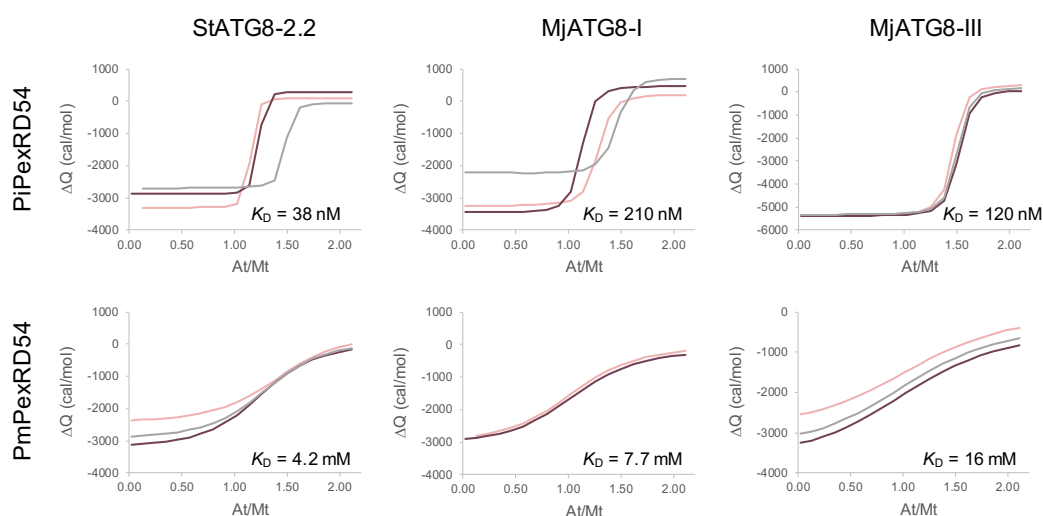


Figure 5.5 *PmPexRD54* peptide binds weakly to ATG8s in isothermal titration calorimetry experiments

The binding affinities between the *PiPexRD54* and *PmPexRD54* peptides and the ATG8 isoforms ATG8-2.2, *MjATG8-I*, and *MjATG8-III*, were determined using isothermal titration calorimetry (ITC). Using AFFINImeter analysis software, the isotherms for each of the experimental replicates were simultaneously fit to the same single site binding model, producing a robust equilibrium dissociation constant (K_D) estimate for each interaction. K_D estimates are listed in nanomolar (nM) for the *PiPexRD54* interactions, and millimolar (mM) for the *PmPexRD54* interactions. The graphs overlay the lines of best fit for the replicate isotherms (pink, grey, purple), with the integration values (ΔQ) plotted against the ratio of ligand to protein (At/Mt). The graphs showing the heat differences and integrated heats of injection for each replicate are shown in **Fig A.5.5** and **Fig A.5.6**, and a table summarizing the thermodynamic information is included in **Table A.5.1**.

5.2.2.4 Synthesis of the co-IP and ITC results

Taking these experiments together, both co-IP and ITC, suggests that *PmPexRD54* is able to interact with the *M. jalapa* ATG8s, although with much lower affinity. The difference between the results of the two methods—one showing no binding, the other showing weak binding—could be due to a number of factors. Firstly, these assays differ in their sensitivities, with isothermal titration calorimetry able to detect even small changes in the heat of dilution. Additionally, the AIM peptide is presented in different contexts in these experiments; in the co-IP assay, the AIM is presented within the full-length protein, whereas the ITC assay was conducted with just the AIM peptide. It is possible that the AIM is more available to bind ATG8 when it is presented as a peptide, rather than at the C-terminus of the *PmPexRD54* protein.

The weak ATG8 binding by any full-length PexRD54 variant or peptide with an AIM sequence of 'DWKIV' fits with the observation that there are no experimentally validated AIMs that have a central lysine residue (Kalvari et al., 2014). However, this finding is in contrast to a previous study that characterized the ability of PexRD54 AIM mutant peptides to bind potato ATG8-2.2 using a peptide array (Maqbool et al., 2016). In this study, Maqbool et al. assayed an array of peptides matching the extended *PiPexRD54* AIM region (residues 372–381, KPLDFDWEIV) and substituted each position with each possible amino acid, for binding with ATG8-2.2. They found that the glutamate position can be occupied by any amino acid, except proline, and the resulting peptide can still bind ATG8-2.2 (Maqbool et al., 2016). In light of my results, this again suggests that presentation of the AIM peptide and assay sensitivity affect the experimental read-out.

5.2.2.5 Is the *PmPexRD54*-*MjATG8* interaction biologically relevant?

Overall, I can conclude that the *PmPexRD54* AIM polymorphism significantly reduces binding to the *M. jalapa* ATG8s. This raises an obvious question: is the weak interaction observed between *PmPexRD54* and the *MjATG8*s biologically relevant? One way to approach this question is to think about the broader biological context of the *PmPexRD54*-*MjATG8* interaction. The role of selective autophagy in *M. jalapa*, or any related Caryophyllales species, has not been characterized. As such, one can only speculate as to whether the *M. jalapa* selective autophagy pathway plays a comparable role in plant immunity to the potato pathway and, more generally, whether the manipulation of this pathway during infection would be advantageous to the pathogen.

Even if one assumes that there is a certain amount of symmetry between the functions of the *M. jalapa* and potato selective autophagy pathways, the weak *PmPexRD54-MjATG8* interaction is likely not relevant to infection. During *P. infestans* infection of potato, the ability of *PiPexRD54* to outcompete JOKA2 for binding to ATG8-2.2 is dependent on its high binding affinity to ATG8-2.2 (Dagdas et al., 2016). Considering the weak, assay-dependent binding of *PmPexRD54* to the *M. jalapa* ATG8s, I hypothesize that *PmPexRD54* would not be able to antagonize *M. jalapa* JOKA2. However, as previously mentioned, *PiPexRD54* has a number of other reported functions (Dagdas et al., 2016), some of which have not been shown to be AIM-independent (unpublished), leaving the possibility that *PmPexRD54* could perturb the selective autophagy pathway through other means.

5.2.3 What is the role of *PmPexRD54* during *P. mirabilis* infection of *M. jalapa*?

5.2.3.1 How does the *PmPexRD54* AIM polymorphism reflect specific challenges posed by the *M. jalapa* host environment?

Since previous experiments showed that *PmPexRD54* likely does not disrupt selective autophagy through interaction with *M. jalapa* host ATG8s, I wanted to understand how this comparative loss-of-function may contribute to successful infection. To do this, I designed constructs to make *M. jalapa* transgenic lines expressing the different PexRD54 variants—*PiPexRD54* and *PmPexRD54*, as well as the reciprocal AIM mutants, *PiPexRD54^{PmAIM}* and *PmPexRD54^{PiAIM}*. My plan was to then infect these plants with *P. mirabilis* and determine how PexRD54-*MjATG8* association strength impacts *P. mirabilis* infection success. I hypothesized that if the *PmPexRD54* AIM polymorphism was adaptive, then I would expect reduced success of infection in the lines expressing PexRD54 variants that successfully target the *M. jalapa* host ATG8s. However, due to methodological limitations, I was not able to carry out these experiments.

M. jalapa is a model organism for molecular studies of the mechanisms underpinning petal expansion and senescence (Xu et al., 2007), as well as for research on secondary metabolite production (Zaccai et al., 2007; Effmert et al., 2005; Brockington et al., 2011). A protocol for *M. jalapa* transformation and regeneration from nodal segments has been previously developed, although it results in a chimeric pattern of transgene expression in

regenerated leaves (Zaccai et al., 2007). The TSL tissue culture team attempted to elaborate on this existing protocol to develop a method to transform and regenerate *M. jalapa* meristematic tissue. Unfortunately, out of close to one hundred plants that I genotyped (data not shown), the repeated attempts to transform *M. jalapa* resulted in no transgenic explants.

An additional strategy to determine the impact of the *P. mirabilis* PexRD54 AIM polymorphism during *M. jalapa* infection—and perhaps an even more elegant one—would be to transform *P. mirabilis* with the different PexRD54 variants, and test these strains for infection success on wild-type *M. jalapa* plants. However, these experiments were not undertaken due to ongoing challenges with *Phytophthora* transformation in the lab, including low transformation rate and reversion of transformant phenotypes. In the future, if a robust, reliable protocol for *P. mirabilis* transformation is developed, this experiment would add significant value to this line of research and address a number of unanswered questions. However, with the limitations as they were, I was not able to infer how the *PmPexRD54* AIM polymorphism reflects specific challenges posed by the *M. jalapa* host environment.

5.2.3.1 *PmPexRD54* does not interact with host vesicle trafficking protein *Rab8a*

The five tandem WY-domains of *PiPexRD54* are thought to be responsible for stimulating autophagosome formation and binding proteins that are taken up into the re-directed autophagy pathway (Maqbool et al., 2016). As such, although the *PmPexRD54* AIM appears non-functional towards *MjATG8* binding, the WY-domains of *PmPexRD54* could be involved in perturbing autophagy via these other means. To gain insight into the role of *PmPexRD54* during infection, I aimed to determine whether *PmPexRD54* interacts with the *M. jalapa* homologs of other potato proteins targeted by *PiPexRD54* during infection.

A number of putative *PiPexRD54* potato host targets were identified in the initial immunoprecipitation with tandem mass spectrometry screen that identified ATG8-2.2 (Dagdas et al., 2016), some of which have been followed up on by our collaborator Tolga Bozkurt. One of these proteins, potato *Rab8a* (*StRab8a*), a small GTPase involved in coordinating vesicle trafficking (Stenmark, 2009), was found to interact with *PiPexRD54* in an AIM-independent manner, contributing to the dysregulation of selective autophagy

(unpublished). I cloned the *M. jalapa* Rab8a ortholog (*MjRab8a*), and tested it for interaction with *PmPexRD54* in a co-IP assay (**Fig 5.6**). I found that *MjRab8a* does not associate with either *PmPexRD54* or *PiPexRD54*, although *StRab8a* associates with both proteins (**Fig 5.6**). These results suggest that *PmPexRD54* does not intersect with the *M. jalapa* selective autophagy pathway via this route, either, leaving the function of *P. mirabilis* PexRD54 during *M. jalapa* infection an open question.

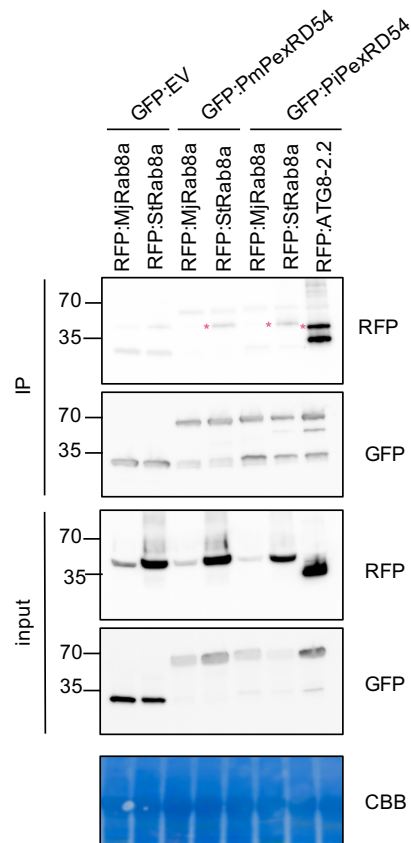


Figure 5.6 *PmPexRD54* does not associate with *M. jalapa* Rab8a

Co-immunoprecipitation experiment between PexRD54 variants (*PmPexRD54* and *PiPexRD54*) and Rab8a homologs from *S. tuberosum* (*StRab8a*) and *M. jalapa* (*MjRab8a*). GFP:EV and GFP:PexRD54 variants were transiently co-expressed with RFP:*StRab8a*, RFP:*MjRab8a*, and—in the case of expression with GFP:*PiPexRD54*—RFP:ATG8-2.2. Immunoprecipitates (IPs) were obtained with anti-GFP antiserum and total protein extracts were immunoblotted with appropriate antisera (listed on the right). Stars indicate expected band sizes.

5.3 Conclusions

Overall, I determined that the *P. mirabilis* PexRD54 has a fixed polymorphism in its AIM which reduces binding to the *M. jalapa* host ATG8s, likely preventing it from targeting the *M. jalapa* selective autophagy pathway through direct ATG8 binding during infection (**Fig 5.6**). I could not determine whether this loss-of-binding mutation reflects specific selective pressures imposed by the host environment, due to methodological constraints. Additionally, I ruled out a role for *Pm*PexRD54 to dysregulate autophagy through interacting with *M. jalapa* Rab8a. With these findings, I have narrowed a potential path for follow-up experiments to address the outstanding questions from this work, including some of those I set out to answer. These questions include (**Fig 5.6**): How has the ATG8-targeting effector PexRD54 evolved in the *Phytophthora* clade 1c lineages? Does the *Pm*PexRD54 AIM polymorphism reflect the specific selective pressures of the *M. jalapa* host environment and, if so, how? And, what is the role of *Pm*PexRD54 during *P. mirabilis* infection of *M. jalapa*?

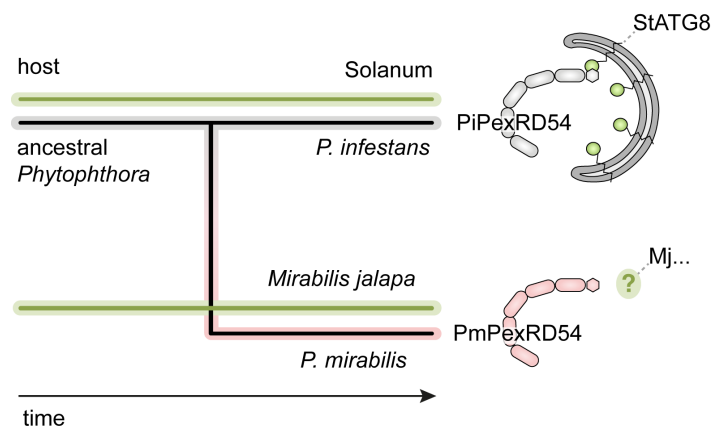


Figure 5.7 Evolutionary dynamics of PexRD54 following a host jump

Schematic view of the *Phytophthora* host jump from Solanum species onto *Mirabilis jalapa*, followed by adaptation and, eventually, speciation, leading to the differentially specialized pathogens *P. infestans* and *P. mirabilis*. This process is associated with changes in the effector repertoire, exemplified by the AIM polymorphism in *P. mirabilis* PexRD54 (*Pm*PexRD54), which precludes its binding to host ATG8s, and perhaps has facilitated adaptation to an alternative host target.

In the previous chapter, I used *Pi*PexRD54 to dissect the potato ATG8 structural elements that underpin interaction specificity with AIM-containing substrates. The work

herein is complementary, approaching the question of ATG8 substrate specificity from the opposing perspective: from that of the substrate. Here, by aiming to explore how the *Phytophthora* clade 1c host environments have shaped the evolution of PexRD54, I discovered that the *Pm*PexRD54 AIM polymorphism reduces ATG8 binding, thus contributing to our understanding of the biochemical basis of ATG8 substrate specificity and further defining the requirements for a functional ATG8-interacting motif.

Chapter 6: Discussion

How the plant autophagy machinery selectively recognizes, recruits, and recycles various cargoes and components remains a huge gap in our understanding of plant homeostatic pathways. Following evidence that the ATG8 family is expanded and diversified in plants, it was hypothesized that plant ATG8 isoforms may form a layer of selectivity in the autophagy pathway by binding distinct substrates. In this thesis, I explored the functional specialization of plant ATG8s in molecular detail, shedding light on the biochemical basis of the plant ATG8 substrate specificity. In chapter 3, I described the potato ATG8 interactome using *in planta* immunoprecipitation followed by mass spectrometry, discovering that potato ATG8 isoforms bind distinct sets of plant proteins with varying degrees of overlap. In chapter 4, I defined the biochemical basis of potato ATG8 specialization. I revealed that the ATG8 N-terminal β -strand underpins binding specificity to substrates that contain ATG8-interacting motifs (AIMs), including the ATG8-targetting effector from the potato late blight pathogen *Phytophthora infestans*, PexRD54. To approach the question of ATG8 substrate specificity from the opposing direction, in chapter 5 I explored the evolutionary dynamics of PexRD54 in different host-specific lineages of *Phytophthora*. I found that the PexRD54 ortholog from *P. mirabilis*, a closely related species to *P. infestans*, has a polymorphism in its AIM which nearly abolishes binding to the ATG8s of its host, *Mirabilis jalapa*, improving our understanding of the requirements for a functional ATG8-interacting motif.

6.1 ATG8 functional specialization: a layer of specificity defining the plant selective autophagy pathway

Across eukaryotic taxa, multiple layers of specificity are thought to define the dynamics of autophagy cargo uptake, sub-cellular trafficking, and turnover. In mammals, it has been proposed that the specificity of the autophagy pathway requires an array of mechanisms, including: spatially restricted membrane sources; the inducible expression, precise cellular localization, and post-translational modification of both autophagy

receptors and core autophagy components; the selective ubiquitylation of autophagy cargoes; and regulation of autophagosome trafficking by intracellular transport proteins.

We only have a nascent understanding of the specificity-determining mechanisms that delimit the plant autophagy pathway, but growing evidence supports the existence of multiple layers of specificity. Previous studies have shown that some plant autophagy components have subfunctionalized with respect to expression patterns, including the ATG8s (Thompson et al., 2005; Contento et al., 2004; Slavikova et al., 2005) and ATG12s (Chung et al., 2010). In addition, a number of autophagy components are regulated through post-translational modification, including ATG13 and ATG6, which are phosphorylated and ubiquitylated, respectively, in a condition-dependent manner (Van Leene et al., 2019; Xie et al., 2015). My work significantly adds to these findings, providing the first large-scale demonstration that plant ATG8 isoforms are functionally specialized, indicating that plant ATG8 substrate selectivity constitutes a layer of specificity in the autophagy pathway.

Although we do not have a complete picture of the many mechanisms that shape the selectivity of the plant autophagy pathway, my hypothesis is that ATG8 is the key specificity-determining component. Based on evidence from my work that plant ATG8 isoforms bind unique sets of cargo, as well as previous findings that ATG8 isoforms are differentially expressed (Hayward et al., 2009; Slavikova et al., 2005), I hypothesize that plant ATG8 isoforms direct distinct, partially redundant autophagy pathways. This is further supported by preliminary evidence from this thesis that ATG8 isoforms preferentially associate with more sequence-related ATG8s, suggesting segregated incorporation into autophagosomes. The compartmentalization of the autophagy pathway could occur at the cellular or subcellular level, with unique ATG8 isoform-specific pathways in different organs, tissues, and cell types.

6.2 What drove the diversification of plant ATG8s?

Although highly conserved across eukaryotes, ATG8 diversified from a single protein in algae to multiple isoforms in higher plants. The topology of the major monophyletic ATG8 clades reflects the chronology of plant evolution, indicating that the presence of multiple ATG8 isoforms is an ancient trait in plants (Kellner et al., 2017). In flowering

plants, each plant family has its own set of ATG8 isoforms that have been maintained over millions of years of evolution (Kellner et al., 2017). I hypothesize that the diversification of ATG8s across plant lineages was driven by the adaptive advantage conferred by both increased phenotypic plasticity and robustness.

To compensate for their lack of mobility, plants employ a number of unique mechanisms to rapidly react to changing environmental conditions, exhibiting remarkable phenotypic plasticity. Autophagy is a key pathway directing the maintenance of cellular homeostasis, involved in responding to starvation, abiotic stress, and pathogen invasion, as well in balancing plant growth and survival under these conditions. The diversification of plant ATG8s could enhance the capacity of the autophagy pathway to efficiently integrate disparate stress signals and alter plant physiology accordingly. The functional specialization of ATG8 isoforms, and the potential compartmentalization of distinct ATG8-specific autophagy pathways, could provide a mechanism to sense and respond to many environmental cues simultaneously.

Robustness—the ability to maintain performance in the face of perturbations and uncertainty—is an inherent property of all biological systems and is strongly favored by evolution (Stelling et al., 2004). At the molecular level, robustness can be conferred to a biological system through “genetic buffering,” with duplicate genes carrying out identical functions, or by different genes constituting alternative, functionally overlapping pathways (Hartman et al., 2001). Partial redundancy between compartmentalized autophagy pathways, facilitated by ATG8 expansion and functional specialization, would enhance the robustness of the autophagy network and safeguard the system against environmental disturbance (Stelling et al., 2004). One of the disturbances particularly relevant to this thesis is the manipulation of the plant autophagy pathway by pathogens, with the *P. infestans* effector PexRD54 as a prime example (Dagdaz et al., 2016). It will be exciting to determine the extent to which other plant pathogens similarly target the autophagy pathway—through direct ATG8 binding, or through alternate means—and to subsequently understand how coevolutionary dynamics may have selected for increased robustness within the pathway.

6.3 Multiple structural features shape ATG8 substrate specificity

The core ATG8 structure is composed of four α -helices and four β -strands, forming a β -grasp fold which is shared with ubiquitin and other ubiquitin-like modifiers (UBLs) (Burroughs et al., 2012). The ATG8 surface features two hydrophobic pockets termed the W-site and L-site, respectively, that serve as the major docking site for ATG8-interacting proteins (Maqbool et al., 2016). I determined that the ATG8 N-terminal β -strand—and, in particular, a single amino acid polymorphism in this region—largely underpins binding specificity to the substrate PexRD54 by shaping the hydrophobic pockets that accommodates this protein's AIM. I also showed that this region determines the broader ATG8 interactor profiles, defining selectivity towards upwards of 80 plant proteins.

Interestingly, the first β -strand had not previously been implicated in ATG8 substrate specificity. In studies of human ATG8s, the second α -helix ($\alpha 2$) and the second β -strand ($\beta 2$) have primarily been identified as the regions involved in determining interaction specificity. These structural features are adjacent to the two surface hydrophobic pockets, with $\beta 2$ sitting directly behind the W- and L-sites. Polymorphic residues in these regions between the two human ATG8 subfamilies, GABARAP and LC3, determine the differential binding of these isoforms to the autophagy adaptor ALFY, which interacts via an AIM (Lystad et al., 2014). Similarly, polymorphisms in ATG8 $\alpha 2$ and $\beta 2$ also underpin the specific interaction between the human ATG8 isoform LC3C and the autophagy receptor NDP52, which binds via a noncanonical AIM (von Muhlinen et al., 2012).

As more studies characterizing the structural determinants of ATG8 substrate specificity are complete, it will be interesting to observe whether ATG8 structural features important for substrate specificity in metazoan ATG8s are found to be similarly important in plant ATG8s, and vice versa. I would hypothesize that, due to constraints on the evolution of the AIM interaction interface—namely, that this region still has to be able to bind AIMS—the variant positions that underpin interaction specificity with AIM-containing substrates will be shared across distantly related ATG8s, although the precise variations may differ. Future experiments should determine the extent to which the biochemical basis of ATG8 interaction specificity has convergently evolved across various eukaryotic lineages.

Recently, a new ATG8 interaction interface was identified, termed the ubiquitin interacting motif (UIM)-docking site (UDS), which is a hydrophobic patch located near the C-terminal glycine on the surface opposite the AIM interaction interface (Marshall et al., 2019). The UDS has been shown to be conserved in yeast and mammalian ATG8s, but it has not yet been explored whether this interface is variable among ATG8 isoforms in eukaryotic lineages. It will be exciting to determine whether this additional interface may be involved in ATG8 functional specialization by preferentially binding distinct substrates.

6.4 Potato ATG8-4: an ATG8 apart?

Across the IP-MS experiments, ATG8-4 exhibited a highly selective interaction pattern compared to the other potato ATG8 isoforms. ATG8-4 presented a comparatively reduced number of interactors and this selectivity was found to be linked, in part, to polymorphisms within the first β -strand. In addition, ATG8-4 consistently interacted with a small number of specific proteins with a diverse set of predicted functions. Intriguingly, ATG8-4 also exhibited a selective interaction pattern with the endogenous *N. benthamiana* ATG8s in the interactome, interacting almost exclusively with the *N. benthamiana* ATG8-4, its closest homolog, supporting a model that autophagosomes may carry different populations of ATG8s. Together, these results suggest that ATG8-4 may perform only a subset of the ancestral ATG8 functions, or may have a completely novel role compared to the other ATG8s.

In both the interactome and the ATG8-4-S3 mutant analysis IP-MS experiments, I could not detect ATG8-4 interaction with a number of core autophagy components and intracellular trafficking proteins, although these proteins showed strong interaction with the other tested potato ATG8 isoforms. ATG8-4 did not interact with the autophagy components ATG1 and ATG4, proteins involved in phagophore initiation and ATG8 processing for membrane insertion, respectively. Interestingly, ATG1 (ULK1 in metazoans) also shows differential interaction with the metazoan ATG8 isoforms, preferentially interacting with both human and *Caenorhabditis elegans* ATG8s that belong to the GABARAP subfamily (Joachim et al., 2017; Wu et al., 2015). This observation has contributed to the understanding that the metazoan ATG8 subfamilies have an

evolutionary separation of function (Rogov et al., 2017), which could also hold true for the plant ATG8 subfamilies, either by major clade (I and II) or by plant-specific subfamilies. In addition, ATG8-4 did not interact with any predicted homologs of the intracellular trafficking proteins myosin XII, myosin-binding protein, early endosome antigen, and Rab11 family interacting protein. The reduced interaction of ATG8-4 with the core autophagy components and intracellular trafficking proteins could suggest that the biogenesis and trafficking of ATG8-4-labelled autophagosomes proceeds by a different mechanism, which would suggest that the plant autophagy pathway is compartmentalized, as well as indicate a potential mechanism for how this is achieved.

Across both of the IP-MS experiments, ATG8-4 specifically interacted with a distinct set of proteins as compared to the other potato ATG8 isoforms. These proteins included autophagy component ATG16, which is involved in the final transfer of ATG8 phosphatidylethanolamine (Kaufmann et al., 2014); 14-3-3 family proteins, which are involved in signal transduction pathways regulated by phosphorylation (DeLille et al., 2001); NADPH sorbitol-6-phosphate dehydrogenases (S6PDH), which reduces glucose-6-phosphate to sorbitol-6-phosphate (Sheveleva et al., 1998); and a lecithin-cholesterol acyltransferase (LCAT), which converts cholesterol and lecithins to cholesteryl esters and lysolecithins (Jonas, 2000). Only ATG16 has a previously characterized connection to autophagy, and there is vanishingly little literature on the latter two proteins.

It is not currently understood how the functions of these seemingly disparate interactors are connected, but I can hypothesize as to how ATG8-4 selectively recruits these proteins. ATG16 has not previously been reported to directly interact with ATG8, and the *N. benthamiana* and *A. thaliana* sequences do not have predicted AIMs. Similarly, none of the 14-3-3 family proteins found to interact with ATG8-4 contain predicted AIMs. For these interactors, it is possible that they interact with ATG8-4 indirectly, through a selective intermediary; that they contain cryptic or noncanonical AIM sequences, tailored to the ATG8-4 AIM binding pockets; or that they directly interact with ATG8-4 through an alternative interface. The other two specific interactors, S6PDH and LCAT, each contain predicted evolutionarily conserved AIM sequences, although the amino acid sequences of the motifs are dissimilar. This suggests that there is not an ATG8-4-specific interaction motif that mediates preferential interaction, in contrast to what has been found for human GABARAP-specific interactors (Rogov et al., 2017).

The enhanced selectivity ATG8-4 suggests that the function of this ATG8 isoform may be a product of subfunctionalization, or perhaps even neofunctionalization. In future research, it will be interesting to estimate the evolutionary timepoint at which functional divergence occurred and determine whether the selectivity of ATG8-4 is specific only to potato, shared among other Solanaceae clade II ATG8 isoforms, or shared amongst a wider swath of clade II ATG8s. It has previously been hypothesized that the polymorphisms within the first ATG8-4 β -strand were selected to evade PexRD54 binding, and thus that the selectivity of this isoform is linked to pathogen coevolution. However, if clade II ATG8s outside of the Solanaceae show a similarly selective interaction pattern, this would cast doubt on this hypothesis, and suggest that the selectivity of clade II ATG8s is a more ancient trait. Overall, studying the evolutionary history of potato ATG8-4 would improve our understanding of the potential compartmentalization of the selective autophagy pathway, as well as generate hypotheses about why this isoform stands apart.

6.5 Aiming higher: improving the accuracy of ATG8-interacting motif predictions

Considering the short length of the ATG8-interacting motif, at just five core amino acid residues, its bioinformatic prediction can result in false positives. To get a sense of the background false AIM prediction rate using the iLIR software (Kalvari et al., 2014), I predicted AIMs within three large sets (260 proteins) of random *N. benthamiana* proteins. In these sets, an average of 35% of the proteins had predicted AIMs, a comparable percentage to the percentage of proteins with predicted AIMs in the ATG8 interactome (40%) and in the ATG8-4-S3 mutant analysis dataset (50%). To filter out potential false predictions, I integrated the parameter of AIM conservation, looking at whether a given AIM was conserved in either *A. thaliana* or the early diverged land plant *Marchantia polymorpha*, both by position and sequence. In doing this, I found that only 27% of the predicted AIMs from the random protein sets were conserved, whereas a majority of AIMs were conserved in the ATG8 interactome (73%) and in the ATG8-4-S3 mutant analysis dataset (70%).

This analysis suggests that conservation is a useful criterion to differentiate between potential false positives and ‘true’ AIMs. I propose that a more advanced approach would also consider the overall amino acid conservation of a given protein when assessing AIM conservation, as well as integrate prediction of whether the putative AIM is in a structurally disordered region of the protein, considering that ATG8 binding requires a flexible AIM conformation (Noda et al., 2010). Overall, having a more accurate AIM prediction tool would increase the power of large-scale ATG8 interactor screens, improving our ability to identify ATG8-interacting candidate proteins. This would facilitate the identification of plant autophagy receptors and adaptors, and thus help fill a large gap in our mechanistic understanding of how the plant autophagy machinery selectively recognizes and recruits various components.

6.6 *Phytophthora mirabilis* PexRD54 has evolved away from direct ATG8 targeting

To understand how changes in the host environment shape effector evolution, I explored the evolutionary dynamics of the effector PexRD54 in different host-specific lineages of *Phytophthora*. I found that the PexRD54 ortholog from *P. mirabilis*, a closely related species to *P. infestans*, has a polymorphism in its AIM which nearly abolishes binding to the ATG8s of its host, *Mirabilis jalapa*. I hypothesize that the weak interaction between *Pm*PexRD54 and the *M. jalapa* ATG8s is likely not relevant to infection, and that *P. mirabilis* PexRD54 has evolved away from direct ATG8 targeting. One potential explanation for the *Pm*PexRD54 evolutionary trajectory is that selective autophagy does not play a role in plant immunity in *M. jalapa*, and thus the manipulation of this pathway during infection does not present an advantage to the pathogen. It is also possible that PexRD54 was fine-tuned to the host environments of the Solanales taxa—which includes the *P. infestans* hosts, potato and tomato, and the *P. ipomeae* host, morning glory—and, due to the large phylogenetic distance that separates *M. jalapa*, targeting ATG8 in this species is not beneficial to infection. Moreover, it is reasonable to propose that an intracellular immune receptor detects the manipulation of autophagy via ATG8 binding in *M. jalapa*, and thus the *Pm*PexRD54 AIM polymorphism represents an attempt to evade detection.

In any of these cases, it may seem somewhat curious that *PmPexRD54* has been maintained in the *P. mirabilis* lineage, especially considering that the gene is localized to a gene-sparse genomic compartment (Raffaele et al., 2010). As part of the ‘two-speed genome model,’ these compartments are hypothesized to serve as cradles for adaptive evolution, featuring increased incidence of duplication, deletion, and recombination. In the *Phytophthora* clade 1c, presence/ absence polymorphisms were found to be thirteen times as abundant in the gene-sparse compared to the gene-dense regions (Raffaele et al., 2010). Indeed, there are countless examples of effector gene loss that can be tied to the host environment, especially in cases where effectors are linked to unstable genomic environment (Raffaele and Kamoun, 2012). And yet, *P. mirabilis* *PexRD54* persists.

I hypothesize that *PexRD54* has been maintained in *P. mirabilis* because it still retains a role in enhancing infection of *M. jalapa*, despite a non-functional AIM. In this, I further propose that the *PmPexRD54* WY-domains are able to carry out the functions, or a subset of the functions, directed by *PiPexRD54* WY-domains during *P. infestans* infection of potato. The five tandem WY-domains of *PiPexRD54* are thought to be responsible for stimulating autophagosome formation and binding proteins that are taken up into the re-directed autophagy pathway (Maqbool et al., 2016). As such, the WY-domains of *PmPexRD54* could be involved in perturbing autophagy via these other means, or through carrying out other as-yet-unknown functions.

6.7 What we talk about when we talk about evolutionary plant-microbe interactions

Performing mechanistic research with an evolutionary perspective pushes the field of plant-microbe interactions beyond the molecular, laying the foundation to ask questions not only about how these systems function, but also about how they came to be that way. Plant-microbe systems are exceptional in that their evolutionary dynamics can be studied across multiple timescales (Upson et al., 2018). In macroevolutionary terms, microbes have shaped the evolution of plants since their arrival on land—and vice versa. With shorter timescales in mind, the arms race that exists between plants and microbes creates a tight interplay, with both plants and pathogens vying for advantage. These dynamics create strong selective pressures and have led to striking examples of rapid adaptive

evolutionary change. I am of the opinion that many experimental systems would benefit from comparative approaches, performed within a robust phylogenetic and ecological framework, that test specific hypotheses about how evolution has modified the mechanisms underpinning plant-microbe interactions. These kinds of evolutionary approaches use evolution as a guide to test molecular models under real-world conditions and thus contribute a more rigorous understanding of plant-microbe systems.

6.8 Concluding remarks and future challenges

There are still many unanswered questions about how ATG8 isoforms interact with specific cargo, as well as the role that these dynamics play in defining the selectivity of the plant autophagy pathway. For example, do other plant family-specific ATG8 clades exhibit similar levels of substrate specificity to the Solanaceae? What other structural regions underpin selectivity in plant ATG8s, both within the Solanaceae and more broadly? Do plant autophagosomes contain unique populations of ATG8 isoforms and, if so, what are the mechanisms that contribute to the compartmentalization of the autophagy pathway? What are the plant autophagy receptors that mediate the degradation of cellular components, and how evolutionarily conserved are these proteins? Are there AIM sequences that are preferential towards binding specific ATG8 isoforms, and how are other ATG8 interaction interfaces involved in cargo selectivity? Do other pathogen species contain effectors that subvert selective autophagy through targeting ATG8s, and what patterns of evolution do these effectors exhibit in closely related pathogen lineages? Answering these fundamental questions will help advance our understanding of plant selective autophagy, providing insights into an essential homeostatic pathway.

Appendix I

Supplemental figures for Chapter 3: Solanaceous ATG8 isoforms associate with distinct sets of plant proteins.

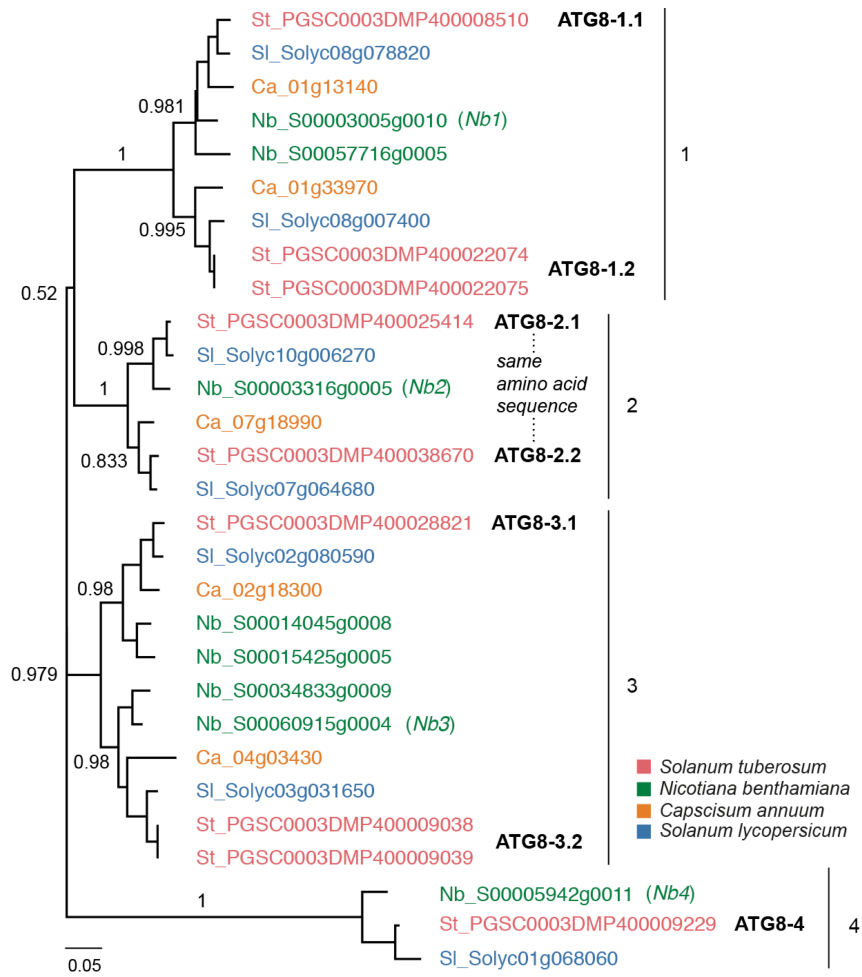


Figure A.1.1 Orthologous relationships between Solanaceous ATG8 isoforms

A more detailed view of Fig 3.1a. Unrooted maximum-likelihood phylogenetic tree of 29 ATG8 homologs with clades marked on the right, and colors indicating plant species. The tree was calculated in MEGA7 (Kumar et al., 2016) from a 369 nucleotide alignment (MUSCLE (Edgar, 2004), codon-based). The bootstrap supports of the major nodes are indicated. The scale bar indicates the evolutionary distance based on nucleotide substitution rate.

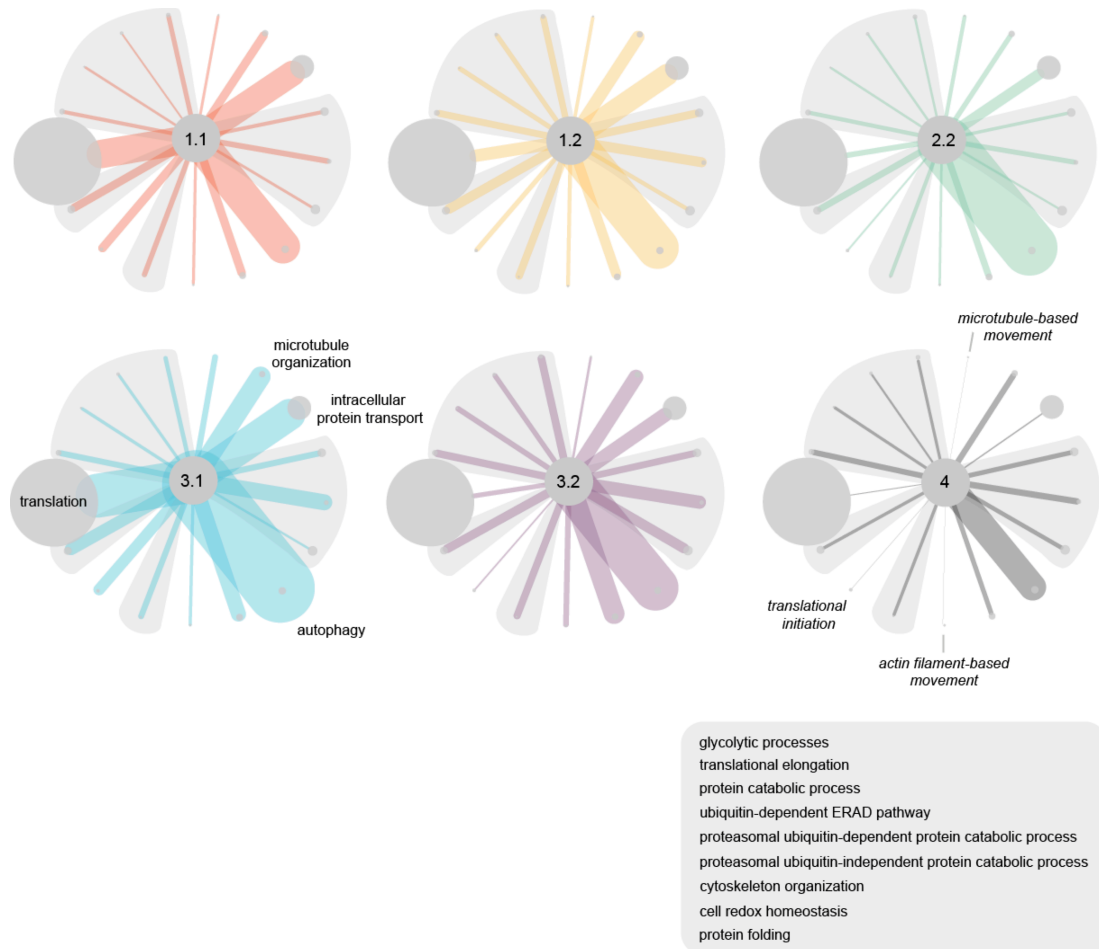


Figure A.1.2 Network representation of the interactions between ATG8s and protein groups defined by biological process gene ontology (GO) annotations

For each interactor in the dataset, the closest *A. thaliana* homolog was predicted using BLAST, and the gene ontology annotations were obtained using Blast2GO (Gotz et al., 2008). Proteins were grouped based on the cellular compartment terms, and a subset of groups were chosen for representation. The sizes of the nodes are scaled to the number of interactors in each respective group, and the edges are weighed to the average PSM values for all the interactors in each respective group for each ATG8. Nodes are labelled where the average PSM value is most differential compared to the other ATG8s. Nodes shaded in gray exhibit similar average PSM values between all ATG8s, and the labels for these are included in the gray box.

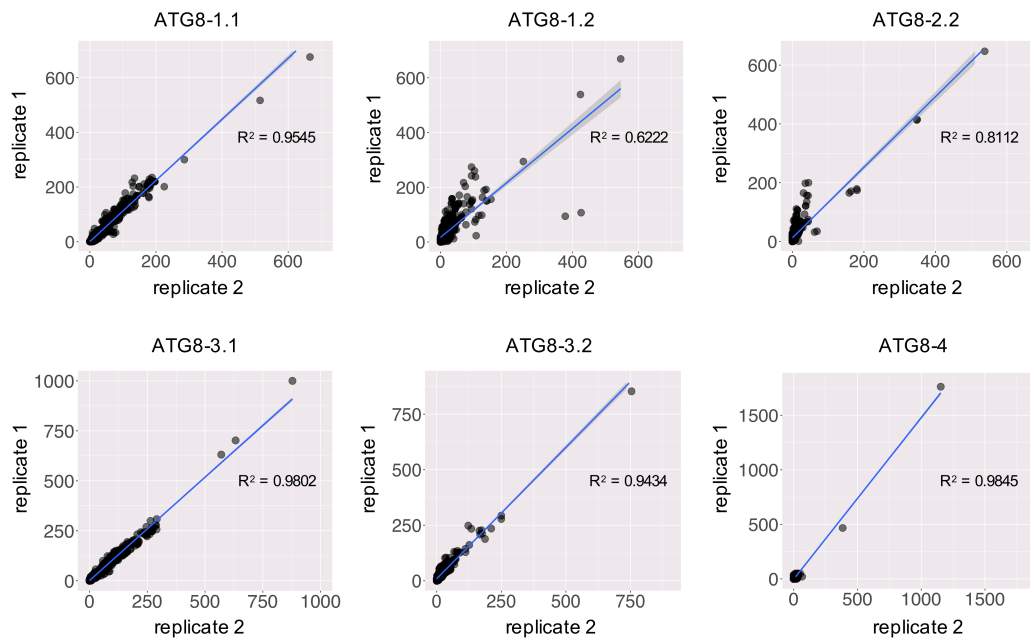


Figure A.1.3 ATG8 interactome data is reproducible across replicates

The PSM values for the two replicates of each ATG8 isoform in the interactome dataset (621 interactors) were plotted in a pairwise fashion with a line of best fit, showing reproducibility across the replicates. The R² values for each correlation are reported for each pair of replicates.

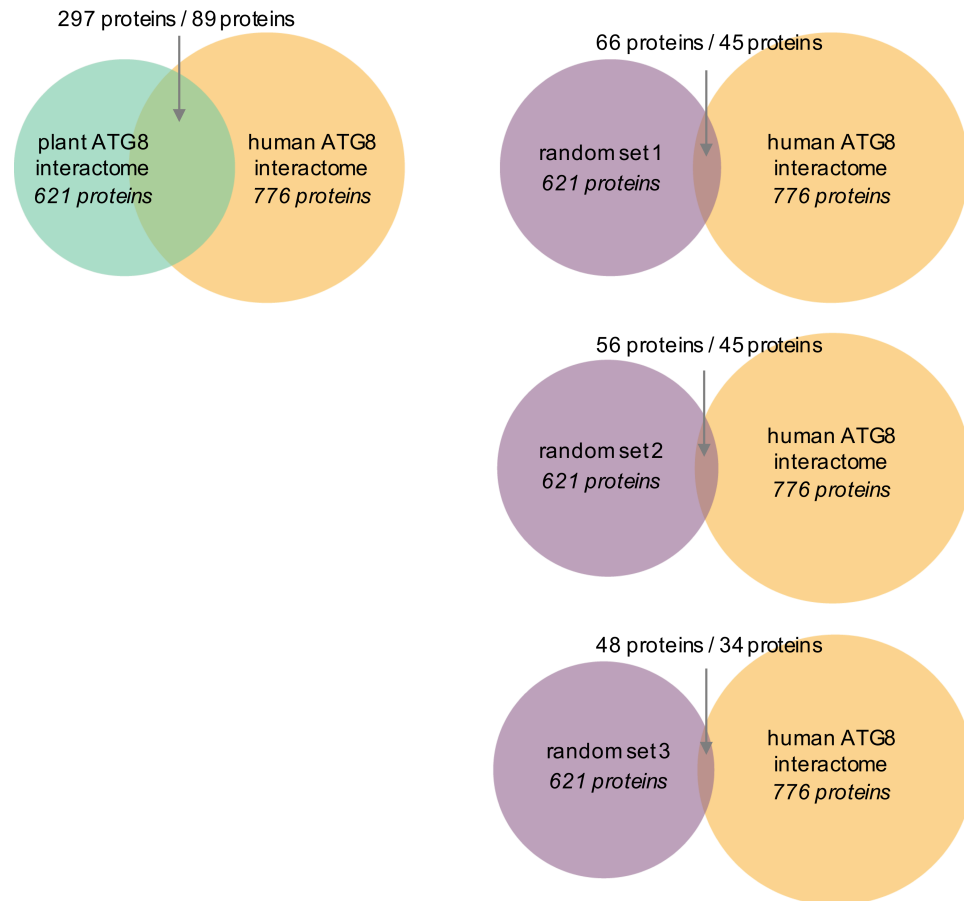


Figure A.1.4 Significant level of overlap between the *N. benthamiana* ATG8 interactome and the human ATG8 interactome from Behrends et al (2010)

(Left) Graphical representation of the related proteins shared between the *N. benthamiana* ATG8 interactome (621 proteins) and the human ATG8 interactome from Behrends et al. (776 proteins) (**Table A.2.2**), with the amount of overlap between the interactome circles scaled to the percent of *N. benthamiana* ATG8 interactors shared. The number of *N. benthamiana* ATG8 interactors with a related protein in the human ATG8 interactome is listed above the gray arrow, to the left, whereas the number of human ATG8 interactors with a related protein in the *N. benthamiana* ATG8 interactome are listed above the gray arrow, to the right. The discrepancy between these numbers is due to the existence of paralogous proteins in *N. benthamiana* or potential false duplications within the *N. benthamiana* proteome. (Right) Analogous graphical representation of the related proteins shared between three random sets of proteins (621 proteins each), separately, and the human ATG8 interactome from Behrends et al. (776 proteins).

Appendix II

Supplemental tables for Chapter 3: Solanaceous ATG8 isoforms associate with distinct sets of plant proteins.

Table A.2.6 ATG8 interactome

For each *N. benthamiana* interactor in the dataset (621 proteins), the closest *A. thaliana* and *M. polymorpha* homologs were predicted using BLAST. Each interactor is thus described, by column: *N. benthamiana* accession ('Nb'), protein identification ('Nb protein ID'); the *A. thaliana* homolog accession number ('At') and protein identification ('At protein ID'); and the *M. polymorpha* homolog accession number ('Mp') and protein identification ('Mp protein ID').

Nb	Nb protein ID	At	At_protein_ID	Mp	Mp protein ID
NbS00025918g0006.1 Nbv6.1trA106497	1 aminocyclopropane 1 carboxylate oxidase	AT1G05010.1	ethylene-forming enzyme	Mapoly0019s0012.1	Oxidoreductase
NbS00056344g0007.1 Nbv6.1trA62570 Nbv6.1trP51988 Nbv6.1trP4045 Nbv6.1trP28238	14 3 3 protein A	AT1G78300.1	general regulatory factor 2	Mapoly0043s0019.1	14-3-3 protein epsilon
NbS00059178g0006.1	14 3 3 protein beta/alpha B	AT5G65430.1	general regulatory factor 8	Mapoly0043s0019.1	14-3-3 protein epsilon
Nbv6.1trA124569	14-3-3 protein 4-like	AT3G02520.2	general regulatory factor 7	Mapoly0043s0019.1	14-3-3 protein epsilon
Nbv6.1trP47675	14-3-3-like protein a	AT5G38480.3	general regulatory factor 3	Mapoly0043s0019.1	14-3-3 protein epsilon
NbS00014887g0017.1 Nbv6.1trA99313 Nbv6.1trA192391 Nbv6.1trA108924	2 oxoglutarate 2OG and FeII dependent oxygenase	AT2G17970.1	2-oxoglutarate (2OG) and Fe(II)-dependent oxygenase superfamily protein	Mapoly0001s0483.1	Uncharacterized conserved protein
Nbv6.1trA1295	2-isopropylmalate synthase a-like	AT1G74040.1	2-isopropylmalate synthase 1	Mapoly0002s0332.1	2-isopropylmalate synthase.
Nbv6.1trA142887 NbS00001524g0009.1 Nbv6.1trA209158 Nbv6.1trA76748 Nbv6.1trP52493	26s protease regulatory subunit 6a homolog	AT3G05530.1	regulatory particle triple-A ATPase 5A	Mapoly0085s0078.1	26S proteasome regulatory subunit T5
Nbv6.1trP58965 NbS00057057g0013.1	26s protease regulatory subunit 7	AT1G53750.1	regulatory particle triple-A 1A	Mapoly0031s0139.1	26S proteasome regulatory subunit T1
Nbv6.1trA106982	26s protease regulatory subunit s10b homolog b	AT1G45000.1	AAA-type ATPase family protein	Mapoly0009s0112.3	26S proteasome regulatory subunit T4
Nbv6.1trA100631 Nbv6.1trA171884 Nbv6.1trA1863 Nbv6.1trP72246	26s proteasome non- atpase regulatory subunit 2 homolog a- like	AT2G20580.1	26S proteasome regulatory subunit S2 1A	Mapoly0136s0010.1	26S proteasome regulatory subunit N1
Nbv6.1trP48624	26s proteasome regulatory subunit 4 homolog a	AT4G29040.1	regulatory particle AAA-ATPase 2A	Mapoly0170s0030.1	26S proteasome regulatory subunit T2
Nbv6.1trA269662 Nbv6.1trP40801	3-ketoacyl- thiolase peroxisomal	AT2G33150.1	peroxisomal 3- ketoacyl-CoA thiolase 3	Mapoly0055s0037.1	Acetyl-CoA C- acyltransferase.
Nbv6.1trA252519 NbS00018083g0002.1	30s ribosomal protein chloroplastic	AT1G79850.1	ribosomal protein S17	Mapoly0027s0119.1	40S RIBOSOMAL PROTEIN S11 FAMILY MEMBER
Nbv6.1trP14272	40s ribosomal protein s13	AT4G00100.1	ribosomal protein S13A	Mapoly0044s0132.1	small subunit ribosomal protein S13e
Nbv6.1trP3841 Nbv6.1trP70032	40s ribosomal protein s14-2	AT3G11510.1	Ribosomal protein S11 family protein	Mapoly0008s0132.1	small subunit ribosomal protein S14e
Nbv6.1trA213884 Nbv6.1trP47007	40s ribosomal protein s15-like	AT5G09500.1	Ribosomal protein S19 family protein	Mapoly0004s0172.1	small subunit ribosomal protein S15e
NbS00013115g0003.1	40S ribosomal protein S15a 1	AT5G59850.1	Ribosomal protein S8 family protein	Mapoly0083s0020.1	small subunit ribosomal protein S15Ae
Nbv6.1trP23049	40s ribosomal protein s16	AT2G09990.1	Ribosomal protein S5 domain 2-like superfamily protein	Mapoly0179s0010.1	small subunit ribosomal protein S16e
NbS00056355g0003.1 Nbv6.1trA264033 Nbv6.1trP19832	40S ribosomal protein S18	AT4G09800.1	S18 ribosomal protein	Mapoly0124s0041.1	small subunit ribosomal protein S18e

Nb	Nb protein ID	At	At_protein_ID	Mp	Mp protein ID
Nbv6.1trA219589	40s ribosomal protein s19-3	AT5G61170.1	Ribosomal protein S19e family protein	Mapoly0002s0140.1	small subunit ribosomal protein S19e
NbS00006107g0001.1 NbS00016839g0002.1	40S ribosomal protein S2 2	AT1G59359.1	Ribosomal protein S5 family protein	Mapoly0027s0187.1	small subunit ribosomal protein S2e
Nbv6.1trP52801	40s ribosomal protein s24-1	AT5G28060.1	Ribosomal protein S24e family protein	Mapoly0014s0159.1	small subunit ribosomal protein S24e
NbS00017796g0009.1	40S ribosomal protein S25 1	AT4G39200.1	Ribosomal protein S25 family protein	Mapoly0114s0042.1	small subunit ribosomal protein S25e
NbS00005996g0006.1 Nbv6.1trA111384 Nbv6.1trA9923	40S ribosomal protein S26	AT2G40590.1	Ribosomal protein S26e family protein	Mapoly0021s0076.1	small subunit ribosomal protein S26e
Nbv6.1trP3553 Nbv6.1trP58727	40s ribosomal protein s3-3	AT5G35530.1	Ribosomal protein S3 family protein	Mapoly0001s0014.1	small subunit ribosomal protein S3e
NbS00002954g0013.1 Nbv6.1trP32198 Nbv6.1trA49019 Nbv6.1trA63784 NbS00004044g0002.1	40S ribosomal protein S3a	AT4G34670.1	Ribosomal protein S3Ae	Mapoly0035s0068.1	small subunit ribosomal protein S3Ae
Nbv6.1trP28367 Nbv6.1trP28368 Nbv6.1trP30065	40s ribosomal protein s4-like	AT5G58420.1	Ribosomal protein S4 (RPS4A) family protein	Mapoly0012s0120.1	small subunit ribosomal protein S4e
NbS00003570g0008.1 NbS00011165g0113.1	40S ribosomal protein S5 2	AT3G11940.2	ribosomal protein 5A	Mapoly0037s0139.1	small subunit ribosomal protein S5e
NbS00000439g0011.1 Nbv6.1trP1324 Nbv6.1trP17350 Nbv6.1trP68267	40S ribosomal protein S6	AT5G10360.1	Ribosomal protein S6e	Mapoly0098s0025.1	small subunit ribosomal protein S6e
Nbv6.1trA118205 Nbv6.1trA228338	40s ribosomal protein s7-like	AT1G48830.2	Ribosomal protein S7e family protein	Mapoly0060s0109.1	small subunit ribosomal protein S7e
Nbv6.1trP19501	40s ribosomal protein s7-like	AT3G02560.3	Ribosomal protein S7e family protein	Mapoly0060s0109.1	small subunit ribosomal protein S7e
Nbv6.1trP47161 NbS00001075g0014.1 Nbv6.1trA237384	50s ribosomal protein chloroplastic	AT1G05190.1	Ribosomal protein L6 family	Mapoly0005s0245.1	60S/50S RIBOSOMAL PROTEIN L6/L9
Nbv6.1trP1337	50s ribosomal protein chloroplastic	AT2G33450.1	Ribosomal L28 family	Mapoly0087s0077.1	39S RIBOSOMAL PROTEIN L28
Nbv6.1trA143068	50s ribosomal protein chloroplastic	AT3G63490.1	Ribosomal protein L1p/L10e family	Mapoly0043s0143.1	RIBOSOMAL PROTEIN L7AE FAMILY MEMBER
Nbv6.1trA53026 Nbv6.1trP19902	50s ribosomal protein chloroplastic-like	AT3G27850.1	ribosomal protein L12-C	Mapoly0071s0038.1	large subunit ribosomal protein L7/L12
NbS00047740g0003.1	50S ribosomal protein L14	AT3G04400.2	Ribosomal protein L14p/L23e family protein	Mapoly0027s0067.1	large subunit ribosomal protein L23e
NbS00007712g0010.1	50S ribosomal protein L16 chloroplastic	ATCG00790.1	ribosomal protein L16	Mapoly0052s0079.1	large subunit ribosomal protein L16
NbS00021394g0006.1	60 ribosomal protein L14	AT4G27090.1	Ribosomal protein L14	Mapoly0030s0040.1	large subunit ribosomal protein L14e

Nb	Nb protein ID	At	At_protein_ID	Mp	Mp protein ID
Nbv6.1trA65372 Nbv6.1trP68173 NbS0000941g0015.1 NbS00021044g0016.1	60s acidic ribosomal protein isoform 1	AT3G44590.2	60S acidic ribosomal protein family	Mapoly0036s0060.1	60S acidic ribosomal protein P2
Nbv6.1trA47361 Nbv6.1trP71351	60s acidic ribosomal protein p0	AT2G40010.1	Ribosomal protein L10 family protein	Mapoly0043s0105.1	large subunit ribosomal protein LP0
NbS00053503g0005.1 Nbv6.1trA117530 Nbv6.1trA168757 Nbv6.1trA242348 Nbv6.1trA117531	60S acidic ribosomal protein P1	AT5G24510.1	60S acidic ribosomal protein family	Mapoly0007s0277.1	large subunit ribosomal protein LP1
Nbv6.1trA7626	60s acidic ribosomal protein p2a-like	AT3G44590.2	60S acidic ribosomal protein family	Mapoly0001s0201.1	large subunit ribosomal protein LP2
Nbv6.1trA254880 Nbv6.1trP41622 Nbv6.1trP66742	60s acidic ribosomal protein p3-like	AT5G57290.3	60S acidic ribosomal protein family	Mapoly0006s0174.1	60S ACIDIC RIBOSOMAL PROTEIN FAMILY MEMBER
Nbv6.1trA213287 Nbv6.1trP65517	60s ribosomal protein l10-like	AT1G26910.1	Ribosomal protein L16p/L10e family protein	Mapoly0020s0158.1	large subunit ribosomal protein L10e
NbS00013207g0009.1 NbS00014760g0001.1 Nbv6.1trA100686 Nbv6.1trP54771 NbS00044021g0003.1	60S ribosomal protein L10a 1	AT1G08360.1	Ribosomal protein L1p/L10e family	Mapoly0006s0264.1	large subunit ribosomal protein L10Ae
Nbv6.1trA198673	60s ribosomal protein l10a-1-like	AT1G08360.1	Ribosomal protein L1p/L10e family	Mapoly0006s0241.3	large subunit ribosomal protein L10Ae
Nbv6.1trP19462 NbS00010427g0115.1	60s ribosomal protein l11-1	AT2G42740.1	ribosomal protein large subunit 16A	Mapoly0038s0097.1	60S RIBOSOMAL PROTEIN L11-RELATED
Nbv6.1trP70429	60s ribosomal protein l11-1	AT2G42740.1	ribosomal protein large subunit 16A	Mapoly0207s0012.1	60S RIBOSOMAL PROTEIN L11-RELATED
Nbv6.1trP77203	60s ribosomal protein l11-1	AT5G45775.2	Ribosomal L5P family protein	Mapoly0038s0097.1	60S RIBOSOMAL PROTEIN L11-RELATED
Nbv6.1trA158121 Nbv6.1trP32299 Nbv6.1trP3838	60s ribosomal protein l12	AT5G60670.1	Ribosomal protein L11 family protein	Mapoly0007s0191.1	large subunit ribosomal protein L12e
NbS00026051g0013.1	60S ribosomal protein L13	AT3G49010.7	breast basic conserved 1	Mapoly0005s0116.1	large subunit ribosomal protein L13e
NbS00030768g0006.1 NbS00041012g0008.1 Nbv6.1trP17644 Nbv6.1trP19568	60S ribosomal protein L13	AT3G49010.7	breast basic conserved 1	Mapoly0055s0071.1	large subunit ribosomal protein L13e
Nbv6.1trP3552 Nbv6.1trP69096 Nbv6.1trA109794 Nbv6.1trP17842	60s ribosomal protein l13a-4-like	AT5G48760.2	Ribosomal protein L13 family protein	Mapoly0054s0044.1	large subunit ribosomal protein L13Ae
Nbv6.1trA74128 Nbv6.1trP76763 Nbv6.1trA75455	60s ribosomal protein l14-1	AT2G20450.1	Ribosomal protein L14	Mapoly0030s0040.1	large subunit ribosomal protein L14e
Nbv6.1trA178237 Nbv6.1trP38388 Nbv6.1trP27073 Nbv6.1trP17614	60s ribosomal protein l15-like	AT4G16720.1	Ribosomal protein L23/L15e family protein	Mapoly0043s0043.1	large subunit ribosomal protein L15e

Nb	Nb protein ID	At	At_protein_ID	Mp	Mp protein ID
Nbv6.1trA110493	60s ribosomal protein l15-like	AT4G17390.1	Ribosomal protein L23/L15e family protein	Mapoly0043s0043.1	large subunit ribosomal protein L15e
NbS00008466g0007.1 Nbv6.1trP54412 Nbv6.1trP13280 Nbv6.1trA12790	60S ribosomal protein L17	AT1G27400.1	Ribosomal protein L22p/L17e family protein	Mapoly0014s0203.2	large subunit ribosomal protein L17e
Nbv6.1trP22752	60s ribosomal protein l18a	AT2G34480.2	Ribosomal protein L18ae/LX family protein	Mapoly0001s0112.1	large subunit ribosomal protein L18Ae
Nbv6.1trA228330 Nbv6.1trP73490	60s ribosomal protein l18a	AT3G14600.1	Ribosomal protein L18ae/LX family protein	Mapoly0001s0112.1	large subunit ribosomal protein L18Ae
NbS00020925g0004.1 NbS00022677g0027.1 NbS00024093g0010.1 NbS00012223g0004.1 NbS00037623g0001.1 Nbv6.1trA65478 Nbv6.1trP56850 Nbv6.1trP58899 Nbv6.1trP65332	60S ribosomal protein L19 2	AT3G16780.1	Ribosomal protein L19e family protein	Mapoly0068s0058.1	large subunit ribosomal protein L19e
Nbv6.1trP56805	60s ribosomal protein l21-1-like	AT1G09690.1	Translation protein SH3-like family protein	Mapoly0052s0065.1	large subunit ribosomal protein L21e
Nbv6.1trA187516 Nbv6.1trP53202 Nbv6.1trP47201	60s ribosomal protein l21-1-like	AT1G57860.1	Translation protein SH3-like family protein	Mapoly0052s0065.1	large subunit ribosomal protein L21e
NbS00017836g0015.1 NbS00024386g0011.1 NbS00056322g0001.1 Nbv6.1trA117657 Nbv6.1trA95896	60S ribosomal protein L22 2	AT3G05560.3	Ribosomal L22e protein family	Mapoly0080s0007.1	60S RIBOSOMAL PROTEIN L22
Nbv6.1trA114306 NbS00004708g0003.1	60s ribosomal protein l23	AT3G04400.1	Ribosomal protein L14p/L23e family protein	Mapoly0047s0085.1	50S/60S RIBOSOMAL PROTEIN L14/L23
NbS00000332g0115.1 Nbv6.1trP27867 Nbv6.1trP46844	60s ribosomal protein l23a-like	AT3G55280.2	ribosomal protein L23AB	Mapoly0028s0094.1	large subunit ribosomal protein L23Ae
NbS00017881g0010.1 Nbv6.1trP1418	60S ribosomal protein L24	AT2G36620.1	ribosomal protein L24	Mapoly0055s0009.1	large subunit ribosomal protein L24e
Nbv6.1trA12405 Nbv6.1trA31978 Nbv6.1trA6916 NbS00035409g0006.1 NbS00059392g0001.1	60s ribosomal protein l26-1	AT3G49910.1	Translation protein SH3-like family protein	Mapoly0026s0085.1	large subunit ribosomal protein L26e
Nbv6.1trP16932 Nbv6.1trA12178 Nbv6.1trA88604	60s ribosomal protein l27	AT4G15000.1	Ribosomal L27e protein family	Mapoly0020s0150.1	large subunit ribosomal protein L27e
NbS00001559g0006.1 Nbv6.1trP30012 Nbv6.1trA6752	60S ribosomal protein L27A	AT1G70600.1	Ribosomal protein L18e/L15 superfamily protein	Mapoly0078s0013.1	large subunit ribosomal protein L27Ae
Nbv6.1trA5091 Nbv6.1trA181920 Nbv6.1trP70380	60s ribosomal protein l28-1-like	AT2G19730.3	Ribosomal L28e protein family	Mapoly0002s0184.2	large subunit ribosomal protein L28e

Nb	Nb protein ID	At	At_protein_ID	Mp	Mp protein ID
Nbv6.1trA251354 Nbv6.1trP48435 NbS00038870g0030.1 Nbv6.1trP61511 Nbv6.1trP43008 Nbv6.1trA211581	60s ribosomal protein l3-like	AT1G61580.1	R-protein L3 B	Mapoly0001s0237.1	large subunit ribosomal protein L3e
Nbv6.1trP71451 NbS00002504g0003.1 Nbv6.1trP53058	60s ribosomal protein l30	AT1G36240.1	Ribosomal protein L7Ae/L30e/S12e/Gadd45 family protein	Mapoly0099s0042.1	large subunit ribosomal protein L30e
Nbv6.1trA29503	60s ribosomal protein l30	AT1G77940.1	Ribosomal protein L7Ae/L30e/S12e/Gadd45 family protein	Mapoly0099s0042.1	large subunit ribosomal protein L30e
Nbv6.1trP3924 Nbv6.1trP73091	60s ribosomal protein l31	AT2G19740.1	Ribosomal protein L31e family protein	Mapoly0102s0008.1	large subunit ribosomal protein L31e
NbS00010505g0011.1 Nbv6.1trA219821 Nbv6.1trP17173 Nbv6.1trP67806 NbS00014354g0008.1 NbS00043519g0007.1	60S ribosomal protein L32 1	AT4G18100.1	Ribosomal protein L32e	Mapoly0003s0256.1	large subunit ribosomal protein L32e
NbS00014666g0005.1	60S ribosomal protein L34	AT1G26880.1	Ribosomal protein L34e superfamily protein	Mapoly0148s0016.1	large subunit ribosomal protein L34e
Nbv6.1trP19660	60s ribosomal protein l34	AT1G69620.1	ribosomal protein L34	Mapoly0148s0016.1	large subunit ribosomal protein L34e
Nbv6.1trA177800 Nbv6.1trA217700 Nbv6.1trA7744	60s ribosomal protein l35-like	AT5G02610.1	Ribosomal L29 family protein	Mapoly0097s0080.1	large subunit ribosomal protein L35e
Nbv6.1trP21419	60s ribosomal protein l35-like	AT5G02610.2	Ribosomal L29 family protein	Mapoly0097s0080.1	large subunit ribosomal protein L35e
NbS00011439g0013.1 NbS00059182g0001.1	60S ribosomal protein L35a	AT1G74270.1	Ribosomal protein L35Ae family protein	Mapoly0014s0079.2	60S RIBOSOMAL PROTEIN L35A
NbS00014429g0017.1	60S ribosomal protein L36	AT3G53740.4	Ribosomal protein L36e family protein	Mapoly0005s0062.1	large subunit ribosomal protein L36e
Nbv6.1trA139422	60s ribosomal protein l36-2-like	AT2G37600.2	Ribosomal protein L36e family protein	Mapoly0005s0062.1	large subunit ribosomal protein L36e
NbS00009780g0005.1	60S ribosomal protein L37 3	AT3G16080.1	Zinc-binding ribosomal protein family protein	Mapoly0029s0031.1	large subunit ribosomal protein L37e
NbS00007843g0209.1 NbS00030533g0009.1	60S ribosomal protein L37a	AT3G10950.1	Zinc-binding ribosomal protein family protein	Mapoly0095s0001.1	large subunit ribosomal protein L37Ae
NbS00032888g0009.1	60S ribosomal protein L38	AT3G59540.1	Ribosomal L38e protein family	Mapoly0009s0137.1	large subunit ribosomal protein L38e
Nbv6.1trA210320 Nbv6.1trP68432 Nbv6.1trA107185 Nbv6.1trA131660 Nbv6.1trA5383 Nbv6.1trA202662	60s ribosomal protein l4-1-like	AT3G09630.1	Ribosomal protein L4/L1 family	Mapoly0116s0033.3	large subunit ribosomal protein L4e
Nbv6.1trP13804	60s ribosomal protein l44	AT4G14320.1	Zinc-binding ribosomal protein family protein	Mapoly0025s0101.1	large subunit ribosomal protein L44e

Nb	Nb protein ID	At	At_protein_ID	Mp	Mp protein ID
Nbv6.1trA239446 Nbv6.1trA239447 Nbv6.1trA244594 Nbv6.1trP74572	60s ribosomal protein l5-like	AT3G25520.3	ribosomal protein L5	Mapoly0054s0045.1	large subunit ribosomal protein L5e
Nbv6.1trA126646 Nbv6.1trP38704 Nbv6.1trA74446 Nbv6.1trP41032 Nbv6.1trP72839	60s ribosomal protein l5-like	AT5G39740.2	ribosomal protein L5 B	Mapoly0054s0045.1	large subunit ribosomal protein L5e
Nbv6.1trA114336 Nbv6.1trA139794 Nbv6.1trP47475 Nbv6.1trA63010 Nbv6.1trA228136 NbS00021581g0010.1 NbS00017572g0018.1	60s ribosomal protein l6-like	AT1G74050.1	Ribosomal protein L6 family protein	Mapoly0037s0030.1	large subunit ribosomal protein L6e
Nbv6.1trA57621	60s ribosomal protein l6-like	AT1G74060.1	Ribosomal protein L6 family protein	Mapoly0037s0030.1	large subunit ribosomal protein L6e
NbS00061153g0003.1	60S ribosomal protein L7	AT2G44120.2	Ribosomal protein L30/L7 family protein	Mapoly0050s0096.1	large subunit ribosomal protein L7e
Nbv6.1trA3389	60s ribosomal protein l7-1	AT1G80750.1	Ribosomal protein L30/L7 family protein	Mapoly0050s0096.1	large subunit ribosomal protein L7e
Nbv6.1trA67492 Nbv6.1trP19854 Nbv6.1trP68164 Nbv6.1trA252389 Nbv6.1trA5223	60s ribosomal protein l7-2	AT3G13580.9	Ribosomal protein L30/L7 family protein	Mapoly0050s0096.1	large subunit ribosomal protein L7e
Nbv6.1trA187926	60s ribosomal protein l7-2-like	AT2G44120.1	Ribosomal protein L30/L7 family protein	Mapoly0050s0096.1	large subunit ribosomal protein L7e
NbS00023515g0003.1 Nbv6.1trP16969 Nbv6.1trP45740 Nbv6.1trP16849 NbS00010173g0011.1	60S ribosomal protein L7a	AT3G62870.1	Ribosomal protein L7Ae/L30e/S12e/Ga dd45 family protein	Mapoly0030s0100.1	large subunit ribosomal protein L7Ae
NbS00017622g0006.1 Nbv6.1trA220169 Nbv6.1trA119089 Nbv6.1trA61976 Nbv6.1trP38162 Nbv6.1trP40677	60S ribosomal protein L8	AT4G36130.1	Ribosomal protein L2 family	Mapoly0068s0027.1	large subunit ribosomal protein L8e
Nbv6.1trA55456	60s ribosomal protein l8-like	AT4G36130.1	Ribosomal protein L2 family	Mapoly0099s0059.1	50S RIBOSOMAL PROTEIN L2
Nbv6.1trA105545 Nbv6.1trP16905 Nbv6.1trA244984 Nbv6.1trA176129	60s ribosomal protein l9-1-like	AT1G33140.1	Ribosomal protein L6 family	Mapoly0020s0166.1	large subunit ribosomal protein L9e
NbS00016445g0012.1	Actin	AT5G09810.1	actin 7	Mapoly0016s0137.1	actin
Nbv6.1trA107517 Nbv6.1trP55562	actin cytoskeleton- regulatory complex protein pan1	AT1G20760.1	Calcium-binding EF hand family protein	Mapoly0065s0050.1	Synaptic vesicle protein EHS-1 and related EH domain proteins
Nbv6.1trA243772 Nbv6.1trA115	actin-like isoform x1	AT3G12110.1	actin-11	Mapoly0016s0137.1	actin
Nbv6.1trA266523	alanine aminotransferase 2- like	AT1G72330.1	alanine aminotransferase 2	Mapoly0036s0030.1	Alanine transaminase.
Nbv6.1trA184988	alpha- partial	AT1G50010.1	tubulin alpha-2 chain	Mapoly0066s0086.1	tubulin alpha
Nbv6.1trP21647	alpha-l-fucosidase 2	AT4G34260.1	1 2C2-alpha-L- fucosidase	Mapoly0115s0027.2	Glycosyl hydrolase family 65

Nb	Nb protein ID	At	At_protein_ID	Mp	Mp protein ID
Nbv6.1trP17728	ankyrin repeat domain-containing protein 2-like	AT2G17390.1	ankyrin repeat-containing 2B	Mapoly0142s0007.1	ANKYRIN REPEAT PROTEIN
Nbv6.1trA65532 Nbv6.1trP63294	ascorbate peroxidase	AT1G07890.8	ascorbate peroxidase 1	Mapoly0188s0011.2	L-ascorbate peroxidase.
Nbv6.1trP4521	atp synthase cf1 alpha subunit	ATCG00120.1	ATP synthase subunit alpha	Mapoly4078s0001.1	F-type H+-transporting ATPase subunit alpha
Nbv6.1trP838	atp synthase cf1 beta subunit	ATCG00480.1	ATP synthase subunit beta	Mapoly0082s0043.1	F-type H+-transporting ATPase subunit beta
NbS00019305g0027.1 Nbv6.1trA77810	ATP synthase subunit beta mitochondrial	AT5G08680.1	ATP synthase alpha/beta family protein	Mapoly0082s0043.1	F-type H+-transporting ATPase subunit beta
Nbv6.1trA197115	atp-binding protein	AT1G73460.2	Protein kinase superfamily protein	Mapoly0049s0040.5	Dual-specificity tyrosine regulated protein kinase 2
Nbv6.1trA272788	atpase subunit 1	ATMG01190.1	ATP synthase subunit 1	Mapoly4078s0001.1	F-type H+-transporting ATPase subunit alpha
Nbv6.1trP19813	autophagy protein 5	AT5G17290.1	autophagy protein Apg5 family	Mapoly0019s0054.4	autophagy-related protein 5
NbS00001756g0014.1 NbS00012195g0005.1 Nbv6.1trA221928 Nbv6.1trA249885 Nbv6.1trA36039	Autophagy related protein 3	AT5G61500.1	autophagy 3 (APG3)	Mapoly0003s0208.1	autophagy-related protein 3
NbS00017537g0009.1	Autophagy related protein 8	AT4G21980.1	Ubiquitin-like superfamily protein	Mapoly0001s0494.2	autophagy-related protein 8
NbS00003005g0010.1	Autophagy related protein 8f (Nb1)	AT4G16520.2	Ubiquitin-like superfamily protein	Mapoly0001s0494.2	autophagy-related protein 8
Nbv6.1trP60922	autophagy-related protein 8c (Nb2)	AT1G62040.1	Ubiquitin-like superfamily protein	Mapoly0001s0494.2	autophagy-related protein 8
Nbv6.1trA236071	autophagy-related protein 8c-like isoform x1 (Nb3)	AT4G21980.2	Ubiquitin-like superfamily protein	Mapoly0001s0494.2	autophagy-related protein 8
Nbv6.1trP17439	autophagy-related protein 8i (Nb4)	AT3G15580.1	Ubiquitin-like superfamily protein	Mapoly0001s0494.2	autophagy-related protein 8
NbS00009154g0017.1 Nbv6.1trP4951	Auxin transport protein BIG	AT3G02260.2	auxin transport protein (BIG)	Mapoly0031s0115.1	E3 ubiquitin-protein ligase UBR4
Nbv6.1trA211552	auxin transport protein big	AT3G02260.3	auxin transport protein (BIG)	Mapoly0031s0115.1	E3 ubiquitin-protein ligase UBR4
Nbv6.1trP21586	beclin-1-like protein	AT3G61710.1	AUTOPHAGY 6	Mapoly0091s0016.1	BECLIN 1
Nbv6.1trP25495	beta- partial	AT3G12110.1	actin-11	Mapoly0016s0139.1	actin
Nbv6.1trA235626 Nbv6.1trA10385	biotin carboxyl carrier protein of acetyl-carboxylase	AT3G56130.1	biotin/lipoyl attachment domain-containing protein	Mapoly0008s0014.2	Pyruvate/acetyl-coa/propionyl-coa carboxylase
NbS00032824g0016.1	C terminal binding protein AN	AT1G01510.1	NAD(P)-binding Rossmann-fold superfamily protein	Mapoly0077s0060.1	2-HYDROXYACID DEHYDROGENAS E-RELATED
Nbv6.1trA32780	carbonic anhydrase 2 isoform x1	AT5G14740.1	carbonic anhydrase 2	Mapoly0105s0019.1	carbonic anhydrase
Nbv6.1trA220150	carbonic anhydrase 2 isoform x2	AT5G14740.9	carbonic anhydrase 2	Mapoly0053s0046.1	carbonic anhydrase

Nb	Nb protein ID	At	At_protein_ID	Mp	Mp protein ID
Nbv6.1trA184404	carbonic anhydrase 2-like isoform x1	AT5G14740.1	carbonic anhydrase 2	Mapoly0053s0046.1	carbonic anhydrase
Nbv6.1trP47090	carbonic chloroplastic-like	AT3G01500.4	carbonic anhydrase 1	Mapoly0053s0046.1	carbonic anhydrase
NbS0006116g0019.1 Nbv6.1trP54093 NbS00012784g0015.1 NbS00003826g0005.1 Nbv6.1trP40491	Catalase	AT4G35090.1	catalase 2	Mapoly0125s0005.1	Catalase.
Nbv6.1trA8369	cdk5rap3-like protein	AT5G06830.1	hypothetical protein	Mapoly0080s0041.1	CDK5 regulatory subunit-associated protein 3
NbS00033917g0007.1 NbS00046481g0008.1	Cell division cycle protein 48	AT5G03340.1	ATPase 2C AAA-type 2C CDC48 protein	Mapoly0096s0020.2	transitional endoplasmic reticulum ATPase
Nbv6.1trA5085 Nbv6.1trP75893	cellulose synthase a catalytic subunit 2	AT5G64740.1	cellulose synthase 6	Mapoly0076s0014.1	Cellulose synthase (UDP-forming).
Nbv6.1trA923	chlorophyll a-b binding protein chloroplastic	AT4G10340.1	light harvesting complex of photosystem II 5	Mapoly0011s0076.1	light-harvesting complex II chlorophyll a/b binding protein 5
Nbv6.1trP69493 Nbv6.1trA110145 Nbv6.1trA15940 Nbv6.1trA34973 Nbv6.1trA60239 Nbv6.1trA95178 Nbv6.1trA95180	clathrin heavy chain 1	AT3G11130.1	Clathrin 2C heavy chain	Mapoly0045s0097.1	clathrin heavy chain
Nbv6.1trA266902	clathrin heavy chain 1-like	AT3G08530.1	Clathrin 2C heavy chain	Mapoly0045s0097.1	clathrin heavy chain
Nbv6.1trA109841 Nbv6.1trA78303	clustered mitochondria protein homolog isoform x1	AT1G01320.3	Tetratricopeptide repeat (TPR)-like superfamily protein	Mapoly0060s0041.2	EUKARYOTIC TRANSLATION INITIATION FACTOR 3 SUBUNIT (EIF-3)
Nbv6.1trA250477 Nbv6.1trA181577 NbS00051557g0007.1 Nbv6.1trP54759 NbS00031319g0001.1	Coatomer alpha subunit protein	AT1G62020.1	Coatomer 2C alpha subunit	Mapoly0007s0005.1	coatomer protein complex
Nbv6.1trP73912 Nbv6.1trP8100 Nbv6.1trA148248	coatomer subunit beta -2-like	AT1G52360.3	Coatomer 2C beta' subunit	Mapoly0022s0125.2	COATOMER BETA SUBUNIT
Nbv6.1trA101014 Nbv6.1trA208246 Nbv6.1trA137980 Nbv6.1trA42176 Nbv6.1trP61756 Nbv6.1trA57795 Nbv6.1trA57793 Nbv6.1trA208241	coatomer subunit beta -2-like	AT1G52360.4	Coatomer 2C beta' subunit	Mapoly0022s0125.2	COATOMER BETA SUBUNIT
Nbv6.1trP8098	coatomer subunit beta -2-like	AT1G79990.1	coatomer subunit beta-2	Mapoly0022s0125.2	COATOMER BETA SUBUNIT
Nbv6.1trA1886 Nbv6.1trP4211	coatomer subunit beta -2-like	AT1G79990.2	coatomer subunit beta-2	Mapoly0022s0125.2	COATOMER BETA SUBUNIT
NbS00017088g0003.1 Nbv6.1trA114667 Nbv6.1trA128366 Nbv6.1trP54756 Nbv6.1trP69288	Coatomer subunit beta 1	AT4G31480.9	Coatomer 2C beta subunit	Mapoly0086s0049.1	COATOMER SUBUNIT BETA

Nb	Nb protein ID	At	At_protein_ID	Mp	Mp protein ID
Nbv6.1trA100206 Nbv6.1trA270047 Nbv6.1trA63178	coatomer subunit beta-1-like	AT4G31480.6	Coatomer 2C beta subunit	Mapoly0086s0049.1	COATOMER SUBUNIT BETA
Nbv6.1trA108594 Nbv6.1trP70667 Nbv6.1trA4145	coatomer subunit delta-like	AT5G05010.2	clathrin adaptor complexes medium subunit family protein	Mapoly0022s0045.1	COATOMER SUBUNIT DELTA
Nbv6.1trP38393 NbS00036341g0012.1	coatomer subunit epsilon-1-like	AT1G30630.1	Coatomer epsilon subunit	Mapoly0002s0056.1	COATOMER SUBUNIT EPSILON
NbS00000812g0012.1 Nbv6.1trP49081 Nbv6.1trP17657 Nbv6.1trA65506 Nbv6.1trA269507 Nbv6.1trA203406	Coatomer subunit gamma	AT4G34450.1	coatomer gamma-2 subunit 2C putative / gamma-2 coat protein 2C putative / gamma- 2 COP	Mapoly0005s0083.1	COATOMER SUBUNIT GAMMA
Nbv6.1trP26130	copper transport protein cch isoform x2	AT3G56240.3	copper chaperone	Mapoly0058s0015.1	Copper transport protein atox1-related
NbS00024389g0004.1	CUE domain containing protein expressed	AT1G03290.5	ELKS/Rab6- interacting/CAST family protein	Mapoly0005s0053.1	(Unknown)
Nbv6.1trP51402	cullin-1-like isoform x1	AT4G02570.4	cullin 1	Mapoly0012s0104.1	CULLIN
Nbv6.1trA186377 Nbv6.1trA135984 Nbv6.1trA186373	cysteine protease atg4-like	AT2G44140.3	Peptidase family C54 protein	Mapoly0153s0038.1	autophagy-related protein 4
Nbv6.1trA76179	ddrgk domain- containing protein 1	AT4G27120.2	DDRKG domain protein	Mapoly0114s0022.1	PROTEIN C20ORF116- RELATED
Nbv6.1trA10975 Nbv6.1trA155393 Nbv6.1trA29799 Nbv6.1trA29801	dead-box atp- dependent rna helicase 38	AT3G53110.1	P-loop containing nucleoside triphosphate hydrolases superfamily protein	Mapoly0035s0045.2	ATP-dependent RNA helicase
Nbv6.1trP19537 Nbv6.1trP72486	dead-box atp- dependent rna helicase 56-like	AT5G11200.1	DEAD/DEAH box RNA helicase family protein	Mapoly0029s0012.2	ATP-dependent RNA helicase
Nbv6.1trA55078	dentin sialophospho	AT5G47940.1	40S ribosomal protein S27	Mapoly0003s0122.1	Domain of unknown function (DUF4506)
Nbv6.1trP14576	dentin sialophosphoprotein	AT1G05087.1	dentin sialophosphoprotein	Mapoly0147s0032.3	(Unknown)
NbS00038989g0006.1	DNA directed RNA polymerase II protein	AT4G08540.1	DNA-directed RNA polymerase II protein	Mapoly0103s0077.6	DNA-DIRECTED RNA POLYMERASE II
Nbv6.1trA76488	dna-directed rna polymerase	AT4G08540.1	DNA-directed RNA polymerase II protein	Mapoly0103s0077.5	DNA-DIRECTED RNA POLYMERASE II
Nbv6.1trA239115 Nbv6.1trP48296 Nbv6.1trA54493 Nbv6.1trA162728 Nbv6.1trP22761	dnaj protein homolog	AT5G22060.1	DNAJ homologue 2	Mapoly0078s0038.1	Molecular chaperone (DnaJ superfamily)
Nbv6.1trP53020	e3 ufm1-protein ligase 1 homolog	AT3G46220.1	E3 UFM1-protein ligase-like protein	Mapoly0007s0143.1	Uncharacterized conserved protein
Nbv6.1trA245897	e3 ufm1-protein ligase 1 homolog	AT3G46220.3	E3 UFM1-protein ligase-like protein	Mapoly0007s0143.2	Uncharacterized conserved protein
NbS00060738g0002.1 Nbv6.1trA148119	Elongation factor 1 alpha	AT5G60390.3	GTP binding Elongation factor Tu family protein	Mapoly0038s0023.1	elongation factor 1- alpha
NbS00030487g0018.1	Elongation factor EF 2	AT1G56070.3	Ribosomal protein S5/Elongation factor G/III/V family protein	Mapoly0055s0033.1	elongation factor EF- 2 [EC:3.6.5.3]

Nb	Nb protein ID	At	At_protein_ID	Mp	Mp protein ID
Nbv6.1trA51090 Nbv6.1trA51091	eukaryotic translation initiation factor 3 subunit b-like	AT5G27640.3	translation initiation factor 3B1	Mapoly0108s0028.1	translation initiation factor 3 subunit B
Nbv6.1trA41766 Nbv6.1trP17478	eukaryotic translation initiation factor 3 subunit g-like	AT3G11400.1	eukaryotic translation initiation factor 3G1	Mapoly0059s0037.1	translation initiation factor 3 subunit G
Nbv6.1trA187403 Nbv6.1trP17033	eukaryotic translation initiation factor 3 subunit i-like	AT2G46290.1	Transducin/WD40 repeat-like superfamily protein	Mapoly0109s0034.1	translation initiation factor 3 subunit I
Nbv6.1trA19802 Nbv6.1trA239564	eukaryotic translation initiation factor 3 subunit j-like	AT1G66070.2	Translation initiation factor eIF3 subunit	Mapoly0038s0048.1	translation initiation factor 3 subunit J
NbS00055086g0001.1 Nbv6.1trP36246 Nbv6.1trA58078 Nbv6.1trA123281	Eukaryotic translation initiation factor 5B	AT1G76810.1	eukaryotic translation initiation factor 2 (eIF-2) family protein	Mapoly0112s0026.1	translation initiation factor 5B
Nbv6.1trA104339 Nbv6.1trP21404 Nbv6.1trA48377 Nbv6.1trA253146 Nbv6.1trA232714 Nbv6.1trA232713 Nbv6.1trA232712 Nbv6.1trA223694 Nbv6.1trA223693 Nbv6.1trA200490 Nbv6.1trA188313 Nbv6.1trA154863	fact complex subunit spt16-like	AT4G10710.2	global transcription factor C	NA	NA
Nbv6.1trA125626 Nbv6.1trP21285	ferredoxin--nadp leaf chloroplastic	AT1G20020.1	ferredoxin-NADP[+]-oxidoreductase 2	Mapoly0062s0041.1	FLAVODOXIN-RELATED
NbS00028064g0012.1 Nbv6.1trP38569 Nbv6.1trA194271 Nbv6.1trP40911 Nbv6.1trP47902 Nbv6.1trP40911 Nbv6.1trA63820	Fructose bisphosphate aldolase	AT4G38970.1	fructose-bisphosphate aldolase 2	Mapoly0053s0082.1	Fructose-bisphosphate aldolase.
NbS00008675g0003.1	Geranylgeranyl diphosphate reductase chloroplastic	AT1G74470.1	Pyridine nucleotide-disulfide oxidoreductase family protein	Mapoly0116s0015.1	Geranylgeranyl diphosphate reductase.
Nbv6.1trA53307 Nbv6.1trA97857 Nbv6.1trP22773	glutamate decarboxylase	AT2G02010.2	glutamate decarboxylase 4	Mapoly0121s0037.1	Glutamate decarboxylase.
Nbv6.1trP59067	glutamate decarboxylase	AT5G17330.1	glutamate decarboxylase	Mapoly0121s0037.1	Glutamate decarboxylase.
Nbv6.1trP25686	glutamate-1-semialdehyde - chloroplastic	AT3G48730.1	glutamate-1-semialdehyde 2 2C1-aminomutase 2	Mapoly0094s0038.1	Glutamate-1-semialdehyde 2
Nbv6.1trP30042	glutaredoxin family protein	AT3G57070.1	Glutaredoxin family protein	Mapoly0022s0043.1	glutaredoxin domain-containing cysteine-rich protein 1
Nbv6.1trA1216 Nbv6.1trA221888	glyceraldehyde-3-phosphate cytosolic	AT1G13440.1	glyceraldehyde-3-phosphate dehydrogenase C2	Mapoly0206s0011.1	Glyceraldehyde-3-phosphate dehydrogenase (phosphorylating).
Nbv6.1trA134724	glyceraldehyde-3-phosphate cytosolic	AT3G04120.1	glyceraldehyde-3-phosphate dehydrogenase C subunit 1	Mapoly0206s0011.1	Glyceraldehyde-3-phosphate dehydrogenase (phosphorylating).
Nbv6.1trA27717	golgin candidate 5	AT1G79830.3	golgin Putative 5	Mapoly0013s0180.1	Transcription factor TMF

Nb	Nb protein ID	At	At_protein_ID	Mp	Mp protein ID
Nbv6.1trA219734 Nbv6.1trA252292	golgin subfamily a member 6-like protein 1	AT4G13670.1	plastid transcriptionally active 5	Mapoly0004s0042.1	Putative peptidoglycan binding domain
NbS00005908g0003.1	Haloacid dehalogenase hydrolase HAD	AT5G59480.5	Haloacid dehalogenase-like hydrolase (HAD) superfamily protein	NA	NA
Nbv6.1trP34322 Nbv6.1trA108466 Nbv6.1trA47396	heat shock cognate protein 80-like	AT5G56000.1	HEAT SHOCK PROTEIN 81.4	Mapoly0002s0217.1	molecular chaperone HtpG
Nbv6.1trP41303	heat shock cognate protein 80-like	AT5G56030.1	heat shock protein 81-2	Mapoly0002s0217.1	molecular chaperone HtpG
Nbv6.1trP4035	histone deacetylase 14 isoform x1	AT4G33470.1	histone deacetylase 14	Mapoly0029s0117.1	HISTONE DEACETYLASE
Nbv6.1trP14845	histone deacetylase 5	AT5G61060.1	histone deacetylase 5	Mapoly0049s0028.1	histone deacetylase 6/10
Nbv6.1trA234445 Nbv6.1trA368 Nbv6.1trA248234	hop-interacting protein thi031	AT5G40690.1	histone-lysine N-methyltransferase trithorax-like protein	Mapoly0030s0028.1	(UnKnown)
NbS00002437g0006.1 Nbv6.1trA68712 Nbv6.1trA226360	hypothetical protein VITISV_033286	AT2G32240.1	early endosome antigen	NA	NA
Nbv6.1trA132118 Nbv6.1trA205096 Nbv6.1trA164576 Nbv6.1trA145479	isocitrate dehydrogenase	AT1G65930.1	cytosolic NADP+-dependent isocitrate dehydrogenase	Mapoly0112s0021.1	Isocitrate dehydrogenase (NADP(+)).
NbS00017142g0001.1	Isocitrate dehydrogenase	AT5G03290.1	isocitrate dehydrogenase V	Mapoly0002s0215.1	Isocitrate dehydrogenase (NAD(+)).
NbS00005985g0007.1 NbS00016411g0025.1	Kinase	AT1G73460.2	Protein kinase superfamily protein	Mapoly0049s0040.1	Dual-specificity tyrosine regulated protein kinase 2
NbS00014166g0016.1	Kinesin protein	AT3G12020.4	P-loop containing nucleoside triphosphate hydrolases superfamily protein	Mapoly0019s0177.2	Kinesin motor domain // Zinc finger
Nbv6.1trA44561	kinesin-related protein 11-like isoform x1	AT4G39050.1	Kinesin motor family protein	Mapoly0019s0177.2	Kinesin motor domain // Zinc finger
Nbv6.1trP72498	kinesin-related protein 4-like	NA	NA	Mapoly0019s0177.2	Kinesin motor domain // Zinc finger
NbS00015568g0013.1	Lecithine cholesterol acyltransferase 4	AT4G19860.1	alpha/beta-Hydrolases superfamily protein	Mapoly0131s0029.1	Lecithine cholesterol acyltransferase-related
Nbv6.1trA174189	leucine-rich repeat-containing protein ddb_g0290503 isoform x2	AT2G32240.1	early endosome antigen	Mapoly0030s0143.1	Uncharacterized coiled-coil protein
Nbv6.1trA208235 Nbv6.1trP35973 Nbv6.1trA106888	leucine-rich repeat-containing protein ddb_g0290503 isoform x2	AT2G32240.1	early endosome antigen	NA	NA
Nbv6.1trA73959	leucine-rich repeat-containing protein ddb_g0290503 isoform x2	AT2G32240.1	early endosome antigen	Mapoly0001s0335.1	E3 ubiquitin ligase involved in syntaxin degradation
Nbv6.1trA203771	low quality protein: myosin heavy cardiac muscle isoform	AT2G32240.1	early endosome antigen	NA	NA

Nb	Nb protein ID	At	At_protein_ID	Mp	Mp protein ID
Nbv6.1trA206321 Nbv6.1trA76622	low-temperature-induced cysteine proteinase-like	AT5G43060.1	Granulin repeat cysteine protease family protein	Mapoly0083s0026.1	CYSTEINE PROTEASE FAMILY C1-RELATED
Nbv6.1trA135785	mag2-interacting protein 2	AT5G24350.3	neuroblastoma-amplified sequence protein	Mapoly0143s0007.1	Secretory pathway protein Sec39
Nbv6.1trA144221 Nbv6.1trP30074	magnesium-dependent phosphatase 1-like	AT2G14110.1	Haloacid dehalogenase-like hydrolase (HAD) superfamily protein	Mapoly0042s0019.8	Magnesium-dependent phosphatase
Nbv6.1trP2377	mannosylglycoprotein endo-beta-mannosidase	AT1G09010.1	glycoside hydrolase family 2 protein	Mapoly0034s0073.1	BETA-GALACTOSIDASE
NbS00004550g0007.1 NbS00019118g0008.1	Myosin XI	AT5G20490.1	myosin family protein with Dil	Mapoly0012s0190.1	MYOSIN
Nbv6.1trA233324	myosin-12 isoform x1	AT2G31900.4	myosin-like protein XIF	Mapoly0012s0190.2	MYOSIN
Nbv6.1trA159973 Nbv6.1trA43810 Nbv6.1trA64141	myosin-12 isoform x2	AT2G31900.4	myosin-like protein XIF	Mapoly0012s0190.1	MYOSIN
Nbv6.1trA121215 Nbv6.1trA52888 Nbv6.1trA48404 Nbv6.1trA22398 Nbv6.1trA145750 Nbv6.1trA145750	myosin-binding protein 1	AT1G08800.4	myosin-binding protein (Protein of unknown function 2C DUF593)	Mapoly0056s0058.8	Zein-binding
NbS00006811g0211.1	NA	AT1G09640.1	Translation elongation factor EF1B 2C gamma chain	Mapoly0062s0115.1	elongation factor 1-gamma
NbS00007010g0113.1	NA	AT5G43960.1	Nuclear transport factor 2 (NTF2) family protein with RNA binding (RRM-RBD-RNP motifs) domain-containing protein	Mapoly0148s0012.1	RasGAP SH3 binding protein rasputin
NbS00017559g0109.1	NA	AT5G65430.2	general regulatory factor 8	Mapoly0043s0019.1	14-3-3 protein epsilon
NbS00017213g0030.1 Nbv6.1trA39226 Nbv6.1trP33140	NADP dependent D sorbitol 6 phosphate dehydrogenase	AT2G21250.1	NAD(P)-linked oxidoreductase superfamily protein	Mapoly0086s0056.3	Aldose-6-phosphate reductase (NADPH).
Nbv6.1trP71475	nadp-dependent malic enzyme	AT5G25880.1	NADP-malic enzyme 3	Mapoly0169s0005.1	Malate dehydrogenase (oxaloacetate-decarboxylating) (NADP(+)).
Nbv6.1trP26187	nodulin-related protein	AT2G03440.1	nodulin-related protein 1	NA	NA
NbS00053127g0003.1	Norcochlorine synthase	NA	NA	Mapoly0063s0024.1	Pathogenesis-related protein Bet v 1 family
NbS00016009g0003.1 NbS00027422g0005.1	Nuclear polyadenylated RNA binding protein 4	AT5G40490.1	RNA-binding (RRM/RBD/RNP motifs) family protein	Mapoly0002s0093.2	heterogeneous nuclear ribonucleoprotein A1/A3
Nbv6.1trP33991	nucleolar gtp-binding protein 1-like	AT1G50920.1	Nucleolar GTP-binding protein	Mapoly0056s0118.1	nucleolar GTP-binding protein

Nb	Nb protein ID	At	At_protein_ID	Mp	Mp protein ID
NbS00040216g0019.1	Nucleolar GTPase	AT1G54920.2	hypothetical protein	Mapoly0011s0030.1	(Unknown)
NbS00020349g0003.1	Octanoyltransferase	AT1G04640.2	lipoyltransferase 2	Mapoly0010s0076.1	Lipoyl(octanoyl) transferase.
NbS00011131g0010.1	Oxidoreductase 2OG Fe oxygenase	AT2G17970.6	2-oxoglutarate (2OG) and Fe(II)-dependent oxygenase superfamily protein	Mapoly0001s0483.1	Uncharacterized conserved protein
NbS00011570g0012.1	P loop containing nucleoside triphosphate hydrolases	AT1G33970.5	P-loop containing nucleoside triphosphate hydrolases superfamily protein	NA	NA
Nbv6.1trP2846	p-loop containing nucleoside triphosphate hydrolases superfamily	AT4G13030.1	P-loop containing nucleoside triphosphate hydrolases superfamily protein	Mapoly0051s0107.1	50S ribosome-binding GTPase
NbS00018333g0014.1 Nbv6.1trA131517	Pentatricopeptide repeat PPR	AT3G49140.1	Pentatricopeptide repeat (PPR) superfamily protein	Mapoly0002s0015.1	CREG1 PROTEIN
Nbv6.1trA28077	peptide methionine sulfoxide reductase chloroplastic	AT1G53670.1	methionine sulfoxide reductase B 1	Mapoly0057s0057.1	Predicted pilin-like transcription factor
Nbv6.1trA5133 NbS00010425g0009.1 Nbv6.1trA87901	peptidoglycan-binding domain-containing family protein	AT4G13670.1	plastid transcriptionally active 5	Mapoly0004s0042.1	Putative peptidoglycan binding domain
Nbv6.1trA11863 Nbv6.1trA122217 Nbv6.1trP32898	phosphatidate phosphatase pah1-like isoform x1	AT3G09560.4	Lipin family protein	Mapoly0089s0039.2	LIPIN // SUBFAMILY NOT NAMED
NbS00054532g0002.1 Nbv6.1trA213284 Nbv6.1trP72093	Phosphatidylinositol 3 kinase	AT1G60490.1	vacuolar protein sorting 34 (Vps34)	Mapoly0003s0185.1	Phosphatidylinositol 3-kinase.
Nbv6.1trA208501 Nbv6.1trP71373 NbS00006821g0002.1	Phosphoglycerate kinase	AT1G56190.1	Phosphoglycerate kinase family protein	Mapoly0111s0004.1	Phosphoglycerate kinase.
Nbv6.1trP23488	phosphoinositide 3-kinase regulatory subunit 4	AT4G29380.1	protein kinase family protein / WD-40 repeat family protein	Mapoly0002s0158.1	phosphoinositide-3-kinase
Nbv6.1trA74738	photosystem i reaction center subunit chloroplastic	AT5G64040.1	photosystem I reaction center subunit PSI-N 2C chloroplast 2C putative / PSI-N 2C putative (PSAN)	Mapoly0116s0042.1	photosystem I subunit PsaN
Nbv6.1trA131125 Nbv6.1trA51800	plasma membrane atpase 3	AT5G62670.1	H[+]-ATPase 11	Mapoly0080s0002.2	Proton-exporting ATPase.
Nbv6.1trP19726	probable cytosolic oligopeptidase a	AT5G65620.2	Zincin-like metalloproteases family protein	Mapoly0137s0031.1	Oligopeptidase A.
Nbv6.1trA120800	probable inactive purple acid phosphatase 27	AT5G50400.1	purple acid phosphatase 27	Mapoly0002s0096.2	ACID PHOSPHATASE RELATED

Nb	Nb protein ID	At	At_protein_ID	Mp	Mp protein ID
NbS00015744g0008.1 Nbv6.1trA29984 Nbv6.1trA56859 Nbv6.1trP30432 NbS00016691g0013.1	probable methionine-tRNA ligase	AT4G13780.1	methionine-tRNA ligase 2C putative / methionyl-tRNA synthetase 2C putative / MetRS	Mapoly0045s0011.1	Methionine-tRNA ligase.
Nbv6.1trA144687 Nbv6.1trA63223	probable phenylalanine-tRNA ligase beta subunit	AT1G72550.1	tRNA synthetase beta subunit family protein	Mapoly0013s0023.1	phenylalanyl-tRNA synthetase beta chain
Nbv6.1trA268018 Nbv6.1trA41512	probable ribose-5-phosphate isomerase chloroplastic	AT5G44520.1	NagB/RpiA/CoA transferase-like superfamily protein	Mapoly0213s0005.1	Ribose-5-phosphate isomerase.
Nbv6.1trP17801	probable uncharacterized protein LOC104107395 isoform X1	AT2G31130.6	hypothetical protein	Mapoly0024s0071.1	(UnKnown)
Nbv6.1trA23960 Nbv6.1trA55250 Nbv6.1trP13243	probable uncharacterized protein LOC104213483	AT3G57990.1	hypothetical protein	Mapoly0061s0112.1	(UnKnown)
Nbv6.1trP28612	probable uncharacterized protein LOC104222222	AT3G57990.1	hypothetical protein	Mapoly0061s0112.1	(UnKnown)
Nbv6.1trA114250	probable uncharacterized protein LOC104225829 isoform X1	AT5G65960.1	GTP binding protein	Mapoly0024s0125.7	Uncharacterized conserved protein
Nbv6.1trA1931	protease do-like chloroplastic	AT3G27925.2	DegP protease 1	Mapoly0003s0078.1	SERINE PROTEASE FAMILY S1C HTRA-RELATED // SUBFAMILY NOT NAMED
Nbv6.1trA100398	proteasome activator subunit 4	AT3G13330.1	proteasome activating protein 200	Mapoly0069s0005.2	proteasome activator subunit 4
Nbv6.1trA120233 Nbv6.1trP51995	protein aspartic protease in guard cell 2-like	AT5G10770.1	Eukaryotic aspartyl protease family protein	Mapoly0271s0001.1	ASPARTYL PROTEASES
Nbv6.1trP744	protein disulfide isomerase-like 1-4	AT5G60640.1	PDI-like 1-4	Mapoly0127s0051.1	PROTEIN DISULFIDE ISOMERASE
Nbv6.1trA162402	protein tic chloroplastic	AT3G46780.1	plastid transcriptionally active 16	Mapoly0154s0018.1	NITROGEN METABOLIC REGULATION PROTEIN NMR-RELATED
Nbv6.1trA1493 Nbv6.1trA201572 NbS00032670g0023.1	protein tipd	AT5G50230.1	Transducin/WD40 repeat-like superfamily protein	Mapoly0102s0055.1	AUTOPHAGY PROTEIN 16-LIKE // SUBFAMILY NOT NAMED
NbS00000183g0014.1	PsbP domain containing protein 6 chloroplastic	AT3G56650.1	thylakoid luminal protein (Mog1/PsbP/DUF1795-like photosystem II reaction center PsbP family protein)	Mapoly0008s0145.1	PsbP
Nbv6.1trA131824 Nbv6.1trA186965 Nbv6.1trA80820 Nbv6.1trA93032	rab11 family-interacting protein 3 isoform x1	AT4G02880.1	ELKS/Rab6-interacting/CAST family protein	Mapoly0005s0053.1	(UnKnown)

Nb	Nb protein ID	At	At_protein_ID	Mp	Mp protein ID
Nbv6.1trA194969 Nbv6.1trP8372	rab3 gtpase-activating protein catalytic subunit	AT5G55060.1	Rab3 GTPase-activating protein catalytic subunit	Mapoly0021s0054.1	BSD domain // Rab3 GTPase-activating protein catalytic subunit
Nbv6.1trP14296 NbS00007750g0014.1 NbS00013932g0015.1 NbS00021061g0110.1 NbS00025676g0010.1	Ribosomal protein L18	AT3G05590.1	ribosomal protein L18	Mapoly0118s0037.1	large subunit ribosomal protein L18e
Nbv6.1trP58182	ribosomal protein l2	ATCG01310.1	ribosomal protein L2	Mapoly0099s0059.1	50S RIBOSOMAL PROTEIN L2
NbS00055601g0001.1	Ribosomal protein S12/S23	AT5G02960.1	Ribosomal protein S12/S23 family protein	Mapoly0015s0153.1	small subunit ribosomal protein S23e
Nbv6.1trP75120	ribosomal protein s3	ATCG00800.1	structural constituent of ribosome	Mapoly0015s0207.1	small subunit ribosomal protein S3
Nbv6.1trP72880	ribosomal protein s4	ATCG00380.1	chloroplast ribosomal protein S4	Mapoly0090s0058.1	small subunit ribosomal protein S4
Nbv6.1trP26194 NbS00037852g0006.1 NbS00041372g0008.1 Nbv6.1trP44670 NbS00009638g0019.1	ribulose bisphosphate carboxylase	AT5G38410.1	Ribulose bisphosphate carboxylase (small chain) family protein	Mapoly0146s0015.1	Ribulose-bisphosphate carboxylase.
Nbv6.1trA262607	ribulose bisphosphate carboxylase oxygenase activase chloroplastic isoform x1	AT2G39730.2	rubisco activase	Mapoly0022s0132.2	26S proteasome regulatory complex
NbC24305910g0003.1 Nbv6.1trA225036	Ribulose bisphosphate carboxylase/oxygenase 2 chloroplastic	AT2G39730.3	rubisco activase	Mapoly0022s0132.2	26S proteasome regulatory complex
Nbv6.1trA82337	ribulose - - bisphosphate carboxylase oxygenase large partial	ATCG00490.1	ribulose-bisphosphate carboxylase	Mapoly0007s0124.1	Ribulose bisphosphate carboxylase large chain
Nbv6.1trA59957	ribulose-phosphate 3-chloroplastic	AT5G61410.2	D-ribulose-5-phosphate-3-epimerase	Mapoly0016s0134.1	Ribulose-phosphate 3-epimerase.
Nbv6.1trA197290 Nbv6.1trA60558 Nbv6.1trA25739	rrp15-like protein	AT1G44770.1	elongation factor	Mapoly0023s0096.2	(UnKnown)
Nbv6.1trA269680 Nbv6.1trA36576 Nbv6.1trA46199 Nbv6.1trA73962 NbS00012224g0007.1	serine threonine-protein kinase atg1	AT2G37840.1	Protein kinase superfamily protein	Mapoly0022s0025.1	serine/threonine-protein kinase ULK/ATG1
Nbv6.1trA70922	serine threonine-protein phosphatase 6 regulatory subunit 3-like isoform x1	AT1G07990.1	SIT4 phosphatase-associated family protein	Mapoly0001s0206.1	SIT4(YEAST)-ASSOCIATING PROTEIN-RELATED
Nbv6.1trA190964 Nbv6.1trA208100 NbS00019018g0007.1	Serine/threonine protein phosphatase 6 regulatory subunit 3	AT3G45190.1	SIT4 phosphatase-associated family protein	Mapoly0001s0206.1	SIT4(YEAST)-ASSOCIATING PROTEIN-RELATED
Nbv6.1trA209536 NbS00005284g0009.1	skp1-like protein 1a	AT1G75950.1	S phase kinase-associated protein 1	Mapoly0007s0013.1	S-phase kinase-associated protein 1

Nb	Nb protein ID	At	At_protein_ID	Mp	Mp protein ID
Nbv6.1trA181809 Nbv6.1trA73422 Nbv6.1trA63517 Nbv6.1trA57246 Nbv6.1trA57245 Nbv6.1trA40617 Nbv6.1trA247721	tbc1 domain family member 15-like	AT5G52580.1	RabGAP/TBC domain-containing protein	Mapoly0045s0037.2	TBC1 DOMAIN FAMILY MEMBER 15
Nbv6.1trA206516	tbc1 domain family member 17 isoform	AT5G52580.3	RabGAP/TBC domain-containing	Mapoly0045s0037.2	TBC1 domain family member 15
NbS00040246g0004.1	Thioredoxin	AT3G15360.1	thioredoxin M-type 4	Mapoly0164s0015.3	THIOREDOXIN
Nbv6.1trP37774 NbS00006010g0008.1	thioredoxin chloroplastic	AT1G76760.1	thioredoxin Y1	Mapoly0166s0016.1	THIOREDOXIN
Nbv6.1trP58422	thioredoxin chloroplastic-like	AT3G02730.1	thioredoxin F-type 1	Mapoly0040s0138.1	THIOREDOXIN
Nbv6.1trA1025 Nbv6.1trA13399 Nbv6.1trA150638	thioredoxin chloroplastic-like	AT3G15360.1	thioredoxin M-type 4	Mapoly0164s0015.3	THIOREDOXIN
Nbv6.1trP26182	thioredoxin peroxidase 1	AT1G65980.1	thioredoxin-dependent peroxidase	Mapoly0057s0026.1	alkyl hydroperoxide reductase subunit C
Nbv6.1trA105231 Nbv6.1trA124653	thioredoxin-like 3-chloroplastic	AT5G06690.1	WCRKC thioredoxin 1	Mapoly0073s0015.1	THIOREDOXIN
Nbv6.1trP22941	titin isoform x7	AT5G40450.2	A-kinase anchor-like	NA	NA
Nbv6.1trA57112	titin-like isoform x1	NA	NA	NA	NA
NbS00008412g0009.1	Transketolase 1	AT2G45290.2	Transketolase	Mapoly0013s0012.2	Transketolase.
NbS00001860g0017.1	Translation initiation factor	AT3G55620.1	Translation initiation factor IF6	Mapoly0001s0181.1	translation initiation factor 6
Nbv6.1trP54998	tripeptidyl-peptidase 2 isoform x1	AT4G20850.1	tripeptidyl peptidase ii	Mapoly0069s0029.1	Tripeptidyl-peptidase II.
NbS00031544g0010.1 NbS00002652g0220.1	Tubulin alpha 7 chain	AT4G14960.2	Tubulin/FtsZ family protein	Mapoly0120s0003.2	tubulin alpha
Nbv6.1trP26162	tubulin alpha chain	AT4G14960.2	Tubulin/FtsZ family protein	Mapoly0061s0068.2	tubulin alpha
Nbv6.1trP73929	tubulin alpha-3 chain	AT5G19780.1	tubulin alpha-5	Mapoly0066s0086.1	tubulin alpha
Nbv6.1trA88398 Nbv6.1trA121378	tubulin beta-1 chain	AT5G23860.2	tubulin beta 8	Mapoly0109s0019.1	tubulin beta
Nbv6.1trP4607 Nbv6.1trP52057 Nbv6.1trP68479	tubulin beta-5 chain	AT5G12250.1	beta-6 tubulin	Mapoly0109s0019.1	tubulin beta
Nbv6.1trA232987 NbS00018426g0019.1	ubiquitin associated UBA/TS N domain containing protein/octicosapeptide/Phox/Bemp1 PB1 domain containing protein	AT4G24690.1	NBR1	Mapoly0100s0042.1	OVARIAN CARCINOMA ANTIGEN CA125-RELATED // SUBFAMILY NOT NAMED
NbS00031715g0004.1	Ubiquitin modifier activating enzyme ATG7	AT5G45900.1	ThiF family protein	Mapoly0015s0071.1	autophagy-related protein 7
Nbv6.1trA5666	upf0415 protein c7orf25 homolog	AT1G73380.1	hypothetical protein	Mapoly0114s0003.2	UNCHARACTERIZED DUF1308
Nbv6.1trA134752	violaxanthin de-epoxidase	AT1G08550.3	non-photochemical quenching 1	Mapoly0111s0023.1	Violaxanthin de-epoxidase.
Nbv6.1trA140086 Nbv6.1trA96560	web family protein chloroplastic-like	AT4G27595.1	WEB family protein (DUF827)	NA	NA
NbS00013825g0003.1 Nbv6.1trA156253 Nbv6.1trA23575 Nbv6.1trP35998	web family protein chloroplastic-like	AT5G16730.1	weak chloroplast movement under blue light protein (DUF827)	NA	NA
Nbv6.1trA102912 Nbv6.1trA84339 Nbv6.1trA121038	zinc ion binding	AT1G29800.1	RING/FYVE/PHD-type zinc finger family protein	Mapoly0037s0060.2	SH3YL1 PROTEIN

Table A.2.7 Overlap between the potato ATG8 interactome and the human ATG8 interactome from Behrends et al (2010)

The gene names of the candidate human ATG8 interactors from Behrends et al (2010) (776 proteins) were used to retrieve the corresponding protein sequences from Ensembl and UniProt (Chen et al., 2010; UniProt: A Worldwide Hub of Protein Knowledge. 2019). Proteins related to the human ATG8 interactors within the ATG8 interactome were determined by BLAST, with an expect (E) value cutoff of $1e-15$. The *N. benthamiana* interactors related to proteins in the human ATG8 interactome (297 proteins) are listed by accession ('Nb'), along with the *N. benthamiana* protein identification ('Nb protein ID'), the gene name of the related human ATG8 interactor ('Human gene name'), and the human protein identification ('Human protein ID').

Nb	Nb protein ID	Human gene name	Human protein ID
Nbv6.1trP40801 Nbv6.1trA269662	3-ketoacyl- thiolase peroxisomal	ACAT1	acetyl-Coenzyme A acetyltransferase 1 (acetoacetyl Coenzyme A thiolase)—Acetyl-CoA acetyltransferase, mitochondrial precursor
Nbv6.1trA115	actin partial	ACTA2	actin, alpha 2, smooth muscle, aorta—Actin, aortic smooth muscle
NbS00016445g0012.1 Nbv6.1trA243772 Nbv6.1trP25495	actin	ACTB	actin, beta—Actin, cytoplasmic 1
Nbv6.1trA270047 Nbv6.1trA63178 Nbv6.1trP69288	coatomer subunit beta-1-like	AP2B1	adaptor-related protein complex 2, beta 1 subunit—Hypothetical protein DKFZp781K0743
Nbv6.1trA186373 Nbv6.1trA186377 Nbv6.1trA135984	cysteine protease atg4-like	ATG4B	ATG4 autophagy related 4 homolog B (S. cerevisiae)—Hypothetical protein DKFZp686G0859
NbS00031715g0004.1	Ubiquitin modifier activating enzyme atg7	ATG7	ATG7 autophagy related 7 homolog (S. cerevisiae)—Isoform 1 of Autophagy-related protein 7
Nbv6.1trA131125 Nbv6.1trA51800	plasma membrane atpase 3	ATPIA1	ATPase, Na ⁺ /K ⁺ transporting, alpha 1 polypeptide—Isoform Long of Sodium/potassium-transporting ATPase alpha-1 chain precursor
Nbv6.1trA110145 Nbv6.1trA15940 Nbv6.1trA266902 Nbv6.1trA34973 Nbv6.1trA60239 Nbv6.1trA95178 Nbv6.1trA95180 Nbv6.1trP69493	clathrin heavy chain 1	CLTC	clathrin, heavy chain (Hc)—Isoform 1 of Clathrin heavy chain 1
NbS00026565g0005.1 NbS00031319g0001.1 NbS00051557g0007.1 Nbv6.1trA181577 Nbv6.1trA250477 Nbv6.1trP54759	Coatomer alpha subunit protein	COPA	coatomer protein complex, subunit alpha—Coatomer subunit alpha
Nbv6.1trP51402	cullin-1-like isoform x1	CUL3	cullin 3—Isoform 1 of Cullin-3
NbS00016009g0003.1 NbS00027422g0005.1	Nuclear polyadenylated RNA binding protein 4	DAZAP1	DAZ associated protein 1—Isoform 1 of DAZ-associated protein 1
Nbv6.1trA54493 Nbv6.1trP48296 Nbv6.1trA239115 Nbv6.1trP22761 Nbv6.1trA162728	dnaj protein homolog	DNAJA1	Dnaj (Hsp40) homolog, subfamily A, member 1—Dnaj homolog subfamily A member 1
NbS00060738g0002.1 Nbv6.1trA148119	Elongation factor 1 alpha	EEF1A1	eukaryotic translation elongation factor 1 alpha 1—EEF1A1 protein
NbS00006811g0211.1	NA	EEF1G	eukaryotic translation elongation factor 1 gamma—Elongation factor 1-gamma
NbS00030487g0018.1	Elongation factor EF 2	EEF2	eukaryotic translation elongation factor 2—Elongation factor 2
Nbv6.1trP72486 Nbv6.1trP19537	dead-box atp-dependent rna helicase 56-like	EIF4A1	eukaryotic translation initiation factor 4A, isoform 1—Eukaryotic initiation factor 4A-I

Nb	Nb protein ID	Human gene name	Human protein ID
Nbv6.1trA29801 Nbv6.1trA10975 Nbv6.1trA155393 Nbv6.1trA29799	dead-box atp-dependent rna helicase 38	EIF4A1	eukaryotic translation initiation factor 4A, isoform 1—Eukaryotic initiation factor 4A-1
Nbv6.1trA236071	autophagy-related protein 8c-like isoform x1 (Nb3)	GABARAPL2	GABA(A) receptor-associated protein-like 2—Gamma-aminobutyric acid receptor-associated protein-like 2
Nbv6.1trP60922	autophagy-related protein 8c (Nb2)	GABARAPL2	GABA(A) receptor-associated protein-like 2—Gamma-aminobutyric acid receptor-associated protein-like 2
NbS00003005g0010.1	Autophagy related protein 8f (Nb1)	GABARAPL2	GABA(A) receptor-associated protein-like 2—Gamma-aminobutyric acid receptor-associated protein-like 2
Nbv6.1trP17439	autophagy-related protein 8i (Nb4)	GABARAPL2	GABA(A) receptor-associated protein-like 2—Gamma-aminobutyric acid receptor-associated protein-like 2
Nbv6.1trA221888 Nbv6.1trA1216 Nbv6.1trA134724	glyceraldehyde-3-phosphate cytosolic-like	GAPDH	glyceraldehyde-3-phosphate dehydrogenase—Glyceraldehyde-3-phosphate dehydrogenase
Nbv6.1trP33991	nucleolar gtp-binding protein 1-like	GTPBP4	GTP binding protein 4—Nucleolar GTP-binding protein 1
Nbv6.1trP14845 Nbv6.1trP4035	histone deacetylase 5	HDAC1	histone deacetylase 1—Histone deacetylase 1
Nbv6.1trA108466 Nbv6.1trP34322 Nbv6.1trP41303 Nbv6.1trA47396	heat shock cognate protein 80-like	HSP90AA1	heat shock protein 90kDa alpha (cytosolic), class A member 1—Heat shock protein HSP 90-alpha 2
NbS00014166g0016.1	Kinesin protein	KIF11	kinesin family member 11—Kinesin-like protein KIF11
Nbv6.1trA44561	kinesin-related protein 11-like isoform x1	KIF5B	kinesin family member 5B—Kinesin heavy chain
NbS00015744g0008.1 NbS00016691g0013.1	methionine tRNA ligase/methionyl tRNA synthetase%2C/MetRS%2C	MARS	methionyl-tRNA synthetase—Methionyl-tRNA synthetase, cytoplasmic
Nbv6.1trA56859 Nbv6.1trP30432 Nbv6.1trA29984	probable methionine--trna ligase	MARS	methionyl-tRNA synthetase—Methionyl-tRNA synthetase, cytoplasmic
Nbv6.1trA232987	probable uncharacterized protein LOC104215021	NBR1	neighbor of BRCA1 gene 1—Isoform 1 of Next to BRCA1 gene 1 protein
NbS00018426g0019.1	ubiquitin associated UBA/TS N domain containing protein/octicosapeptide/Phox/Bemp1 PB1 domain containing protein	NBR1	neighbor of BRCA1 gene 1—Isoform 1 of Next to BRCA1 gene 1 protein
Nbv6.1trP744	protein disulfide isomerase-like 1-4	P4HB	procollagen-proline, 2-oxoglutarate 4-dioxygenase (proline 4-hydroxylase), beta polypeptide—Protein disulfide-isomerase precursor
Nbv6.1trA36576 Nbv6.1trA46199 NbS00012224g0007.1 Nbv6.1trA73962	serine threonine-protein kinase atg1	PRKAA1	protein kinase, AMP-activated, alpha 1 catalytic subunit—5'-AMP-activated protein kinase catalytic subunit alpha-1
Nbv6.1trA269680	serine threonine-protein kinase atg1	PRKCI	protein kinase C, iota—protein kinase C, iota
Nbv6.1trA197115 NbS00005985g0007.1 NbS00016411g0025.1	Kinase	PRPF4B	PRP4 pre-mRNA processing factor 4 homolog B (yeast)—Serine/threonine-protein kinase PRP4 homolog
Nbv6.1trA194969 Nbv6.1trP8372	rab3 gtpase-activating protein catalytic subunit	RAB3GAP1	RAB3 GTPase activating protein subunit 1 (catalytic)—Similar to RAB3 GTPase-activating protein

Nb	Nb protein ID	Human gene name	Human protein ID
NbS00013207g0009.1 NbS00014760g0001.1 Nbv6.1trA100686 NbS00044021g0003.1 Nbv6.1trP54771 Nbv6.1trA198673 Nbv6.1trA213287 Nbv6.1trP65517	60S ribosomal protein L10a1	RPL10A	ribosomal protein L10a—60S ribosomal protein L10a
Nbv6.1trP77203 Nbv6.1trP19462 NbS00010427g0115.1 Nbv6.1trP70429	60s ribosomal protein l11-1	RPL11	ribosomal protein L11—Isoform 1 of 60S ribosomal protein L11
Nbv6.1trP32299 Nbv6.1trP3838 Nbv6.1trA158121	60s ribosomal protein l12	RPL12	ribosomal protein L12—60S ribosomal protein L12
NbS00041012g0008.1 Nbv6.1trP17644 NbS00026051g0013.1 NbS00030768g0006.1 Nbv6.1trP19568	60S ribosomal protein L13	RPL13	ribosomal protein L13—60S ribosomal protein L13
Nbv6.1trP3552 Nbv6.1trP17842 Nbv6.1trA109794 Nbv6.1trP69096	60s ribosomal protein l13a-4-like	RPL13A	ribosomal protein L13a—60S ribosomal protein L13a
Nbv6.1trP76763 Nbv6.1trA74128 Nbv6.1trA75455 NbS00021394g0006.1	probable 60s ribosomal protein l14	RPL14	ribosomal protein L14—RPL14 protein
Nbv6.1trP17614 Nbv6.1trA178237 Nbv6.1trP38388 Nbv6.1trP27073 Nbv6.1trA110493 NbS00007010g0113.1	60s ribosomal protein l15-like	RPL15	ribosomal protein L15—26 kDa protein
Nbv6.1trP54412 Nbv6.1trA12790 NbS00008466g0007.1 Nbv6.1trP13280	60S ribosomal protein L17	RPL17	ribosomal protein L17—60S ribosomal protein L17
NbS00021061g0110.1 NbS00013932g0015.1 NbS00007750g0014.1 Nbv6.1trP14296 NbS00025676g0010.1	Ribosomal protein L18	RPL18	ribosomal protein L18—60S ribosomal protein L18
Nbv6.1trP22752 Nbv6.1trP73490 Nbv6.1trA228330	60s ribosomal protein l18a	RPL18A	ribosomal protein L18a—60S ribosomal protein L18a

Nb	Nb protein ID	Human gene name	Human protein ID
NbS00022677g0027.1 NbS00020925g0004.1 NbS00024093g0010.1 NbS00012223g0004.1 Nbv6.1trP56850 Nbv6.1trP65332 NbS00037623g0001.1 Nbv6.1trP58899 Nbv6.1trA65478	60S ribosomal protein L19	RPL19	ribosomal protein L19—60S ribosomal protein L19
Nbv6.1trP53202 Nbv6.1trP56805 Nbv6.1trP47201 Nbv6.1trA187516	60s ribosomal protein l21-1-like	RPL21	ribosomal protein L21—60S ribosomal protein L21
NbS00017836g0015.1 NbS00056322g0001.1 Nbv6.1trA117657 Nbv6.1trA95896 NbS00024386g0011.1	60S ribosomal protein L22 2	RPL22	ribosomal protein L22—60S ribosomal protein L22
Nbv6.1trA114306 NbS00004708g0003.1 NbS00047740g0003.1	60s ribosomal protein l23	RPL23	ribosomal protein L23—60S ribosomal protein L23
Nbv6.1trP27867 Nbv6.1trP46844 NbS00000332g0115.1	60s ribosomal protein l23a-like	RPL23A	ribosomal protein L23a—60S ribosomal protein L23a
NbS00017881g0010.1 Nbv6.1trP1418	60S ribosomal protein L24	RPL24	ribosomal protein L24—60S ribosomal protein L24
Nbv6.1trA6916 NbS00059392g0001.1 Nbv6.1trA12405 Nbv6.1trA31978 NbS00035409g0006.1	60s ribosomal protein l26-1	RPL26L1	ribosomal protein L26-like 1—60S ribosomal protein L26-like 1
Nbv6.1trA12178 Nbv6.1trA88604 Nbv6.1trP16932	60s ribosomal protein l27	RPL27	ribosomal protein L27—60S ribosomal protein L27
Nbv6.1trA5091 Nbv6.1trA181920	60s ribosomal protein l28-1-like	RPL28	ribosomal protein L28—60S ribosomal protein L28
NbS00038870g0030.1 Nbv6.1trP61511 Nbv6.1trP48435 Nbv6.1trP43008 Nbv6.1trA251354 Nbv6.1trA211581	Ribosomal protein L3	RPL3	ribosomal protein L3—60S ribosomal protein L3
Nbv6.1trP53058	60s ribosomal protein l30-like	RPL30	ribosomal protein L30—60S ribosomal protein L30
NbS00002504g0003.1 Nbv6.1trP71451 Nbv6.1trA29503	60s ribosomal protein L30	RPL30	ribosomal protein L30—60S ribosomal protein L30
Nbv6.1trP73091 Nbv6.1trP3924	60s ribosomal protein l31	RPL31	ribosomal protein L31—60S ribosomal protein L31
NbS00014429g0017.1 Nbv6.1trA139422	60S ribosomal protein L36	RPL36	ribosomal protein L36—60S ribosomal protein L36

Nb	Nb protein ID	Human gene name	Human protein ID
NbS00007843g0209.1 NbS00030533g0009.1	60S ribosomal protein L37a	RPL37A	ribosomal protein L37a—60S ribosomal protein L37a
NbS00032888g0009.1	60S ribosomal protein L38	RPL38	ribosomal protein L38—60S ribosomal protein L38
Nbv6.1trA210320 Nbv6.1trA107185 Nbv6.1trA5383 Nbv6.1trA131660 Nbv6.1trP68432 Nbv6.1trA202662	60s ribosomal protein l4-like	RPL4	ribosomal protein L4—60S ribosomal protein L4
Nbv6.1trP72839 Nbv6.1trA239446 Nbv6.1trP41032 Nbv6.1trA126646 Nbv6.1trP74572 Nbv6.1trP38704 Nbv6.1trA74446 Nbv6.1trA244594	60s ribosomal protein l5-like	RPL5	ribosomal protein L5—60S ribosomal protein L5
Nbv6.1trP47475 Nbv6.1trA228136 Nbv6.1trA63010 NbS00021581g0010.1 Nbv6.1trA139794 NbS00017572g0018.1 Nbv6.1trA114336 Nbv6.1trA57621	60s ribosomal protein l6-like	RPL6	ribosomal protein L6—60S ribosomal protein L6
Nbv6.1trA67492 Nbv6.1trA187926 Nbv6.1trP68164 Nbv6.1trP19854	60s ribosomal protein l7-2	RPL7	ribosomal protein L7—60S ribosomal protein L7
Nbv6.1trA252389 Nbv6.1trA5223	60s ribosomal protein l7-4	RPL7	ribosomal protein L7—60S ribosomal protein L7
NbS00061153g0003.1 Nbv6.1trA3389	60S ribosomal protein L7	RPL7	ribosomal protein L7—60S ribosomal protein L7
NbS00010173g0011.1 NbS00023515g0003.1 Nbv6.1trP16849	Ribosomal protein L7a	RPL7A	ribosomal protein L7a—60S ribosomal protein L7a
Nbv6.1trP45740 Nbv6.1trP16969	60s ribosomal protein l7a-2-like	RPL7A	ribosomal protein L7a—60S ribosomal protein L7a
Nbv6.1trP38162 NbS00017622g0006.1 Nbv6.1trA61976 Nbv6.1trA55456 Nbv6.1trP40677 Nbv6.1trA220169 Nbv6.1trA119089 Nbv6.1trP58182	60S ribosomal protein L8	RPL8	ribosomal protein L8—60S ribosomal protein L8
Nbv6.1trA105545 Nbv6.1trP16905 Nbv6.1trA244984 Nbv6.1trA176129	60s ribosomal protein l9-1-like	RPL9	ribosomal protein L9—60S ribosomal protein L9

Nb	Nb protein ID	Human gene name	Human protein ID
Nbv6.1trA47361 Nbv6.1trP71351	60s acidic ribosomal protein p0	RPLP0	ribosomal protein, large, P0—60S acidic ribosomal protein P0
Nbv6.1trA117530 Nbv6.1trA168757 Nbv6.1trA117531 NbS00053503g0005.1	60s acidic ribosomal protein p1	RPLP1	ribosomal protein, large, P1—60S acidic ribosomal protein P1
NbS00021044g0016.1 Nbv6.1trA65372 NbS00000941g0015.1 Nbv6.1trP68173 Nbv6.1trA7626	60s acidic ribosomal protein	RPLP2	ribosomal protein, large, P2—60S acidic ribosomal protein P2
Nbv6.1trP14272	40s ribosomal protein s13	RPS13	ribosomal protein S13—40S ribosomal protein S13
Nbv6.1trP3841 Nbv6.1trP70032	40s ribosomal protein s14-2	RPS14	ribosomal protein S14—40S ribosomal protein S14
Nbv6.1trP47007 Nbv6.1trA213884	40s ribosomal protein s15-like	RPS15	ribosomal protein S15—40S ribosomal protein S15
NbS00013115g0003.1	40S ribosomal protein S15a 1	RPS15A	ribosomal protein S15a—40S ribosomal protein S15a
Nbv6.1trP23049	40s ribosomal protein s16	RPS16	ribosomal protein S16—40S ribosomal protein S16
NbS00056355g0003.1 Nbv6.1trA264033 Nbv6.1trP19832	40S ribosomal protein S18	RPS18	ribosomal protein S18—40S ribosomal protein S18
Nbv6.1trA219589	40s ribosomal protein s19-3	RPS19	ribosomal protein S19—40S ribosomal protein S19
NbS00006107g0001.1 NbS00016839g0002.1	40S ribosomal protein S2 2	RPS2	ribosomal protein S2—40S ribosomal protein S2
NbS00055601g0001.1	Ribosomal protein S12/S23	RPS23	ribosomal protein S23—40S ribosomal protein S23
Nbv6.1trP52801	40s ribosomal protein s24-1	RPS24	ribosomal protein S24—Isoform 1 of 40S ribosomal protein S24
NbS00017796g0009.1	40S ribosomal protein S25 1	RPS25	ribosomal protein S25—40S ribosomal protein S25
Nbv6.1trP3553 Nbv6.1trP58727	40s ribosomal protein s3-3	RPS3	ribosomal protein S3—40S ribosomal protein S3
	40s ribosomal protein s3-3-like	RPS3	ribosomal protein S3—40S ribosomal protein S3
Nbv6.1trP30065 Nbv6.1trP28367 Nbv6.1trP28368	40s ribosomal protein s4-like	RPS4X	ribosomal protein S4, X-linked—40S ribosomal protein S4, X isoform
NbS00003570g0008.1 NbS00011165g0113.1	40S ribosomal protein S5 2	RPS5	ribosomal protein S5—40S ribosomal protein S5
Nbv6.1trP1324 Nbv6.1trP68267 Nbv6.1trP17350 NbS00000439g0011.1	40s ribosomal protein s6-like	RPS6	ribosomal protein S6—40S ribosomal protein S6
Nbv6.1trA118205 Nbv6.1trA228338 Nbv6.1trP19501	40s ribosomal protein s7-like	RPS7	ribosomal protein S7—40S ribosomal protein S7
Nbv6.1trA187403 Nbv6.1trP17033	eukaryotic translation initiation factor 3 subunit i-like	STRAP	serine/threonine kinase receptor associated protein—Serine-threonine kinase receptor-associated protein
NbS00002652g0220.1 NbS00031544g0010.1 Nbv6.1trP26162 Nbv6.1trP73929 Nbv6.1trA184988	tubulin alpha chain	TUBA1C	tubulin, alpha 1c—TUBA1C protein

Nb	Nb protein ID	Human gene name	Human protein ID
Nbv6.1trA121378 Nbv6.1trA88398 Nbv6.1trP4607 Nbv6.1trP52057 Nbv6.1trP68479	tubulin beta-2 chain	TUBB2A	tubulin, beta 2A—Tubulin beta-2A chain
Nbv6.1trP58422	thioredoxin chloroplastic-like	TXN	thioredoxin—Thioredoxin
NbS00033917g0007.1 NbS00046481g0008.1	ATPase AAA type/ cell division cycle protein 48	VCP	valosin-containing protein—Transitional endoplasmic reticulum ATPase
Nbv6.1trA1493 Nbv6.1trA201572 NbS00032670g0023.1	protein tipd	WDR5	WD repeat domain 5—WD repeat protein 5
Nbv6.1trP28238 Nbv6.1trP4045 Nbv6.1trP51988 Nbv6.1trA62570 NbS00056344g0007.1 Nbv6.1trP47675 NbS00059178g0006.1 NbS00017559g0109.1 Nbv6.1trA124569	14-3-3 protein	YWHAE	tyrosine 3-monooxygenase/ tryptophan 5-monooxygenase activation protein, epsilon polypeptide—14-3-3 protein epsilon

Appendix III

Supplemental figures for Chapter 4: N-terminal β -strand underpins biochemical specialization of a plant ATG8 isoform

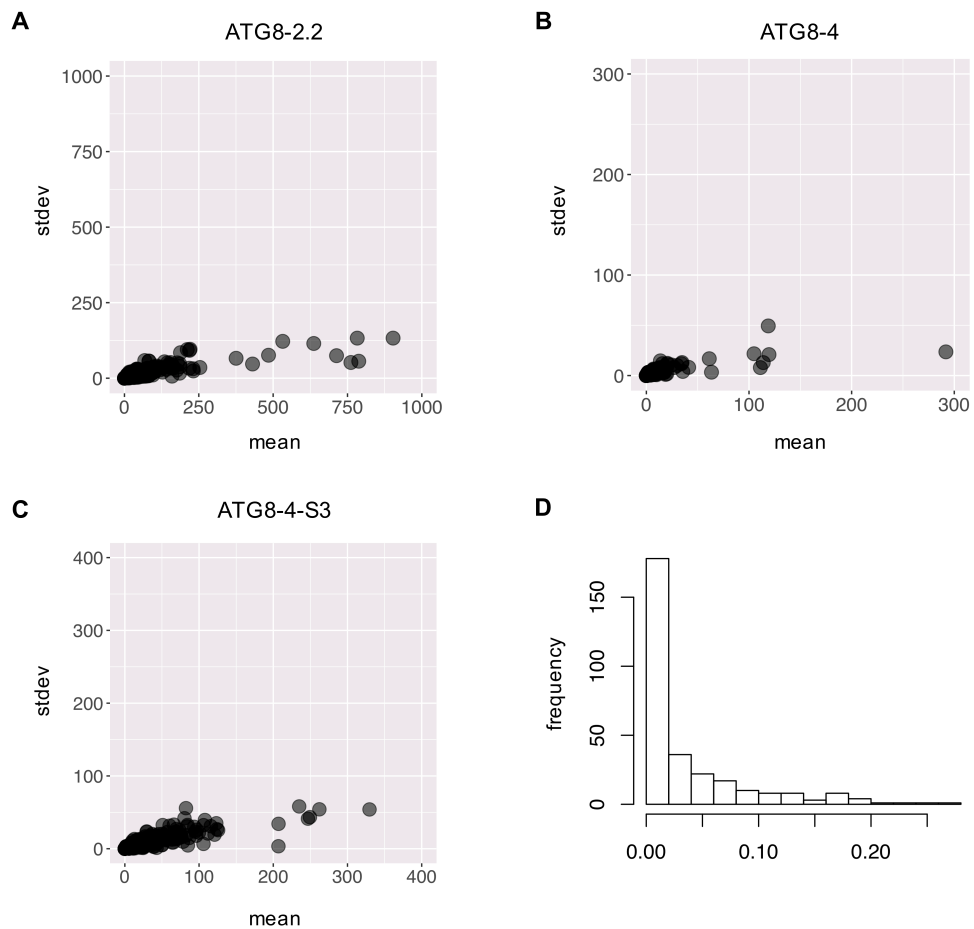


Figure A.3.1 Normal distribution of comparative ATG8-4-S3 mutant IP-MS data
 The standard deviation (stdev) versus mean is plotted for the GFP normalized peptide count data for three replicates of each construct tested in IP-MS, (a) ATG8-2.2, (b) ATG8-4, and (c) ATG8-4-S3, showing a normal distribution in each. (d) A histogram of ANOVA p-values showing the high level of significance within the dataset.

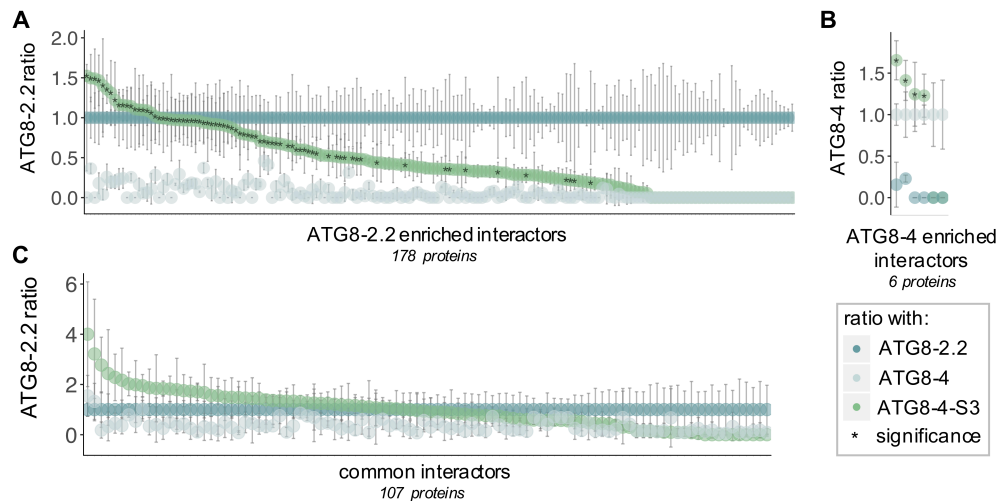


Figure A.3.2 The first β -strand of ATG8 underpins interaction with plant proteins

For each interactor in the dataset, the average peptide count data for ATG8-2.2 (teal), ATG8-4 (light grey), and ATG8-4-S3 (green) were normalized to either ATG8-2.2 or ATG8-4 data based on the enrichment category being analyzed: (a) values for ATG8-2.2 enriched interactors were normalized to ATG8-2.2, (b) values for ATG8-4 enriched interactors were normalized to ATG8-4, and (c) values for common interactors were normalized to ATG8-2.2. For (a) ATG8-2.2 enriched interactors and (b) ATG8-4 enriched interactors, this highlights the difference in how ATG8-2.2 and ATG8-4 interact with each protein in the set and how the ATG8-4-S3 interactions compare. For (a) ATG8-2.2 enriched interactors, the asterisk (*) marks proteins that showed no statistical difference in their interaction with ATG8-4-S3 as compared to ATG8-2.2 (in **Fig 4.5**, '(+) S3 enrichment'); for (b) ATG8-4 enriched interactors, the asterisk (*) marks proteins that showed no statistical difference in their interaction with ATG8-4-S3 as compared to ATG8-4. For (c) common interactors, the graph highlights the similarity in how ATG8-2.2, ATG8-4, and ATG8-4-S3 interact with each protein in the set; due to the lack of statistical difference, this feature is not marked.

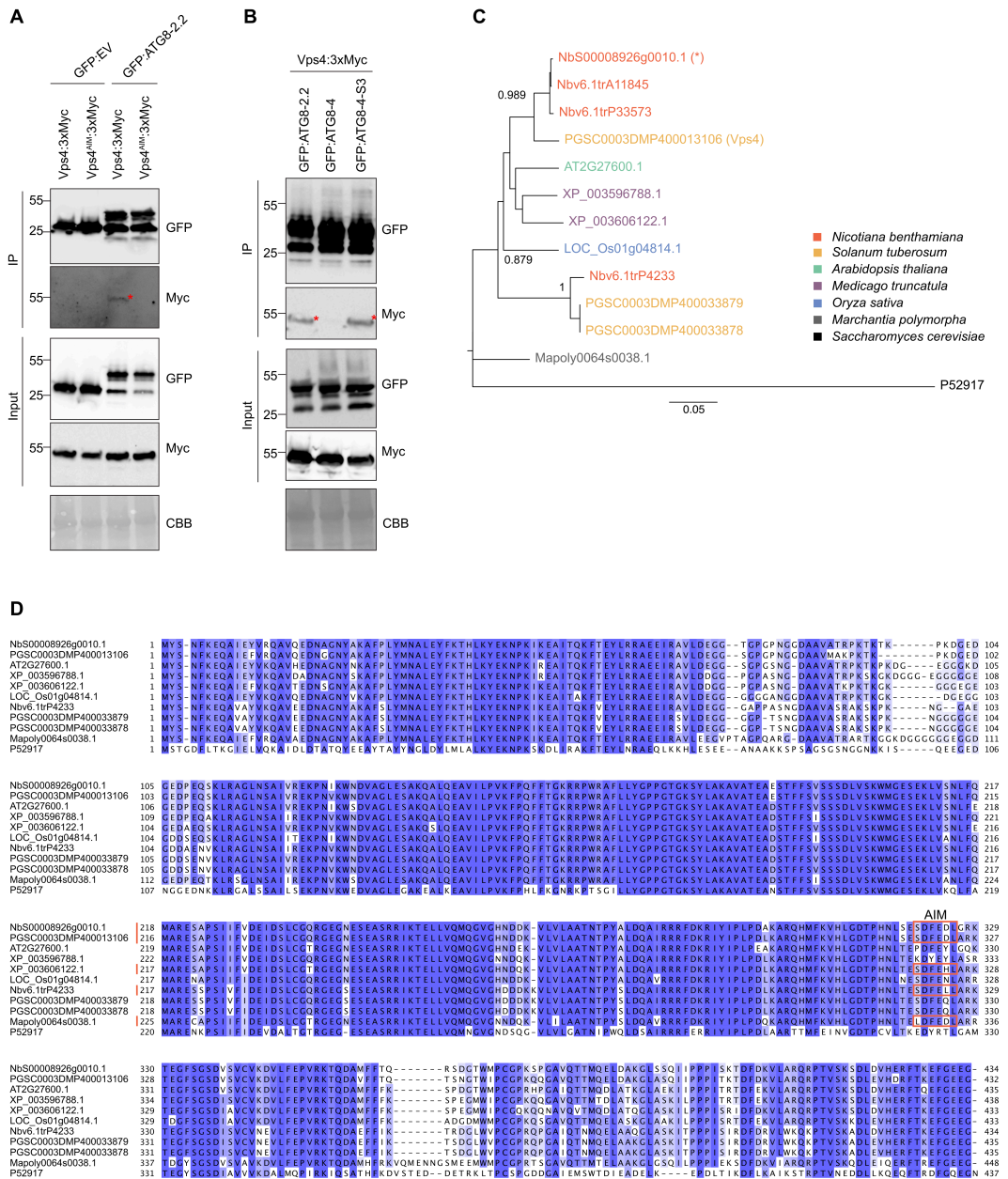


Figure A.3.3 The ATG8 region surrounding the first β -strand is responsible for discriminatory binding to potato Vps4

(a) Co-Immunoprecipitation experiment between potato Vps4 and the Vps4 AIM mutant (Vps4AIM)—changing the AIM sequence of SDFEDL to SDAEDA—with ATG8-2.2. Vps4:3xMyc and Vps4AIM:3xMyc were transiently co-expressed with GFP:EV and GFP:ATG8-2.2, respectively. (b) Co-Immunoprecipitation experiment between Vps4 and ATG8-2.2, ATG8-4, and ATG8-4-S3. Vps4:3xMyc was transiently co-expressed with GFP:ATG8-2.2, GFP:ATG8-4, and GFP:ATG8-4-S3. For (a- b), immunoprecipitates (IPs) were obtained with anti-GFP antiserum and total protein extracts were immunoblotted with appropriate antisera (listed on the

right). Stars indicate expected band sizes. These experiments were performed by project collaborator Yasin Dagdas. (c) Unrooted maximum-likelihood phylogenetic tree of orthologs of *Saccharomyces cerevisiae* (yeast) Vps4 from across select plant species, with the *N. benthamiana* Vps4 identified in the IP-MS experiment starred (*) and the *S. tuberosum* Vps4 tested in co-immunoprecipitation experiments marked ('Vps4'). Colors indicate species, and bootstrap supports are noted when >0.7. The tree was calculated in MEGA7 (Kumar et al., 2016) from a 448 amino acid alignment (MUSCLE (Edgar, 2004) codon-based). The scale bar indicates the evolutionary distance based on amino acid substitution rate. (d) Alignment of Vps4 sequences included in the phylogenetic tree in (c), excluding the Nbv6.1trA11845 and Nbv6.1trP33573 sequences, which are almost sequence identical to NbS00008926g0010.1. The presence of a predicted AIM as determined by iLIR is marked with a red box (Kalvari et al., 2014).

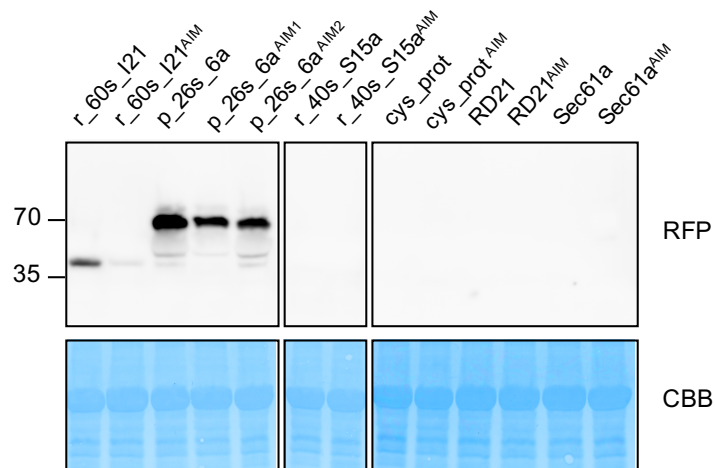


Figure A.3.4 Candidate ATG8-interacting proteins do not express *in planta*

Western blot experiment of showing no expression of the candidate ATG8-interacting proteins and their respective AIM mutants—40s ribosomal protein S15a (r_40s_S15a), low-temperature-induced cysteine protease (cys_prot), cathepsin B cysteine protease (RD21), and Sec61a subunit α -like (Sec61a). The proteins 60s ribosomal protein I21-1 (r_60s_I21) and 26s proteasome regulatory subunit 6a (26a_p_6a) were included as positive controls. RFP-tagged proteins were transiently co-expressed, and total protein extracts were immunoblotted with anti-RFP antisera.

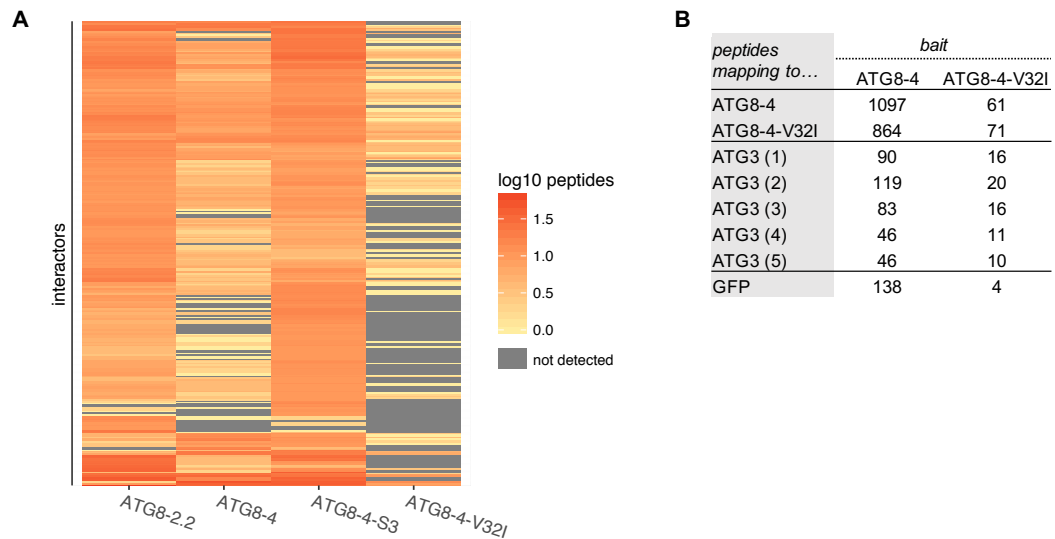


Figure A.3.5 The ATG8-4-V32I bait construct is weakly expressed

(a) Heatmap showing the interactor profiles of ATG8-2.2, ATG8-4, ATG8-4-S3, and ATG8-4-V32I. The average peptide value data for the three replicates was filtered to remove any interactors where empty vector showed peptide count values >5 . The data for the remaining interactors (403 proteins) was log₁₀ normalized and used to construct a hierarchically clustered heatmap with the scale as shown. Experiment performed by a collaborator. (b) Average peptide count values for the ATG8-4 and ATG8-4-V32I bait proteins, mapping to ATG8-4 and ATG8-4-V32I; autophagy-related protein 3 (ATG3) isoforms; and green fluorescent protein (GFP).

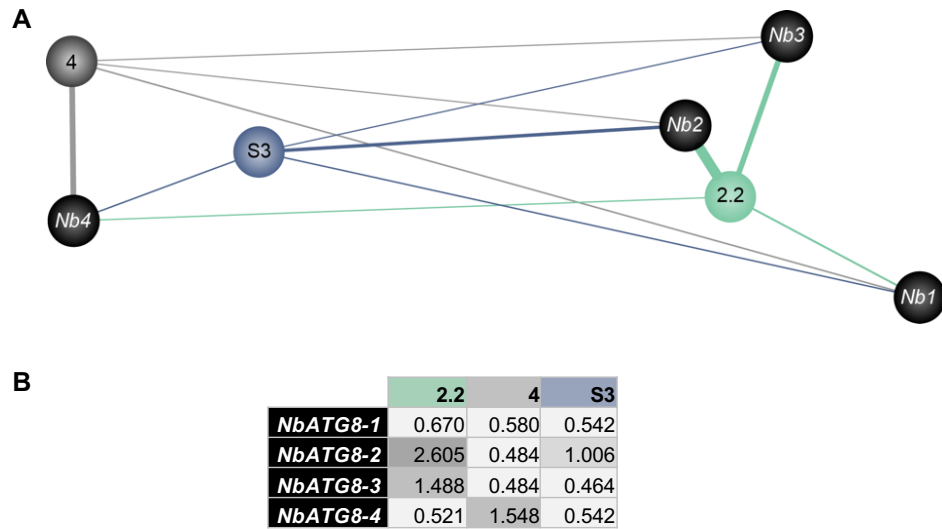


Figure A.3.6 Network representation of the interaction between ATG8-2.2, ATG8-4, and ATG8-4-S3 and endogenous *N. benthamiana* ATG8s

Network representation of the interactions between ATG8-2.2, ATG8-4, and ATG8-4-S3 and endogenous *N. benthamiana* ATG8s. The edge widths are weighted to GFP normalized peptide counts shown in (b). The spatial relationships between the ATG8s are scaled to amino acid sequence identity, with more sequence related ATG8s clustering together, using Cytoscape (Shannon et al., 2003). The four *N. benthamiana* ATG8s present in the dataset—labelled NbATG8-1- NbATG8-4—are correspondingly labelled in Fig A.1.1 for reference.

Appendix IV

Supplemental table for Chapter 4: N-terminal β -strand underpins biochemical specialization of a plant ATG8 isoform.

Table A.4.8 Comparative ATG8-4-S3 mutant analysis dataset

For each *N. benthamiana* interactor in the dataset (291 proteins), the closest *A. thaliana* and *M. polymorpha* homologs were predicted using BLAST. Each interactor is thus described, by column: *N. benthamiana* accession ('Nb'), protein identification ('Nb protein ID'); the *A. thaliana* homolog accession number ('At') and protein identification ('At protein ID'); and the *M. polymorpha* homolog accession number ('Mp') and protein identification ('Mp protein ID'). This dataset was cross-referenced with the ATG8 interactome (**Table A.2.1**) by *N. benthamiana* accession and protein identification; interactors shared between the datasets are marked ('Int.').

Nb	Nb protein ID	At	At protein ID	Mp	Mp protein ID	Int.
Nbv6.1trA214512	14-3-3-like protein gfl4 kappa	AT5G65430.1	general regulatory factor 8	Mapoly0043s0019.1	14-3-3 protein epsilon	
Nbv6.1trA99313	2-oxoglutarate and fe - dependent oxygenase superfamily protein isoform 1	AT2G17970.1	2-oxoglutarate (2OG) and Fe(II)-dependent oxygenase	Mapoly0001s0483.1	uncharacterized conserved protein	x
NbS00048541g0015.1	26S protease regulatory subunit	AT1G45000.1	AAA-type ATPase family protein	Mapoly0009s0112.3	26S proteasome regulatory subunit T4	
Nbv6.1trP48334	26s protease regulatory subunit 6a homolog	AT3G05530.1	regulatory particle triple-A ATPase 5A	Mapoly0085s0078.1	26S proteasome regulatory subunit T5	x
Nbv6.1trA116345	26s protease regulatory subunit 6b homolog	AT5G58290.1	regulatory particle triple-A ATPase 3	Mapoly0008s0139.1	26S proteasome regulatory subunit T3	
Nbv6.1trP58965	26s protease regulatory subunit 7	AT1G53750.1	regulatory particle triple-A ATPase 1A	Mapoly0031s0139.1	26S proteasome regulatory subunit T1	x
Nbv6.1trA103869	26s protease regulatory subunit 8 homolog a	AT5G19990.3	regulatory particle triple-A ATPase 6A	Mapoly0005s0178.1	26S proteasome regulatory subunit T6	
NbS00013187g0013.1	26S proteasome non ATPase regulatory subunit 6	AT4G24820.2	26 proteasome regulatory subunit Rpn7	Mapoly0014s0216.1	26S proteasome regulatory subunit N7	
NbS00007460g0008.1	26S proteasome regulatory subunit	AT2G32730.1	26 proteasome regulatory complex 2C	Mapoly0034s0048.1	26S proteasome regulatory subunit N2	
NbS00011906g0010.1	3 oxoacyl	AT1G74960.3	fatty acid biosynthesis 1	Mapoly0035s0037.1	beta-ketoacyl-[acyl-carrier-protein]	
Nbv6.1trP37282	3-ketoacyl- synthase 6	AT1G68530.1	3-ketoacyl-acyl carrier protein synthase 6	Mapoly0005s0001.1	FAE1/ Type III polyketide synthase-like protein	
Nbv6.1trP48824	3-oxoacyl-	AT5G46290.1	3-ketoacyl-acyl carrier protein synthase	Mapoly0002s0312.1	polyketide synthase-related	
Nbv6.1trA81966	3beta-hydroxysteroid-dehydrogenase decarboxylase isoform 2	AT2G26260.1	3beta-hydroxysteroid-dehydrogenase/decarb oxylase isoform 2	Mapoly0001s0030.1	NAD dependent epimerase/ dehydratase	
NbS00013115g0003.1	40S ribosomal protein S15a 1	AT5G59850.1	ribosomal protein S8 family protein	Mapoly0083s0020.1	small subunit ribosomal protein S15Ae	x
NbS00016839g0002.1	40S ribosomal protein S2 2	AT1G59359.1	Ribosomal protein S5 family protein	Mapoly0027s0187.1	small subunit ribosomal protein S2e	x
Nbv6.1trA62456	40s ribosomal protein s3-3-like	AT2G31610.1	Ribosomal protein S3 family protein	Mapoly0001s0014.1	small subunit ribosomal protein S3e	x
Nbv6.1trP64367	40s ribosomal protein s4-like	AT5G58420.1	Ribosomal protein S4 (RPS4A) family protein	Mapoly0012s0120.1	small subunit ribosomal protein S4e	x
Nbv6.1trP19501	40s ribosomal protein s7-like	AT3G02560.3	ribosomal protein S7e family protein	Mapoly0060s0109.1	small subunit ribosomal protein S7e	x
Nbv6.1trA174217	50s ribosomal protein chloroplastic-like	AT1G35680.1	Ribosomal protein L21	Mapoly0034s0066.1	50s ribosomal protein L21	x
NbS00015607g0008.1	50S ribosomal protein L2	AT4G36130.1	Ribosomal protein L2 family	Mapoly0068s0027.1	large subunit ribosomal protein L8e	
NbS00010171g0006.1	60S ribosomal protein L10a 1	AT1G08360.1	ribosomal protein L1p/L10e family	Mapoly0006s0264.1	large subunit ribosomal protein L10Ae	x
Nbv6.1trA141068	60s ribosomal protein l11	AT5G45775.2	Ribosomal L5P family protein	Mapoly0038s0097.1	60s ribosomal protein L11-related	x
NbS00029456g0001.1	60S ribosomal protein L12	AT5G60670.1	Ribosomal protein L11 family protein	Mapoly0007s0191.1	large subunit ribosomal protein L12e	x

Nb	Nb protein ID	At	At protein ID	Mp	Mp protein ID	Int.
Nbv6.1trP42422	60S ribosomal protein l13-1-like	AT3G49010.7	breast basic conserved 1	Mapoly0055s0071.1	large subunit ribosomal protein L13e	x
Nbv6.1trA75455 NbS00009111g0021.1	60S ribosomal protein L14-1	AT2G20450.1	Ribosomal protein L14	Mapoly0030s0040.1	large subunit ribosomal protein L14e	x
NbS00036485g0008.1	60S ribosomal protein L17	AT1G27400.1	Ribosomal protein L22p/L17e family protein	Mapoly0014s0203.2	large subunit ribosomal protein L17e	x
NbS00022260g0005.1	60S ribosomal protein L21 protein	AT1G57860.1	translation protein SH3-like family protein	Mapoly0052s0065.1	large subunit ribosomal protein L21e	
Nbv6.1trP56805	60S ribosomal protein l21-1-like	AT1G09690.1	Translation protein SH3-like family protein	Mapoly0052s0065.1	large subunit ribosomal protein L21e	x
Nbv6.1trP4365	60S ribosomal protein l23a	AT3G55280.2	ribosomal protein L23AB	Mapoly0028s0094.1	large subunit ribosomal protein L23Ae	x
Nbv6.1trA6916 NbS00059392g0001.1	60S ribosomal protein L26-1	AT3G49910.1	translation protein SH3-like family protein	Mapoly0026s0085.1	large subunit ribosomal protein L26e	x
Nbv6.1trA6752	60S ribosomal protein l27a-3-like	AT1G70600.1	Ribosomal L28e/L15 superfamily protein	Mapoly0033s0117.1	large subunit ribosomal protein L27Ae	x
Nbv6.1trP30012	60S ribosomal protein l27a-3-like	AT1G70600.1	ribosomal protein L18/L15 superfamily protein	Mapoly0078s0013.1	large subunit ribosomal protein L27Ae	x
NbS00005975g0012.1	60S ribosomal protein L28	AT2G19730.3	Ribosomal L28e protein family	Mapoly0002s0184.2	large subunit ribosomal protein L28e	
Nbv6.1trP61511	60S ribosomal protein l3	AT1G61580.1	R-protein L3 B	Mapoly0001s0237.1	large subunit ribosomal protein L3c	x
NbS00014666g0005.1	60S ribosomal protein L34	AT1G26880.1	Ribosomal protein L34e superfamily protein	Mapoly0148s0016.1	large subunit ribosomal protein L34e	x
Nbv6.1trA177800	60S ribosomal protein l35-like	AT5G02610.1	Ribosomal L29 family protein	Mapoly0097s0080.1	large subunit ribosomal protein L35e	x
NbS00026258g0017.1	60S ribosomal protein L36	AT3G53740.4	ribosomal protein L36e family protein	Mapoly0005s0062.1	large subunit ribosomal protein L36e	x
Nbv6.1trA162946 Nbv6.1trA202660	60S ribosomal protein l4-1-like	AT3G09630.1	Ribosomal protein L4/L1 family	Mapoly0116s0033.3	large subunit ribosomal protein L4e	x
Nbv6.1trA1344 Nbv6.1trP38704	60S ribosomal protein l5-like	AT5G39740.2	ribosomal protein L5 B	Mapoly0054s0045.1	large subunit ribosomal protein L5e	x
Nbv6.1trP27978 Nbv6.1trA114336 Nbv6.1trA57621	60S ribosomal protein l6-like	AT1G74050.1	Ribosomal protein L6 family	Mapoly0037s0030.1	large subunit ribosomal protein L6e	x
Nbv6.1trA159125	60S ribosomal protein l7-2-like	AT3G13580.9	Ribosomal protein L30/L7 family protein	Mapoly0050s0096.1	large subunit ribosomal protein L7e	x
Nbv6.1trA1317	acetolactate synthase small subunit chloroplastic-like	AT5G16290.2	valine-tolerant 1	Mapoly0007s0273.1	acetolactate synthase I/III small subunit	
Nbv6.1trA269378	acetyl-coenzyme a carboxylase carboxyl transferase subunit chloroplastic	AT2G38040.2	acetyl co-enzyme a carboxylase carboxyltransferase	Mapoly0083s0025.2	acetyl-CoA carboxylase carboxyl transferase	
NBR1-a	added_for_Tolga	NA	NA	NA	NA	
NbS00043181g0003.1	ADP ATP carrier protein%2C mitochondrial Fragment	AT5G13490.2	ADP/ATP carrier 2	Mapoly0117s0032.3	solute carrier family 25	
NbS00003232g0016.1	Aldehyde dehydrogenase 22A1	AT3G66658.2	aldehyde dehydrogenase 22A1	NbS00003232g0016.1	predicted: similar to aldehyde dehydrogenase	

Nb	Nb protein ID	At	At protein ID	Mp	Mp protein ID	Int.
NbS00047628g0009.1	Aldehyde dehydrogenase expressed	AT1G44170.2	aldehyde dehydrogenase 3H1	Mapoly0030s0099.1	aldehyde dehydrogenase	
Nbv6.1trP47800	aldehyde dehydrogenase family 3 member f1-like	AT4G36250.1	aldehyde dehydrogenase 3F1	Mapoly0030s0099.1	ALDEHYDE DEHYDROGENAS E	
Nbv6.1trA6964	alpha beta hydrolase family protein	AT1G74640.1	alpha/beta-Hydrolases superfamily protein	Mapoly0229s0006.1	predicted hydrolase/ acyltransferase	
Nbv6.1trA159249	alpha beta-hydrolases superfamily protein isoform 1	AT1G52510.1	alpha/beta-Hydrolases superfamily protein	Mapoly0030s0015.1	alpha/beta hydrolase fold-containing protein	
Nbv6.1trP21647	alpha-L-fucosidase 2	AT4G34260.1	alpha-L-fucosidase	Mapoly0115s0027.2	glycosyl hydrolase family 65	x
NbS00029456g0006.1	Aquaporin 1	AT2G37170.2	plasma membrane intrinsic protein 2	Mapoly0041s0003.1	aquaporin PIP	
Nbv6.1trA111126	argininosuccinate chloroplastic	AT4G24830.1	argininosuccinate synthase family	Mapoly0038s0028.1	argininosuccinate synthase	
NbS00054590g0004.1	Arginyl tRNA synthetase	AT4G26300.5	arginyl-tRNA synthetase 2C class 1c	Mapoly0066s0109.1	arginine-tRNA ligase	
NbS00062043g0007.1	Ascorbate peroxidase	AT4G35000.1	ascorbate peroxidase	Mapoly0015s0180.2	L-ascorbate peroxidase	x
Nbv6.1trA268603	atp sulfurylase chloroplastic-like	AT3G22890.1	ATP sulfurylase 1	Mapoly0142s0006.1	sulfate adenylyltransferase	
NbS00012584g0001.1	ATP synthase gamma chain chloroplastic	AT4G04640.1	ATPase 2C F1 complex 2C gamma subunit protein	Mapoly0206s0012.1	F-type H+-transporting ATPase subunit gamma	
Nbv6.1trA49071	atp-dependent clp protease proteolytic subunit-related protein chloroplastic	AT1G09130.3	ATP-dependent caseolytic (Clp) protease/crotonase family protein	Mapoly0091s0025.1	ATP-dependent CLP protease proteolytic subunit	x
Nbv6.1trA11859 Nbv6.1trA36039 Nbv6.1trA59159 Nbv6.1trA190771	autophagy-related protein 3	AT5G61500.1	autophagy 3 (ATG3)	Mapoly0003s0208.1	autophagy-related protein 3	x
Nbv6.1trA177743	auxin-binding protein abp19a-like	AT5G20630.1	germin 3	Mapoly0028s0003.1	Cpin, nutrient reservoir activity	
NbS00024548g0007.1	B cell receptor associated protein 31 containing protein	AT5G42570.1	B-cell receptor-associated 31-like protein	Mapoly0006s0178.1	BCR-associated protein, BAP	
NbS00023298g0013.1	beta ketoacyl reductase 1	AT1G67730.1	beta-ketoacyl reductase 1	Mapoly0014s0112.1	17 beta-hydroxysteroid	
Nbv6.1trA11249	bifunctional l-3-cyanoalanine synthase cysteine synthase mitochondrial	AT3G61440.1	cysteine synthase C1	Mapoly0008s0245.1	cysteine synthase	
Nbv6.1trA1915	binding isoform 1	AT2G22125.1	binding protein	Mapoly0058s0070.1	beta catenin-related armadillo repeat-containing	
Nbv6.1trA147492	brefeldin a-inhibited guanine nucleotide-exchange protein 5	AT3G43300.3	HOPM interactor 7 (AtMIN7)	Mapoly0003s0171.4	guanine nucleotide-exchange factor	
Nbv6.1trA42882	caax prenyl protease 1 homolog	AT4G01320.1	Peptidase family M48 family protein	Mapoly0151s0045.1	Ste24 endopeptidase	
NbS00028901g0010.1	Calcium binding protein	AT5G08580.2	Calcium-binding EF hand protein	Mapoly0097s0037.1	EF-hand calcium-binding domain containing protein	

Nb	Nb protein ID	At	At protein ID	Mp	Mp protein ID	Int.
NbS00004134g0009.1	Calcium transporting ATPase 1	AT1G27770.4	autoinhibited Ca ²⁺ -ATPase 1	Mapoly0034s0113.1	calcium-transporting ATPase	
NbS00001483g0005.1	Calcium transporting ATPase endoplasmic reticulum type	AT4G09900.2	ER-type Ca ²⁺ -ATPase	Mapoly0013s0119.3	calcium-transporting ATPase	
Nbv6.1trA12125	calcium-transporting atpase endoplasmic reticulum-type-like	AT1G07670.2	endomembrane-type CA-ATPase	Mapoly0013s0119.3	calcium-transporting ATPase	
Nbv6.1trA98659 Nbv6.1trA128302	calnexin homolog	AT5G61790.1	calnexin 1	Mapoly0114s0016.1	calnexin	
Nbv6.1trA5196 NbS00006116g0019.1 Nbv6.1trP22723	catalase isozyme 1	AT4G35090.1	catalase 2	Mapoly0125s0005.1	catalase	x
NbC26208175g0003.1	Cathepsin B cysteine proteinase	AT1G47128.1	Granulin repeat cystein protease family protein (RD21)	Mapoly0083s0026.1	cysteine protease family C1-related	
NbS00007177g0022.1	CDK5 regulatory subunit associated protein 3	AT5G06830.1	hypothetical protein	Mapoly0080s0041.1	CDK5 regulatory subunit-associated protein 3	x
Nbv6.1trA1845	cell division cycle protein 48 homolog	AT5G03340.1	ATPase 2C AAA-type 2C CDC48 protein	Mapoly0096s0020.2	transitional endoplasmic reticulum ATPase	x
Nbv6.1trA114043	cell division protein homolog 2-chloroplastic-like	AT3G52750.3	Tubulin/FtsZ family protein	Mapoly0048s0025.1	cell division protein FtsZ-related	
Nbv6.1trA30804	cell division protein homolog chloroplastic-like	AT5G55280.1	homolog of bacterial cytokinesis Z-ring protein	Mapoly0029s0085.1	cell division protein FtsZ	
Nbv6.1trA68003	cellulose synthase a catalytic subunit 1	AT4G32410.1	cellulose synthase	Mapoly0076s0014.1	cellulose synthase (UDP-forming)	
Nbv6.1trP75893	cellulose synthase a catalytic subunit 2	AT5G64740.1	cellulose synthase 6	Mapoly0076s0014.1	cellulose synthase (UDP-forming)	x
Nbv6.1trA108645	cellulose synthase a catalytic subunit 3	AT5G05170.1	cellulose synthase	Mapoly0076s0014.1	cellulose synthase (UDP-forming)	
NbS00027305g0008.1	Chlorophyll a b binding protein 6A chloroplastic	AT3G08940.2	light harvesting complex photosystem II	Mapoly0001s0025.1	light-harvesting complex II chlorophyll a/b binding protein 4	x
Nbv6.1trA188376	chloroplast stem-loop binding protein of 41 kda chloroplastic	AT1G09340.1	chloroplast RNA binding protein	Mapoly0014s0058.1	NAD dependent epimerase/dehydratase	
NbS00002272g0002.1	cinnamate 4 hydroxylase	AT2G30490.1	cinnamate-4-hydroxylase	Mapoly0163s0018.1	trans-cinnamate 4-monooxygenase	
Nbv6.1trA109294	clathrin light chain 1-like	AT2G20760.1	clathrin light chain protein	Mapoly0075s0069.1	clathrin light chain	
NbS00052354g0005.1	Cleft lip and palate associated transmembrane protein	AT5G08500.1	Transmembrane CLPIM1 family protein	Mapoly0020s0073.1	cleft lip and palate associated transmembrane protein-related	
Nbv6.1trP45587	clustered mitochondria protein homolog isoform x1	AT1G01320.3	tetratricopeptide repeat (TPR)-like superfamily protein	Mapoly0060s0041.2	eukaryotic translation initiation factor 3	x
NbS00036341g0012.1	Coatomer protein epsilon subunit	AT1G30630.1	Coatomer epsilon subunit	Mapoly0002s0056.1	coatomer subunit epsilon	x
Nbv6.1trA203551	coatomer subunit alpha-1-like	AT1G62020.1	Coatomer 2c alpha subunit	Mapoly0007s0005.1	coatomer protein complex	x

Nb	Nb protein ID	At	At protein ID	Mp	Mp protein ID	Int.
Nbv6.1trA235897 Nbv6.1trP19534 Nbv6.1trP52462	coatomer subunit alpha-1-like	AT1G62020.1	Coatomer 2c alpha subunit	Mapoly0007s0005.1	coatomer protein complex	
Nbv6.1trA203775 Nbv6.1trA57793	coatomer subunit beta-2-like	AT1G52360.4	coatomer 2c beta subunit	Mapoly0022s0125.2	coatomer beta subunit	x
Nbv6.1trA70802	coatomer subunit beta-1-like	AT4G31480.9	coatomer 2C beta subunit	Mapoly0086s0049.1	coatomer subunit beta	x
Nbv6.1trA212907	coatomer subunit gamma	AT4G34450.1	coatomer gamma-2 subunit	Mapoly0005s0083.1	coatomer subunit gamma	x
Nbv6.1trA11495	cobw domain-containing protein 1	AT1G80480.1	plastid transcriptionally active 17	Mapoly0005s0038.1	PRLI-interacting factor L	
NbS00028772g0004.1	Cyclin delta 3	AT4G34090.1	cyclin delta-3	Mapoly0032s0004.1	unknown	
Nbv6.1trA48437	cysteine desulfurase chloroplastic	AT1G08490.1	chloroplastic NIFS-like cysteine desulfurase	Mapoly0010s0063.1	Selenocysteine lyase	
Nbv6.1trA11488	cysteine desulfurase mitochondrial	AT5G65720.3	nitrogen fixation S (NIFS)-like 1	Mapoly0184s0007.1	cysteine desulfurase	
Nbv6.1trA108027 Nbv6.1trA199742	cysteine protease atg4-like	AT2G44140.3	peptidase family C54 protein (ATG4A)	Mapoly0153s0038.1	autophagy-related protein 4	x
NbS00047751g0012.1	Cytochrome b5	AT2G32720.1	cytochrome B5 isoform B	Mapoly0153s0010.1	cytochrome b5	
NbS00007170g0004.1	Cytochrome P450	AT4G36220.1	ferulic acid 5-hydroxylase 1	Mapoly0109s0053.1	cytochrome P450 CYP2 subfamily	
NbS00016582g0009.1	Cytochrome P450	AT3G14690.1	cytochrome P450 2C family	Mapoly0052s0003.1	cytochrome P450 CYP4/CYP19/CYP26 subfamilies	
Nbv6.1trA125819	cytochrome p450 98a2-like	AT2G40890.1	cytochrome P450 2C family	Mapoly0037s0087.1	coumaroylquinate(coumaroylshikimate) 3-monoxygenase	
Nbv6.1trP32614	delta-1-pyrroline-5-carboxylate synthase-like	AT3G55610.1	delta 1-pyrroline-5-carboxylate synthase	Mapoly0102s0016.2	glutamate-5-semialdehyde dehydrogenase	
Nbv6.1trA6306	dna repair atpase-related family protein	AT4G31340.1	myosin heavy chain-like protein	Mapoly0004s0241.1	unknown	
Nbv6.1trP38618	dnaj homolog mitochondrial-like	AT2G22360.1	DNAJ heat shock family protein	Mapoly0020s0120.1	molecular chaperone DnaJ	
NbS00005851g0011.1 Nbv6.1trA74221	Dolichyl diphosphooligosaccharide protein glycosyltransferase subunit 2	AT4G21150.3	ribophorin II (RPN2) family protein	Mapoly0028s0115.1	ribophorin II	
Nbv6.1trP47320 Nbv6.1trA113800	dolichyl-diphosphooligosaccharide-protein glycosyltransferase 48 kda subunit	AT5G66680.1	dolichyl-diphosphooligosaccharide-protein glycosyltransferase	Mapoly0103s0006.1	oligosaccharyltransferase complex subunit beta	
Nbv6.1trP74340	dolichyl-diphosphooligosaccharide-protein glycosyltransferase subunit 1a	AT1G76400.1	Ribophorin I	Mapoly0008s0275.1	oligosaccharyltransferase complex subunit alpha	
Nbv6.1trP17332	dolichyl-diphosphooligosaccharide-protein glycosyltransferase subunit 1b	AT2G01720.1	Ribophorin I	Mapoly0008s0275.1	oligosaccharyltransferase complex subunit alpha	

Nb	Nb protein ID	At	At protein ID	Mp	Mp protein ID	Int.
Nbv6.1trA55014	e3 ubiquitin-protein ligase keg isoform x1	AT5G13530.1	protein kinase ubiquitin-protein ligase (KEG)	Mapoly0002s0111.2	protein kinase domain	
Nbv6.1trP4945	e3 ubiquitin-protein ligase upl2-like	AT1G55860.1	LOW protein: E3 ubiquitin ligase-like protein	Mapoly0090s0059.1	E3 ubiquitin-protein ligase HUWE1	
Nbv6.1trP41060	e3 ufm1-protein ligase 1 homolog	AT3G46220.1	E3 UFM1-protein ligase-like protein	Mapoly0007s0143.1	uncharacterized conserved protein	x
Nbv6.1trA130325	elongation factor 1-gamma 2-like isoform x2	AT1G09640.1	translation elongation factor EF1B 2C gamma chain	Mapoly0062s0115.1	elongation factor 1-gamma	
Nbv6.1trP48914 Nbv6.1trA38007	elongation factor mitochondrial	AT4G02930.1	GTP binding Elongation factor Tu	Mapoly0153s0015.1	translation factor	
Nbv6.1trA113674	er membrane protein complex subunit 10	AT1G65270.3	ER membrane protein complex subunit-like protein	Mapoly0069s0067.1	uncharacterized conserved protein	
Nbv6.1trP50123	er membrane protein complex subunit 8 9 homolog	AT5G55940.1	Uncharacterized protein family	Mapoly0118s0025.1	uncharacterized conserved protein encoded by sequence overlapping the COX4 gene	
Nbv6.1trA35837	erlin-2-b	AT2G03510.1	SPFH/Band 7/PHB domain-containing membrane-associated	Mapoly0041s0056.2	prohibitin-related membrane protease subunits	
Nbv6.1trA86334	ethylene-insensitive protein 2	AT5G03280.1	NRAMP metal ion transporter family protein	Mapoly0001s0226.1	ethylene-insensitive protein 2	
NbS00038062g0006.1	Eukaryotic translation initiation factor 3 subunit 4	AT3G11400.1	eukaryotic translation initiation factor 3G1	Mapoly0059s0037.1	translation initiation factor 3 subunit G	
Nbv6.1trA45700	eukaryotic translation initiation factor 3 subunit i-like	AT2G46290.1	Transducin/WVD40 repeat-like superfamily protein	Mapoly0109s0034.1	translation initiation factor 3 subunit I	
NbS00032531g0004.1 Nbv6.1trA239564	Eukaryotic translation initiation factor 3 subunit J	AT1G66070.2	Translation initiation factor eIF3 subunit	Mapoly0038s0048.3	translation initiation factor 3 subunit J	x
NbS00008738g0001.1	Fatty acid elongase 3 ketoacyl CoA synthase	AT1G07720.2	3-ketoacyl-CoA synthase	Mapoly0055s0025.1	FAE1/ Type III polyketide synthase-like protein	
Nbv6.1trA95890	fc-s cluster assembly factor chloroplastic isoform x1	AT3G24430.1	ATP binding protein	Mapoly0100s0060.1	nucleotide-binding protein NBP35 (yeast)-related	
Nbv6.1trA125626	ferredoxin--nadp leaf chloroplastic	AT1G20020.1	ferredoxin-NADP[+]-oxidoreductase 2	Mapoly0062s0041.1	flavodoxin-related	x
NbS00028584g0008.1	FG GAP repeat containing protein	AT3G51050.1	FG-GAP repeat-containing protein	Mapoly0159s0016.1	unknown	
NbS00036753g0005.1	Fructokinase protein 1	AT3G54090.1	fructokinase-like 1	Mapoly0051s0110.1	sugare kinase	
Nbv6.1trA1421	fructose-bisphosphate aldolase chloroplastic-like	AT4G38970.1	fructose-bisphosphate aldolase 2	Mapoly0053s0082.1	fructose-bisphosphate aldolase	x
NbS00021088g0005.1	Glucose 1 phosphate adenyltransferase small subunit chloroplastic/amyoplastic	AT5G48300.1	ADP glucose pyrophosphorylase	Mapoly0033s0108.1	sugar-1-phosphate guanyl transferase	

Nb	Nb protein ID	At	At protein ID	Mp	Mp protein ID	Int.
Nbv6.1trA261159	glucose-1-phosphate adenylyltransferase large subunit chloroplastic amyloplastic	AT5G19220.1	ADP glucose pyrophosphorylase large subunit	Mapoly0101s0020.1	glucose-1-phosphate adenylyltransferase	
NbS00040601g0015.1	Glycerol 3 phosphate acyltransferase 4	AT1G01610.1	glycerol-3-phosphate acyltransferase 4	Mapoly0046s0032.1	glycerol-3-phosphate acyltransferase	
Nbv6.1trP39071	glycerol-3-phosphate acyltransferase 3	AT5G60620.1	glycerol-3-phosphate acyltransferase 9	Mapoly0113s0056.1	glycerol-3-phosphate O-acyltransferase 3/4	
Nbv6.1trP5121	glycine-tRNA ligase chloroplastic mitochondrial isoform x1	AT3G48110.1	glycine-tRNA ligase	Mapoly0186s0003.1	glycyl-tRNA synthetase	
Nbv6.1trA51581	gram domain-containing protein 1a	AT1G02120.1	GRAM domain family protein	Mapoly0083s0023.1	Uncharacterized conserved protein	
NbS00031957g0003.1	Hydrolase alpha/beta fold	AT2G36290.1	alpha/beta-Hydrolases superfamily protein	Mapoly0005s0202.1	alpha/beta hydrolase fold-containing protein	
Nbv6.1trA78626	importin-9	AT1G26170.1	ARM repeat superfamily protein	Mapoly0176s0015.1	importin 9	
NbS00017142g0001.1	Isocitrate dehydrogenase	AT5G03290.1	isocitrate dehydrogenase V	Mapoly0002s0215.1	isocitrate dehydrogenase	x
Nbv6.1trP4964	isoflavone 2 - hydroxylase-like	AT4G37370.1	cytochrome P450 2C family	Mapoly0025s0014.1	flavonoid 3' monooxygenase	
NbS00025777g0007.1	Kinase	AT4G29380.1	VPS15	Mapoly0002s0158.1	phosphoinositide-3-kinase, regulatory subunit4	x
Nbv6.1trP30916	lecithin-cholesterol acyltransferase-like 4	AT4G19860.1	alpha/beta-Hydrolases superfamily protein	Mapoly0131s0029.1	lecithine cholesterol acyltransferase-related	
NbS00002437g0006.1 Nbv6.1trA226360 Nbv6.1trP76357	leucine-rich repeat-containing protein ddb_g0290503	AT2G32240.1	early endosome antigen	Mapoly0001s0335.1	E3 ubiquitin ligase involved in syntaxin degradation	x
Nbv6.1trP764	long chain acyl-synthetase 1	AT2G47240.3	AMP-dependent synthetase and ligase family protein	Mapoly0099s0012.1	Long-chain-fatty-acid-CoA ligase	
Nbv6.1trA184467	long chain acyl-synthetase 4	AT4G23850.1	AMP-dependent synthetase and ligase family protein	Mapoly0099s0012.1	long-chain-fatty-acid COA ligase	
NbS00019858g0012.1	Long chain fatty acid CoA ligase 3	AT2G04350.2	AMP-dependent synthetase and ligase family protein	Mapoly0002s0259.1	acyl-CoA synthetase	
Nbv6.1trA201272	low-temperature-induced cysteine proteinase-like	AT5G43060.1	Granulin repeat cystein protease family protein	Mapoly0083s0026.1	cysteine protease family C1-related	x
Nbv6.1trP19733	lysophospholipid acyltransferase 1-like	AT1G12640.1	MBOAT (membrane bound O-acyl transferase) family	Mapoly0004s0125.1	porcupine	
NbS00024469g0004.1 Nbv6.1trA199873	MADS box interactor/ rrp15-like protein	AT1G44770.1	elongation factor	Mapoly0023s0095.2	unknown	x
Nbv6.1trA188547	mag2-interacting protein 2	AT5G24350.3	neuroblastoma-amplified sequence protein	Mapoly0143s0007.1	secretory pathway protein Sec39	x
Nbv6.1trA1123	magnesium-protoporphyrin ix monomethyl ester	AT3G56940.1	dicarboxylate diiron protein 2C	Mapoly0124s0017.1	magnesium-protoporphyrin IX monomethyl ester cyclase	
Nbv6.1trA216541	mannose-1-phosphate guanyltransferase alpha-b-like	AT1G74910.2	ADP-glucose pyrophosphorylase family protein	Mapoly0163s0013.4	SUGAR-1-PHOSPHATE GUANYL TRANSFERASE	

Nb	Nb protein ID	At	At protein ID	Mp	Mp protein ID	Int.
Nbv6.1trP58673	mannose-1-phosphate guanylyltransferase 1	AT2G39770.3	Glucose-1-phosphate adenylyltransferase family protein	Mapoly0034s0043.1	mannose-1-phosphate guanylyltransferase	
Nbv6.1trA45428	mannosyl-oligosaccharide glucosidase gcs1-like	AT1G67490.1	glucosidase 1	Mapoly0071s0095.1	mannosyl-oligosaccharide glucosidase	
Nbv6.1trP2377	mannosylglycoprotein endo-beta-mannosidase	AT1G09010.1	glycoside hydrolase family 2 protein	Mapoly0034s0073.1	beta-galactosidase	x
Nbv6.1trA227595 Nbv6.1trP74344	mitochondrial outer membrane protein porin of 36 kda	AT3G01280.1	voltage dependent anion channel 1	Mapoly0001s0240.1	voltage-dependent anion channel protein 1	
NbS00004550g0007.1	Myosin XI	AT5G20490.2	myosin family protein with Dil	Mapoly0012s0190.1	myosin	x
Nbv6.1trA64146	myosin-12 isoform x2	AT2G31900.4	myosin-like protein XIF	Mapoly0012s0190.1	myosin	x
Nbv6.1trA24849	myosin-binding protein 1	AT1G08800.4	myosin-binding protein	Mapoly0056s0058.8	zein-binding	x
Nbv6.1trA264276	nadh--cytochrome b5 reductase 1	AT5G17770.1	NADH:cytochrome B5 reductase	Mapoly0013s0176.1	cytochrome-b5 reductase	
NbS00017213g0030.1	NADP dependent D sorbitol 6 phosphate dehydrogenase	AT2G21250.1	NAD (P)-linked oxidoreductase superfamily protein	Mapoly0086s0056.3	aldose-6-phosphate reductase	x
Nbv6.1trA211118 Nbv6.1trP59491	nadh--cytochrome p450 reductase	AT4G24520.1	P450 reductase	Mapoly0159s0022.1	NADPH-hemoprotein reductase	
NbS00005969g0104.1	NbS00005969g0104.1	AT1G02560.1	nuclear encoded CLP protease 5	Mapoly0055s0124.1	ATP-dependent CLP protease proteolytic subunit	
NbS00007615g0209.1	NbS00007615g0209.1	AT2G39770.3	glucose-1-phosphate adenylyltransferase family protein	Mapoly0034s0043.1	mannose-1-phosphate guanylyltransferase	
NbS00008760g0210.1	NbS00008760g0210.1	AT2G34480.2	Ribosomal protein L18ae/LX family protein	Mapoly0001s0112.1	large subunit ribosomal protein L18Ae	
NbS00010886g0114.1	NbS00010886g0114.1	AT3G20560.1	PDI-like 5-3	Mapoly0033s0073.1	thioredoxin-related	
NbS00021769g0023.1	Nicalin	AT3G44330.1	M28 Zn-peptidase nicastrin	Mapoly0185s0020.1	predicted aminopeptidases - M20/M25/M40 family	
Nbv6.1trA59280 Nbv6.1trA59274	nodal modulator 1	AT3G62360.2	Carbohydrate-binding-like fold	Mapoly0002s0320.1	carboxypeptidase regulatory region-containing	
NbS00030615g0019.1	Oligosaccharyl transferase SIT3 subunit	AT1G34130.1	staurosporin and temperature sensitive 3-like B	Mapoly0130s0037.1	oligosaccharyl transferase	
NbS00046616g0009.1	Oligosaccharyl transferase SIT3 subunit	AT5G19690.1	staurosporin and temperature sensitive 3-like A	Mapoly0108s0026.1	oligosaccharyl transferase	
NbS00011570g0012.1	P loop containing nucleoside triphosphate hydrolases	AT1G33970.5	P-loop containing nucleoside triphosphate hydrolase	Mapoly0063s0085.1	GTPase, IMPA family member-related	x
Nbv6.1trA203942 Nbv6.1trP21997	pdr-type acb transporter	AT1G15520.1	pleiotropic drug resistance 12	Mapoly0021s0156.2	ATP-binding cassette transporter	
Nbv6.1trA131517	pentatricopeptide repeat superfamily isoform 1	AT3G49140.1	Pentatricopeptide repeat (PPR) superfamily protein	Mapoly0002s0015.1	CREG1 protein	x

Nb	Nb protein ID	At	At protein ID	Mp	Mp protein ID	Int.
Nbv6.1trA393	pentatricopeptide repeat-containing protein chloroplastic	nexin.1	pentatricopeptide repeat (PPR) superfamily protein	Mapoly0036s0094.1	PPR repeat family	
NbS00046742g0003.1	Phospho 2 dehydro 3 deoxyheptonate aldolase 2 chloroplastic	AT4G39980.1	3-deoxy-D-arabino-heptulosonate 7-phosphate synthase	Mapoly0008s0188.1	3-deoxy-7-phosphoheptulonate synthase	
Nbv6.1trP4906	photosystem i p700 apoprotein a2	ATCG00340.1	Photosystem I 2C PsaA/PsaB protein	Mapoly0043s0109.1	photosystem II P700 chlorophyll a apoprotein A2	
Nbv6.1trA254975	photosystem i reaction center subunit chloroplastic	AT1G31330.1	photosystem I subunit F	Mapoly0075s0057.1	photosystem I subunit III	x
Nbv6.1trP4567	photosystem ii cp43 chlorophyll partial	ATCG00280.1	photosystem II reactoin center protein C	none	NA	
Nbv6.1trA87986	photosystem ii protein d1	AT1G71810.1	Protein kinase superfamily protein	Mapoly0121s0049.1	CHAPERONE-ACTIVITY OF BC1 COMPLEX (CABC1)-RELATED	
Nbv6.1trP59901	photosystem ii protein d1	ATCG00020.1	photosystem II reaction center protein A	Mapoly0093s0016.1	photosystem II P680 reaction centre protein	
Nbv6.1trP45067	photosystem ii protein d2	ATCG00270.1	photosystem II reaction center protein D	Mapoly0093s0016.1	photosystem II P680 reaction centre protein	
NbS00005958g0009.1	plastid transcriptionally active 12	AT2G34640.1	plastid transcriptionally active 12	Mapoly0061s0053.1	unknown	
NbS00010425g0009.1	plastid transcriptionally active 5	AT4G13670.1	plastid transcriptionally active 5	Mapoly0004s0042.1	putative peptidoglycan binding domain	x
Nbv6.1trA6871	pra1 family protein f2-like	AT1G55190.1	PRA1 (prenylated rab acceptor) family protein	Mapoly0065s0006.1	prenylated rab acceptor 1	
Nbv6.1trP4996	premnaspirodiene oxygenase-like	AT3G26310.1	cytochrome P450 2C family	Mapoly0025s0014.1	flavonoid 3' monooxygenase	
NbS00018433g0002.1	Prenylated rab acceptor PRA1	AT2G38360.1	prenylated RAB acceptor 1.B4	Mapoly0065s0006.1	prenylated rab acceptor 1	
Nbv6.1trA203605	probable -trehalose-phosphate synthase	AT1G06410.3	trehalose-phosphatase/synthase 7	Mapoly0128s0020.1	trehalose-phosphatase	
Nbv6.1trP16938	probable 1-deoxy-d-xylulose-5-phosphate chloroplastic	AT4G15560.1	Deoxyxylulose-5-phosphate synthase	Mapoly0015s0196.1	1-deoxy-D-xylulose-5-phosphate synthase	
Nbv6.1trA8540	probable manganese-transporting atpase pdr2	AT5G23630.1	phosphate deficiency response 2	Mapoly0002s0327.1	ATPase	
Nbv6.1trA56860	probable methionine--trna ligase	AT4G13780.1	methionine-tRNA ligase 2C putative	Mapoly0045s0011.1	methionine-tRNA ligase	x
Nbv6.1trP1387	probable mitochondrial chaperone bcs1-b	AT3G50930.1	cytochrome BC1 synthesis	Mapoly0165s0017.1	BCS1 AAA-type ATPase	
Nbv6.1trA22057	probable ribose-5-phosphate isomerase chloroplastic	AT5G44520.2	NagB/RpiA/CoA transferase-like superfamily protein	Mapoly0213s0005.1	ribose-5-phosphate isomerase	x
Nbv6.1trP51466	probable threonine--trna cytoplasmic	AT2G04842.2	threonyl-tRNA synthetase 2C	Mapoly0096s0034.2	Threonine-tRNA ligase	
Nbv6.1trA100080	probable uncharacterized protein At5g49945-like	AT4G24330.1	hypothetical protein (DUF1682)	Mapoly0037s0012.1	adipocyte-specific protein 4-related	
Nbv6.1trP34674	probable uncharacterized protein LOC104216996	AT4G16180.2	transmembrane protein	Mapoly0066s0100.1	unknown	
Nbv6.1trP16911	protein argonaute 4-like	AT2G27040.2	Argonaute family protein	Mapoly0065s0059.1	eukaryotic translation initiation factor 2c	

Nb	Nb protein ID	At	At protein ID	Mp	Mp protein ID	Int.
NbS00006168g0008.1	Protein ASPARTIC PROTEASE IN GUARD CELL 2	AT1G01300.1	Eukaryotic aspartyl protease family protein	Mapoly0271s0001.1	aspartyl protease	
Nbv6.1trP16940	protein root hair defective 3-like	AT3G13870.1	root hair defective 3 GTP-binding protein	Mapoly0153s0041.1	MSS1/ TRME-related GTP-binding protein	
Nbv6.1trP48508 Nbv6.1trA1393	protein tic chloroplastic	AT3G46780.1	plastid transcriptionally active 16	Mapoly0154s0018.1	nitrogen metabolic regulation protein	x
NbS00009984g0010.1	Protein transport protein sec31	AT3G63460.1	transducin/WD40 repeat-like superfamily protein	Mapoly0156s0008.1	protein transport protein SEC31	
Nbv6.1trP32384	protein transport protein sec61 subunit alpha-like	AT2G34250.3	SecY protein transport family protein	Mapoly0026s0118.1	protein transport protein SEC61 subunit alpha	
Nbv6.1trA200682	protochlorophyllide reductase-like	AT5G54190.1	protochlorophyllide oxidoreductase A	Mapoly0030s0118.2	protochlorophyllide reductase	
Nbv6.1trP30388	proton pump-interactor 1-like	AT4G27500.2	proton pump interactor 1	Mapoly0003s0069.1	unknown	
Nbv6.1trP50802	protoporphyrinogen oxidase chloroplastic	AT4G01690.1	Flavin containing amine oxidoreductase family	Mapoly0001s0469.1	protoporphyrinogen oxidase	
Nbv6.1trP41948	psbp domain-containing protein chloroplastic	AT3G56650.1	thylakoid luminal protein (Mog1/PsbP/DUF179 5-like photosystem II reaction center PsbP family protein)	Mapoly0008s0145.1	PsbP	
Nbv6.1trA221327	pyruvate cytosolic isozyme	AT5G08570.3	pyruvate kinase family protein	Mapoly0023s0129.2	pyruvate kinase	
Nbv6.1trA191817	pyruvate cytosolic isozyme-like	AT3G52990.1	pyruvate kinase family protein	Mapoly0074s0068.3	pyruvate kinase	
Nbv6.1trA86604 Nbv6.1trA242429	rab11 family-interacting protein 3 isoform x1	AT4G02880.2	ELKS/Rab6-interacting/CAST family protein	Mapoly0005s0053.1	unknown	x
Nbv6.1trA93034	rab11 family-interacting protein 3 isoform x1	AT1G62020.1	ELKS/Rab6-interacting/CAST family protein	Mapoly0005s0053.1	unknown	x
Nbv6.1trP13425	rab11 family-interacting protein 3 isoform x1	AT4G02880.1	ELKS/Rab6-interacting/CAST family protein	Mapoly0005s0053.1	unknown	x
Nbv6.1trA74626 Nbv6.1trA125101	ras-related protein rabe1c-like	AT5G59840.1	Ras-related small GTP-binding family protein	Mapoly0116s0012.1	GTP-binding protein SEC4	
NbS00003909g0012.1	Reticulon	AT2G46170.1	reticulon family protein	Mapoly0035s0106.2	reticulon-related (plant)	
NbS00028552g0005.1	Rhodanese related sulfurtransferase	AT4G01050.1	thylakoid rhodanese-like protein	Mapoly0027s0106.1	chitinase	
NbS00050038g0007.1	Ribosomal protein L10	AT1G26910.1	Ribosomal protein L16p/L10e family protein	Mapoly0020s0158.1	large subunit ribosomal protein L10e	
NbS00049696g0008.1	Ribosomal protein L15	AT4G16720.1	ribosomal protein L23/L15e family protein	Mapoly0043s0043.1	large subunit ribosomal protein L15e	
NbS00013932g0015.1 NbS00021061g0110.1	Ribosomal protein L18	AT3G05590.1	ribosomal protein L18	Mapoly0118s0037.1	large subunit ribosomal protein L18e	x
Nbv6.1trP58182	ribosomal protein L2	ATCG01310.1	ribosomal protein L2	Mapoly0099s0059.1	50s ribosomal protein L2	x
NbS00002504g0003.1	Ribosomal protein L30	AT1G36240.1	ribosomal protein L7Ae/L30e/S12e/gad d45 family protein	Mapoly0099s0042.1	large subunit ribosomal protein L30e	x
NbS00053639g0015.1	Ribosomal protein L32	AT4G18100.1	ribosomal protein L32e	Mapoly0003s0256.1	large subunit ribosomal protein L23e	x

Nb	Nb protein ID	At	At protein ID	Mp	Mp protein ID	Int.
Nbv6.1trP75120	ribosomal protein s3	ATCG00800.1	structural constituent of ribosome	Mapoly0015s0207.1	small subunit ribosomal protein S3	x
Nbv6.1trP15300	rna polymerase alpha subunit	ATCG00740.1	RNA polymerase subunit alpha	Mapoly0026s0099.1	DNA-directed RNA polymerase subunit alpha	
Nbv6.1trP44911	rna polymerase beta subunit	ATCG00190.1	RNA polymerase subunit beta	Mapoly0091s0005.1	DNA-directed RNA polymerase subunit beta	
Nbv6.1trA206109	ru large subunit-binding protein subunit chloroplastic	AT3G13470.1	TCP-1/cpn60 chaperonin family protein	Mapoly0001s0499.1	rubisco subunit binding-protein beta subunit	
Nbv6.1trA120596 Nbv6.1trA195533	serine threonine-protein phosphatase 2a 65 kda regulatory subunit a beta isoform	AT3G25800.3	protein phosphatase 2A subunit A2	Mapoly0107s0027.1	serine/threonine-protein phosphatase 2A regulatory subunit A	
Nbv6.1trA143338	sh3 domain-containing protein	AT1G29800.1	RING/FYVE/PHD-type zinc finger family protein	Mapoly0037s0060.2	SH3YL1 protein	
Nbv6.1trP13185	sh3 domain-containing protein isoform 3	AT2G07360.1	SH3 domain-containing protein	Mapoly0015s0202.1	formin binding protein and related proteins	
NbS00016433g0002.1	Squalene synthase	AT4G34640.1	squalene synthase	Mapoly0098s0008.1	squalene synthase	
Nbv6.1trA1373	strictosidine synthase 3	AT1G08470.1	strictosidine synthase-like 3	Mapoly0164s0010.1	strictosidine synthase-related	
NbS00048356g0005.1	T complex protein 1 subunit alpha	AT3G20050.1	T-complex protein alpha subunit	NbS00048356g0005.1	chaperonin complex, TCP-1 alpha subunit (CCT1)	
Nbv6.1trA63517 Nbv6.1trP17352	tbc1 domain family member 15-like	AT5G52580.1	RabGAP/TBC domain-containing protein	Mapoly0045s0037.2	TBC1 domain family member 15	x
Nbv6.1trA164394	thioredoxin family protein isoform 2	AT5G03880.1	Thioredoxin family protein	Mapoly0060s0005.1	glutathione s-transferase, GST	
Nbv6.1trP45557	threonine--trna mitochondrial	AT5G26830.1	Threonyl-tRNA synthetase	Mapoly0065s0074.1	threonine-tRNA ligase	
Nbv6.1trA272945	trab domain-containing protein	AT1G05270.1	TraB family protein	Mapoly0043s0066.1	gb def. hypothetical protein At2g32340	
Nbv6.1trA82735	trafficking protein particle complex subunit 10 isoform x1	AT5G54440.1	CLUB	Mapoly0031s0138.1	epilepsy holoprosencephaly candidate 1/ TMEM1	
Nbv6.1trA267408	transducin wd40 repeat-like superfamily protein isoform 2	AT3G50590.2	transducin/WD40 repeat-like superfamily protein	Mapoly0038s0024.1	autophagy protein 16-like	
Nbv6.1trA1924	translational activator gcn1	AT1G64790.1	ILITYHIA (ILV)	Mapoly0135s0025.1	translational activator GCN1-related	
NbS00002458g0031.1	Translocation protein SEC63	AT1G79940.3	DnaJ/ Sec63 Br1 domain-containing protein	Mapoly0090s0076.1	translocation protein SEC63	
Nbv6.1trP21340	translocon-associated protein subunit beta	AT5G14030.4	translocon-associated protein beta (TRAPB) family	Mapoly0091s0054.1	translocon-associated protein subunit beta	
Nbv6.1trP35974	transmembrane protein 120 homolog	AT4G10430.3	TMPPT-like protein	Mapoly0153s0034.3	transmembrane protein induced by tumor necrosis	
Nbv6.1trA261157 Nbv6.1trA164758	transmembrane protein 214	AT1G70770.2	transmembrane protein	Mapoly0031s0122.1	uncharacterized conserved protein	

Nb	Nb protein ID	At	At protein ID	Mp	Mp protein ID	Int.
Nbv6.1trP19476	transmembrane protein 33 homolog	AT3G02420.1	dihydroflavonol 4-reductase/flavanone protein	Mapoly0013s0171.1	uncharacterized protein family (UPF0121)	
NbS00030328g0010.1	Transportin 1	AT2G16950.2	transportin 1	NbS00030328g0010.1	transportin-1	
NbS00031715g0004.1	Ubiquitin modifier activating enzyme atg7	AT5G45900.1	ThiF family protein (ATG7)	Mapoly0015s0071.1	autophagy related protein 7	x
Nbv6.1trP13803	uncharacterized aarf domain-containing protein kinase chloroplastic	AT3G24190.1	protein kinase superfamily protein	Mapoly0134s0032.1	ABC1 family protein kinase	
Nbv6.1trA44984	uncharacterized membrane protein at1g75140-like	AT1G75140.1	membrane protein	Mapoly0094s0054.2	Sec31-related protein	
Nbv6.1trA85749	uncharacterized oxidoreductase chloroplastic	AT1G06690.1	NAD(P)-linked oxidoreductase superfamily protein	Mapoly0064s0050.1	aldo/keto reductase	
NbS00018339g0004.1 Nbv6.1trA33291	uncharacterized protein LOC100242119	AT3G57990.1	hypothetical protein	Mapoly0061s0112.1	unknown	x
Nbv6.1trA5666	upf0415 protein c7orf25 homolog	AT1G73380.1	hypothetical protein	Mapoly0114s0003.2	uncharacterized DUF1308	x
Nbv6.1trP54873	uroporphyrinogen decarboxylase	AT2G40490.1	Uroporphyrinogen decarboxylase	Mapoly0103s0078.1	METHYLTETRAHYDROFOLATE:HOMOCYSTEINE METHYLTRANSFERASE RELATED	
Nbv6.1trP70104	v-type proton atpase subunit b2	AT4G38510.5	ATPase 2C subunit B protein	Mapoly0093s0019.1	v-type H ⁺ -transporting ATPase subunit B	
NbS00008926g0010.1	Vacuolar protein sorting associated protein 4B	AT2G27600.1	AAA-type ATPase family protein	Mapoly0064s0038.1	vacuolar protein-sorting-associated protein 4	
Nbv6.1trA143295	vesicle-associated membrane protein 727	AT3G54300.3	vesicle-associated membrane protein 727 (VAMP727)	Mapoly0076s0053.1	vesicle-associated membrane protein 72	
NbS00050269g0002.1	WD 40 repeat protein	AT5G50230.1	Transducin/WD40 repeat-like superfamily protein	Mapoly0102s0055.1	Autophagy protein 16-like	x
NbS00000049g0010.1 Nbv6.1trP76606 Nbv6.1trA73825 Nbv6.1trP35998	web family protein chloroplastic-like	AT5G16730.1	weak chloroplast movement under blue light protein	Mapoly0004s0133.1	unknown	x
Nbv6.1trA215778	zeaxanthin epoxidase	AT5G67030.1	zeaxanthin epoxidase (ZEP) (ABA1)	Mapoly0028s0084.1	Zeaxanthin epoxidase	

Appendix V

Supplemental figures for Chapter 5: Evolutionary dynamics of the *Phytophthora* effector PexRD54 following a host jump.

		signal peptide	
<i>P. infestans</i> PexRD54	1	MR FQS I MMLT I T CAGTCLA EGLAP SDQAYRPTMT GLK SRLNDPRPL STAT I ATSSERFLRFDTV	64
<i>P. ipomoeae</i> PexRD54	1	MR FQS I MMLT I T CAGTCLA EGLAP SDQAYRPTMT GLK SRLNDPRPL STAT I ATSSERFLRFDTA	64
<i>P. mirabilis</i> PexRD54	1	MR FQS I MMLT I T CAGTCLA EGLAP SDQAYRPTMT GLK SRLNDPRPL STAT I ATSSERFLRFDTA	64
<i>P. infestans</i> PexRD54	65	AR DTAGNDEERVGP SWLAK V DGLMHKMTV SSLSA EEAQLK VVIQ SQ IHPREL FGV LSLGKRAAK	128
<i>P. ipomoeae</i> PexRD54	65	AR DTAGNDEERVGP SWL SKVDGLMHKMTV SSLSA EEAQLK VVIQ SQ IHPREL FGV LSLGKRAAK	128
<i>P. mirabilis</i> PexRD54	65	AR DTAGNDEERVGP SWL SKVDGLMHKMTV SSLSA EEAQLK VVIQ SQ IHPREL FGV LSLGKRAAK	128
<i>P. infestans</i> PexRD54	129	LDDNP D FVQWLR LVKDFRANNGNQAF SDDL I YLLKTN SPEQLK L LFETLRHTPGMTK I GASM	192
<i>P. ipomoeae</i> PexRD54	129	LDDNP D FVQWLR LVKDFRANNGNQAF SDDL I YLLKTN SPEQLK L LFETLRHTPGMTK I GASM	192
<i>P. mirabilis</i> PexRD54	129	LDDNP D FVQWLR LVKDFRANNGNQAF SDDL I YLLKTN SPEQLK L LFETLRHTPGMTK I GASM	192
<i>P. infestans</i> PexRD54	193	EK SLSGNW I RKA LEQDTYPT I VYNTLRLK DAGTKLDDT PMFRQWLE YVEKYWNKNAGA FFGDTQ	256
<i>P. ipomoeae</i> PexRD54	193	EK SLSGNW I RKA LEQDTYPT I VYNTLRLK DAGTKLDDT PMFRQWLE YVEKYWNKNAGA FFGDTQ	256
<i>P. mirabilis</i> PexRD54	193	EK SLSGNW I RKA LEQDTYPT I VYNTLRLK DAGTKLDDT PMFRQWLE YVEKYWNKNAGA FFGDTQ	256
<i>P. infestans</i> PexRD54	257	ML TLFQKTMT EEEDI I KLVHMLRN NPGMK SHADK LERY LLLT SESSHKT MADVWLKARETPEEV	320
<i>P. ipomoeae</i> PexRD54	257	ML TLFQKTMT EEEDI I KLVHMLRN NPGMK SHADK LERY LLLT SESSHKT MADVWLKARETPEEV	320
<i>P. mirabilis</i> PexRD54	257	ML TLFQKTMT EEEDI I KLVHMLRN NPGMK SHADK LERY LLLT SESSHKT MADVWLKARETPEEV	320
			AIM
<i>P. infestans</i> PexRD54	321	FR I LRLAEKQTAA ADDNRMLNLWLR YQT YRDK I DKNAFSDA EALQFFR KAKPLDFDWEI V	381
<i>P. ipomoeae</i> PexRD54	321	FR I LRLAEKQTAA ADDNRMLNLWLR YQT YRDK I DKNAFSDA EALQFFR KAKPLDFDWEI V	381
<i>P. mirabilis</i> PexRD54	321	FR I LRLAEKQTAVT DDPMLNLWLR YQT YRDK I DKNAFSDA EALQFFR KAKPLDFDWEI V	381

Figure A.5.1 Diversity of *Phytophthora* clade 1c PexRD54 sequences

Alignment of *Phytophthora* clade 1c PexRD54 sequences (MUSCLE (Edgar, 2004)) from *P. infestans* (strain T30-4), *P. ipomoeae* (strains P10225, P10226, P10227, P99167), *P. mirabilis* (strains P99114, P3005, P3006, P3007, P3008, P3010, P10229, P10230), visualized with Jalview. The PexRD54 sequence and structural motifs are designated.

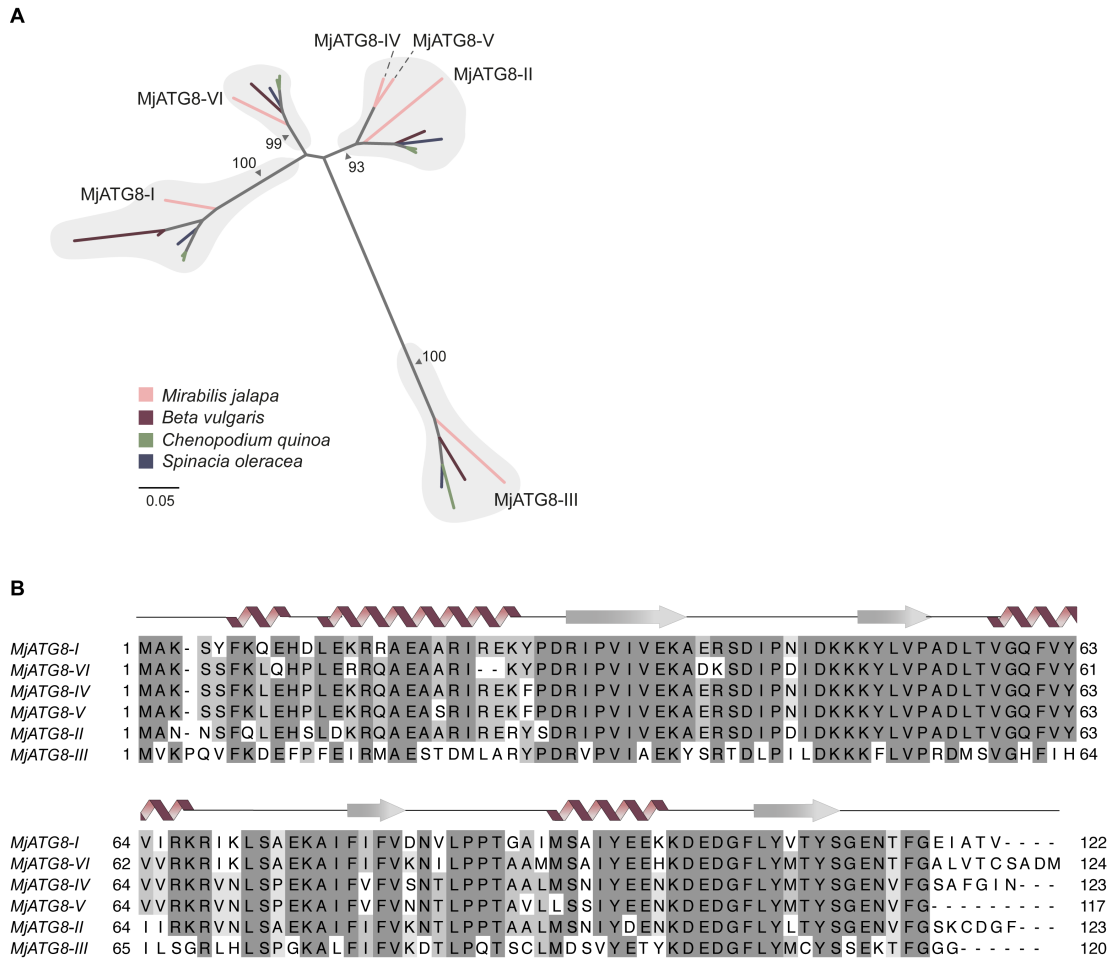


Figure A.5.2 Sequence diversity of *M. jalapa* ATG8s

(a) Orthologous relationships between Caryophyllales ATG8 isoforms. Unrooted maximum-likelihood phylogenetic tree of 22 ATG8 isoforms with gray shading highlighting clades, and colors indicated plant species. The tree was calculated in MEGA7 (Kumar et al., 2016) from a 375 nucleotide alignment (MUSCLE (Edgar, 2004), codon-based). The bootstrap supports of the major nodes are indicated. The scale bar indicates the evolutionary distance based on substitution rate. (b) Sequence diversity among *M. jalapa* ATG8 isoforms. Alignment of all *M. jalapa* ATG8s (MUSCLE (Edgar, 2004)), visualized with Jalview, with the protein model above corresponding to the StATG8-2.2 structure.

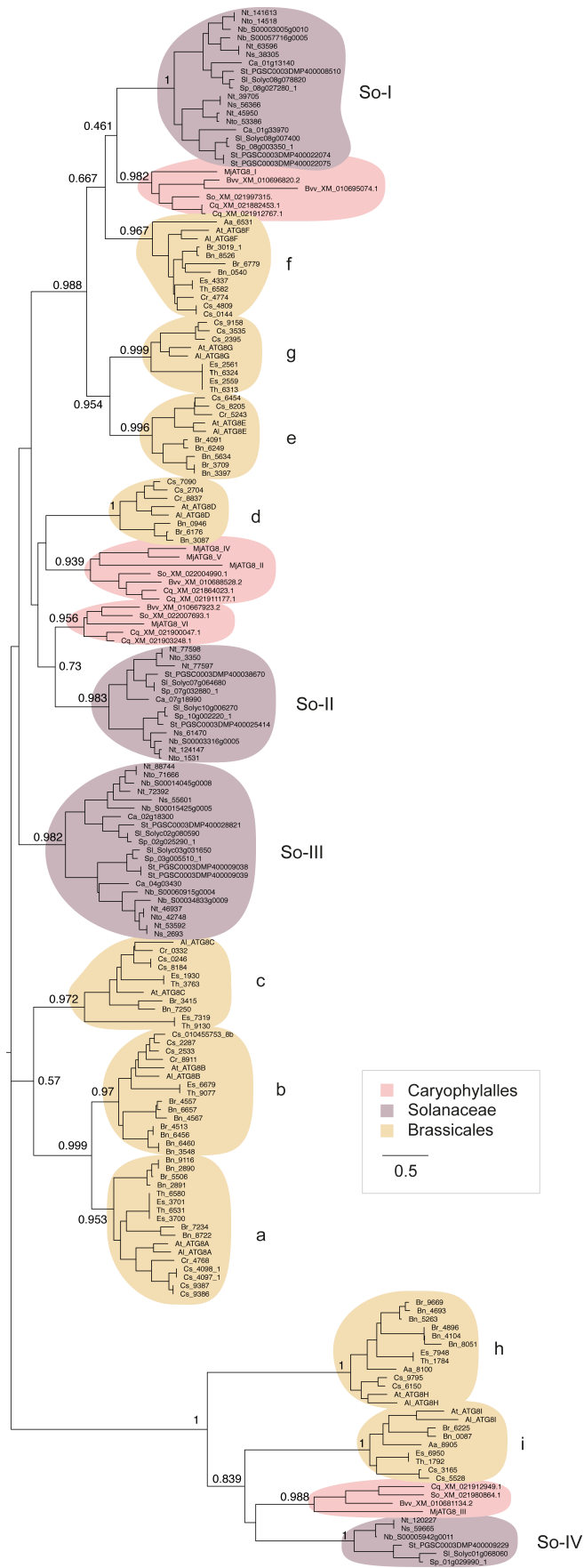


Figure A.5.3 *Mirabilis jalapa* ATG8s are not orthologous to ATG8s from other plant taxa

Phylogenetic relationship between ATG8s from the Caryophyllales, Solanales, and Brassicales. Unrooted maximum-likelihood tree of 186 ATG8 isoforms, with clades marked and colored as in **Fig 5.3**. The tree was calculated in MEGA7 (Kumar et al., 2016) from a 445 nucleotide alignment (MUSCLE (Edgar, 2004), codon-based). The Solanales and Brassicales ATG8 clades are named following the conventions in Kellner et al. 2016. The bootstrap values of the major nodes are indicated. The scale bar indicates the evolutionary distance based on nucleotide substitution rate.

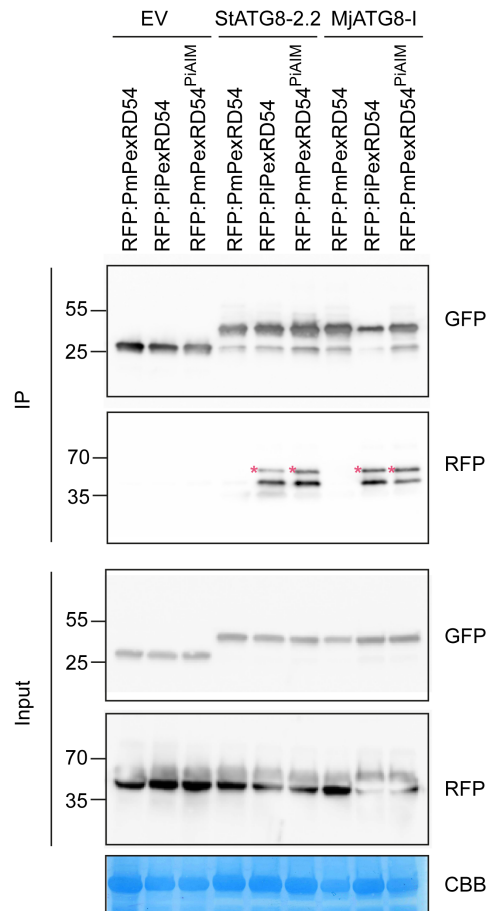


Figure A.5.4 Mutation of the *P. mirabilis* PexRD54 AIM to match the *P. infestans* sequence is sufficient to reconstitute ATG8 binding

Co-immunoprecipitation experiment between PexRD54 variants (*Pm*PexRD54, *Pi*PexRD54, *Pm*PexRD54^{PiAIM}) and ATG8s. RFP:PexRD54 variants were transiently co-expressed with GFP:EV, GFP:*St*ATG8-2.2, and GFP:*Mj*ATG8-I. Immunoprecipitates (IPs) were obtained with anti-GFP antiserum and total protein extracts were immunoblotted with appropriate antisera (listed on the right). Stars indicate expected band sizes.

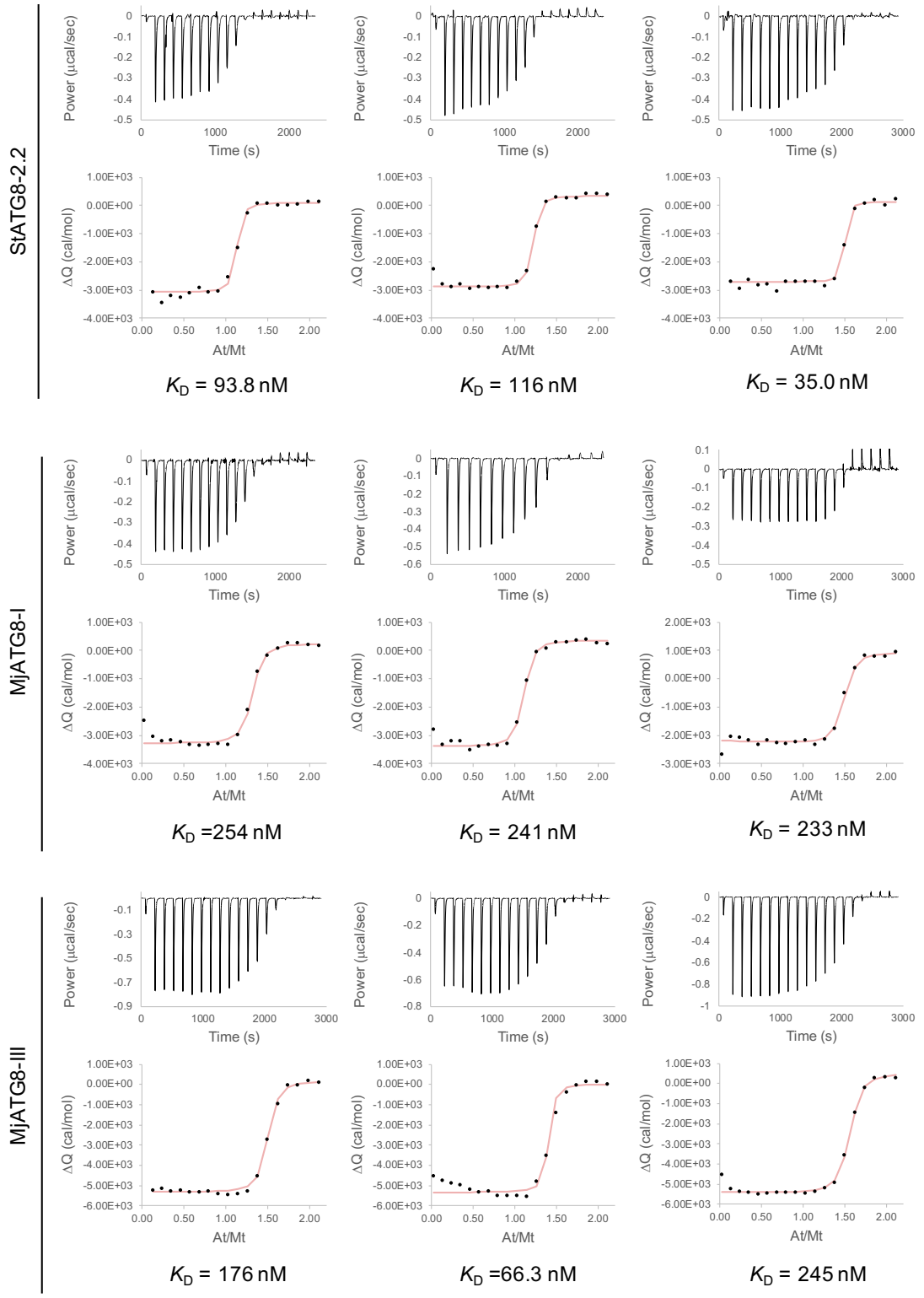


Figure A.5.5 *PiPexRD54* AIM peptide interaction with *StATG8-2.2*, *MjATG8-I* and *MjATG8-III* in isothermal titration calorimetry

Figure A.5.5 *PiPexRD54* AIM peptide interaction with *StATG8-2.2*, *MjATG8-I* and *MjATG8-III* in isothermal titration calorimetry

The binding affinities between *PiPexRD54* AIM peptide and *StATG8-2.2*, *MjATG8-I*, and *MjATG8-III* were determined using isothermal titration calorimetry (ITC). The top panels show heat differences upon injection of peptide ligands, and the lower panels show integrated heats of injection (•) and the best fit (pink line) to a single site binding model using AFFINImeter analysis software.

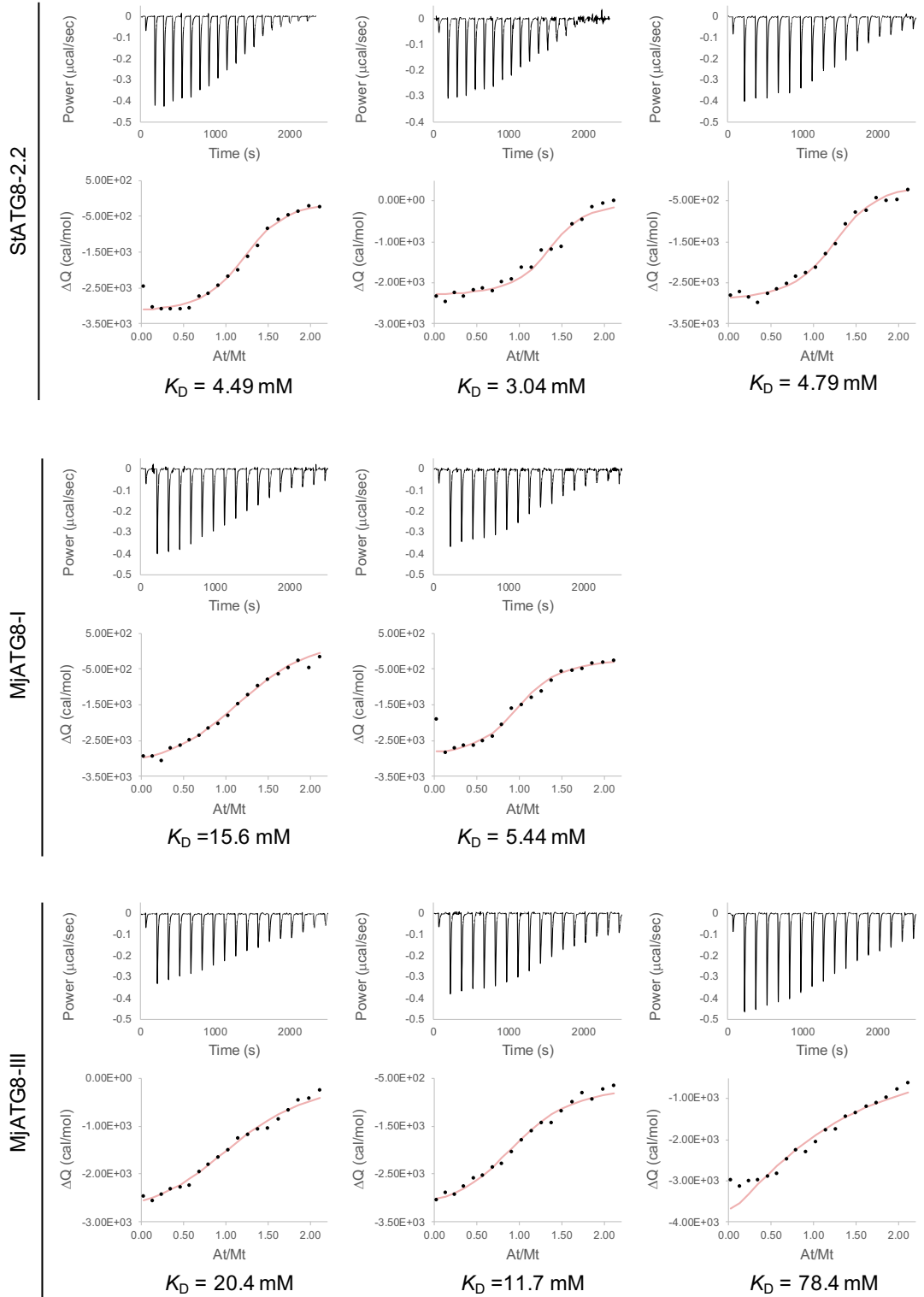


Figure A.5.6 *PmPexRD54* AIM peptide interaction with *StATG8-2.2*, *MjATG8-I* and *MjATG8-III* in isothermal titration calorimetry

Figure A.5.6 *PmPexRD54* AIM peptide interaction with *StATG8-2.2*, *MjATG8-I* and *MjATG8-III* in isothermal titration calorimetry

The binding affinities between *PmPexRD54* AIM peptide and *StATG8-2.2*, *MjATG8-I*, and *MjATG8-III* were determined using isothermal titration calorimetry (ITC). The top panels show heat differences upon injection of peptide ligands, and the lower panels show integrated heats of injection (•) and the best fit (pink line) to a single site binding model using AFFINImeter analysis software.

Peptide	ATG8	Rep.	KD [M]	rM	ΔH [cal/mol]	ΔG [cal/mol]
PiPexRD54	StATG8-2.2	1	9.39E-08± 2.96e-8	1.08± 7.70e-3	-3.18E+03± 5.11e+1	-9.59E+03± 1.87e+2
PiPexRD54	StATG8-2.2	2	1.16E-07± 3.19e-8	1.17± 4.38e-3	-3.27E+03± 3.76e+1	-9.46E+03± 1.63e+2
PiPexRD54	StATG8-2.2	3	3.50E-08± 1.83e-8	1.45± 6.11e-3	-2.85E+03± 3.93e+1	-1.02E+04± 3.10e+2
PiPexRD54	MjATG8-I	1	2.55E-07± 4.13e-8	1.27± 8.01e-3	-3.55E+03± 2.33e+1	-9.00E+03± 9.60e+1
PiPexRD54	MjATG8-I	2	2.41E-07± 3.05e-8	1.06± 4.50e-3	-3.78E+03± 4.10e+1	-9.03E+03± 7.51e+1
PiPexRD54	MjATG8-I	3	2.34E-07± 5.55e-8	1.44± 1.04e-2	-3.28E+03± 9.38e+1	-9.05E+03± 1.41e+2
PiPexRD54	MjATG8-III	1	1.76E-07± 1.19e-8	1.45± 1.50e-3	-5.50E+03± 1.75e+1	-9.21E+03± 4.01e+1
PiPexRD54	MjATG8-III	2	6.63E-08± 1.73e-8	1.35± 8.04e-3	-5.33E+03± 1.06e+1	-9.79E+03± 1.55e+2
PiPexRD54	MjATG8-III	3	2.45E-07± 2.54e-8	1.51± 4.46e-3	-5.99E+03± 5.03e+1	-9.02E+03± 6.12e+1
PmRD54	StATG8-2.2	1	4.49E-06± 2.38e-7	1.23± 8.95e-3	-3.23E+03± 2.50e+1	-7.30E+03± 3.14e+1
PmRD54	StATG8-2.2	2	3.04E-06± 5.77e-7	1.35± 1.44e-2	-2.34E+03± 3.90e+1	-7.53E+03± 1.13e+2
PmRD54	StATG8-2.2	3	4.79E-06± 5.12e-7	1.27± 1.28e-2	-2.98E+03± 4.27e+1	-7.26E+03± 6.34e+1
PmRD54	MjATG8-I	1	1.56E-05± 3.22e-6	1.32± 7.2 8e-2	-4.12E+03± 3.94e+2	-6.56E+03± 1.22e+2
PmRD54	MjATG8-I	2	5.44E-06± 5.21e-7	1.00± 0.00	-2.74E+03± 7.30e+1	-7.18E+03± 5.68e+1
PmRD54	MjATG8-III	1	2.04E-05± 1.78e-6	1.23± 1.89e-2	-3.02E+03± 8.34e+1	-6.40E+03± 5.16e+1
PmRD54	MjATG8-III	2	1.17E-05± 1.95e-6	1.00± 0.00	-2.55E+03± 1.56e+2	-6.73E+03± 9.89e+1
PmRD54	MjATG8-III	3	7.84E-05± 2.13e-6	1.00± 0.00	-6.93E+03± 7.65e+1	-5.60E+03± 1.61e+1

Table A.5.7 Summary of the thermodynamic and kinetic data for the isothermal titration calorimetry experiments

Table summarizing the thermodynamic and kinetic data for the isothermal titration calorimetry experiments presented in **Fig A.5.5** and **Fig A.5.6**.

References

- Akagi, Yasunori, Hajime Akamatsu, Hiroshi Otani, and Motoichiro Kodama. 2009. Horizontal Chromosome Transfer, a Mechanism for the Evolution and Differentiation of a Plant-Pathogenic Fungus. *Eukaryot. Cell* 8: 1732–38.
- Alemu, Endalkachew Ashenafi, Trond Lamark, Knut Martin Torgersen, Aasa Birna Birgisdottir, Kenneth Bowitz Larsen, Ashish Jain, Hallvard Olsvik, Aud Overvatn, Vladimir Kirkin, and Terje Johansen. 2012. ATG8 Family Proteins Act as Scaffolds for Assembly of the ULK Complex: Sequence Requirements for LC3-Interacting Region (LIR) Motifs. *J. Biol. Chem.* 287: 39275–90.
- Alfano, James R, and Alan Collmer. 2004. Type III Secretion System Effector Proteins: Double Agents in Bacterial Disease and Plant Defense. *Annu. Rev. Phytopathol.* 42: 385–414.
- Allen, Rebecca L, Peter D Bittner-Eddy, Laura J Grenville-Briggs, Julia C Meitz, Anne P Rehmany, Laura E Rose, and Jim L Beynon. 2004. Host-Parasite Coevolutionary Conflict between Arabidopsis and Downy Mildew. *Science* 306: 1957–60.
- An, Heeseon, and J Wade Harper. 2018. Systematic Analysis of Ribophagy in Human Cells Reveals Bystander Flux during Selective Autophagy. *Nat. Cell Biol.* 20: 135–43.
- Anding, Allyson L, and Eric H Baehrecke. 2017. Cleaning House: Selective Autophagy of Organelles. *Dev. Cell* 41: 10–22.
- Avin-Wittenberg, Tamar, Krzysztof Bajdzienko, Gal Wittenberg, Saleh Alseikh, Takayuki Tohge, Ralph Bock, Patrick Giavalisco, and Alisdair R Fernie. 2015. Global Analysis of the Role of Autophagy in Cellular Metabolism and Energy Homeostasis in Arabidopsis Seedlings under Carbon Starvation. *Plant Cell* 27: 306–22.
- Avin-Wittenberg, Tamar, Arik Honig, and Gad Galili. 2012. Variations on a Theme: Plant Autophagy in Comparison to Yeast and Mammals. *Protoplasma* 249: 285–99.
- Baer, Charles F, Michael M Miyamoto, and Dee R Denver. 2007. Mutation Rate Variation in Multicellular Eukaryotes: Causes and Consequences. *Nat. Rev. Genet.* 8: 619–31.
- Balderhaar, Henning J Kleine, Henning Arlt, Clemens Ostrowicz, Cornelia Brocker, Frederik Sundermann, Roland Brandt, Markus Babst, and Christian Ungermann.

2010. The Rab GTPase Ypt7 Is Linked to Retromer-Mediated Receptor Recycling and Fusion at the Yeast Late Endosome. *J. Cell Sci.* 123: 4085–94.
- Bars, Romain Le, Jessica Marion, Remi Le Borgne, Beatrice Satiat-Jeunemaitre, and Michele Wolfe Bianchi. 2014. ATG5 Defines a Phagophore Domain Connected to the Endoplasmic Reticulum during Autophagosome Formation in Plants. *Nat. Commun.* 5: 4121.
- Becker, Walter. 2012. Emerging Role of DYRK Family Protein Kinases as Regulators of Protein Stability in Cell Cycle Control. *Cell Cycle* 11: 3389–94.
- Behrends, Christian, Mathew E Sowa, Steven P Gygi, and J Wade Harper. 2010. Network Organization of the Human Autophagy System. *Nature* 466: 68–76.
- Bento, Carla F, Maurizio Renna, Ghita Ghislat, Claudia Puri, Avraham Ashkenazi, Mariella Vicinanza, Fiona M Menzies, and David C Rubinsztein. 2016. Mammalian Autophagy: How Does It Work? *Annu. Rev. Biochem.* 85: 685–713.
- Berrow, Nick S, David Alderton, Sarah Sainsbury, Joanne Nettleship, Rene Assenberg, Nahid Rahman, David I Stuart, and Raymond J Owens. 2007. A Versatile Ligation-Independent Cloning Method Suitable for High-Throughput Expression Screening Applications. *Nucleic Acids Res.* 35: e45.
- Bertipaglia, Chiara, Sarah Schneider, Arjen J Jakobi, Abul K Tarafder, Yury S Bykov, Andrea Picco, Wanda Kukulski, et al. 2016. Higher-Order Assemblies of Oligomeric Cargo Receptor Complexes Form the Membrane Scaffold of the Cvt Vesicle. *EMBO Rep.* 17: 1044–60.
- Biemelt, Sophia, and Uwe Sonnewald. 2006. Plant-Microbe Interactions to Probe Regulation of Plant Carbon Metabolism. *J. Plant Physiol.* 163: 307–18.
- Birgisdottir, Asa Birna, Trond Lamark, and Terje Johansen. 2013. The LIR Motif - Crucial for Selective Autophagy. *J. Cell Sci.* 126: 3237–47.
- Block, Anna, and James R Alfano. 2011. Plant Targets for Pseudomonas Syringae Type III Effectors: Virulence Targets or Guarded Decoys? *Curr. Opin. Microbiol.* 14: 39–46.
- Bolton, Melvin D, H Peter van Esse, Jack H Vossen, Ronnie de Jonge, Ioannis Stergiopoulos, Iris J E Stulemeijer, Grady C M van den Berg, et al. 2008. The Novel Cladosporium Fulvum Lysin Motif Effector Ecp6 Is a Virulence Factor with Orthologues in Other Fungal Species. *Mol. Microbiol.* 69: 119–36.

- Boutemy, Laurence S, Stuart R F King, Joe Win, Richard K Hughes, Thomas A Clarke, Tharin M A Blumenschein, Sophien Kamoun, and Mark J Banfield. 2011. Structures of Phytophthora RXLR Effector Proteins: A Conserved but Adaptable Fold Underpins Functional Diversity. *J. Biol. Chem.* 286: 35834–42.
- Boyle, Keith B, and Felix Randow. 2013. The Role of “eat-Me” Signals and Autophagy Cargo Receptors in Innate Immunity. *Curr. Opin. Microbiol.* 16: 339–48.
- Bozkurt, Tolga O, Sebastian Schornack, Joe Win, Takayuki Shindo, Muhammad Ilyas, Ricardo Oliva, Liliana M Cano, et al. 2011. Phytophthora Infestans Effector AVRblb2 Prevents Secretion of a Plant Immune Protease at the Haustorial Interface. *Proc. Natl. Acad. Sci.* 108: 20832 LP – 20837.
- Breeze, Emily, Elizabeth Harrison, Stuart McHattie, Linda Hughes, Richard Hickman, Claire Hill, Steven Kiddle, et al. 2011. High-Resolution Temporal Profiling of Transcripts during Arabidopsis Leaf Senescence Reveals a Distinct Chronology of Processes and Regulation. *Plant Cell* 23: 873–94.
- Brockington, Samuel F, Rachel H Walker, Beverley J Glover, Pamela S Soltis, and Douglas E Soltis. 2011. Complex Pigment Evolution in the Caryophyllales. *New Phytol.* 190: 854–64.
- Broda, Martyna, A Harvey Millar, and Olivier Van Aken. 2018. Mitophagy: A Mechanism for Plant Growth and Survival. *Trends Plant Sci.* 23: 434–50.
- Burg, Harrold A van den, Stuart J Harrison, Matthieu H A J Joosten, Jacques Vervoort, and Pierre J G M de Wit. 2006. Cladosporium Fulvum Avr4 Protects Fungal Cell Walls against Hydrolysis by Plant Chitinases Accumulating during Infection. *Mol. Plant. Microbe. Interact.* 19: 1420–30.
- Burgyan, Jozsef, and Zoltan Havelda. 2011. Viral Suppressors of RNA Silencing. *Trends Plant Sci.* 16: 265–72.
- Burroughs, Alexander Maxwell, Lakshminarayan M Iyer, and L Aravind. 2012. The Natural History of Ubiquitin and Ubiquitin-Related Domains. *Front. Biosci. (Landmark Ed.* 17: 1433–60.
- Carroll, Adam. 2013. The Arabidopsis Cytosolic Ribosomal Proteome: From Form to Function. *Front. Plant Sci.* 4: 32.
- Chandra, Sreeganga, Peter F Heinstejn, and Philip S Low. 1996. The activation of phospholipase A by plant defense elicitors. *Plant Physiol.* 110: 979-986.

- Chen, Guanquan, Michael S Greer, Ida Lager, Jenny Lindberg Yilmaz, Elzbieta Mietkiewska, Anders S Carlsson, Sten Stymne, Randall J Weslake. 2012. Identification and characterization of an LCAT-like *Arabidopsis thaliana* gene encoding a novel phospholipase A. *Febs Lett* 586: 373-377.
- Chen, Yuan, Fiona Cunningham, Daniel Rios, William M McLaren, James Smith, Bethan Pritchard, Giulietta M Spudich, et al. 2010. Ensembl Variation Resources. *BMC Genomics* 11: 293.
- Cheng, Xiaofang, Yingli Wang, Yukang Gong, Faxiang Li, Yujiao Guo, Shichen Hu, Jianping Liu, and Lifeng Pan. 2016. Structural Basis of FYCO1 and MAP1LC3A Interaction Reveals a Novel Binding Mode for Atg8-Family Proteins. *Autophagy* 12: 1330–39.
- Chisholm, Stephen T, Gitta Coaker, Brad Day, and Brian J Staskawicz. 2006. Host-Microbe Interactions: Shaping the Evolution of the Plant Immune Response. *Cell* 124: 803–14.
- Chou, Seemay, Ksenia V Krasileva, James M Holton, Adam D Steinbrenner, Tom Alber, and Brian J Staskawicz. 2011. Hyaloperonospora Arabidopsis ATR1 Effector Is a Repeat Protein with Distributed Recognition Surfaces. *Proc. Natl. Acad. Sci. U. S. A.* 108: 13323–28.
- Chuma, Izumi, Chihiro Isobe, Yuma Hotta, Kana Ibaragi, Natsuru Futamata, Motoaki Kusaba, Kentaro Yoshida, et al. 2011. Multiple Translocation of the AVR-Pita Effector Gene among Chromosomes of the Rice Blast Fungus *Magnaporthe Oryzae* and Related Species. *PLoS Pathog.* 7: e1002147.
- Chung, Taijoon, Allison R Phillips, and Richard D Vierstra. 2010. ATG8 Lipidation and ATG8-Mediated Autophagy in *Arabidopsis* Require ATG12 Expressed from the Differentially Controlled ATG12A AND ATG12B Loci. *Plant J.* 62: 483–93.
- Chung, Taijoon, Anongpat Suttangkakul, and Richard D Vierstra. 2009. The ATG Autophagic Conjugation System in Maize: ATG Transcripts and Abundance of the ATG8-Lipid Adduct Are Regulated by Development and Nutrient Availability. *Plant Physiol.* 149: 220 LP – 234.
- Cianciotto, N. 2005. Type II secretion: a protein secretion system for all seasons. *Trends in Micro.* 13: 581- 588.
- Coll, N S, P Epple, and J L Dangl. 2011. Programmed Cell Death in the Plant Immune

- System. *Cell Death Differ.* 18: 1247–56.
- Contento, Anthony L, Sang-Jin Kim, and Diane C Bassham. 2004. Transcriptome Profiling of the Response of Arabidopsis Suspension Culture Cells to Suc Starvation. *Plant Physiol.* 135: 2330–47.
- Couto, Daniel, and Cyril Zipfel. 2016. Regulation of Pattern Recognition Receptor Signalling in Plants. *Nat. Rev. Immunol.* 16: 537–52.
- Croll, Daniel, and Bruce A McDonald. 2012. The Accessory Genome as a Cradle for Adaptive Evolution in Pathogens. *PLoS Pathog.* 8: e1002608.
- Cuomo, Christina A, Ulrich Guldener, Jin-Rong Xu, Frances Trail, B Gillian Turgeon, Antonio Di Pietro, Jonathan D Walton, et al. 2007. The Fusarium Graminearum Genome Reveals a Link between Localized Polymorphism and Pathogen Specialization. *Science* 317: 1400–1402.
- Dagdas, Yasin F, Khaoula Belhaj, Abbas Maqbool, Angela Chaparro-Garcia, Pooja Pandey, Benjamin Petre, Nadra Tabassum, et al. 2016. An Effector of the Irish Potato Famine Pathogen Antagonizes a Host Autophagy Cargo Receptor. Edited by Jean T Greenberg. *Elife* 5: e10856.
- Dagdas, Yasin F, Pooja Pandey, Yasin Tumtas, Nattapong Sanguankiattichai, Khaoula Belhaj, Cian Duggan, Alexandre Y Leary, et al. 2018. Host Autophagy Machinery Is Diverted to the Pathogen Interface to Mediate Focal Defense Responses against the Irish Potato Famine Pathogen. Edited by Jian-Min Zhou. *Elife* 7: e37476.
- Damasceno, Cynthia M B, John G Bishop, Daniel R Ripoll, Joe Win, Sophien Kamoun, and Jocelyn K C Rose. 2008. Structure of the Glucanase Inhibitor Protein (GIP) Family from Phytophthora Species Suggests Coevolution with Plant Endo-Beta-1,3-Glucanases. *Mol. Plant. Microbe. Interact.* 21: 820–30.
- Damme, Mireille van, Tolga O Bozkurt, Cahid Cakir, Sebastian Schornack, Jan Sklenar, Alexandra M E Jones, and Sophien Kamoun. 2012. The Irish Potato Famine Pathogen Phytophthora Infestans Translocates the CRN8 Kinase into Host Plant Cells. *PLoS Pathog.* 8: e1002875.
- Dauphinee, Adrian N, Catarina Cardoso, Kerstin Dalman, Jonas A Ohlsson, Stina Berglund Fick, Stephanie Robert, Glenn R Hicks, Peter Bozhkov, and Elena A Minina. 2019. Chemical Screening Pipeline for Identification of Specific Plant Autophagy Modulators. *Plant Physiol.*, September.

- DeLille, Justin M, Paul C Sehnke, and Robert J Ferl. 2001. The Arabidopsis 14-3-3 Family of Signaling Regulators. *Plant Physiol.* 126: 35–38.
- Deng, Yan, Sabrina Humbert, Jian-Xiang Liu, Renu Srivastava, Steven J Rothstein, and Stephen H Howell. 2011. Heat Induces the Splicing by IRE1 of a MRNA Encoding a Transcription Factor Involved in the Unfolded Protein Response in Arabidopsis. *Proc. Natl. Acad. Sci. U. S. A.* 108: 7247–52.
- Deosaran, Elizabeth, Kenneth B Larsen, Rong Hua, Graeme Sargent, Yuqing Wang, Sarah Kim, Trond Lamark, et al. 2013. NBR1 Acts as an Autophagy Receptor for Peroxisomes. *J. Cell Sci.* 126: 939–52.
- Derevnina, Lida, Sophien Kamoun, and Chih-hang Wu. 2019. Dude, Where Is My Mutant? *Nicotiana Benthamiana* Meets Forward Genetics. *New Phytol.* 221: 607–10.
- Dikic, Ivan. 2017. Proteasomal and Autophagic Degradation Systems. *Annu. Rev. Biochem.* 86: 193–224.
- Dikic, Ivan, and Zvulun Elazar. 2018. Mechanism and Medical Implications of Mammalian Autophagy. *Nat. Rev. Mol. Cell Biol.* 19: 349–64.
- Dodds, Peter N, Gregory J Lawrence, Ann-Maree Catanzariti, Trazel Teh, Ching-I A Wang, Michael A Ayliffe, Bostjan Kobe, and Jeffrey G Ellis. 2006. Direct Protein Interaction Underlies Gene-for-Gene Specificity and Coevolution of the Flax Resistance Genes and Flax Rust Avirulence Genes. *Proc. Natl. Acad. Sci. U. S. A.* 103: 8888–93.
- Dodds, Peter N, and John P Rathjen. 2010. Plant Immunity: Towards an Integrated View of Plant-Pathogen Interactions. *Nat. Rev. Genet.* 11: 539–48.
- Doelling, Jed H, Joseph M Walker, Eric M Friedman, Allison R Thompson, and Richard D Vierstra. 2002. The APG8/12-Activating Enzyme APG7 Is Required for Proper Nutrient Recycling and Senescence in Arabidopsis Thaliana. *J. Biol. Chem.* 277: 33105–14.
- Domingues, Mariane Noronha, Tiago Antonio De Souza, Raul Andres Cernadas, Maria Luiza Peixoto de Oliveira, Cassia Docena, Chuck Shaker Farah, and Celso Eduardo Benedetti. 2010. The Xanthomonas Citri Effector Protein PthA Interacts with Citrus Proteins Involved in Nuclear Transport, Protein Folding and Ubiquitination Associated with DNA Repair. *Mol. Plant Pathol.* 11: 663–75.
- Dong, Suomeng, Sylvain Raffaele, and Sophien Kamoun. 2015. The Two-Speed

- Genomes of Filamentous Pathogens: Waltz with Plants. *Curr. Opin. Genet. Dev.* 35: 57–65.
- Dong, Suomeng, Remco Stam, Liliana M Cano, Jing Song, Jan Sklenar, Kentaro Yoshida, Tolga O Bozkurt, et al. 2014. Effector Specialization in a Lineage of the Irish Potato Famine Pathogen. *Science* 343: 552–55.
- Dorfer, Viktoria, Peter Pichler, Thomas Stranzl, Johannes Stadlmann, Thomas Taus, Stephan Winkler, and Karl Mechtler. 2014. MS Amanda, a Universal Identification Algorithm Optimized for High Accuracy Tandem Mass Spectra. *J. Proteome Res.* 13: 3679–84.
- Dupont, Nicolas, Shanya Jiang, Manohar Pilli, Wojciech Ornatowski, Dhruva Bhattacharya, and Vojo Deretic. 2011. Autophagy-Based Unconventional Secretory Pathway for Extracellular Delivery of IL-1 β . *EMBO J.* 30: 4701–11.
- Edgar, Robert C. 2004. MUSCLE: Multiple Sequence Alignment with High Accuracy and High Throughput. *Nucleic Acids Res.* 32: 1792–97.
- Effmert, Uta, Jana Grosse, Ursula S R Rose, Fred Ehrig, Ralf Kagi, and Birgit Piechulla. 2005. Volatile Composition, Emission Pattern, and Localization of Floral Scent Emission in *Mirabilis Jalapa* (Nyctaginaceae). *Am. J. Bot.* 92: 2–12.
- Faino, Luigi, Michael F Seidl, Xiaoqian Shi-Kunne, Marc Pauper, Grady C M van den Berg, Alexander H J Wittenberg, and Bart P H J Thomma. 2016. Transposons Passively and Actively Contribute to Evolution of the Two-Speed Genome of a Fungal Pathogen. *Genome Res.* 26: 1091–1100.
- Farré, Jean-Claude, and Suresh Subramani. 2016. Mechanistic Insights into Selective Autophagy Pathways: Lessons from Yeast. *Nat. Rev. Mol. Cell Biol.* 17: 537.
- Feng, Feng, and Jian-Min Zhou. 2012. Plant-Bacterial Pathogen Interactions Mediated by Type III Effectors. *Curr. Opin. Plant Biol.* 15: 469–76.
- Feschotte, Cedric. 2008. Transposable Elements and the Evolution of Regulatory Networks. *Nat. Rev. Genet.* 9: 397–405.
- Filimonenko, Maria, Susanne Stuffers, Camilla Raiborg, Ai Yamamoto, Lene Malerod, Elizabeth M C Fisher, Adrian Isaacs, Andreas Brech, Harald Stenmark, and Anne Simonsen. 2007. Functional Multivesicular Bodies Are Required for Autophagic Clearance of Protein Aggregates Associated with Neurodegenerative Disease. *J. Cell Biol.* 179: 485–500.

- Fu, Zheng Qing, Ming Guo, Byeong-ryool Jeong, Fang Tian, Thomas E Elthon, Ronald L Cerny, Dorothee Staiger, and James R Alfano. 2007. A Type III Effector ADP-Ribosylates RNA-Binding Proteins and Quells Plant Immunity. *Nature* 447: 284–88.
- Fujioka, Yuko, Nobuo N Noda, Hitoshi Nakatogawa, Yoshinori Ohsumi, and Fuyuhiko Inagaki. 2010. Dimeric Coiled-Coil Structure of *Saccharomyces Cerevisiae* Atg16 and Its Functional Significance in Autophagy. *J. Biol. Chem.* 285: 1508–15.
- Fujita, Naonobu, Eiji Morita, Takashi Itoh, Atsushi Tanaka, Megumi Nakaoka, Yuki Osada, Tetsuo Umemoto, et al. 2013. Recruitment of the Autophagic Machinery to Endosomes during Infection Is Mediated by Ubiquitin. *J. Cell Biol.* 203: 115–28.
- Gao, Caiji, Xiaohong Zhuang, Yong Cui, Xi Fu, Yilin He, Qiong Zhao, Yonglun Zeng, Jinbo Shen, Ming Luo, and Liwen Jiang. 2015. Dual Roles of an Arabidopsis ESCRT Component FREE1 in Regulating Vacuolar Protein Transport and Autophagic Degradation. *Proc. Natl. Acad. Sci. U. S. A.* 112: 1886–91.
- Ge, Liang, Min Zhang, and Randy Schekman. 2014. Phosphatidylinositol 3-Kinase and COPII Generate LC3 Lipidation Vesicles from the ER-Golgi Intermediate Compartment. *Elife* 3: e04135.
- Gomez, Rodrigo Enrique, Jerome Joubes, Nicolas Valentin, Henri Batoko, Beatrice Satiat-Jeunemaitre, and Amelie Bernard. 2018. Lipids in Membrane Dynamics during Autophagy in Plants. *J. Exp. Bot.* 69: 1287–99.
- Gotz, Stefan, Juan Miguel Garcia-Gomez, Javier Terol, Tim D Williams, Shivashankar H Nagaraj, Maria Jose Nueda, Montserrat Robles, Manuel Talon, Joaquin Dopazo, and Ana Conesa. 2008. High-Throughput Functional Annotation and Data Mining with the Blast2GO Suite. *Nucleic Acids Res.* 36: 3420–35.
- Graef, Martin, Jonathan R Friedman, Christopher Graham, Mohan Babu, and Jodi Nunnari. 2013. ER Exit Sites Are Physical and Functional Core Autophagosome Biogenesis Components. *Mol. Biol. Cell* 24: 2918–31.
- Grant, Sarah R, Emily J Fisher, Jeff H Chang, Beth M Mole, and Jeffery L Dangl. 2006. Subterfuge and Manipulation: Type III Effector Proteins of Phytopathogenic Bacteria. *Annu. Rev. Microbiol.* 60: 425–49.
- Guerroue, Francois Le, Franziska Eck, Jennifer Jung, Tatjana Starzetz, Michel Mittelbronn, Manuel Kaulich, and Christian Behrends. 2017. Autophagosomal

- Content Profiling Reveals an LC3C-Dependent Piecemeal Mitophagy Pathway. *Mol. Cell* 68: 786-796.e6.
- Guiboileau, Anne, Liliana Avila-Ospina, Kohki Yoshimoto, Fabienne Soulay, Marianne Azzopardi, Anne Marmagne, Jeremy Lothier, and Celine Masclaux-Daubresse. 2013. Physiological and Metabolic Consequences of Autophagy Deficiency for the Management of Nitrogen and Protein Resources in Arabidopsis Leaves Depending on Nitrate Availability. *New Phytol.* 199: 683–94.
- Guillen, Karine de, Diana Ortiz-Vallejo, Jerome Gracy, Elisabeth Fournier, Thomas Kroj, and Andre Padilla. 2015. Structure Analysis Uncovers a Highly Diverse but Structurally Conserved Effector Family in Phytopathogenic Fungi. *PLoS Pathog.* 11: e1005228.
- Gutierrez, Maximiliano G, Daniela B Munafo, Walter Beron, and Maria I Colombo. 2004. Rab7 Is Required for the Normal Progression of the Autophagic Pathway in Mammalian Cells. *J. Cell Sci.* 117: 2687–97.
- Haas, Brian J, Sophien Kamoun, Michael C Zody, Rays H Y Jiang, Robert E Handsaker, Liliana M Cano, Manfred Grabherr, et al. 2009. Genome Sequence and Analysis of the Irish Potato Famine Pathogen *Phytophthora Infestans*. *Nature* 461: 393–98.
- Hachez, Charles, Vasko Veljanovski, Hagen Reinhardt, Damien Guillaumot, Celine Vanhee, Francois Chaumont, and Henri Batoko. 2014. The Arabidopsis Abiotic Stress-Induced TSP0-Related Protein Reduces Cell-Surface Expression of the Aquaporin PIP2;7 through Protein-Protein Interactions and Autophagic Degradation. *Plant Cell* 26: 4974–90.
- Hacker, J, and J B Kaper. 2000. Pathogenicity Islands and the Evolution of Microbes. *Annu. Rev. Microbiol.* 54: 641–79.
- Hafren, Anders, Jean-Luc Macia, Andrew J Love, Joel J Milner, Martin Drucker, and Daniel Hofius. 2017. Selective Autophagy Limits Cauliflower Mosaic Virus Infection by NBR1-Mediated Targeting of Viral Capsid Protein and Particles. *Proc. Natl. Acad. Sci. U. S. A.* 114: E2026–35.
- Han, Shaojie, Yan Wang, Xiyin Zheng, Qi Jia, Jinping Zhao, Fan Bai, Yiguo Hong, and Yule Liu. 2015. Cytoplasmic Glyceraldehyde-3-Phosphate Dehydrogenases Interact with ATG3 to Negatively Regulate Autophagy and Immunity in *Nicotiana Benthamiana*. *Plant Cell* 27: 1316–31.

- Han, Y, X Liu, U Benny, H C Kistler, and H D VanEtten. 2001. Genes Determining Pathogenicity to Pea Are Clustered on a Supernumerary Chromosome in the Fungal Plant Pathogen *Nectria Haematococca*. *Plant J.* 25: 305–14.
- Hanaoka, Hideki, Takeshi Noda, Yumiko Shirano, Tomohiko Kato, Hiroaki Hayashi, Daisuke Shibata, Satoshi Tabata, and Yoshinori Ohsumi. 2002. Leaf Senescence and Starvation-Induced Chlorosis Are Accelerated by the Disruption of an Arabidopsis Autophagy Gene. *Plant Physiol.* 129: 1181–93.
- Hartman, J L 4th, B Garvik, and L Hartwell. 2001. Principles for the Buffering of Genetic Variation. *Science* 291: 1001–4.
- Have, Marien, Anne Marmagne, Fabien Chardon, and Celine Masclaux-Daubresse. 2017. Nitrogen Remobilization during Leaf Senescence: Lessons from Arabidopsis to Crops. *J. Exp. Bot.* 68: 2513–29.
- Hayward, Andrew P, and S P Dinesh-Kumar. 2011. What Can Plant Autophagy Do for an Innate Immune Response? *Annu. Rev. Phytopathol.* 49: 557–76.
- Hayward, Andrew P, Jeffrey Tsao, and S P Dinesh-Kumar. 2009. Autophagy and Plant Innate Immunity: Defense through Degradation. *Semin. Cell Dev. Biol.* 20: 1041–47.
- He, Jinqiu, Wenwu Ye, Du Seok Choi, Baixing Wu, Yi Zhai, Baodian Guo, Shuyi Duan, et al. 2019. Structural Analysis of Phytophthora Suppressor of RNA Silencing 2 (PSR2) Reveals a Conserved Modular Fold Contributing to Virulence. *Proc. Natl. Acad. Sci.* 116: 8054–59.
- Hecker, Christina-Maria, Matthias Rabiller, Kaisa Haglund, Peter Bayer, and Ivan Dikic. 2006. Specification of SUMO1- and SUMO2-Interacting Motifs. *J. Biol. Chem.* 281: 16117–27.
- Hegedus, Krisztina, Szabolcs Takats, Attila Boda, Andras Jipa, Peter Nagy, Kata Varga, Attila L Kovacs, and Gabor Juhasz. 2016. The Ccz1-Mon1-Rab7 Module and Rab5 Control Distinct Steps of Autophagy. *Mol. Biol. Cell* 27: 3132–42.
- Hemetsberger, Christoph, Christian Herrberger, Bernd Zechmann, Morten Hillmer, and Gunther Doehlemann. 2012. The *Ustilago Maydis* Effector Pep1 Suppresses Plant Immunity by Inhibition of Host Peroxidase Activity. *PLoS Pathog.* 8: e1002684.
- Heo, Jin-Mi, Alban Ordureau, Joao A Paulo, Jesse Rinehart, and J Wade Harper. 2015. The PINK1-PARKIN Mitochondrial Ubiquitylation Pathway Drives a Program of OPTN/NDP52 Recruitment and TBK1 Activation to Promote Mitophagy. *Mol.*

Cell 60: 7–20.

- Hofius, Daniel, Liang Li, Anders Hafren, and Nuria S Coll. 2017. Autophagy as an Emerging Arena for Plant-Pathogen Interactions. *Curr. Opin. Plant Biol.* 38: 117–23.
- Hogenhout, Saskia A, Renier A L Van der Hoorn, Ryohei Terauchi, and Sophien Kamoun. 2009. Emerging Concepts in Effector Biology of Plant-Associated Organisms. *Mol. Plant. Microbe. Interact.* 22: 115–22.
- Honig, Arik, Tamar Avin-Wittenberg, Shai Ufaz, and Gad Galili. 2012. A New Type of Compartment, Defined by Plant-Specific Atg8-Interacting Proteins, Is Induced upon Exposure of Arabidopsis Plants to Carbon Starvation. *Plant Cell* 24: 288–303.
- Hua-Van, Aurelie, Arnaud Le Rouzic, Thibaud S Boutin, Jonathan Filee, and Pierre Capy. 2011. The Struggle for Life of the Genome's Selfish Architects. *Biol. Direct* 6: 19.
- Huang, Ju, Weina Si, Qiming Deng, Ping Li, and Sihai Yang. 2014. Rapid Evolution of Avirulence Genes in Rice Blast Fungus Magnaporthe Oryzae. *BMC Genet.* 15: 45.
- Huang, Rui, Yinfeng Xu, Wei Wan, Xin Shou, Jiali Qian, Zhiyuan You, Bo Liu, et al. 2015. Deacetylation of Nuclear LC3 Drives Autophagy Initiation under Starvation. *Mol. Cell* 57: 456–66.
- Hughes, David P, and Frederic Libersat. 2019. Parasite Manipulation of Host Behavior. *Curr. Biol.* 29: R45–47.
- Ichimura, Y, T Kirisako, T Takao, Y Satomi, Y Shimonishi, N Ishihara, N Mizushima, et al. 2000. A Ubiquitin-like System Mediates Protein Lipidation. *Nature* 408: 488–92.
- Ichimura, Yoshinobu, Taichi Kumanomidou, Yu-shin Sou, Tsunehiro Mizushima, Junji Ezaki, Takashi Ueno, Eiki Kominami, Takashi Yamane, Keiji Tanaka, and Masaaki Komatsu. 2008. Structural Basis for Sorting Mechanism of P62 in Selective Autophagy. *J. Biol. Chem.* 283: 22847–57.
- Inoue, Yuko, Takao Suzuki, Masaki Hattori, Kohki Yoshimoto, Yoshinori Ohsumi, and Yuji Moriyasu. 2006. AtATG Genes, Homologs of Yeast Autophagy Genes, Are Involved in Constitutive Autophagy in Arabidopsis Root Tip Cells. *Plant Cell Physiol.* 47: 1641–52.
- Isakson, Pauline, Alf Hakon Lystad, Kamilla Breen, Gerbrand Koster, Harald Stenmark, and Anne Simonsen. 2013. TRAF6 Mediates Ubiquitination of KIF23/MKLP1

- and Is Required for Midbody Ring Degradation by Selective Autophagy. *Autophagy* 9: 1955–64.
- Ishida, Hiroyuki, Kohki Yoshimoto, Masanori Izumi, Daniel Reisen, Yuichi Yano, Amane Makino, Yoshinori Ohsumi, Maureen R Hanson, and Tadahiko Mae. 2008. Mobilization of Rubisco and Stroma-Localized Fluorescent Proteins of Chloroplasts to the Vacuole by an ATG Gene-Dependent Autophagic Process. *Plant Physiol.* 148: 142–55.
- Ismayil, Asigul, Meng Yang, and Yule Liu. 2019. Role of Autophagy during Plant-Virus Interactions. *Semin. Cell Dev. Biol.*, July.
- Izumi, Masanori, Hiroyuki Ishida, Sakuya Nakamura, and Jun Hidema. 2017. Entire Photodamaged Chloroplasts Are Transported to the Central Vacuole by Autophagy. *Plant Cell* 29: 377–94.
- Izumi, Masanori, Shinya Wada, Amane Makino, and Hiroyuki Ishida. 2010. The Autophagic Degradation of Chloroplasts via Rubisco-Containing Bodies Is Specifically Linked to Leaf Carbon Status but Not Nitrogen Status in Arabidopsis. *Plant Physiol.* 154: 1196–1209.
- Jacomín, Anne-Claire, Siva Samavedam, Vasilis Promponas, and Ioannis P Nezis. 2016. ILIR Database: A Web Resource for LIR Motif-Containing Proteins in Eukaryotes. *Autophagy* 12: 1945–53.
- Jahreiss, Luca, Fiona M Menzies, and David C Rubinsztein. 2008. The Itinerary of Autophagosomes: From Peripheral Formation to Kiss-and-Run Fusion with Lysosomes. *Traffic* 9: 574–87.
- Janjusevic, Radmila, Robert B Abramovitch, Gregory B Martin, and C Erec Stebbins. 2006. A Bacterial Inhibitor of Host Programmed Cell Death Defenses Is an E3 Ubiquitin Ligase. *Science* 311: 222–26.
- Joachim, Justin, Harold B J Jefferies, Minoos Razi, David Frith, Ambrosius P Snijders, Probir Chakravarty, Delphine Judith, and Sharon A Tooze. 2015. Activation of ULK Kinase and Autophagy by GABARAP Trafficking from the Centrosome Is Regulated by WAC and GM130. *Mol. Cell* 60: 899–913.
- Joachim, Justin, Minoos Razi, Delphine Judith, Martina Wirth, Emily Calamita, Vesela Encheva, Brian D Dynlacht, et al. 2017. Centriolar Satellites Control GABARAP Ubiquitination and GABARAP-Mediated Autophagy. *Curr. Biol.* 27: 2123-2136.e7.

- Johansen, Terje, and Trond Lamark. 2011. Selective Autophagy Mediated by Autophagic Adapter Proteins. *Autophagy* 7: 279–96.
- Jonas, Ana. 2000. Lecithin Cholesterol Acyltransferase. *Biochim. Biophys. Acta - Mol. Cell Biol. Lipids* 1529: 245–56.
- Jones, Jonathan D G, and Jeffery L Dangl. 2006. The Plant Immune System. *Nature* 444: 323–29.
- Jonge, Ronnie de, Melvin D Bolton, Anja Kombrink, Grardy C M van den Berg, Koste A Yadeta, and Bart P H J Thomma. 2013. Extensive Chromosomal Reshuffling Drives Evolution of Virulence in an Asexual Pathogen. *Genome Res.* 23: 1271–82.
- Jonge, Ronnie de, Melvin D Bolton, and Bart P H J Thomma. 2011. How Filamentous Pathogens Co-Opt Plants: The Ins and Outs of Fungal Effectors. *Curr. Opin. Plant Biol.* 14: 400–406.
- Jurkiewicz, Pawel, Su Melser, Mickael Maucourt, Haitham Ayeb, Vasko Veljanovski, Lilly Maneta-Peyret, Mark Hooks, Dominique Rolin, Patrick Moreau, and Henri Batoko. 2018. The Multistress-Induced Translocator Protein (TSPO) Differentially Modulates Storage Lipids Metabolism in Seeds and Seedlings. *Plant J.* 96: 274–86.
- Kabbage, Mehdi, Brett Williams, and Martin B Dickman. 2013. Cell Death Control: The Interplay of Apoptosis and Autophagy in the Pathogenicity of *Sclerotinia Sclerotiorum*. *PLoS Pathog.* 9: e1003287.
- Kadandale, Pavan, and Amy A Kiger. 2010. Role of Selective Autophagy in Cellular Remodeling: “Self-Eating” into Shape. *Autophagy* 6: 1194–95.
- Kaessmann, Henrik. 2010. Origins, Evolution, and Phenotypic Impact of New Genes. *Genome Res.* 20: 1313–26.
- Kalinowska, Kamila, and Erika Isono. 2018. All Roads Lead to the Vacuole-Autophagic Transport as Part of the Endomembrane Trafficking Network in Plants. *J. Exp. Bot.* 69: 1313–24.
- Kalvari, Ioanna, Stelios Tsompanis, Nitha C Mulakkal, Richard Osgood, Terje Johansen, Ioannis P Nezis, and Vasilis J Promponas. 2014. ILIR: A Web Resource for Prediction of Atg8-Family Interacting Proteins. *Autophagy* 10: 913–25.
- Kanzaki, Hiroyuki, Kentaro Yoshida, Hiromasa Saitoh, Koki Fujisaki, Akiko Hirabuchi, Ludovic Alaux, Elisabeth Fournier, Didier Tharreau, and Ryohei Terauchi. 2012. Arms Race Co-Evolution of Magnaporthe Oryzae AVR-Pik and Rice Pik Genes

- Driven by Their Physical Interactions. *Plant J.* 72: 894–907.
- Karimi, Mansour, Dirk Inze, and Ann Depicker. 2002. GATEWAY Vectors for Agrobacterium-Mediated Plant Transformation. *Trends Plant Sci.* 7: 193–95.
- Katsiarimpa, Anthi, Kamila Kalinowska, Franziska Anzenberger, Corina Weis, Maya Ostertag, Chie Tsutsumi, Claus Schwechheimer, Frederic Brunner, Ralph Huckelhoven, and Erika Isono. 2013. The Deubiquitinating Enzyme AMSH1 and the ESCRT-III Subunit VPS2.1 Are Required for Autophagic Degradation in Arabidopsis. *Plant Cell* 25: 2236–52.
- Kaufmann, Anna, Viola Beier, Henri G Franquelim, and Thomas Wollert. 2014. Molecular Mechanism of Autophagic Membrane-Scaffold Assembly and Disassembly. *Cell* 156: 469–81.
- Kaufmann, Anna, and Thomas Wollert. 2014. Scaffolding the Expansion of Autophagosomes. *Autophagy* 10: 1343–45.
- Kellner, Ronny, Juan Carlos De la Concepcion, Abbas Maqbool, Sophien Kamoun, and Yasin F Dagdas. 2017. ATG8 Expansion: A Driver of Selective Autophagy Diversification? *Trends Plant Sci.* 22: 204–14.
- Khaminets, Aliaksandr, Christian Behl, and Ivan Dikic. 2016. Ubiquitin-Dependent And Independent Signals In Selective Autophagy. *Trends Cell Biol.* 26: 6–16.
- Kirisako, T, Y Ichimura, H Okada, Y Kabeya, N Mizushima, T Yoshimori, M Ohsumi, T Takao, T Noda, and Y Ohsumi. 2000. The Reversible Modification Regulates the Membrane-Binding State of Apg8/Aut7 Essential for Autophagy and the Cytoplasm to Vacuole Targeting Pathway. *J. Cell Biol.* 151: 263–76.
- Kirkin, Vladimir, Trond Lamark, Yu-Shin Sou, Geir Bjorkoy, Jennifer L Nunn, Jack-Ansgar Bruun, Elena Shvets, et al. 2009. A Role for NBR1 in Autophagosomal Degradation of Ubiquitinated Substrates. *Mol. Cell* 33: 505–16.
- Klionsky, Daniel J. 2007. Autophagy: From Phenomenology to Molecular Understanding in Less than a Decade. *Nat. Rev. Mol. Cell Biol.* 8: 931–37.
- Klionsky, Daniel J, and Brenda A Schulman. 2014. Dynamic Regulation of Macroautophagy by Distinctive Ubiquitin-like Proteins. *Nat. Struct. Mol. Biol.* 21: 336–45.
- Kolb, Cornelia, Marie-Kristin Nagel, Kamila Kalinowska, Jorg Hagmann, Mie Ichikawa, Franziska Anzenberger, Angela Alkofer, Masa H Sato, Pascal Braun, and Erika

- Isono. 2015. FYVE1 Is Essential for Vacuole Biogenesis and Intracellular Trafficking in Arabidopsis. *Plant Physiol.* 167: 1361–73.
- Kraft, Claudine, and Sascha Martens. 2012. Mechanisms and Regulation of Autophagosome Formation. *Curr. Opin. Cell Biol.* 24: 496–501.
- Kraft, Claudine, Matthias Peter, and Kay Hofmann. 2010. Selective Autophagy: Ubiquitin-Mediated Recognition and Beyond. *Nat. Cell Biol.* 12: 836–41.
- Kulich, Ivan, Tamara Pecenkova, Juraj Sekeres, Ondrej Smetana, Matyas Fendrych, Ilse Foissner, Margit Hoftberger, and Viktor Zarsky. 2013. Arabidopsis Exocyst Subcomplex Containing Subunit EXO70B1 Is Involved in Autophagy-Related Transport to the Vacuole. *Traffic* 14: 1155–65.
- Kumar, Sudhir, Glen Stecher, and Koichiro Tamura. 2016. MEGA7: Molecular Evolutionary Genetics Analysis Version 7.0 for Bigger Datasets. *Mol. Biol. Evol.* 33: 1870–74.
- Kumar, Suresh, Ashish Jain, Farzin Farzam, Jingyue Jia, Yuexi Gu, Seong Won Choi, Michal H Mudd, et al. 2018. Mechanism of Stx17 Recruitment to Autophagosomes via IRGM and Mammalian Atg8 Proteins. *J. Cell Biol.* 217: 997–1013.
- Kwon, Soon Il, Hong Joo Cho, Sung Ryul Kim, and Ohkmae K Park. 2013. The Rab GTPase RabG3b Positively Regulates Autophagy and Immunity-Associated Hypersensitive Cell Death in Arabidopsis. *Plant Physiol.* 161: 1722–36.
- Lai, Zhibing, Fei Wang, Zuyu Zheng, Baofang Fan, and Zhixiang Chen. 2011. A Critical Role of Autophagy in Plant Resistance to Necrotrophic Fungal Pathogens. *Plant J.* 66: 953–68.
- Lakatos, Lorant, Gyorgy Szittyá, Daniel Silhavy, and Jozsef Burgyan. 2004. Molecular Mechanism of RNA Silencing Suppression Mediated by P19 Protein of Tombusviruses. *EMBO J.* 23: 876–84.
- Lamb, Christopher A, Tamotsu Yoshimori, and Sharon A Tooze. 2013. The Autophagosome: Origins Unknown, Biogenesis Complex. *Nat. Rev. Mol. Cell Biol.* 14: 759–74.
- Lastdrager, Jeroen, Johannes Hanson, and Sjef Smeekens. 2014. Sugar Signals and the Control of Plant Growth and Development. *J. Exp. Bot.* 65: 799–807.
- Lazarou, Michael, Danielle A Sliter, Lesley A Kane, Shireen A Sarraf, Chunxin Wang, Jonathon L Burman, Dionisia P Sideris, Adam I Fogel, and Richard J Youle. 2015.

- The Ubiquitin Kinase PINK1 Recruits Autophagy Receptors to Induce Mitophagy. *Nature* 524: 309–14.
- Leary, Alexandre Y, Zachary Savage, Yasin Tumtas, and Tolga O Bozkurt. 2019. Contrasting and Emerging Roles of Autophagy in Plant Immunity. *Curr. Opin. Plant Biol.* 52: 46–53.
- Lederberg, J. 1999. J. B. S. Haldane (1949) on Infectious Disease and Evolution. *Genetics* 153: 1–3.
- Lee, Amy Huei-Yi, Brenden Hurley, Corinna Felsensteiner, Carmen Yea, Wenzislava Ckurshumova, Verena Bartetzko, Pauline W Wang, et al. 2012. A Bacterial Acetyltransferase Destroys Plant Microtubule Networks and Blocks Secretion. *PLoS Pathog.* 8: e1002523.
- Lee, Amy Huei-Yi, Maggie A Middleton, David S Guttman, and Darrell Desveaux. 2013. Phytopathogen Type III Effectors as Probes of Biological Systems. *Microb. Biotechnol.* 6: 230–40.
- Lee, Han Nim, Xavier Zarza, Jeong Hun Kim, Min Ji Yoon, Sang-Hoon Kim, Jae-Hoon Lee, Nadine Paris, Teun Munnik, Marisa S Otegui, and Taijoon Chung. 2018. Vacuolar Trafficking Protein VPS38 Is Dispensable for Autophagy. *Plant Physiol.* 176: 1559–72.
- Lee, Jin-A, Anne Beigneux, S Tariq Ahmad, Stephen G Young, and Fen-Biao Gao. 2007. ESCRT-III Dysfunction Causes Autophagosome Accumulation and Neurodegeneration. *Curr. Biol.* 17: 1561–67.
- Leene, Jelle Van, Chao Han, Astrid Gadeyne, Dominique Eeckhout, Caroline Matthijs, Bernard Cannoot, Nancy De Winne, et al. 2019. Capturing the Phosphorylation and Protein Interaction Landscape of the Plant TOR Kinase. *Nat. Plants* 5: 316–27.
- Li, Faqiang, Taijoon Chung, Janice G Pennington, Maria L Federico, Heidi F Kaeppler, Shawn M Kaeppler, Marisa S Otegui, and Richard D Vierstra. 2015. Autophagic Recycling Plays a Central Role in Maize Nitrogen Remobilization. *Plant Cell* 27: 1389–1408.
- Li, Faqiang, and Richard D Vierstra. 2012. Autophagy: A Multifaceted Intracellular System for Bulk and Selective Recycling. *Trends Plant Sci.* 17: 526–37.
- Li, Yurong, Mehdi Kabbage, Wende Liu, and Martin B Dickman. 2016. Aspartyl Protease-Mediated Cleavage of BAG6 Is Necessary for Autophagy and Fungal

- Resistance in Plants. *Plant Cell* 28: 233–47.
- Liu, Fen, Richard S Marshall, and Faqiang Li. 2018. Understanding and Exploiting the Roles of Autophagy in Plants through Multi-Omics Approaches. *Plant Sci.* 274: 146–52.
- Liu, J, and J Debnath. 2016. The Evolving, Multifaceted Roles of Autophagy in Cancer. *Adv. Cancer Res.* 130: 1–53.
- Liu, Yimo, and Diane C Bassham. 2010. TOR Is a Negative Regulator of Autophagy in *Arabidopsis Thaliana*. *PLoS One* 5: e11883.
- . 2012. Autophagy: Pathways for Self-Eating in Plant Cells. *Annu. Rev. Plant Biol.* 63: 215–37.
- Liu, Yimo, Junmarie Soto Burgos, Yan Deng, Renu Srivastava, Stephen H Howell, and Diane C Bassham. 2012. Degradation of the Endoplasmic Reticulum by Autophagy during Endoplasmic Reticulum Stress in *Arabidopsis*. *Plant Cell* 24: 4635–51.
- Liu, Yimo, Yan Xiong, and Diane C Bassham. 2009. Autophagy Is Required for Tolerance of Drought and Salt Stress in Plants. *Autophagy* 5: 954–63.
- Liu, Yule, Michael Schiff, Kirk Czymmek, Zsolt Talloczy, Beth Levine, and S P Dinesh-Kumar. 2005. Autophagy Regulates Programmed Cell Death during the Plant Innate Immune Response. *Cell* 121: 567–77.
- Liu, Zhenyu, Jorunn I B Bos, Miles Armstrong, Stephen C Whisson, Luis da Cunha, Trudy Torto-Alalibo, Joe Win, et al. 2005. Patterns of Diversifying Selection in the Phytotoxin-like Scr74 Gene Family of *Phytophthora Infestans*. *Mol. Biol. Evol.* 22: 659–72.
- Lystad, Alf Hakon, Yoshinobu Ichimura, Kenji Takagi, Yinjie Yang, Serhiy Pankiv, Yumi Kanegae, Shun Kageyama, et al. 2014. Structural Determinants in GABARAP Required for the Selective Binding and Recruitment of ALFY to LC3B-Positive Structures. *EMBO Rep.* 15: 557–65.
- Ma, Li-Jun, H Charlotte van der Does, Katherine A Borkovich, Jeffrey J Coleman, Marie-Josee Daboussi, Antonio Di Pietro, Marie Dufresne, et al. 2010. Comparative Genomics Reveals Mobile Pathogenicity Chromosomes in *Fusarium*. *Nature* 464: 367–73.
- Macho, Alberto P., and Cyril Zipfel. 2014. Plant PRRs and the Activation of Innate

- Immune Signaling. *Mol. Cell* 54: 263–72.
- Maqbool, A, H Saitoh, M Franceschetti, C E M Stevenson, A Uemura, H Kanzaki, S Kamoun, R Terauchi, and M J Banfield. 2015. Structural Basis of Pathogen Recognition by an Integrated HMA Domain in a Plant NLR Immune Receptor. *Elife* 4.
- Maqbool, Abbas, Richard K Hughes, Yasin F Dagdas, Nicholas Tregidgo, Erin Zess, Khaoula Belhaj, Adam Round, Tolga O Bozkurt, Sophien Kamoun, and Mark J Banfield. 2016. Structural Basis of Host Autophagy-Related Protein 8 (ATG8) Binding by the Irish Potato Famine Pathogen Effector Protein PexRD54. *J. Biol. Chem.* 291: 20270–82.
- Marshall, Richard S, Zhihua Hua, Sujina Mali, Fionn McLoughlin, and Richard D Vierstra. 2019. ATG8-Binding UIM Proteins Define a New Class of Autophagy Adaptors and Receptors. *Cell* 177: 766-781.e24.
- Marshall, Richard S, Faqiang Li, David C Gempertine, Adam J Book, and Richard D Vierstra. 2015. Autophagic Degradation of the 26S Proteasome Is Mediated by the Dual ATG8/Ubiquitin Receptor RPN10 in Arabidopsis. *Mol. Cell* 58: 1053–66.
- Marshall, Richard S, and Richard D Vierstra. 2018. Autophagy: The Master of Bulk and Selective Recycling. *Annu. Rev. Plant Biol.* 69: 173–208.
- Martens, Sascha, and Andreas Bachmair. 2015. How Cells Coordinate Waste Removal through Their Major Proteolytic Pathways. *Nat. Cell Biol.* 17: 841–42.
- Masclaux-Daubresse, Celine, Qinwu Chen, and Marien Have. 2017. Regulation of Nutrient Recycling via Autophagy. *Curr. Opin. Plant Biol.* 39: 8–17.
- Masclaux-Daubresse, Celine, Gilles Clement, Pauline Anne, Jean-Marc Routaboul, Anne Guiboileau, Fabienne Soulay, Ken Shirasu, and Kohki Yoshimoto. 2014. Stitching Together the Multiple Dimensions of Autophagy Using Metabolomics and Transcriptomics Reveals Impacts on Metabolism, Development, and Plant Responses to the Environment in Arabidopsis. *Plant Cell* 26: 1857–77.
- Matsumoto, Gen, Koji Wada, Misako Okuno, Masaru Kurosawa, and Nobuyuki Nukina. 2011. Serine 403 Phosphorylation of P62/SQSTM1 Regulates Selective Autophagic Clearance of Ubiquitinated Proteins. *Mol. Cell* 44: 279–89.
- McEwan, David G, Doris Popovic, Andrea Gubas, Seigo Terawaki, Hironori Suzuki, Daniela Stadel, Fraser P Coxon, et al. 2015. PLEKHM1 Regulates

- Autophagosome-Lysosome Fusion through HOPS Complex and LC3/GABARAP Proteins. *Mol. Cell* 57: 39–54.
- Mellacheruvu, Dattatreya, Zachary Wright, Amber L Couzens, Jean-Philippe Lambert, Nicole A St-Denis, Tuo Li, Yana V Miteva, et al. 2013. The CRAPome: A Contaminant Repository for Affinity Purification-Mass Spectrometry Data. *Nat. Methods* 10: 730–36.
- Michaeli, Simon, Gad Galili, Pascal Genschik, Alisdair R Fernie, and Tamar Avin-Wittenberg. 2016. Autophagy in Plants--What's New on the Menu? *Trends Plant Sci.* 21: 134–44.
- Michaeli, Simon, Arik Honig, Hanna Levanony, Hadas Peled-Zehavi, and Gad Galili. 2014. Arabidopsis ATG8-INTERACTING PROTEIN1 Is Involved in Autophagy-Dependent Vesicular Trafficking of Plastid Proteins to the Vacuole. *Plant Cell* 26: 4084–4101.
- Mitchum, Melissa G, Richard S Hussey, Thomas J Baum, Xiaohong Wang, Axel A Elling, Martin Wubben, and Eric L Davis. 2013. Nematode Effector Proteins: An Emerging Paradigm of Parasitism. *New Phytol.* 199: 879–94.
- Mizushima, N, T Noda, T Yoshimori, Y Tanaka, T Ishii, M D George, D J Klionsky, M Ohsumi, and Y Ohsumi. 1998. A Protein Conjugation System Essential for Autophagy. *Nature* 395: 395–98.
- Mizushima, Noboru. 2018. A Brief History of Autophagy from Cell Biology to Physiology and Disease. *Nat. Cell Biol.* 20: 521–27.
- Moreau, Kevin, Brinda Ravikumar, Maurizio Renna, Claudia Puri, and David C Rubinsztein. 2011. Autophagosome Precursor Maturation Requires Homotypic Fusion. *Cell* 146: 303–17.
- Mostowy, Serge, Vanessa Sancho-Shimizu, Melanie Anne Hamon, Roxane Simeone, Roland Brosch, Terje Johansen, and Pascale Cossart. 2011. P62 and NDP52 Proteins Target Intracytosolic Shigella and Listeria to Different Autophagy Pathways. *J. Biol. Chem.* 286: 26987–95.
- Muhlinen, Natalia von, Masato Akutsu, Benjamin J Ravenhill, Agnes Foeglein, Stuart Bloor, Trevor J Rutherford, Stefan M V Freund, David Komander, and Felix Randow. 2012. LC3C, Bound Selectively by a Noncanonical LIR Motif in NDP52, Is Required for Antibacterial Autophagy. *Mol. Cell* 48: 329–42.

- Nakamura, Sakuya, and Masanori Izumi. 2018. Regulation of Chlorophagy during Photoinhibition and Senescence: Lessons from Mitophagy. *Plant Cell Physiol.* 59: 1135–43.
- Nakatogawa, Hitoshi, Yoshinobu Ichimura, and Yoshinori Ohsumi. 2007. Atg8, a Ubiquitin-like Protein Required for Autophagosome Formation, Mediates Membrane Tethering and Hemifusion. *Cell* 130: 165–78.
- Nakatogawa, Hitoshi, Shiran Ohbayashi, Machiko Sakoh-Nakatogawa, Soichiro Kakuta, Sho W Suzuki, Hiromi Kirisako, Chika Kondo-Kakuta, Nobuo N Noda, Hayashi Yamamoto, and Yoshinori Ohsumi. 2012. The Autophagy-Related Protein Kinase Atg1 Interacts with the Ubiquitin-like Protein Atg8 via the Atg8 Family Interacting Motif to Facilitate Autophagosome Formation. *J. Biol. Chem.* 287: 28503–7.
- Nakatogawa, Hitoshi, Kuninori Suzuki, Yoshiaki Kamada, and Yoshinori Ohsumi. 2009. Dynamics and Diversity in Autophagy Mechanisms: Lessons from Yeast. *Nat. Rev. Mol. Cell Biol.* 10: 458–67.
- Noda, Nobuo N, Hiroyuki Kumeta, Hitoshi Nakatogawa, Kenji Satoo, Wakana Adachi, Junko Ishii, Yuko Fujioka, Yoshinori Ohsumi, and Fuyuhiko Inagaki. 2008. Structural Basis of Target Recognition by Atg8/LC3 during Selective Autophagy. *Genes to Cells* 13: 1211–18.
- Noda, Nobuo N, Yoshinori Ohsumi, and Fuyuhiko Inagaki. 2010. Atg8-Family Interacting Motif Crucial for Selective Autophagy. *FEBS Lett.* 584: 1379–85.
- Nolan, Trevor M, Benjamin Brennan, Mengran Yang, Jiani Chen, Mingcai Zhang, Zhaohu Li, Xuelu Wang, Diane C Bassham, Justin Walley, and Yanhai Yin. 2017. Selective Autophagy of BES1 Mediated by DSK2 Balances Plant Growth and Survival. *Dev. Cell* 41: 33-46.e7.
- Norizuki, Takuya, Takehiko Kanazawa, Naoki Minamino, Hirokazu Tsukaya, and Takashi Ueda. 2019. *Marchantia Polymorpha*, a New Model Plant for Autophagy Studies. *Front. Plant Sci.* 10: 935.
- Nukarinen, Ella, Thomas Nagele, Lorenzo Pedrotti, Bernhard Wurzinger, Andrea Mair, Ramona Landgraf, Frederik Bornke, et al. 2016. Quantitative Phosphoproteomics Reveals the Role of the AMPK Plant Ortholog SnRK1 as a Metabolic Master Regulator under Energy Deprivation. *Sci. Rep.* 6: 31697.
- Orbach, M J, L Farrall, J A Sweigard, F G Chumley, and B Valent. 2000. A Telomeric

- Avirulence Gene Determines Efficacy for the Rice Blast Resistance Gene Pi-Ta. *Plant Cell* 12: 2019–32.
- Ortiz, Diana, Karine de Guillen, Stella Cesari, Véronique Chalvon, Jérôme Gracy, André Padilla, and Thomas Kroj. 2017. Recognition of the Magnaporthe Oryzae Effector AVR-Pia by the Decoy Domain of the Rice NLR Immune Receptor RGA5. *Plant Cell* 29: 156–68.
- Pankiv, Serhiy, Endalkachew A Alemu, Andreas Brech, Jack-Ansgar Bruun, Trond Lamark, Aud Overvatn, Geir Bjorkoy, and Terje Johansen. 2010. FYCO1 Is a Rab7 Effector That Binds to LC3 and PI3P to Mediate Microtubule plus End-Directed Vesicle Transport. *J. Cell Biol.* 188: 253–69.
- Pankiv, Serhiy, Terje Hoyvarde Clausen, Trond Lamark, Andreas Brech, Jack-Ansgar Bruun, Heidi Outzen, Aud Overvatn, Geir Bjorkoy, and Terje Johansen. 2007. P62/SQSTM1 Binds Directly to Atg8/LC3 to Facilitate Degradation of Ubiquitinated Protein Aggregates by Autophagy. *J. Biol. Chem.* 282: 24131–45.
- Patel, Shalaka, and Savithramma P Dinesh-Kumar. 2008. Arabidopsis ATG6 Is Required to Limit the Pathogen-Associated Cell Death Response. *Autophagy* 4: 20–27.
- Pfeilmeier, Sebastian, Delphine L Caly, and Jacob G Malone. 2016. Bacterial Pathogenesis of Plants: Future Challenges from a Microbial Perspective: Challenges in Bacterial Molecular Plant Pathology. *Mol. Plant Pathol.* 17: 1298–1313.
- Phillips, Allison R, Anongpat Suttangkakul, and Richard D Vierstra. 2008. The ATG12-Conjugating Enzyme ATG10 Is Essential for Autophagic Vesicle Formation in Arabidopsis Thaliana. *Genetics* 178: 1339 LP – 1353.
- Popa, Crina, Liang Li, Sergio Gil, Laura Tatjer, Keisuke Hashii, Mitsuaki Tabuchi, Nuria S Coll, Joaquin Arino, and Marc Valls. 2016. The Effector AWR5 from the Plant Pathogen Ralstonia Solanacearum Is an Inhibitor of the TOR Signalling Pathway. *Sci. Rep.* 6: 27058.
- Popelka, Hana, and Daniel J Klionsky. 2015. One Step Closer to Understanding Mammalian Macroautophagy Initiation: Interplay of 2 HORMA Architectures in the ULK1 Complex. *Autophagy* 11: 1953–55.
- Pozuelo-Rubio, Mercedes. 2012. 14-3-3 Proteins Are Regulators of Autophagy. *Cells* 1: 754–73.

- Pu, Yunting, Xinjuan Luo, and Diane C Bassham. 2017. TOR-Dependent and -Independent Pathways Regulate Autophagy in Arabidopsis Thaliana. *Front. Plant Sci.* 8: 1204.
- Qi, Hua, Fan-Nv Xia, Li-Juan Xie, Lu-Jun Yu, Qin-Fang Chen, Xiao-Hong Zhuang, Qian Wang, et al. 2017. TRAF Family Proteins Regulate Autophagy Dynamics by Modulating AUTOPHAGY PROTEIN6 Stability in Arabidopsis. *Plant Cell* 29: 890 LP – 911.
- Rabinowitz, Joshua D, and Eileen White. 2010. Autophagy and Metabolism. *Science* 330: 1344–48.
- Raffaele, Sylvain, Rhys A Farrer, Liliana M Cano, David J Studholme, Daniel MacLean, Marco Thines, Rays H Y Jiang, et al. 2010. Genome Evolution Following Host Jumps in the Irish Potato Famine Pathogen Lineage. *Science* 330: 1540–43.
- Raffaele, Sylvain, and Sophien Kamoun. 2012. Genome Evolution in Filamentous Plant Pathogens: Why Bigger Can Be Better. *Nat. Rev. Microbiol.* 10: 417–30.
- Randow, Felix, and Richard J Youle. 2014. Self and Nonself: How Autophagy Targets Mitochondria and Bacteria. *Cell Host Microbe* 15: 403–11.
- Reggiori, Fulvio, and Daniel J Klionsky. 2013. Autophagic Processes in Yeast: Mechanism, Machinery and Regulation. *Genetics* 194: 341–61.
- Reggiori, Fulvio, and Christian Ungermann. 2017. Autophagosome Maturation and Fusion. *J. Mol. Biol.* 429: 486–96.
- Reyes, Francisca C, Rafael A Buono, Hannetz Roschztardt, Simone Di Rubbo, Li Huey Yeun, Eugenia Russinova, and Marisa S Otegui. 2014. A Novel Endosomal Sorting Complex Required for Transport (ESCRT) Component in Arabidopsis Thaliana Controls Cell Expansion and Development. *J. Biol. Chem.* 289: 4980–88.
- Rich, Melanie, and Pierre-Marc Delaux. 2018. Taking the Step: From Evo-Devo to Plant-Microbe Interaction Evolution with the Liverwort Marchantia. *New Phytol.* 218: 882–84.
- Robberecht, Caroline, Thierry Voet, Masoud Zamani Esteki, Beata A Nowakowska, and Joris R Vermeesch. 2013. Nonallelic Homologous Recombination between Retrotransposable Elements Is a Driver of de Novo Unbalanced Translocations. *Genome Res.* 23: 411–18.
- Rodriguez-Herva, Jose J, Pablo Gonzalez-Melendi, Raquel Cuartas-Lanza, Maria

- Antunez-Lamas, Isabel Rio-Alvarez, Ziduo Li, Gema Lopez-Torrejon, et al. 2012. A Bacterial Cysteine Protease Effector Protein Interferes with Photosynthesis to Suppress Plant Innate Immune Responses. *Cell. Microbiol.* 14: 669–81.
- Rogov, Vladimir, Volker Dotsch, Terje Johansen, and Vladimir Kirkin. 2014. Interactions between Autophagy Receptors and Ubiquitin-like Proteins Form the Molecular Basis for Selective Autophagy. *Mol. Cell* 53: 167–78.
- Rogov, Vladimir V, Alexandra Stolz, Arvind C Ravichandran, Diana O Rios-Szwed, Hironori Suzuki, Andreas Kniss, Frank Lohr, et al. 2017. Structural and Functional Analysis of the GABARAP Interaction Motif (GIM). *EMBO Rep.* 18: 1382–96.
- Rooney, Henrietta C E, John W Van't Klooster, Renier A L van der Hoorn, Matthieu H A J Joosten, Jonathan D G Jones, and Pierre J G M de Wit. 2005. Cladosporium Avr2 Inhibits Tomato Rcr3 Protease Required for Cf-2-Dependent Disease Resistance. *Science* 308: 1783–86.
- Rose, Tatiana Lundgren, Laurent Bonneau, Christophe Der, Daniele Marty-Mazars, and Francis Marty. 2006. Starvation-Induced Expression of Autophagy-Related Genes in Arabidopsis. *Biol. Cell* 98: 53–67.
- Rubinsztein, David C, Tomer Shpilka, and Zvulun Elazar. 2012. Mechanisms of Autophagosome Biogenesis. *Curr. Biol.* 22: R29-34.
- Rusten, Tor Erik, Thomas Vaccari, Karine Lindmo, Lina M W Rodahl, Ioannis P Nezis, Catherine Sem-Jacobsen, Franz Wendler, et al. 2007. ESCRTs and Fab1 Regulate Distinct Steps of Autophagy. *Curr. Biol.* 17: 1817–25.
- Ryu, Kook Hui, Ling Huang, Hyun Min Kang, and John Schiefelbein. 2019. Single-Cell RNA Sequencing Resolves Molecular Relationships Among Individual Plant Cells. *Plant Physiol.* 179: 1444–56.
- Sanjana, Neville E, Le Cong, Yang Zhou, Margaret M Cunniff, Guoping Feng, and Feng Zhang. 2012. A Transcription Activator-like Effector Toolbox for Genome Engineering. *Nat. Protoc.* 7: 171–92.
- Schornack, Sebastian, Matthew J Moscou, Eric R Ward, and Diana M Horvath. 2013. Engineering Plant Disease Resistance Based on TAL Effectors. *Annu. Rev. Phytopathol.* 51: 383–406.
- Schurholz, Ann-Kathrin, Vadir Lopez-Salmeron, Zhenni Li, Joachim Forner, Christian Wenzl, Christophe Gaillochet, Sebastian Augustin, et al. 2018. A Comprehensive

- Toolkit for Inducible, Cell Type-Specific Gene Expression in Arabidopsis. *Plant Physiol.* 178: 40–53.
- Seay, Montrell, Shalaka Patel, and Savithamma P Dinesh-Kumar. 2006. Autophagy and Plant Innate Immunity. *Cell. Microbiol.* 8: 899–906.
- Shannon, Paul, Andrew Markiel, Owen Ozier, Nitin S Baliga, Jonathan T Wang, Daniel Ramage, Nada Amin, Benno Schwikowski, and Trey Ideker. 2003. Cytoscape: A Software Environment for Integrated Models of Biomolecular Interaction Networks. *Genome Res.* 13: 2498–2504.
- Shao, Feng, Catherine Golstein, Jules Ade, Mark Stoutemyer, Jack E Dixon, and Roger W Innes. 2003. Cleavage of Arabidopsis PBS1 by a Bacterial Type III Effector. *Science* 301: 1230–33.
- Sharma, Rahul, Bagdevi Mishra, Fabian Runge, and Marco Thines. 2014. Gene Loss Rather than Gene Gain Is Associated with a Host Jump from Monocots to Dicots in the Smut Fungus *Melanopsichium pennsylvanicum*. *Genome Biol. Evol.* 6: 2034–49.
- Sheveleva, Elena V, Sheila Marquez, Wendy Chmara, Abreeza Zegeer, Richard G Jensen, and Hans J Bohnert. 1998. Sorbitol-6-Phosphate Dehydrogenase Expression in Transgenic Tobacco. *Plant Physiol.* 117: 831–39.
- Shibutani, Shusaku T, and Tamotsu Yoshimori. 2014. Autophagosome Formation in Response to Intracellular Bacterial Invasion. *Cell. Microbiol.* 16: 1619–26.
- Shin, Jun-Hye, Kohki Yoshimoto, Yoshinori Ohsumi, Jong-Seong Jeon, and Gynheung An. 2009. OsATG10b, an Autophagosome Component, Is Needed for Cell Survival against Oxidative Stresses in Rice. *Mol. Cells* 27: 67–74.
- Shulse, Christine N, Benjamin J Cole, Doina Ciobanu, Junyan Lin, Yuko Yoshinaga, Mona Gouran, Gina M Turco, et al. 2019. High-Throughput Single-Cell Transcriptome Profiling of Plant Cell Types. *Cell Rep.* 27: 2241–2247.e4.
- Slavikova, Silvia, Galia Shy, Youli Yao, Rina Glozman, Hanna Levanony, Shmuel Pietrokovski, Zvulun Elazar, and Gad Galili. 2005. The Autophagy-Associated Atg8 Gene Family Operates Both under Favourable Growth Conditions and under Starvation Stresses in Arabidopsis Plants. *J. Exp. Bot.* 56: 2839–49.
- Slobodkin, Moran Rawet, and Zvulun Elazar. 2013. The Atg8 Family: Multifunctional Ubiquitin-like Key Regulators of Autophagy. *Essays Biochem.* 55: 51–64.

- Sone, Teruo, Saori Takeuchi, Shinsuke Miki, Yuki Satoh, Keisuke Ohtsuka, Ayumi Abe, and Kozo Asano. 2013. Homologous Recombination Causes the Spontaneous Deletion of AVR-Pia in Magnaporthe Oryzae. *FEMS Microbiol. Lett.* 339: 102–9.
- Song, Jing, Joe Win, Miaoying Tian, Sebastian Schornack, Farnusch Kaschani, Muhammad Ilyas, Renier A L van der Hoorn, and Sophien Kamoun. 2009. Apoplastic Effectors Secreted by Two Unrelated Eukaryotic Plant Pathogens Target the Tomato Defense Protease Rcr3. *Proc. Natl. Acad. Sci. U. S. A.* 106: 1654–59.
- Soto-Burgos, Junmarie, and Diane C Bassham. 2017. SnRK1 Activates Autophagy via the TOR Signaling Pathway in Arabidopsis Thaliana. *PLoS One* 12: e0182591.
- Souza, Tiago Antonio de, Adriana Santos Soprano, Nayara Patricia Vieira de Lira, Alexandre Jose Christino Quaresma, Bianca Alves Pauletti, Adriana Franco Paes Leme, and Celso Eduardo Benedetti. 2012. The TAL Effector PthA4 Interacts with Nuclear Factors Involved in RNA-Dependent Processes Including a HMG Protein That Selectively Binds Poly(U) RNA. *PLoS One* 7: e32305.
- Spitzer, Christoph, Faqiang Li, Rafael Buono, Hannetz Roschzttardtz, Taijoon Chung, Min Zhang, Katherine W Osteryoung, Richard D Vierstra, and Marisa S Otegui. 2015. The Endosomal Protein CHARGED MULTIVESICULAR BODY PROTEIN1 Regulates the Autophagic Turnover of Plastids in Arabidopsis. *Plant Cell* 27: 391–402.
- Spitzer, Christoph, Francisca C Reyes, Rafael Buono, Marek K Sliwinski, Thomas J Haas, and Marisa S Otegui. 2009. The ESCRT-Related CHMP1A and B Proteins Mediate Multivesicular Body Sorting of Auxin Carriers in Arabidopsis and Are Required for Plant Development. *Plant Cell* 21: 749–66.
- Stanley, Robin E, Michael J Ragusa, and James H Hurley. 2014. The Beginning of the End: How Scaffolds Nucleate Autophagosome Biogenesis. *Trends Cell Biol.* 24: 73–81.
- Stegmann, Martin, Ryan G Anderson, Lore Westphal, Sabine Rosahl, John M McDowell, and Marco Trujillo. 2013. The Exocyst Subunit Exo70B1 Is Involved in the Immune Response of Arabidopsis Thaliana to Different Pathogens and Cell Death. *Plant Signal. Behav.* 8: e27421.
- Stelling, Jorg, Uwe Sauer, Zoltan Szallasi, Francis J 3rd Doyle, and John Doyle. 2004.

- Robustness of Cellular Functions. *Cell* 118: 675–85.
- Stenmark, Harald. 2009. Rab GTPases as Coordinators of Vesicle Traffic. *Nat. Rev. Mol. Cell Biol.* 10: 513.
- Stephani, Madlen, and Yasin Dagdas. 2019. Plant Selective Autophagy - Still an Uncharted Territory with a Lot of Hidden Gems. *J. Mol. Biol.*
- Stolz, Alexandra, Andreas Ernst, and Ivan Dikic. 2014. Cargo Recognition and Trafficking in Selective Autophagy. *Nat. Cell Biol.* 16: 495–501.
- Stukenbrock, Eva H, Frank G Jorgensen, Marcello Zala, Troels T Hansen, Bruce A McDonald, and Mikkel H Schierup. 2010. Whole-Genome and Chromosome Evolution Associated with Host Adaptation and Speciation of the Wheat Pathogen *Mycosphaerella Graminicola*. *PLoS Genet.* 6: e1001189.
- Sugio, Akiko, Heather N Kingdom, Allyson M MacLean, Victoria M Grieve, and Saskia A Hogenhout. 2011. Phytoplasma Protein Effector SAP11 Enhances Insect Vector Reproduction by Manipulating Plant Development and Defense Hormone Biosynthesis. *Proc. Natl. Acad. Sci. U. S. A.* 108: E1254-63.
- Suttangkakul, Anongpat, Faqiang Li, Taijoon Chung, and Richard D Vierstra. 2011. The ATG1/ATG13 Protein Kinase Complex Is Both a Regulator and a Target of Autophagic Recycling in Arabidopsis. *Plant Cell* 23: 3761–79.
- Suzuki, Sho W, Hayashi Yamamoto, Yu Oikawa, Chika Kondo-Kakuta, Yayoi Kimura, Hisashi Hirano, and Yoshinori Ohsumi. 2015. Atg13 HORMA Domain Recruits Atg9 Vesicles during Autophagosome Formation. *Proc. Natl. Acad. Sci. U. S. A.* 112: 3350–55.
- Svenning, Steingrim, and Terje Johansen. 2013. Selective Autophagy. *Essays Biochem.* 55: 79–92.
- Svenning, Steingrim, Trond Lamark, Kirsten Krause, and Terje Johansen. 2011. Plant NBR1 Is a Selective Autophagy Substrate and a Functional Hybrid of the Mammalian Autophagic Adapters NBR1 and P62/SQSTM1. *Autophagy* 7: 993–1010.
- Takahashi, Yoshinori, Haiyan He, Zhenyuan Tang, Tatsuya Hattori, Ying Liu, Megan M Young, Jacob M Serfass, et al. 2018. An Autophagy Assay Reveals the ESCRT-III Component CHMP2A as a Regulator of Phagophore Closure. *Nat. Commun.* 9: 2855.

- Tan, Dongyan, Yiyang Cai, Juan Wang, Jinzhong Zhang, Shekar Menon, Hui-Ting Chou, Susan Ferro-Novick, Karin M Reinisch, and Thomas Walz. 2013. The EM Structure of the TRAPP3 Complex Leads to the Identification of a Requirement for COPII Vesicles on the Macroautophagy Pathway. *Proc. Natl. Acad. Sci. U. S. A.* 110: 19432–37.
- Tanaka, Hirokazu, Saeko Kitakura, Riet De Rycke, Ruth De Groot, and Jiri Friml. 2009. Fluorescence Imaging-Based Screen Identifies ARF GEF Component of Early Endosomal Trafficking. *Curr. Biol.* 19: 391–97.
- Taus, Thomas, Thomas Kocher, Peter Pichler, Carmen Paschke, Andreas Schmidt, Christoph Henrich, and Karl Mechtler. 2011. Universal and Confident Phosphorylation Site Localization Using PhosphoRS. *J. Proteome Res.* 10: 5354–62.
- Teh, Ooi-Kock, and Daniel Hofius. 2014. Membrane Trafficking and Autophagy in Pathogen-Triggered Cell Death and Immunity. *J. Exp. Bot.* 65: 1297–1312.
- Thompson, Allison R, Jed H Doelling, Anongpat Suttangkakul, and Richard D Vierstra. 2005. Autophagic Nutrient Recycling in Arabidopsis Directed by the ATG8 and ATG12 Conjugation Pathways. *Plant Physiol.* 138: 2097 LP – 2110.
- Thompson, Allison R, and Richard D Vierstra. 2005. Autophagic Recycling: Lessons from Yeast Help Define the Process in Plants. *Curr. Opin. Plant Biol.* 8: 165–73.
- Thon, Michael R, Huaqin Pan, Stephen Diener, John Papalas, Audrey Taro, Thomas K Mitchell, and Ralph A Dean. 2006. The Role of Transposable Element Clusters in Genome Evolution and Loss of Synteny in the Rice Blast Fungus *Magnaporthe Oryzae*. *Genome Biol.* 7: R16.
- Thumm, M, R Egner, B Koch, M Schlumpberger, M Straub, M Veenhuis, and D H Wolf. 1994. Isolation of Autophagocytosis Mutants of *Saccharomyces Cerevisiae*. *FEBS Lett.* 349: 275–80.
- Thurston, Teresa L M, Grigory Ryzhakov, Stuart Bloor, Natalia von Muhlinen, and Felix Randow. 2009. The TBK1 Adaptor and Autophagy Receptor NDP52 Restricts the Proliferation of Ubiquitin-Coated Bacteria. *Nat. Immunol.* 10: 1215–21.
- Tian, Miaoying, Edgar Huitema, Luis Da Cunha, Trudy Torto-Alalibo, and Sophien Kamoun. 2004. A Kazal-like Extracellular Serine Protease Inhibitor from *Phytophthora Infestans* Targets the Tomato Pathogenesis-Related Protease P69B. *J. Biol. Chem.* 279: 26370–77.

- Tian, Miaoying, Joe Win, Jing Song, Renier van der Hoorn, Esther van der Knaap, and Sophien Kamoun. 2007. A *Phytophthora Infestans* Cystatin-like Protein Targets a Novel Tomato Papain-like Apoplastic Protease. *Plant Physiol.* 143: 364–77.
- Tooze, Sharon A, Adi Abada, and Zvulun Elazar. 2014. Endocytosis and Autophagy: Exploitation or Cooperation? *Cold Spring Harb. Perspect. Biol.* 6: a018358–a018358.
- Tooze, Sharon A, and Ivan Dikic. 2016. Autophagy Captures the Nobel Prize. *Cell* 167: 1433–35.
- Trinkle-Mulcahy, Laura, Séverine Boulon, Yun Wah Lam, Roby Urcia, François-Michel Boisvert, Franck Vandermoere, Nick A Morrice, et al. 2008. Identifying Specific Protein Interaction Partners Using Quantitative Mass Spectrometry and Bead Proteomes. *J. Cell Biol.* 183: 223–39.
- Tsukada, Miki, and Yoshinori Ohsumi. 1993. Isolation and Characterization of Autophagy-Defective Mutants of *Saccharomyces Cerevisiae*. *FEBS Lett.* 333: 169–74.
- Tzfadia, Oren, and Gad Galili. 2013. The Arabidopsis Exocyst Subcomplex Subunits Involved in a Golgi-Independent Transport into the Vacuole Possess Consensus Autophagy-Associated Atg8 Interacting Motifs. *Plant Signal. Behav.* 8: e26732.
- UniProt: A Worldwide Hub of Protein Knowledge. 2019. *Nucleic Acids Res.* 47: D506–15.
- Upton, Jessica L, Erin K Zess, Aleksandra Bialas, Chih-Hang Wu, and Sophien Kamoun. 2018. The Coming of Age of EvoMPMI: Evolutionary Molecular Plant-Microbe Interactions across Multiple Timescales. *Curr. Opin. Plant Biol.* 44: 108–16.
- Ustun, Suayib, Anders Hafren, Qinsong Liu, Richard S Marshall, Elena A Minina, Peter V Bozhkov, Richard D Vierstra, and Daniel Hofius. 2018. Bacteria Exploit Autophagy for Proteasome Degradation and Enhanced Virulence in Plants. *Plant Cell* 30: 668–85.
- Vanhee, Celine, Grzegorz Zapotoczny, Daniele Masquelier, Michel Ghislain, and Henri Batoko. 2011. The Arabidopsis Multistress Regulator TSPO Is a Heme Binding Membrane Protein and a Potential Scavenger of Porphyrins via an Autophagy-Dependent Degradation Mechanism. *Plant Cell* 23: 785–805.
- Vicinanza, Mariella, Viktor I Korolchuk, Avraham Ashkenazi, Claudia Puri, Fiona M Menzies, Jonathan H Clarke, and David C Rubinsztein. 2015. PI(5)P Regulates

- Autophagosome Biogenesis. *Mol. Cell* 57: 219–34.
- Vizcaino, Juan Antonio, Attila Csordas, Noemi del-Toro, Jose A Dianas, Johannes Griss, Ilias Lavidas, Gerhard Mayer, et al. 2016. 2016 Update of the PRIDE Database and Its Related Tools. *Nucleic Acids Res.* 44: D447-56.
- von Muhlinen, Natalia, Masato Akutsu, Benjamin J. Ravenhill, Ágnes Foeglein, Stuart Bloor, Trevor J. Rutherford, Stefan M.V. Freund, David Komander, and Felix Randow. 2012. LC3C, Bound Selectively by a Noncanonical LIR Motif in NDP52, Is Required for Antibacterial Autophagy. *Mol. Cell* 48: 329–42.
- Wang, Heng-Long, Ping-Du Lee, Li-Fei Liu, and Jong-Ching Su. 1999. Effect of sorbitol induced osmotic stress on the changes of carbohydrate and free amino acid pools in sweet potato cell suspension cultures. *Bot. Bull. Acad. Sin.* 40: 219-225.
- Wang, Ming, Nicholas Thomas and Hailing Jin. 2017. Cross-Kingdom RNA Trafficking and Environmental RNAi for Powerful Innovative Pre- and Post-Harvest Plant Protection. *Curr. Opin. Plant Biol.* 38: 133–41.
- Wang, Ping, Yosia Mugume, and Diane C Bassham. 2018. New Advances in Autophagy in Plants: Regulation, Selectivity and Function. *Semin. Cell Dev. Biol.* 80: 113–22.
- Wang, Wei-Ying, Li Zhang, Shufan Xing, Zhiqiang Ma, Jingjing Liu, Hongya Gu, Genji Qin, and Li-Jia Qu. 2012. Arabidopsis AtVPS15 Plays Essential Roles in Pollen Germination Possibly by Interacting with AtVPS34. *J. Genet. Genomics* 39: 81–92.
- Wang, Yan, Bingjie Yu, Jinping Zhao, Jiangbo Guo, Ying Li, Shaojie Han, Lei Huang, et al. 2013. Autophagy Contributes to Leaf Starch Degradation. *Plant Cell* 25: 1383–99.
- Wang, Yu, Shuyu Cai, Lingling Yin, Kai Shi, Xiaojian Xia, Yanhong Zhou, Jingquan Yu, and Jie Zhou. 2015. Tomato HsfA1a Plays a Critical Role in Plant Drought Tolerance by Activating ATG Genes and Inducing Autophagy. *Autophagy* 11: 2033–47.
- Weber, Ernst, Carola Engler, Ramona Gruetzner, Stefan Werner, and Sylvestre Marillonnet. 2011. A Modular Cloning System for Standardized Assembly of Multigene Constructs. *PLoS One* 6: e16765.
- Wei, Ping, Wilson W Wong, Jason S Park, Ethan E Corcoran, Sergio G Peisajovich, James J Onuffer, Arthur Weiss, and Wendell A Lim. 2012. Bacterial Virulence Proteins as Tools to Rewire Kinase Pathways in Yeast and Immune Cells. *Nature*

488: 384.

- Weiberg, Arne, Ming Wang, Feng-Mao Lin, Hongwei Zhao, Zhihong Zhang, Isgouhi Kaloshian, Hsien-Da Huang, and Hailing Jin. 2013. Fungal Small RNAs Suppress Plant Immunity by Hijacking Host RNA Interference Pathways. *Science* 342: 118–23.
- Weidberg, Hilla, Elena Shvets, Tomer Shpilka, Frida Shimron, Vera Shinder, and Zvulun Elazar. 2010. LC3 and GATE-16/GABARAP Subfamilies Are Both Essential yet Act Differently in Autophagosome Biogenesis. *EMBO J.* 29: 1792–1802.
- Welters, P, K Takegawa, S D Emr, and M J Chrispeels. 1994. AtVPS34, a Phosphatidylinositol 3-Kinase of Arabidopsis Thaliana, Is an Essential Protein with Homology to a Calcium-Dependent Lipid Binding Domain. *Proc. Natl. Acad. Sci. U. S. A.* 91: 11398–402.
- Wen, Xin, and Daniel J Klionsky. 2016. An Overview of Macroautophagy in Yeast. *J. Mol. Biol.* 428: 1681–99.
- Wicker, Thomas, Simone Oberhaensli, Francis Parlange, Jan P Buchmann, Margarita Shatalina, Stefan Roffler, Roi Ben-David, et al. 2013. The Wheat Powdery Mildew Genome Shows the Unique Evolution of an Obligate Biotroph. *Nat. Genet.* 45: 1092–96.
- Wild, Philipp, Hesso Farhan, David G McEwan, Sebastian Wagner, Vladimir V Rogov, Nathan R Brady, Benjamin Richter, et al. 2011. Phosphorylation of the Autophagy Receptor Optineurin Restricts Salmonella Growth. *Science* 333: 228–33.
- Wild, Philipp, David G McEwan, and Ivan Dikic. 2014. The LC3 Interactome at a Glance. *J. Cell Sci.* 127: 3 LP – 9.
- Win, J, A Chaparro-Garcia, K Belhaj, D G O Saunders, K Yoshida, S Dong, S Schornack, et al. 2012. Effector Biology of Plant-Associated Organisms: Concepts and Perspectives. *Cold Spring Harb. Symp. Quant. Biol.* 77: 235–47.
- Win, Joe, Sophien Kamoun, and Alexandra M E Jones. 2011. Purification of Effector-Target Protein Complexes via Transient Expression in *Nicotiana Benthamiana*. *Methods Mol. Biol.* 712: 181–94.
- Win, Joe, William Morgan, Jorunn Bos, Ksenia V Krasileva, Liliana M Cano, Angela Chaparro-Garcia, Randa Ammar, Brian J Staskawicz, and Sophien Kamoun. 2007.

- Adaptive Evolution Has Targeted the C-Terminal Domain of the RXLR Effectors of Plant Pathogenic Oomycetes. *Plant Cell* 19: 2349 LP – 2369.
- Winer, Hila, Milana Fraiberg, Adi Abada, Tali Dadosh, Bat-Chen Tamim-Yecheskel, and Zvulun Elazar. 2018. Autophagy Differentially Regulates TNF Receptor Fn14 by Distinct Mammalian Atg8 Proteins. *Nat. Commun.* 9: 3744.
- Wirth, Martina, Wenxin Zhang, Mino Razi, Lynet Nyoni, Dhira Joshi, Nicola O'Reilly, Terje Johansen, Sharon A Tooze, and Stéphane Mouilleron. 2019. Molecular Determinants Regulating Selective Binding of Autophagy Adapters and Receptors to ATG8 Proteins. *Nat. Commun.* 10: 2055.
- Wittenberg, Alexander H J, Theo A J van der Lee, Sarrah Ben M'barek, Sarah B Ware, Stephen B Goodwin, Andrzej Kilian, Richard G F Visser, Gert H J Kema, and Henk J Schouten. 2009. Meiosis Drives Extraordinary Genome Plasticity in the Haploid Fungal Plant Pathogen *Mycosphaerella Graminicola*. *PLoS One* 4: e5863.
- Woo, Jongchan, Eunsook Park, and S P Dinesh-Kumar. 2014. Differential Processing of Arabidopsis Ubiquitin-like Atg8 Autophagy Proteins by Atg4 Cysteine Proteases. *Proc. Natl. Acad. Sci. U. S. A.* 111: 863–68.
- Wu, Chih-Hang, Ahmed Abd-El-Halim, Tolga O Bozkurt, Khaoula Belhaj, Ryohei Terauchi, Jack H Vossen, and Sophien Kamoun. 2017. NLR Network Mediates Immunity to Diverse Plant Pathogens. *Proc. Natl. Acad. Sci. U. S. A.* 114: 8113–18.
- Wu, Fan, Yasunori Watanabe, Xiang-Yang Guo, Xin Qi, Peng Wang, Hong-Yu Zhao, Zheng Wang, et al. 2015. Structural Basis of the Differential Function of the Two *C. Elegans* Atg8 Homologs, LGG-1 and LGG-2, in Autophagy. *Mol. Cell* 60: 914–29.
- Wurzer, Bettina, Gabriele Zaffagnini, Dorotea Fracchiolla, Eleonora Turco, Christine Abert, Julia Romanov, and Sascha Martens. 2015. Oligomerization of P62 Allows for Selection of Ubiquitinated Cargo and Isolation Membrane during Selective Autophagy. *Elife* 4: e08941.
- Xia, Kuaifei, Tao Liu, Jie Ouyang, Ren Wang, Tian Fan, and Mingyong Zhang. 2011. Genome-Wide Identification, Classification, and Expression Analysis of Autophagy-Associated Gene Homologues in Rice (*Oryza Sativa* L.). *DNA Res.* 18: 363–77.
- Xiang, Tingting, Na Zong, Yan Zou, Yong Wu, Jie Zhang, Weiman Xing, Yan Li, et al.

2008. Pseudomonas Syringae Effector AvrPto Blocks Innate Immunity by Targeting Receptor Kinases. *Curr. Biol.* 18: 74–80.
- Xie, Qingjun, Oren Tzfadia, Matan Levy, Efrat Weithorn, Hadas Peled-Zehavi, Thomas Van Parys, Yves Van de Peer, and Gad Galili. 2016. HFAIM: A Reliable Bioinformatics Approach for in Silico Genome-Wide Identification of Autophagy-Associated Atg8-Interacting Motifs in Various Organisms. *Autophagy* 12: 876–87.
- Xie, Yangchun, Rui Kang, Xiaofang Sun, Meizuo Zhong, Jin Huang, Daniel J Klionsky, and Daolin Tang. 2015. Posttranslational Modification of Autophagy-Related Proteins in Macroautophagy. *Autophagy* 11: 28–45.
- Xiong, Yan, Anthony L Contento, and Diane C Bassham. 2005. AtATG18a Is Required for the Formation of Autophagosomes during Nutrient Stress and Senescence in Arabidopsis Thaliana. *Plant J.* 42: 535–46.
- Xiong, Yan, Anthony L Contento, Phan Quang Nguyen, and Diane C Bassham. 2007. Degradation of Oxidized Proteins by Autophagy during Oxidative Stress in Arabidopsis. *Plant Physiol.* 143: 291–99.
- Xu, Guoyong, Shanshan Wang, Shaojie Han, Ke Xie, Yan Wang, Jinlin Li, and Yule Liu. 2017. Plant Box Inhibitor-1 Interacts with ATG6 to Regulate Autophagy and Programmed Cell Death. *Autophagy* 13: 1161–75.
- Xu, Xinjia, Tim Gookin, Cai-Zhong Jiang, and Michael Reid. 2007. Genes Associated with Opening and Senescence of Mirabilis Jalapa Flowers. *J. Exp. Bot.* 58: 2193–2201.
- Xue, Minfeng, Jun Yang, Zhigang Li, Songnian Hu, Nan Yao, Ralph A Dean, Wensheng Zhao, et al. 2012. Comparative Analysis of the Genomes of Two Field Isolates of the Rice Blast Fungus Magnaporthe Oryzae. *PLoS Genet.* 8: e1002869.
- Yaeno, Takashi, Hua Li, Angela Chaparro-Garcia, Sebastian Schornack, Seizo Koshiba, Satoru Watanabe, Takanori Kigawa, Sophien Kamoun, and Ken Shirasu. 2011. Phosphatidylinositol Monophosphate-Binding Interface in the Oomycete RXLR Effector AVR3a Is Required for Its Stability in Host Cells to Modulate Plant Immunity. *Proc. Natl. Acad. Sci. U. S. A.* 108: 14682–87.
- Yamamoto, Hayashi, Yuko Fujioka, Sho W Suzuki, Daisuke Noshiro, Hironori Suzuki, Chika Kondo-Kakuta, Yayoi Kimura, et al. 2016. The Intrinsically Disordered Protein Atg13 Mediates Supramolecular Assembly of Autophagy Initiation

- Complexes. *Dev. Cell* 38: 86–99.
- Yamamoto, Hayashi, Soichiro Kakuta, Tomonobu M Watanabe, Akira Kitamura, Takayuki Sekito, Chika Kondo-Kakuta, Rie Ichikawa, Masataka Kinjo, and Yoshinori Ohsumi. 2012. Atg9 Vesicles Are an Important Membrane Source during Early Steps of Autophagosome Formation. *J. Cell Biol.* 198: 219–33.
- Yang, Xiaochen, and Diane C Bassham. 2015. New Insight into the Mechanism and Function of Autophagy in Plant Cells. *Int. Rev. Cell Mol. Biol.* 320: 1–40.
- Yang, Xiaochen, Renu Srivastava, Stephen H Howell, and Diane C Bassham. 2016. Activation of Autophagy by Unfolded Proteins during Endoplasmic Reticulum Stress. *Plant J.* 85: 83–95.
- Yang, Zhifen, and Daniel J Klionsky. 2010. Eaten Alive: A History of Macroautophagy. *Nat. Cell Biol.* 12: 814.
- Yoshida, Kentaro, Hiromasa Saitoh, Shizuko Fujisawa, Hiroyuki Kanzaki, Hideo Matsumura, Kakoto Yoshida, Yukio Tosa, et al. 2009. Association Genetics Reveals Three Novel Avirulence Genes from the Rice Blast Fungal Pathogen *Magnaporthe Oryzae*. *Plant Cell* 21: 1573–91.
- Yoshida, Kentaro, Diane G O Saunders, Chikako Mitsuoka, Satoshi Natsume, Shunichi Kosugi, Hiromasa Saitoh, Yoshihiro Inoue, et al. 2016. Host Specialization of the Blast Fungus *Magnaporthe Oryzae* Is Associated with Dynamic Gain and Loss of Genes Linked to Transposable Elements. *BMC Genomics* 17: 370.
- Yoshida, Kiyotsugu. 2008. Role for DYRK Family Kinases on Regulation of Apoptosis. *Biochem. Pharmacol.* 76: 1389–94.
- Yoshimoto, Kohki, Hideki Hanaoka, Shusei Sato, Tomohiko Kato, Satoshi Tabata, Takeshi Noda, and Yoshinori Ohsumi. 2004. Processing of ATG8s, Ubiquitin-like Proteins, and Their Deconjugation by ATG4s Are Essential for Plant Autophagy. *Plant Cell* 16: 2967–83.
- Youle, Richard J, and Derek P Narendra. 2011. Mechanisms of Mitophagy. *Nat. Rev. Mol. Cell Biol.* 12: 9–14.
- Young, Pierce G, Michael J Passalacqua, Kevin Chappell, Roxanna J Llinas, and Bonnie Bartel. 2019. A Facile Forward-Genetic Screen for Arabidopsis Autophagy Mutants Reveals Twenty-One Loss-of-Function Mutations Disrupting Six ATG Genes. *Autophagy* 15: 941–59.

- Zaccai, Michele, Guixia Jia, Xinlu Chen, Oksana Genis, Danit Feibin, and Revital Gesua. 2007. Regeneration and Transformation System in *Mirabilis Jalapa*. *Sci. Hort. (Amsterdam)*. 111: 304–9.
- Zaffagnini, Gabriele, and Sascha Martens. 2016. Mechanisms of Selective Autophagy. *J. Mol. Biol.* 428: 1714–24.
- Zess, Erin K, Cassandra Jensen, Neftaly Cruz-Mireles, Juan Carlos De la Concepcion, Jan Sklenar, Madlen Stephani, Richard Imre, et al. 2019. N-Terminal β -Strand Underpins Biochemical Specialization of an ATG8 Isoform. *PLOS Biol.* 17: e3000373.
- Zhang, Lichao, and Joshua E Elias. 2017. Relative Protein Quantification Using Tandem Mass Tag Mass Spectrometry BT - Proteomics: Methods and Protocols. In , edited by Lucio Comai, Jonathan E Katz, and Parag Mallick, 185–98. New York, NY: Springer New York.
- Zhang, Peixiang, M Anthony Verity, and Karen Reue. 2014. Lipin-1 Regulates Autophagy Clearance and Intersects with Statin Drug Effects in Skeletal Muscle. *Cell Metab.* 20: 267–79.
- Zheng, Yiyu T, Shahab Shahnazari, Andreas Brech, Trond Lamark, Terje Johansen, and John H Brumell. 2009. The Adaptor Protein P62/SQSTM1 Targets Invading Bacteria to the Autophagy Pathway. *J. Immunol.* 183: 5909–16.
- Zhou, Fan, Zulin Wu, Mengzhu Zhao, Rakhilya Murtazina, Juan Cai, Ao Zhang, Rui Li, et al. 2019. Rab5-Dependent Autophagosome Closure by ESCRT. *J. Cell Biol.* 218: 1908 LP – 1927.
- Zhou, Jie, Jian Wang, Yuan Cheng, Ying-Jun Chi, Baofang Fan, Jing-Quan Yu, and Zhixiang Chen. 2013. NBR1-Mediated Selective Autophagy Targets Insoluble Ubiquitinated Protein Aggregates in Plant Stress Responses. *PLoS Genet.* 9: e1003196.
- Zhou, Jie, Zhe Wang, Xiaoting Wang, Xifeng Li, Zhenchao Zhang, Baofang Fan, Cheng Zhu, and Zhixiang Chen. 2018. Dicot-Specific ATG8-Interacting ATI3 Proteins Interact with Conserved UBAC2 Proteins and Play Critical Roles in Plant Stress Responses. *Autophagy* 14: 487–504.
- Zhou, Jie, Jing-Quan Yu, and Zhixiang Chen. 2014. The Perplexing Role of Autophagy in Plant Innate Immune Responses. *Mol. Plant Pathol.* 15: 637–45.

- Zhou, Jie, Yan Zhang, Jingxia Qi, Yingjin Chi, Baofang Fan, Jing-Quan Yu, and Zhixiang Chen. 2014. E3 Ubiquitin Ligase CHIP and NBR1-Mediated Selective Autophagy Protect Additively against Proteotoxicity in Plant Stress Responses. *PLOS Genet.* 10: e1004116.
- Zhou, Xue-mei, Peng Zhao, Wei Wang, Jie Zou, Tian-he Cheng, Xiong-bo Peng, and Meng-xiang Sun. 2015. A Comprehensive, Genome-Wide Analysis of Autophagy-Related Genes Identified in Tobacco Suggests a Central Role of Autophagy in Plant Response to Various Environmental Cues. *DNA Res.* 22: 245–57.
- Zhuang, Xiaohong, Kin Pan Chung, Yong Cui, Weili Lin, Caiji Gao, Byung-Ho Kang, and Liwen Jiang. 2017. ATG9 Regulates Autophagosome Progression from the Endoplasmic Reticulum in Arabidopsis. *Proc. Natl. Acad. Sci. U. S. A.* 114: E426–35.
- Zhuang, Xiaohong, Hao Wang, Sheung Kwan Lam, Caiji Gao, Xiangfeng Wang, Yi Cai, and Liwen Jiang. 2013. A BAR-Domain Protein SH3P2, Which Binds to Phosphatidylinositol 3-Phosphate and ATG8, Regulates Autophagosome Formation in Arabidopsis. *Plant Cell* 25: 4596 LP – 4615.
- Zientara-Rytter, Katarzyna, Jolanta Lukomska, Grzegorz Moniuszko, Rafal Gwozdecki, Przemyslaw Surowiecki, Malgorzata Lewandowska, Frantz Liszewska, Anna Wawrzynska, and Agnieszka Sirko. 2011. Identification and Functional Analysis of Joka2, a Tobacco Member of the Family of Selective Autophagy Cargo Receptors. *Autophagy* 7: 1145–58.
- Zimmermann, Philip, Matthias Hirsch-Hoffmann, Lars Hennig, and Wilhelm Gruissem. 2004. GENEVESTIGATOR. Arabidopsis Microarray Database and Analysis Toolbox. *Plant Physiol.* 136: 2621–32.